STAT1 potentiates oxidative stress revealing a targetable vulnerability that sensitizes breast cancers to mitochondrial complex I inhibitors.

Stephanie Totten
Division of Experimental Medicine, Department of Medicine
McGill University, Montreal, Canada
April 2023

A thesis submitted to McGill University in partial fulfillment of the requirements for the degree of Doctor of Philosophy

Table of Contents

Abstract

Improved understanding of metabolic modifications and dependencies of neoplastic cells may reveal clinically targetable vulnerabilities. Reactive oxygen species (ROS) are produced by multiple metabolic pathways in normal and cancer cells. Moderate increases in the production of reactive oxygen species favours neoplastic growth and progression, however these must be held in balance with compensatory increases in ROS scavengers to limit oxidative stress and cell death. Phenformin is a mitochondrial complex I inhibitor that induces bioenergetic stress. Herein, we report that multiple human and mouse breast cancer cell lines were sensitized to phenformin when combined with the pro-inflammatory cytokine interferon gamma (IFNγ). Similarly, we find that an elevated inflammatory response, stimulated by polyIC synergizes with phenformin to attenuate breast tumor growth.

By inhibiting complex I of the electron transport chain, phenformin suppresses mitochondrial-dependent ATP generation and simultaneously increases production of mitochondrial ROS. We find that functionally, the mitochondrial ROS scavenger, MitoTempo, reverses the ability of the inflammatory mediators, IFNγ and polyIC to sensitize tumor models to phenformin. Through RNA sequencing, we identify Nqo1 as a target gene that decreases upon IFNγ treatment of breast cancer cells. Nqo1 is a 2-electron reductase that is upregulated in many tumors and has important roles in ROS scavenging and cellular stress responses. Decreasing Nqo1 by genetic suppression or pharmacologically with β-lapachone, cooperatively sensitizes human and mouse cell lines, and HER2+ and basal-like cells from patient-derived xenografts (PDX), as well as *in vivo* tumor growth to phenformin. Given that glutathione is a major ROS scavenger in cancer cells, we further show that combined treatment with phenformin and an inhibitor of glutathione synthesis (BSO) cooperate in breast cancer cell lines and PDX cell lines. Using the immortalized epithelial cell line, NMuMG, and its HER2/Neu transformed counterpart, breast cancer cells are sensitized to co-treatment of phenformin with BSO or β-lapachone, while sparing normal non-transformed cells. Overall, we find that therapies that target ROS scavengers increase the anti-neoplastic efficacy on ROS-inducing mitochondrial complex I inhibitors.

Abrégé

Une meilleure compréhension des modifications métaboliques et des dépendances des cellules néoplasiques peut révéler des vulnérabilités cliniquement ciblables. Les espèces réactives de l'oxygène (ERO) sont produites par de multiples voies métaboliques. Des augmentations modérées de la production d'espèces réactives de l'oxygène favorisent la croissance et la progression néoplasiques, mais celles-ci doivent être maintenues en équilibre avec des augmentations compensatoires des capacités cellulaire antioxydante pour limiter le stress oxydant et la mort cellulaire. La phenformine est un inhibiteur du complexe I mitochondrial qui induit un stress bioénergétique. Nous rapportons que plusieurs lignées cellulaires de cancer du sein humain et models murin ont été sensibilisées à la phenformine lorsqu'elles sont combinées avec la cytokine pro-inflammatoire interféron gamma (IFNγ). De même, nous constatons qu'une réponse inflammatoire élevée, stimulée par polyIC est coopère avec la phenformine pour atténuer la croissance tumorale.

En inhibant le complexe I de la chaîne de transport d'électrons, la phenformine supprime simultanément la génération d'ATP dépendante des mitochondries et augmente la production d'ERO mitochondriales. Sur le plan fonctionnel, l'antioxydant mitochondrial, MitoTempo, inverse la capacité des médiateurs anti-inflammatoires, IFNγ et polyIC à sensibiliser les tumeursavec la phenformine. Grâce au séquençage de l'ARN, nous identifions Nqo1 comme gène cible qui diminue lors du traitement des cellules cancéreuses du sein avec IFNγ. Nqo1 est une réductase à deux électrons qui est surrexprimé dans de nombreuses tumeurs et qui joue un rôle important d'antioxidant, détoxification des quinones, et les réponses au stress cellulaire. Le ciblage de Nqo1 par ablation génétique, ou pharmacologique avec la β-lapachone, sensibilise les lignées cellulaires humaines et murines, et les xénogreffes dérivées de patients de cancers du sein HER2+ et de type-basale, et la croissance tumorale de xénogreffe *in vivo* à la phenformine. Dans le même ordre d'idées, un traitement combiné à la phenformine et à un inhibiteur de la synthèse du glutathion coopère dans les lignées cellulaires du cancer du sein et les lignées cellulaires PDX. Enfin, en utilisant la lignée cellulaire épithéliale immortalisée, NMuMG, et son homologue transformé HER2/Neu, les cellules cancéreuses du sein sont sensibilisées au co-traitement de la phenformine avec l'inhibiteur de la synthèse du glutathion ou avec la β-lapachone, tout en épargnant les cellules normales non transformées. Dans l'ensemble, nous constatons que les thérapies qui ciblent les antioxydants augmentent l'efficacité anti-néoplasique des inhibiteurs du complexe mitochondrial I, en induisant le stress oxydant.

Acknowledgements

This research and thesis would not have been possible, nor would this journey have been nearly as enjoyable, without the following people:

Firstly, I would like to acknowledge my supervisor and mentor, Dr. Josie Ursini-Siegel. Josie, thank you for welcoming me into your group, and for the opportunity to work on this intriguing project. Your passion and thoroughness are remarkable. Thank you for your open-door policy, your guidance and support to pursue various ideas and collaborations throughout my doctorate. You have helped me grow both as a scientist and a person.

I would also like to acknowledge my thesis advisory committee members: Dr. Antonis Koromilas, Dr. Peter Siegel, Dr. Morag Park, my advisor Dr. Michael Witcher and external examiner, Dr. Lawrence Kazak, for their time, expertise, recommendations for experiments, and encouragement throughout my PhD.

Thank you to my thesis defence committee members: Dr. Donna Senger, Dr. Isaac Harris, Dr. Janusz Rak and Dr. Lawrence Kazak for their time, feedback, thought-provoking questions and discussion, and revisions.

A huge thank you to our many collaborators. Your contributions in terms of materials, experiments, data analysis, exchange of ideas, and editorial help made addressing our research question, the manuscript, and this thesis possible. Please refer to contribution of authors section for details of these contributions. Working with each of you and learning from you were highlights of my PhD.

To my colleagues and friends both current and past in the JUS lab, thank you for your support and for the stimulating conversations. Throughout these years, you helped me grow as a researcher and an individual. I am grateful that our paths crossed.

Thank you to McGill's MD-PhD program director Dr. Mark Eisenberg for his support. To my colleagues in the program present and past, I value your friendship and encouragement throughout these 8 years.

A big thank you to my family for their love and support. Special thanks to my Dad for his advice and strength, as well as for fostering my inquisitiveness. To Ann, thank you for your unwavering encouragement. To my brother and sister, for your love and encouragement.

To my Nana, Papa and Aunt Pen, thank you for your love and understanding.
A huge thank you to my friends who are like family. Aly, Zoy, Jackie, Pedj, Rach, Piotr, Ed, Kyle, Mandie, Nats, Lashanda, Shriya, Libby, Eden, Celine and Kait, thank you for your love, support, encouragement and advice throughout my PhD, medical school and in writing this thesis.

Finally, this thesis would not have been possible without the support of my love, Andrey. I can't thank you enough for encouraging me when I needed it most, for your advice, your listening ear, your edits, and for all the ways you have and continue to show up for me. Thank you for embarking on this journey with me and supporting my pursuit of a career as a clinician-scientist.

I wish to acknowledge funding received from the Canadian Institutes of Health Research's Frederick Banting and Charles Best Graduate Doctoral award, McGill's MD-PhD program, the Hilton J. McKeown Scholarship, the George Corcoran Scholarship, the Dr. Raymond and Leora Kahn Summer Research Bursary in memory of Marion Kahn and the McGill Graduate Excellence Entrance Scholarship.

Dedication

***For my Nana Totten**, I miss you tremendously.*

***For patients and advocates** whose contributions have advanced female reproductive rights and health, and improved outcomes and quality of life for all individuals facing a cancer diagnosis.*

Preface

The following doctoral thesis is written in traditional monograph-based format and contains 6 chapters.

Chapter 1: Literature Review

Chapter 2: Methods

Chapter 3: Results

Chapter 4: Discussion

Chapter 5: Conclusion and summary

Chapter 6: References

This thesis was written in accordance with the guidelines outlined by McGill's Graduate and Postdoctoral Studies organization.

Publication arising from this research

Totten SP, Im YK, Cepeda Cañedo E, Najyb O, Nguyen A, Hébert S, Ahn R, Lewis K, Lebeau B, La Selva R, Sabourin V, Martínez C, Savage P, Kuasne H, Avizonis D, Santos Martínez N, Chabot C, Aguilar-Mahecha A, Goulet ML, Dankner M, Witcher M, Petrecca K, Basik M, Pollak M, Topisirovic I, Lin R, Siegel PM, Kleinman CL, Park M, St-Pierre J, Ursini-Siegel J. STAT1 potentiates oxidative stress revealing a targetable vulnerability that increases phenformin efficacy in breast cancer. Nature Communications. 2021 Jun 3;12(1):3299.

Additional contributions throughout MD-PhD

Cepeda Cañedo E, Totten S, Ahn R, Savage P, MacNeil D, Hudson J, Autexier C, Deblois G, Park M, Witcher M, Ursini-Siegel J. p66ShcA potentiates the cytotoxic response of triple negative breast cancers to PARP inhibitors. JCI Insight., 2021 Jan 21:138382.

Ahn R, Sabourin V, Bolt AM, Hebert S, Totten S, De Jay N, Festa MC, Young YK, Im Y, Pawson T, Koromilas AE, Muller WJ, Mann KK, Kleinman CL, Ursini-Siegel J. The Shc1 adaptor simultaneously balances Stat1 and Stat3 activity to promote breast cancer immune suppression. Nature Communications, 2017, 8: 14638.

Totten S, Xu J. Chapter 15: Completing your project, in Eisenberg M.J. and Cox A.L. (eds.). The Essential MD-PhD Guide. McGraw Hill, pp. 115-124.

Contribution to original knowledge

1. We provide the first evidence that IFNγ-driven STAT1 activation sensitizes multiple mouse and human breast cancer cell lines to phenformin-induced anti-tumorigenic effects.

2. We also demonstrate that tumor inflammation driven by polyIC treatment induces robust anti-tumorigenic responses when combined with phenformin, in a STAT1-dependent manner in multiple *in vivo* models of breast cancer.

3. We find that IFNγ and polyIC sensitization of breast cancer cells to phenformin depends on mitochondrial ROS production and that combination treatment increases oxidative stress in tumors.

4. We characterize metabolic impacts of single IFNγ treatment of breast cancers and find that it modestly reduces the maximal respiration and bioenergetic flexibility of breast cancer cells in a STAT1-dependent manner. IFNγ increases steady state levels of lactate, pyruvate and the α-ketoglutarate levels, as well as increases the lactate/pyruvate and the α-ketoglutarate/citrate ratio in a STAT1-dependent manner.

5. We establish Nqo1 (an NAD(P)H-dependent two-electron reductase that scavenges reactive oxygen species) as a target decreased upon IFNγ treatment in multiple human and mouse breast cancer models.

6. We find that combining phenformin and an inhibitor of glutathione cooperate as anti-cancer agents in multiple human and mouse models of breast cancer.

7. We show the first evidence that decreasing NQO1 levels with shRNA, sensitizes multiple breast cancer cell lines to phenformin, revealing NQO1 as an important ROS scavenger that protects breast tumors from phenformin anti-tumorigenic activity.

8. We also find that an NQO1 bioactivatable drug, β-lapachone, sensitizes both *in vitro* and *in vivo* breast cancer models to phenformin or the small molecule mitochondrial complex I inhibitor, IACS-010759, by inducing oxidative damage.

9. We demonstrate that phenformin in combination with β-lapachone or BSO selectively sensitize breast cancer cells, while sparing non-transformed cell models.

10. We find that targetable ROS scavenging mechanisms can be alleviated to preferentially sensitize patient-derived human breast cancer cells of the HER2+ and basal-like subtypes to phenformin.

Contribution of authors

-Stephanie Totten prepared the thesis, including the literature review, the methods, results, and discussion, conclusion. She also performed most of the experiments, data analysis and figure preparation that are presented in this thesis. ST and Dr. Josie Ursini-Siegel also conceptualized most of the experiments.
-Dr. Josie Ursini-Siegel reviewed and edited the thesis. ST and JUS wrote the manuscript for which this thesis was based. JUS prepared 3.18h and 3.20 and IHC analysis.
-Dr. Claudia L. Kleinman, Dr. Julie St-Pierre and Dr. Rongtuan Lin also contributed to specific experimental design, see details below.
-Dr. Michael Pollak and Dr. Ivan Topisirovic contributed by providing essential input in the early stages of this project.
-Thesis advisory committee members, Dr. Michael Witcher, Dr. Antonis Koromilas, Dr. Peter Siegel, Dr. Morag Park provided support, suggestions, and valuable recommendations throughout various stages of this project.
-Young Im, performed the initial experiments that set the groundwork for this project, he specifically contributed to Figure 3.1a-c, Figure 3.2a, b, e, f; Figure 3.3a-c, e; 3.9a; 3.13 e,f; 3.15 a-d.
-Eduardo Cepeda Cañedo performed the immunoblots in Figure 3.14c, d and ran and analysed the multiple RT-qPCRs in Figure 3.14a.
-Dr. Ouafa Najyb performed the seahorse experiments in Figure 3.6a-f ; GC-MS for Figure 3.7 a,b, h and i, during which she also kindly trained ST.
-Alice Nguyen assisted with the cell counts for Figures 3.11a and b; Figure 3.12a.
-Steven Hebert performed the RNA sequencing analysis under the supervision of Dr. Claudia L. Kleinman, presented in Figure 3.13 a-d.
-Dr. Ryujin Ahn prepared the original STAT1-CRISPR cell lines and the observation that Shc313F cell lines have increased STAT1 expression was made from her work.
-Kyle Lewis analyzed the GC-MS data in Figure 3.7c, d, f, g.
-Dr. Benjamin Lebeau performed the CHIP-qPCR, under the supervision of Dr. Michael Witcher. Figure 3.14e.
-Valerie Sabourin assisted with various steps of IHC, including slide preparation, for some of the experiments, and for others, antigen retrieval and staining in Figure 3.9b. She also is responsible for optimizing many of the IHC conditions used in other panels.

-Dr. Morag Park Dr. Constanza Martínez and Dr. Paul Savage the Hellen Kuasne provided the GCRC PDX models used in Figure 3.19 c-h.
-Dr. Daina Avizonis and the Goodman Cancer Research Centre Metabolomics' core that ran the LC-MS samples, offered GC-MS support, and assisted with the analysis.
- Dr. Mark Basik, Dr. Nancy Santos Martínez, Dr. Catherine Chabot and Dr. Adriana Aguilar-Mahecha, prepared and provided the PDX CRC 132 used in Figures 3.19 c and d.
-Dr. Kevin Petrecca Dr. Peter M. Siegel and Dr. Matthew Dankner provided lysates from the lung cancer brain metastases PDXs used in Figure 3.14d.
-Dr. Rongtuan Lin and Marie-Line Goulet provided the VSV, supported experimental design, as well as initial training ST for VSV-intratumoral injections for Figure 3.3d.

List of abbreviations

Abbreviation	Term
^{18}FDG-PET	^{18}F-fluorodeoxyglucose positron-emission tomography
4E-BP	Eukaryotic initiation factor 4E-binding proteins
8 oxo-dG	8-Oxo-2'-deoxyguanosine
AhR	Aryl hydrocarbon receptor
AMPK	5'-AMP-activated protein kinase
APC	Antigen presenting cell
ARN	Acide ribonucléique
ATM	Ataxia-telangiectasia mutated
ATP	Adenosine triphosphate
B2M	β2 microglobulin
BRCA1	BReast CAncer gene 1
BRCA2	BReast CAncer gene 2
BrdU	5-Bromo-2´-Deoxyuridine
BRIP1	BRCA1 interacting Helicase 1
BSA	Bovine serum albumin
BSO	Buthionine sulfoxime
CAF	Cancer associated fibroblast
CAT	Catalase
CAT1	Carnitine palmitoyltransferase I
CAT2	Carnitine acetyl-CoA transferase
CD8	Cluster of differentiation 8
CDH1	Cadherin-1
cDNA	Complementary DNA
cGAS	Cytosolic DNA sensor cyclic GMP-AMP synthase
CHEK2	Checkpoint kinase 2
ChIP-qPCR	Chromatin immunoprecipitation-quantitative real-time polymerase chain reaction
CoQ	Coenzyme Q/Ubiquinone
CRISPR	Clustered Regularly Interspaced Short Palindromic Repeats
CSC	Cancer stem cells
CTL	Cytotoxic T lymphocytes
CTLA-4	Cytotoxic T lymphocyte-associated protein 4
CXCL9	Chemokine ligand 9
DAMPs	Damage associated molecular patterns
DAPI	4′,6-diamidino-2-phenylindole
DCIS	Ductal Carcinoma in situ
DMEM	Dulbecco's Modified Eagle's Medium
DMSO	Dimethyl sulfoxide
ECAR	Extracellular acidification rate
EDTA	Ethylenediaminetetraacetic acid
EGFR	Epidermal Growth factor receptor

EMT	Epithelial-mesenchymal transition
ER	Estrogen receptor
Erap1	Endoplasmic Reticulum Aminopeptidase 1
ERO	Espèces réactives de l'oxygène
ESI	Electrospray ionization
ETC	Electron transport chain
FAO	Fatty Acid oxidation
FBS	Fetal bovine serum
GAPDH	Glyceraldehyde 3-phosphate dehydrogenase
GAS	Gamma-activated sequence
GC-MS	Gas Chromatography-Mass Spectrometry
GCL	Glutamate-cysteine ligase
GCLC	Glutamate-cysteine ligase modulatory subunit
GCLM	Glutamate-cysteine ligase catalytic subunit
GLS1	Glutaminase-1
GLUD	Glutamate dehydrogenase
GnRH	Gonadotrophin-releasing hormone agonists
GOT1	Glutamic-oxaloacetic transaminase 1
GPX	Glutathione peroxidase
GR	Glutathione reductase
GS	Glutathione synthetase
GSEA	Gene Set Enrichment analysis
GSH	Glutathione
GSSG	Glutathione disulfide
HEPES	Hydroxyethyl piperazine ethanesulfonic acid
HER2	Human epidermal growth factor receptor 2
HIF	Hypoxia-inducible factor
HPβCD	Hydroxypropyl-β-cyclodextrin
HR	Hormone receptors
HRE	Hypoxia response elements
IBC	Invasive breast carcinomas
IDC	Invasive (infiltrating) ductal carcinoma (IDC
IDH	Isocitrate dehydrogenases
IDO	Indoleamine 2,3-dioxygenase
IFNγ	Interferon gamma
IgG	Immunoglobulin G
IHC	Immunohistochemistry
IL	Interleukins
Irf1	Interferon regulatory factor 1
IRF7	Interferon Regulatory Factor 7
Irf9	Interferon regulatory factor 9
ISRE	Interferon-stimulated response elements
JAK	Janus Kinase
KEAP1	Kelch-like erythroid cell-derived protein with CNC homology [ECH]-associated protein 1

KO	Knock-out
LAR	Luminal androgen receptor
LC-MS	Liquid Chromatography-Mass Spectrometry (LC-MS)
LCIS	Lobular Carcinoma in situ
LKB1	Liver kinase B1
LN	Lymph nodes
LTR	Long terminal repeat
MaSc	Mammary stem cells
MATE	Multi-drug and toxin extrusion protein
MEGS	Mammary epithelial growth supplement
MFP	Mammary fat pad
MHC	Major histocompatibility complex
MMTV	Mouse mammary tumor virus
MPO	Myeloperoxidase
MRM	Multiple reaction monitoring
mTORC	Mammalian/mechanistic target of rapamycin complex
NAD+	Nicotinamide adenine dinucleotide
NADH	Nicotinamide adenine dinucleotide + hydrogen
NADP+	Nicotinamide adenine dinucleotide phosphate
NADPH	Nicotinamide adenine dinucleotide phosphate +Hydrogen
NF-kB	Nuclear factor kappa-light chain-enhancer of activate B cell
NK	Natural Killer
NKT	Natural killer T cell
NQO1	NAD(P)H Quinone Dehydrogenase 1
NRF2	Nuclear factor erythroid 2–related factor 2
NRH	Dihydronicotinamide riboside
OCR	Oxygen consumption rate
OCT	Organic cation transporters
OGG1	8-oxoguanine DNA glycosylase
ORF	Open reading frame
OXPHOS	Oxidative phosphorylation
PALB2	Partner and localizer of BRCA2
PAMPs	Pathogen associated molecular patterns
PARP	Poly (ADP-ribose) polymerase
PARP	Poly (ADP-ribose) polymerase
PBS	Phosphate buffered saline
PCOS	Multi-drug and toxin extrusion protein
PCR	Polymerase chain reaction
PD1	Programmed cell death protein
PDH	Pyruvate dehydrogenase
PDK1	Pyruvate dehydrogenase kinase 1
PDL1	Programmed cell death protein ligand
PDX	Patient-derived xenografts
PFU	Particle forming units

PGC-1α	Peroxisome proliferator-activated receptor gamma coactivator 1-alpha
PHD2	Prolyl hydroxylase domain protein 2
PI	Propidium iodide
PI3K	5'-AMP-activated protein kinase
PolyAU	Polyadenylic–polyuridylic acid
PolyIC	Polyinosinic-polycytidylic acid
PPP	Pentose phosphate pathway
PR	Progesterone Recepor
PRDX4	Peroxiredoxin 4
Psmb8	Proteasome subunit beta type-8
PTEN	Phosphatase and tensin homolog
RAD51C	RAD51 homolog C
RAD51D	RAD51 homolog D
RAGE	Receptor for advanced glycation end products
RIG	Retinoic acid-inducible gene I
RLR	Retinoic acid-inducible gene I (RIG-I)-like receptors
RNA	Ribonucleic acid
RNS	Reactive nitrogen species
ROS	Reactive Oxygen Species
RPMI	Roswell Park Memorial Institute
RT-qPCR	Quantitative reverse transcription polymerase chain reaction
S6K	Ribosomal protein S6
SD	Standard deviation
SDS	Sodium dodecyl sulfate
SEM	Standard Error of the Mean
shRNA	Short hairpin ribonucleic acid
SNP	Small nucleotide polymorphisms
SOCS	Suppressor of cytokine signaling molecules
SOD3	Superoxide dismutase 3
STAT1	Signal transducer and activator of transcription 1
STK11	Serine/threonine kinase 11
TAM	Tumor associated macrophage
TAP1	Transporter 1, ATP Binding Cassette Subfamily B Member
TBS	Tris buffered saline
TCA	Tricarboxylic acid
TDLU	Terminal duct lobular units
TIL	Tumor-infiltrating lymphocyte
TIM-3	T-cell immunoglobulin and mucin domain 3
TLR	Toll-like receptors
TME	Tumor microenvironment
TNBC	Triple negative breast cancer
TNF	Tumor necrosis factor
TNM	Tumor, node, metastasis
TP53	Tumor protein 53

TSS	Transcription start site
TXN	Thioredoxin
VSV	Vesicular stomatitis virus
WT	Wild type
XRE	Xenobiotic response element

List of figures and tables

Chapter 1: Introduction

1.1 Introduction to literature review

In the following literature review, an overview of normal breast tissue and breast cancer is provided. Next, current treatment strategies are explored, highlighting current limitations, particularly for patients who experience relapse/resistant breast cancer and/or metastatic disease and those who initially present with disseminated disease [1-3]. Tumor-intrinsic and tumor-extrinsic (microenvironmental) factors, including cellular components, nutrients and oxygen availability contribute to tumor development, tumor heterogeneity and ultimately to variable responses to therapies and outcomes. A particular focus of this literature review is on our current understanding of breast cancer metabolism, which is contrasted with normal mammary epithelial cell metabolism.

Cancer cell survival depends on the orchestration of metabolic pathways to create the biomass, energy, and maintenance of redox balance necessary for proliferation and metastasis. The objective of characterizing breast cancer metabolism is to identify tumor-specific and essential metabolic dependencies that can then be targeted clinically while sparing normal cells. Given the heterogeneity of breast cancers, this task remains a challenging one. Certain metabolic vulnerabilities in different cancer models, including breast cancer have been described, although many of these are subtype- and even model-restricted. It is now understood that many breast cancers rely on mitochondrial metabolism. Furthermore, many resistant cells have increased dependency on oxidative phosphorylation. Considering this, pharmacological inhibitors of complex I within the electron transport chain have shown promise as anti-cancer agents. Our current understanding of mitochondrial complex I inhibitors, including the class biguanides (metformin and phenformin) is addressed. A particular focus of this literature review is on redox balance, including key cellular antioxidants, as well as the current state of understanding of therapeutic strategies involved in promoting oxidative stress in cancer cells. As it pertains to the findings in this thesis, the topics of inflammation, interferon gamma and signal transducer and activator of transcription 1 (STAT1), in cancer are also overviewed. Finally, our current understanding of the intersection of metabolism and inflammation is addressed.

1.2 Normal breast anatomy, histology, development and function

Mammary glands are one of the characteristic features of the class Mammalia. In females, these exocrine glands have the potential to produce milk intended for nourishment and immunologic protection of infants [reviewed in [4]]. In humans, breasts are generally bilateral

and are comprised of tree-like glandular tissue embedded within a fibroadipose stromal compartment, located on the anterior thoracic wall. Our understanding of the development of the human breast and its pathologies has evolved considerably since Sir Astley Cooper's anatomical description and general remarks of the human breasts in 1875 [5].

Breast development begins in utero around the fifth week of gestation in humans [6]. Our current understanding is that breasts develop from ectoderm, which then gives rise to mammary stem cells (MaSc) [7] that have the capacity to entirely repopulate the mammary gland. MaSc further differentiate into lineage-restricted luminal and basal progenitors, with more limited differentiation capacity, but can expand to respectively maintain each lineage of terminally differentiated cell types that constitute the mammary gland: including luminal ductal cells and luminal alveolar cells as well as, myoepithelial cells [8-10]. Distinct progenitor cells along this hierarchy are the putative cells of origin of breast cancers from distinctive molecular subtypes, and are discussed below in the *Breast cancer pathogenesis* section [11]. The structure and function of mammary glands vary substantially according to sex, stage of development, medication including hormone replacement therapy as well as physiological status, including puberty, menarche, pregnancy, lactation, and menopause. To meet such demands, breasts are metabolically dynamic organs.

Each breast is between the superficial layer of superficial fascia anteriorly and rests upon the deep layer of superficial fascia, with fibrous connections between the two that contribute to the support of the breast tissue components called Cooper's suspensory ligaments. These two fascial layers come together circumferentially to create the circum-mammary ligament. Each breast extends from the clavicles bilaterally, to the inframammary fold inferiorly, to the sternum medially and laterally to the anterior border of the latissimus dorsi muscle as well as to the axilla, referred to as the axillary tail. Each nipple has a base, called the areola, and Montgomery glands that aid in lubrication during breastfeeding. The nipple-areolar complex varies between individuals and throughout the life-cycle, in terms of shape, pigmentation and size. Smooth muscle fiber bundles under the nipple-areolar complex are responsible for nipple erection in response to different stimuli such as cold and breastfeeding. Invasion of these fibers by carcinoma can cause nipple retraction, most often unilaterally, can be an early physical exam finding suggestive of breast cancer. Importantly, retraction is to be differentiated from congenital nipple inversion, which is benign [12].

Each adult breast is divided into 12-20 lobes each with an individual excretory lactiferous duct. Each lactiferous duct leads to an independent opening in the nipple, considering this, each lobe is a functionally independent gland. Approximately 1-2 years after the onset of menses,

each lobe is made up of approximately 20-40 terminal duct lobular units (TDLU), which are comprised of the terminal ducts that terminate to form 10-100 alveolar buds. These alveolar ductal structures further differentiate and branch to form ductules or mature acini, depending on the menstrual cycle phase and/or during pregnancy. Ducts and alveoli are usually comprised of a single layer of cuboidal epithelial cells (luminal layer) surrounded by a myoepithelial layer (basal layer), which rests on the basement membrane. The myoepithelial cells are functionally a hybrid of epithelial and smooth muscle cells that contract to stimulate milk ejection during lactation, and also contribute to the synthesis of the compact basement membrane made of laminin, proteoglycans and collagen IV (See Figure 1.1) [13]. The breast stroma is made of collagen-rich connective tissue with fibroblasts, immune cells, adipocytes, with nerves, blood and lymphatics vessel networks. More specifically, intralobular stroma is within a TDLU surrounding the acini and ductules and loose connective tissue with hormonally-responsive fibroblasts and various immune cells. It can be distinguished from interlobular stroma made of more dense connective tissue and adipose tissue [14].

Beginning in puberty, the mammary gland of females begins morphogenesis under the control of primarily estrogen, yet growth hormone, epidermal growth factor [15] and insulin-like growth factor have also been shown to play roles in this process, in mouse models [reviewed in[16]]. The primary changes to the female mammary glands during puberty include ductal elongation and corresponding increases in fibroadipose stroma. Breast maturation proceeds with TDLU development, branching and alveolar budding [17], which is directed primarily by progesterone. During each menstrual cycle the mammary gland undergoes proliferation and differentiation through activation of stem/progenitor cell pools [18]. More specifically, during the luteal phase of the menstrual cycle, the TDLUs proliferate to branch further, and alveolar buds are formed. If fertilization does not occur, then progesterone levels decrease back to baseline levels, leading the breast tissue to return to its inactive state, called involution through alveolar cell apoptosis. Contrastingly, during pregnancy, mammary glands undergo significant expansion and proliferation, under the control of progesterone, prolactin, estrogen, insulin, cortisol and human placental lactogen [19]. In what is referred to as an active breast (or lactating breast), the glandular tissue is comprised of highly branched TDLUs ending in secretory alveoli. After delivery, progesterone and estrogen levels fall, prolactin's actions are therefore uninhibited, allowing for milk secretion. To support these changes and metabolic demands, the breast tissue receives blood supply originating from the internal mammary artery and some supply from the lateral thoracic arteries, with a rich branching of small blood vessels to capillaries within the stroma. The venous outflow of the breast is divided into superficial veins and deep veins that

ultimately drain into the internal thoracic vein, or the posterior intercostal veins and axillary vein, respectively. Each breast is drained by both superficial and deep lymphatic vessels, with the lymph traveling from the superficial to deep lymphatic towards either the axillary, internal mammary and clavicular lymph nodes. While drainage to the axillary lymph nodes is most common, lymphatic drainage patterns have particular relevance in breast cancer staging and surgical management in the case of lymphatic invasion/metastasis [20] (discussed in the current treatment and limitations section below.)

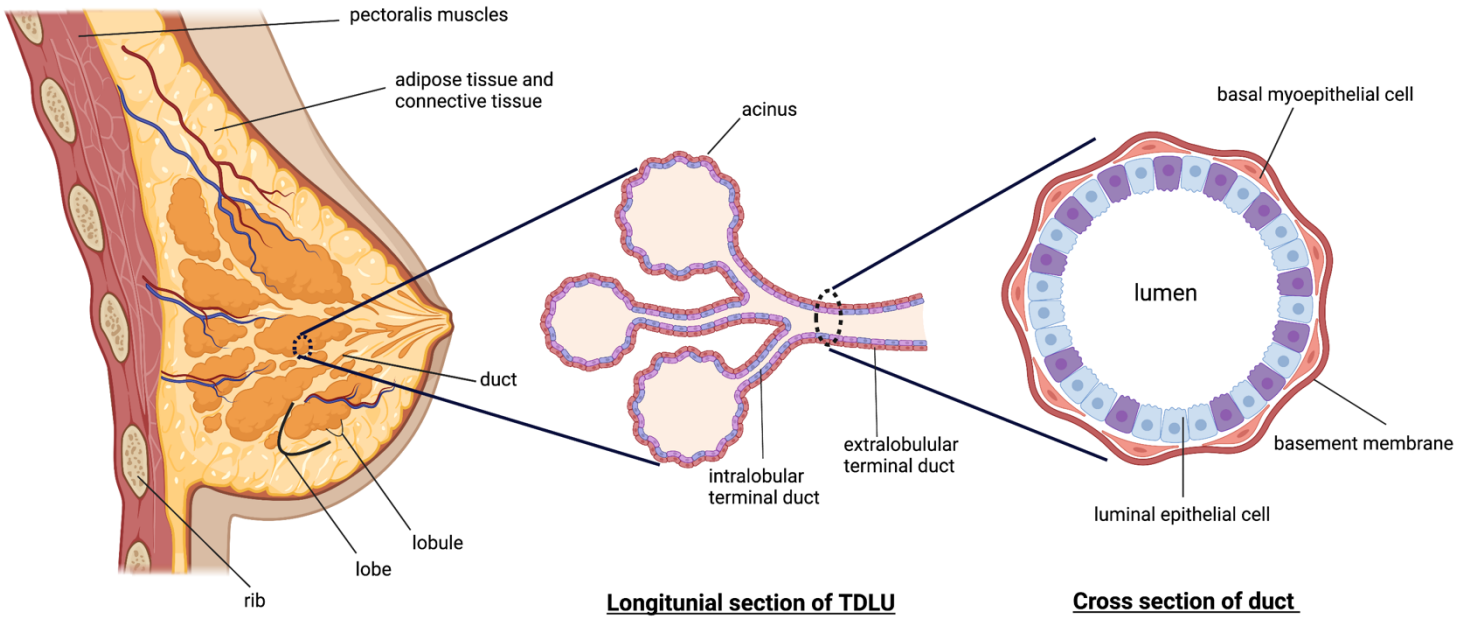

Figure 1.1: Overview of normal breast anatomy and terminal duct lobular unit morphology
Simplified representation of breast anatomy, longitudinal section of terminal duct lobular unit, and cross-section of duct. Adult human breast is divided into 12-20 lobes each with an individual excretory lactiferous duct. Each lobe has about 20-40 terminal duct lobular units. In a lactating breast, these end in milk-producing acini. Ducts and acini are composed of 1 layer of cuboidal luminal epithelial cells, which is surrounded by a myoepithelial basal cell layer which rests on a basement membrane. TDLU: terminal duct lobular unit. **Created with** BioRender.com

1.3 Breast cancer introduction and epidemiology

Breast cancer is a heterogeneous collection of diseases. Most breast cancers are carcinomas, arising primarily from the epithelial cells lining the ducts and lobules, which will be the focus of this review. However, it is worth noting, that the term breast cancer, also encompasses stromal cancers of the breast, including angiosarcoma, leiomyosarcoma, liposarcoma and others. Histologically, epithelial tumors of the breast are separated into non-invasive disease, such as ductal carcinoma in situ (DCIS) and (LCIS); and invasive breast cancers, the most common being invasive (infiltrating) ductal carcinoma (IDC) (about 70-80 % of invasive breast cancers) and second most common, invasive lobular carcinoma (5-10% of invasive breast cancers) [21, 22].

Breast cancer is the most common cancer worldwide, surpassing lung cancer in 2020 [23]. In Canada, it is estimated that 28 900 females will be diagnosed with breast cancer in 2022, which represents 25% of cancers occurring in females. After lung cancer, breast cancer is also projected to be the second leading cause of cancer deaths in females, accounting for 14% of cancer-associated mortalities [24]. Breast cancer affects females predominantly, with less than 1% of breast cancer occurring in males and an estimated 270 new breast cancers will be diagnosed in males this year [25]. Risk factors for breast cancer are family history of breast and ovarian cancer, increasing age, female sex, early menarche, increased age at first full-term pregnancy [26], nulliparity or low parity [27], later menopause, hormone replacement therapy, a higher body mass index and perimenopausal weight gain in postmenopausal women, (in premenopausal women increased body mass index is associated with lower risk of breast cancer), tall stature, and smoking. According to a nationwide cohort study in the Netherlands, transgender women using gender affirming hormone treatment had an increased incidence of breast cancer compared to cisgender men. Transgender men using gender affirming hormone replacement therapy have slightly decreased rates of breast cancer when compared to cisgender women [28].

Approximately 5-10% of breast cancers are familial and have a hereditary background. Pathogenic germline variants in tumor suppressor genes *BRCA1* (BReast CAncer gene 1) and *BRCA2 (*BReast CAncer gene 2) account for about 25-28% of familial risk and are associated with earlier onset and bilateral breast cancers [29-32]. With an autosomal inheritance pattern, pathogenic variants (a term to replace what was previously referred to as “mutation”) [33]) in *BRCA1* and *BRCA2* are highly penetrant, increasing the average cumulative risk of a female developing a breast cancer by the age of 80, from 55-72% and 45-69% respectively; as well as ovarian and fallopian cancer (39-44% and 20-30% respectively), as well as other cancers such

as prostate and pancreatic cancers. Other high-risk breast cancer genes, include genes encoding tumor protein 53 (*TP53*), phosphatase and tensin homolog (*PTEN)*, RAD51 homolog C (*RAD51C)*, RAD51 homolog D (*RAD51D)*, Cadherin-1 (*CDH1)* and serine/threonine kinase 11 (*STK11*) also called liver kinase B1 (*LKB1*). Many of these genes are implicated in multiple cancer syndromes, such as Li-fraumeni syndrome (*TP53*), Peutz-Jeghers syndrome (*STK11/LKB1*), and both Cowden syndrome and Bannayan-Riley-Ruvalcaba syndromes (*PTEN*). Moderate-risk alleles include *PALB2* (Partner and localizer of BRCA2)*, CHEK2* (Checkpoint kinase 2)*, BRIP1* (BRCA1 interacting Helicase 1) *and ATM* (Ataxia-telangiectasia mutated), yet our understanding of these pathogenic variants remains limited as they have been found in less than 1% of breast cancer cases [34]. A commonality between many of these genes is their role in DNA repair mechanisms and maintaining genomic integrity. Since pathogenic variants in known breast cancer susceptibility genes account for only a fraction of familial breast cancers, there is increasing interest in characterizing polygenic risks. Individual low-penetrance breast cancer susceptibility alleles may be low, but risks of breast cancer can be substantial as the risks of each combine in a multiplicative fashion, as such, polygenic risk scores are being refined to address this [35, 36].

1.3.1 Breast cancer classification and heterogeneity

Breast cancers are currently classified by an integration of histological analysis, molecular characterization, and clinical information with the goal of guiding treatment and improving the outcome for patients. Importantly, the classification of breast tumors continues to evolve. Histologically, the most common invasive carcinoma, is invasive (infiltrating) ductal carcinoma (IDC) (or infiltrating ductal carcinoma not otherwise specified) since it does not have specific identifying histological features of other breast carcinomas). IDC represents 70-80% of all invasive breast carcinomas (IBC). The second most common is invasive lobular carcinoma [21] representing 5-10% of all IBC [37]. The remaining invasive breast carcinomas are classified histologically as: ductal/lobular, mucinous, tubular, medullary, papillary and metaplastic, collectively these represent about 10-15% of IBC; whereas other less common subtypes make up less than 1 % of IBC [22].

In addition to histopathological appearance, the nuclear expression of two hormone receptors (HR), estrogen receptor (ER) and progesterone receptor (PR), are evaluated, stemming from evidence of their utility as prognostic factors and in determining which patients will benefit most from endocrine therapy [38]. The first written observations of the link between ovarian hormones and breast cancer progression were made in 1896 by Beatson who

eloquently reported two patients whose recurrent breast carcinomas began to shrink in size after bilateral salpingo-oophorectomy [39]. Almost 80 years later, McGuire reported that 55-60% of patients with ER-positive patients had tumor regression with endocrine therapies [40]. However, not all individuals with ER-positive tumors at that time responded to endocrine therapies (please see the *Current Treatment landscape and limitations* section below for the types of endocrine therapies).

Combined with the fact that PR is estrogen-dependent, Horwitz and McGuire thus hypothesized that PR expression may be a better indicator of tumors under estrogen control, and thus predict sensitivity to endocrine therapy [41]. Tumors from 189 patients with stage II breast cancer, stained for PR and ER, revealed that patients with tumors with lower PR levels had shorter disease-free survival than patients with higher levels [42]. Although there is evidence that PR expression status may have additional prognostic value for patients with ER-positive tumors, the prognostic implications of differential PR expression levels have not been validated. Consequently, ER expression is most often used to guide therapy decisions in the clinic [43].

HER2, a member of the epidermal growth factor receptor family was functionally shown to be an oncogene [44-46]. Next, Slamon et al. found that HER2 was overexpressed in 30% of breast cancers, and was a predictor of relapse, decreased overall survival and increased risk of metastasis [47]. HER2 is normally expressed on the cell surface (HER2/neu or ERBB2) and considerable work showed that amplification of the *HER2* gene results in HER2 overexpression, promoting tumorigenesis in women, by upregulating several processes, including cellular proliferation, survival and angiogenesis [48]. Considering its pivotal role in breast tumorigenesis, a HER2 targeting monoclonal therapy, called trastuzumab, was developed [49]. Clinically, trastuzumab (Herceptin) was shown to improve patient survival and delay disease progression in women with HER2-positive metastatic breast cancers [50, 51]. Since then, new anti-HER2 therapies have been developed, and use of trastuzumab has been expanded to first-line adjuvant and even in some cases in the neoadjuvant setting in combination with chemotherapy [52]. Considering this, IBC are therefore routinely evaluated for HER2 levels.

Interpretation of PR, ER and HER2 expression levels by pathologists, are still used in the diagnosis of breast cancer biopsies and surgical specimens, in addition to histological features and architecture. Presently, PR, ER and HER2 are determined on histological sections with immunohistochemistry (IHC) and in the case of HER2-positive being equivocal by IHC, then fluorescence in situ hybridization is used [53].

In addition to type, histological grading of IDCs have prognostic implications, which influences clinical management. The grading system most commonly used is based on Scarff-Bloom-Richardson's histological grade from 1957 [54] which was later modified by Elston and Ellis to make the criteria more objective [55]. Also referred to as the Nottingham grading system, tumors are graded out of 3 (with grade 1 being a well-differentiated tumor, grade II is moderately differentiated and grade III is poorly-differentiated), based on percentage of tubule formation, nuclear pleomorphism (variability in size, shape) and mitotic count (per microscopic field area) [56].

Breast cancer is widely accepted to comprise of diverse molecular "intrinsic" subtypes based on molecular classification. In 2000, Perou, Sørlie and Brown et al. first described five intrinsic molecular subtypes of breast tumors that were revealed through cDNA microarrays as: ER-positive/luminal-like; HER2-positive (also called Erb-B2-positive); basal-like (with gene expression profile that is similar to the basal-myoepithelial layer of normal breast, with high expression of cytokeratins 5,6, 17); as well as a normal-like group (fibroadenoma and normal breast) [57]. A follow up study divided the luminal-like breast cancers into luminal A and luminal B groups [58].

The Cancer Genome study characterized 510 breast tumors by integrating information across 6 different platforms: genomic DNA copy number, whole-exome sequencing, mRNA arrays, DNA methylation and miRNA sequencing and reverse-phase protein expression [59]. This study revealed likely genomic drivers of the major breast cancer subtypes. They also showed evidence that ER negative tumors are comprised mainly of two biologically distinct groups, namely the HER2-positive and Basal-like subtypes. Genomic and transcriptomic characterization of breast cancers continues to evolve [60].

High-throughput transcriptome analysis remains expensive, so surrogate intrinsic subtypes were developed based on immunohistochemical analysis of ER, PR and HER2 levels and also the percent Ki67 positivity being frequently used clinically [61]. Luminal A-like breast cancers represent about 60-70% of invasive breast tumors, and they have strong ER staining, are PR-positive and HER2-negative. They typically have a low ki67 proliferation index and are typically low grade. Luminal B-like HER2-negative, represent about 10-20% of IBC and have ER expression, but the expression of PR is either negative or low, with higher ki67 proliferation index, and usually higher grade. Luminal B-like HER2-positive breast cancer, are ER-positive but have lower ER expression levels than Luminal A-like group; are PR-positive or negative, are HER2 overexpressed/amplified, with a high ki67 proliferation index, and tend to be of a higher grade. HER2-positive (non-luminal) are ER-negative, PR-negative, HER2

overexpressed/amplified, with high grade and a high ki67 proliferation index. HER2-positive IBCs represent about 13-15% of all invasive breast cancers. Triple-negative breast cancer (TNBC) is used to describe breast cancers that lack IHC staining for ER, PR, HER2 (or negative FISH for HER2-positive, in the case where IHC is equivocal result), account for 15% of all invasive breast cancers [62]. The prognosis for each of these subtypes by staging is discussed in the current treatment section below.

TNBC is used as a surrogate for basal-like breast cancers. While TNBCs overlap with basal-like intrinsic subtypes, importantly, the two are not biologically synonymous. The claudin-low subtype was described in 2007 by Herschkowitz et al. [63] to have features suggestive of a "cancer stem cell-like/less differentiated phenotype," including low expression of cell-cell adhesions claudin 3, 4, 7, and E-cadherin, features of an epithelial-mesenchymal transition (EMT), and marked immune stromal cell infiltration [64, 65]. Several studies have proposed additional subtypes of TNBC, including pathogenic variant, copy number, transcriptomic, epigenetic, proteomic and phospho-proteomic patterns, including two basal-like (BL1, BL2), mesenchymal (M) and a luminal androgen receptor (LAR). However clinical utility of these groupings remains unclear [66, 67]. The discussion of treatment options for TNBC is elaborated upon below.

While IHC is the foundation of pathological diagnosis to guide clinical decision-making, molecular assays have been developed and are commercially available, such as Oncotype Dx, which is a qRT-PCR assay that measures HER2 and ER expression as well as ER-regulated transcripts to provide a recurrence score. Oncotype Dx is used in many Canadian institutions only in a subset of patients. More specifically, to predict the risk of recurrence of individuals with ER-positive, lymph-node-negative disease treated with tamoxifen, to determine which individuals would benefit from adjuvant chemotherapy and those who could be spared the harsh treatment [68, 69].

1.3.2 Breast cancer pathogenesis

The progression to breast carcinoma is classically understood based on histological and clinical stages, where inherited or acquired variants and epigenetic insults of normal TDLU cells lead to the gain of proliferative phenotypes, causing lesions like atypical hyperplasia. Further genomic and/or epigenetic aberrations and promote the proliferation of these cells, leading to progression to pre-invasive cancer, such as DCIS and LCIS (wherein the integrity of the basement membrane is still maintained), then progression to invasive breast cancer, IDC and

ILC, respectively, (which is defined histologically by cancer invasion of the basement membrane), to ensuing metastasis to lymph nodes (LN) and/or distant organs [70].

The metastatic cascade is then used to describe the stepwise hurdles cancer cells must overcome to metastasize. These include cancer cells invading through the basement membrane of their primary tumor site, migrating toward and entering the blood or lymph vessels (early stages), where they then must survive while circulating to other organ sites, successfully exiting these vessels, evading the immune system and then surviving in their new microenvironments; and ultimately re-entering the cell cycle forming often lethal metastases (later stages of the metastatic cascade) [71]. The most common sites of distant metastases are bone, liver, lung and pleura, and brain ([72, 73]. Although many patients with metastatic disease will often eventually develop metastases in more than one distant site, breast cancer subtypes seem to have propensities for certain metastatic sites. Bone metastases are the most common among all subtypes except Basal-like tumors. TNBC and Basal-like tumors metastasize more to the brain and lung than luminal subtypes. The most common site for luminal A and B tumors is bone [73-76].

On the cellular level, two models exist to conceptualize breast cancer origin and heterogeneity. The first is the clonal evolution model, wherein epigenetic and genetic pathogenic variants lead to clones of cells with varying survival advantages. In this model, dominant clonal populations outcompete others, yet failure of them to do so leads to subclonal populations, contributing to tumor heterogeneity. The second model is the hierarchical cancer stem cell model, wherein, stem-cell like progenitors that closely resemble the normal mammary stem cells (MaSc) and progenitor cells, are the cells of origin of breast cancer, and that they sustain cancer progression through self-renewal [77]. At the top of this hierarchy are MaSc that differentiate into lineage-restricted luminal and basal progenitors, with more limited differentiation capacity, but can expand to respectively maintain each lineage of terminally differentiated cell types that constitute the mammary gland: including luminal ductal cells and luminal alveolar cells as well as, myoepithelial cells [8-10]. As discussed above, distinct progenitor cells along this hierarchy are the putative cells of origin of breast cancers from distinctive molecular subtypes [78, 79] (see Figure 1.2). Evidence supports that claudin-low tumors originate from MaSc [80-82]. Specifically in *BRCA1* pathogenic variant IBC, tumors of Basal-like subtype were found to likely derive from a luminal progenitor, whereas those of luminal subtype were found to most closely resemble mature luminal progenitors [83].

An important concept in breast cancer is heterogeneity. Indeed, genomic and transcriptome profiling of tumors reveals extensive intrinsic heterogeneity in breast cancer. Yet,

there are certain genetic perturbations that occur at a higher frequency among breast cancers and within molecular subtypes. Genome/exome sequencing, targeted deep sequencing to validate SNVs and high-throughput RNA sequencing of 104 primary TNBCs revealed the most frequently genetic driver is *TP53* with 62% of basal and 43% of non-basal TNBC found to have validated *TP53* pathogenic variants [84]. The second most frequent pathogenic variants were identified in *PIK3CA* (10.2%). They also showed that clonal frequencies are more variable in the basal subtype of TNBC compared to non-basal TNBC. While somatic pathogenic variants in *TP53*, *PIK3CA* and *PTEN* in TNBCs are clonally dominant, there are some tumors, in which clonal frequencies were low, suggesting they were not founding events [84]. *TP53* pathogenic variants are found in about 75% of HER2-positive cancers [85]. Activating *PIK3CA* pathogenic variants (which encodes the p100 alpha subunit of PI3K) occur in about 40-50% of Luminal A tumors, approximately 30% of Luminal B subtype and 40% of HER2-positive breast cancers, causing hyperactivation of the PI3K pathway [85]. *PTEN* pathognic variants or loss is observed in 13-35% of breast cancers across molecular subtypes. *GATA3* (encoding GATA binding protein 3) pathogenic variants are found in about 14% of Luminal A tumors [85].

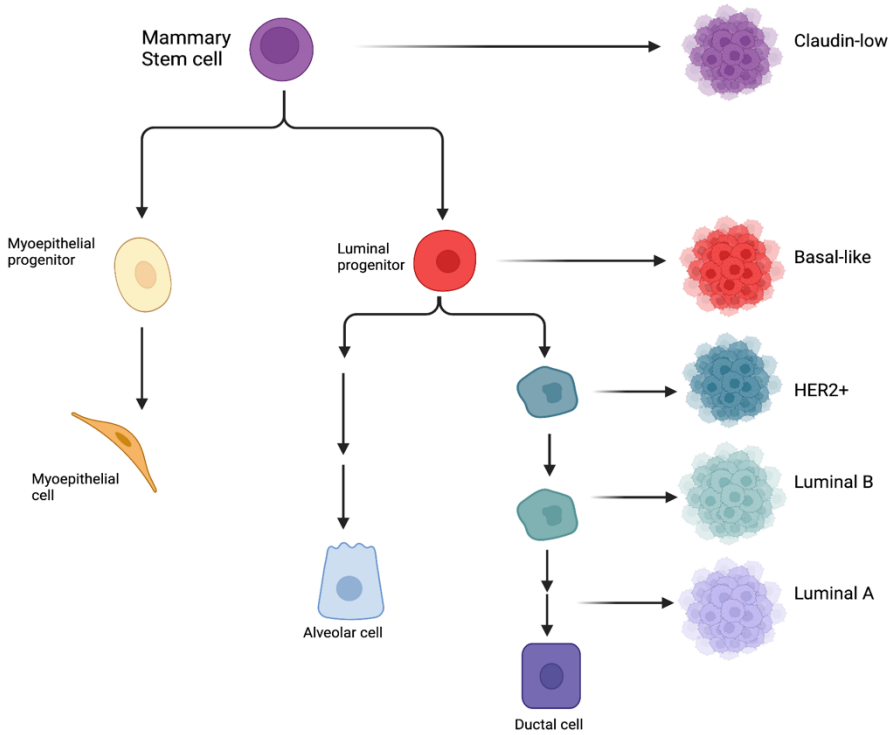

Figure 1.2: Hierarchical breast cancer stem cell model
Simplified schematic of the hierarchy of stem cells and progenitor cells of breast epithelial cell types and the closest normal epithelial counterparts of breast cancer subtypes, based on gene expression, adapted from (Visvader 2009) (Cristea and Polyak 2018). **Created with** BioRender.com

The most recent version of Hanahan and Weinberg's "Hallmarks of cancer", which is a heuristic model of understanding the capabilities of tumor cells that enable their progression from normal to neoplastic states and are fundamental to forming malignant tumors; includes 8 hallmark and 2 enabling characteristics [86]. The hallmark capabilities are: "resisting cell death", "activating invasion and metastasis", "enabling replicative immortality", "avoiding immune destruction", "evading growth suppressors", "sustaining proliferative signaling" and "deregulating cellular metabolism". The two enabling characteristics include "genome instability and mutation" and "tumor promoting inflammation" [86]. Two of these are core to this thesis, include "**deregulating cellular metabolism**" and "**tumor promoting inflammation**" which will be explored in greater detail in below sections.

In addition to tumor intrinsic mechanisms contributing to heterogeneity, breast cancers develop in complex and heterogeneous microenvironments. Paget is credited with sparking the first interest in the tumor microenvironment (TME) [87], when developing the "seed and soil" hypothesis to understand metastases in 1889 [88]. This includes cancer-associated fibroblasts (CAFs), blood vessels, various immune cells and adipose cells as well as hormones, growth factors, cytokines, chemokines, nutrients, oxygen and other non-cellular components [89, 90], [reviewed in [91]]. Tumor-TME crosstalk, including the impact of TME structure and phenotype on tumor phenotypes and treatment response is continually being elucidated [92]. Indeed, anti-tumor immune mechanisms are understood to target and control cancer cells during the early stages of breast tumorigenesis. Cytotoxic T lymphocytes (CTLs) gained attention as key anti-tumor immune cells. To progress, cancer cells must escape the immune system. Diverse immune evasion mechanisms have been reported, including tumor surface expression of immune checkpoint ligands, such as PDL1, that dampen the anti-tumor immune response by binding to their cognate receptors, (such as programmed cell death receptor-1 (PD-1)) on the surface of T cells. This forms the basis for anti-tumor immunotherapy strategies, that block PD-1 interaction with its ligand PD-L1 to reactivate CTL function, with noted success in some clinical settings, including a small subset of breast cancers [reviewed in [93]]. Quantification of tumor-infiltrating lymphocyte (TIL) density may have clinical value in subsets of breast cancer patients, particularly women with TNBC and HER2-positive disease. Indeed, TIL density is relatively increased in HER2-positive and TNBC tumors, where it is associated with improved response to neoadjuvant therapy and better outcomes [94-97]. However, it will be important to characterize these populations, as only CTL density is predominately predictive of positive prognosis [98]. Importantly, unresolved immune responses have been shown to instead contribute to chronic inflammation that promotes tumor progression and metastasis [99].

1.3.3 Current Treatment landscape and limitations

The surgical and clinical management of breast cancer have evolved significantly since the radical operations described by Halsted in 1907 [100]. Veronesi, Fisher and others then pioneered breast conserving surgery, when in a trial starting in 1976, they compared total mastectomy with segmental mastectomy, or segmental mastectomy combined with local radiation, for the treatment of women with Stage I and II breast cancers that were less than 4 cm at presentation. All women in the trial, received axillary node dissections, and those with node-positive disease also received chemotherapy [21]. They found that disease-free survival was improved after segmental mastectomy plus radiation in comparison to that of total mastectomy [101]. Presently, local therapy, including surgical resection (usually a segmental mastectomy and sometimes a modified radical mastectomy) with sentinel lymph node(s) biopsy; with/without post-operative radiation therapy, and combined with systemic treatment strategies, mostly guided by ER, PR and HER2 IHC staining; are at the core of management for most patients with early-stage breast cancer. Exceptions to this approach, including advanced stage IV disease, whereby individuals are not considered to be surgical candidates, or due to patient preferences. In certain cases, neoadjuvant chemotherapy followed by surgery, or chemotherapy alone will be selected. Segmental mastectomy (also referred to as partial mastectomy and breast conserving surgery) is usually combined with post-operative radiotherapy to the resection area (tumor bed).

Tumor, node, metastasis (TNM) staging is used to guide treatment. It can either be clinical stage, evaluated by physical exam, imaging with or without biopsy results; or pathological stage, after surgical resection incorporating tumor margins, sentinel lymph node assessment and imaging for distant metastases. The majority of management decisions rest on expression of ER, PR, and HER2, as well as stage. Neoadjuvant (before surgery) systemic therapy such as chemotherapy or HER2- targeting therapy is sometimes selected for patients with either large tumors who would benefit from tumors being first reduced in size prior to the operation, and also for some individuals for whom information on whether their tumors had pathologic complete response (complete absence of cancer cells in the breast after the completion of neoadjuvant therapy) would have prognostic implications for their disease [102].

Pre-operative imaging (including mammography and ultrasound) and the physical exam (particularly for lymph nodes, or skin involvement of tumors), play pivotal roles in evaluating the extent of primary tumors, guiding surgical decision making as well as determining possible lymph node involvement, that would warrant lymph node biopsy. Depending on the extent of suspected lymph node involvement and intra-operative findings the decision to perform a more

extensive axillary lymph node dissection rather than a sentinel lymph node biopsy may be taken. Staging of breast cancer either pre-operatively with lymph node biopsy or post-operatively with sentinel lymph node dissection is performed. Patients are evaluated for the presence of macrometastases or isolated tumor cells and micrometastases, as those even with isolated tumor cells and micrometastases (<2 mm) benefit from adjuvant therapy with improved five-year disease-free survival rates [103]. Lymph node-positive disease in some subtypes, such as TNBC, will also favour axillary radiation.

Irrespective of HER2 status, individuals with HR-positive tumors should be offered adjuvant endocrine therapies, such as tamoxifen (selective estrogen receptor modulator) in premenopausal women; letrozole, anastrozole and exemestane (aromatase inhibitor) typically postmenopausal women, goserelin (gonadotrophin-releasing hormone, GnRH agonists) as an add-on for some premenopausal women [104]. The duration of endocrine therapy is usually five years. In addition, some patients with HR-positive but HER2-negative tumors, particularly tumors that are greater than 0.5 cm and with lymph node involvement, may benefit from chemotherapy [104]. Deciding which of these patients will likely benefit from receiving chemotherapy and those who can be spared the harsh side effects differ between centres but usually includes the patient's age, menopausal status, tumor size, and lymph node involvement. Gene expression signature tools such as Oncotype Dx may also be used to aid in decision making (mentioned above) [2, 105].

For HER2-amplified tumors, depending on tumor size and nodal involvement, neoadjuvant or adjuvant HER2 blockade is offered. For example, for patients with tumors that are greater than 2 cm or with nodal involvement, typically chemotherapy (anthracycline-taxane typically) plus dual HER2-blockade (trastuzumab and pertuzumab) will be offered in the neoadjuvant setting, followed by surgery and then by either trastuzumab or dual HER2 blockade or HER2-targeted antibody–drug conjugate trastuzumab emtansine (T-DM1), depending on whether complete pathological response was obtained with neoadjuvant therapy. In patients with HER2-positive tumors that either are less than 2 cm and have no evidence of LN involvement are typically offered upfront surgery for smaller tumors with adjuvant chemotherapy (usually paclitaxel) and HER2 blockade (trastuzumab for one year).

For women with early-stage TNBC (non-metastatic), chemotherapy consisting typically of an anthracycline and a taxane is used in the neoadjuvant setting, followed by surgery and then if non-pathological complete response, typically will be offered capecitabine in the adjuvant setting [106].

Breast cancer cell-intrinsic and extrinsic factors produce inter-tumor heterogeneity (patient to patient differences), contributing to the wide variability in presentation stages, responses to therapies, and time to relapse for patients. While tumor-specific characteristics that predict response to targeted therapies such as anti-HER2 and endocrine therapies have improved outcomes for many patients, there remains variability in response. Moreover, TNBCs are extensively heterogeneous tumors, consequentially lacking targeted therapies. In addition, a single patient's breast cancer and metastatic lesions can include several distinct subpopulations of tumor cells as a result of both tumor cell intrinsic differences, as well as interactions with the TME [107, 108]. Importantly, there is a wide window of relapse for women with breast cancer, further elucidating this heterogeneity.

Outcomes for women with breast cancer are increasingly favourable, yet, women treated for IBC are at risk of recurrence and/or progression to metastatic disease [109, 110]. Subtype differences have been noted in terms of recurrence rates [3]. In a retrospective study of 1,951 patients with node-negative early-stage IBC at a median follow-up of 12 years, individuals with Luminal A-like tumors had a higher 10-year breast cancer free interval (86%) compared to those with Luminal B-like (76%), HER2 (73%), and TNBC (71%) subtypes [111]. Overall, patients with Luminal A subtype experience the longest survival, followed by Luminal B, HER2-enriched subtypes, and triple-negative subtype with the shortest average survival [112]. Locoregional recurrences in the breast (either the ipsilateral breast or chest wall; local) or ipsilateral lymph nodes (regional), typically undergo re-excision (often mastectomy if previously breast-conserving therapy), and these patients may additionally be offered radiation treatment. TNBC and ER-positive tumor recurrences are typically also treated with chemotherapy (considering the therapy the patient has previously received). Currently, there is no evidence to support the use of genomic signatures in recurrences. HER2-positive recurrences are typically treated with a combination of HER2-directed therapy and chemotherapy. If prior chemotherapy was given, patients should receive different regimens.

Length of survival for individuals with metastatic disease is significantly reduced. 6-10% of individuals with breast cancer, are found to have metastatic disease when first diagnosed with their breast cancer, referred to as stage IV disease. 20-30% of individuals who first present with early-stage breast cancers will go on to develop metastatic disease [113, 114]. Metastatic disease remains incurable, yet treatments are primarily aimed to relieve symptoms and quality-adjusted life expectancy. Poly (ADP-ribose) polymerase (PARP) inhibitors are approved for use in patients with *BRCA* germline pathogenic variants, thus all patients with metastatic breast cancer should undergo germline testing [115]. Clinical trial evidence is accumulating for use of

PARP inhibitors in patients with “BRCA-like tumors” (tumors with somatic *BRCA1/2* mutations, *BRCA1* methylation and non-*BRCA1/2* homologous repair-associated gene germline pathogenic variants) [116]. Some treatments being explored in the metastatic disease including checkpoint inhibitors, include combination approaches, and anti-body drug conjugates [117]. However, metastatic disease remains incurable.

Despite a wide array of ongoing clinical trials, disease recurrence and metastasis remain realities for many women with breast cancer. At the metastatic stage, breast cancer is incurable highlighting the need for novel treatments that target tumor-specific essential vulnerabilities which, while sparing normal cells, effectively kill malignant cells. For this thesis, work in the understanding tumor metabolism and potential targetable metabolic vulnerabilities will be explored.

1.4 Overview of metabolic pathways

Metabolism encompasses the biochemical reactions in cells that either generate or consume energy of a living organism to sustain life. Broadly, these main metabolic reactions serve to provide cells with energy, synthesize a diversity of biomolecules and maintain redox balance. Blood supplies nutrients and oxygen to breast cells, as well as the hormones that direct many of the processes. The body exists broadly in two states, insulin, and glucagon states. In response to increased blood glucose levels after a meal, the pancreatic beta cells secrete insulin. Insulin’s main actions are on the muscle cells as well as the liver to decrease gluconeogenesis (de novo glucose synthesis), stimulate glycogen synthesis and increase lipogenesis [reviewed in [118]]. In contrast, when blood glucose levels are low, glucagon is released from the pancreatic alpha cells, which primarily functions on the liver to increase glycogenolysis, stimulate gluconeogenesis, inhibit glycogenesis, glycolysis (glucose breakdown) and lipogenesis [reviewed in [119]]. Once glucose reaches the tissue, it will be taken up by cells with glucose transporters expressed on their cells. There are 14 glucose transporters that have been identified. GLUT1 is broadly expressed on various cell types, including breast epithelial cells. GLUT4 is insulin-responsive and primarily found on adipocytes and muscle cells. Once in the cell, glucose can then be used for energy generation, biomass production and redox homeostasis.

Energy is required for many cellular processes such as active ion transport, nerve propagation, muscle contraction and synthesis of macromolecules, etc. Cellular energy is obtained through the oxidation of molecules such as carbohydrates (primarily glucose), amino acids, proteins, and lipids. Free energy can then be store in high energy bonds such as

adenosine 5'-triphosphate (ATP). ATP is also used in cellular signaling and biomolecular synthesis. ATP is generated through glycolysis and the tricarboxylic acid cycle (TCA) through oxidative phosphorylation (which will be explained below) [120][reviewed in [121]].

Glycolysis is the set of 10 enzymatic reactions in the cytoplasm that breaks down glucose, to yield 2 pyruvate molecules, 2 reduced nicotinamide adenine dinucleotide (NADH) molecules (from NAD+) [122] and a net two ATP molecules. Glycolysis is therefore a NAD+ dependent pathway. In conditions with adequate oxygen, acetyl CoA (derived from either pyruvate, amino acids, or fatty acids), undergoes 8 enzymatic reactions collectively referred to as the tricarboxylic acid cycle (TCA cycle) [120]. The TCA cycle is an amphibolic pathway in that it involves catabolism (break down of molecules into smaller units for energy as well as anabolism (the synthesis of building blocks) and the formation of ATP.

The TCA cycle produces reducing equivalents, like NADH and flavin adenine dinucleotide ($FADH_2$). Oxidative phosphorylation is the process wherein the electrons from these reducing equivalents are funneled through the electron transport chain, which pumps protons into the intermembrane space of the mitochondria, generating a membrane potential, which is used by ATP synthase to generates ATP and consumes oxygen. In anaerobic conditions, glycolysis can run uncoupled from oxidative phosphorylation, and produce ATP. Anaerobic glycolysis produces the end-product lactate, which allows for the replenishment of NAD+, an essential co-factor for glycolysis to continuously run [reviewed in [123]].

Another source of acetyl CoA for the TCA cycle is fatty-acid β-oxidation. β-oxidation is the primary pathway for breakdown of fatty acids to either form ketones (liver) or to enter the TCA cycle (primarily in skeletal muscle, cardiac muscle and kidneys). During periods of fasting, lipase is secreted from adipose tissue in response to glucagon and/or epinephrine, releasing fatty acids. Fatty acids are then taken up by a target cell through transport mechanisms relying on the membrane fatty acid-binding protein. The first step of β-oxidation involves Fatty acyl CoA Synthetases, which activate the fatty acids. Short chain fatty acids (1-12 carbons) can typically diffuse freely into the mitochondrial matrix. Whereas long fatty acids (14-20 carbons), are first activated in the cytoplasm, by Fatty Acyl CoA synthetase and then rely on the carnitine transport system to enter the mitochondria. Very long chain fatty acids >20 carbons are oxidized in peroxisomes. The Carnitine transport system, consists of Carnitine palmitoyltransferase I (CAT1), which adds a carnitine to fatty acyl for entry into the mitochondrial matrix, and then once in the matrix, Carnitine acetyl-CoA transferase (CAT2) converts the acylcarnitine to Fatty acyl-CoA [124]. Fatty acyl-CoA then undergoes the four steps of mitochondrial β-oxidation, namely dehydrogenation, hydration, oxidation and thiolysis to eventually produce acetyl-CoA,

which can either be used in the TCA cycle or to make ketone bodies. The TCA cycle is an amphibolic pathway since it involves catabolism (break down of molecules into smaller units for energy as well as anabolism (the synthesis of building blocks).

Both glycolysis and the TCA cycle produce metabolites that can be used in additional biosynthetic pathways, for example glucose 6-phosphate can enter the pentose phosphate pathway, generating NADPH, and precursors for nucleotide and amino acid synthesis [125]. NADPH is an important co-factor in redox homeostasis and synthesis of biomolecules such as cholesterol, fatty acids, as well as amino acids. NADPH can also be generated through the glutamate dehydrogenase pathway, where glutamate is converted to alpha-ketoglutarate [126]. Finally, NADPH can also be generated through pathways involving TCA cycle intermediates isocitrate and malate, with the enzymatic activity of isocitrate dehydrogenases (IDH1 and IDH2) and malic enzymes (ME1, ME2, and ME3) [127, 128]. NADH is a key cofactor for redox homeostasis, generated from NAD+ in glycolysis, the TCA cycle and fatty acid oxidation (FAO). NAD+ can be synthesized *de novo* through several pathways, including from salvage pathways from nicotinamide (NAM) and Preiss-Handler pathway from nicotinic acid (NA). Alternatively, NAD+ be generated from NADH, through the electron transport chain and by lactate dehydrogenase through the generation of lactate from pyruvate. NAD+ is a co-factor for many enzymes including PARPs, RNA polymerases and sirtuins [129, 130]. Redox homeostasis refers to the balance of reducing and oxidizing reactions and products within the cell and will be addressed further below.

1.4.1 Electron transport chain

The electron transport chain (ETC) is made of four inner mitochondrial complexes; Complex I (NADH: ubiquinone oxidoreductase), Complex II (or succinate dehydrogenase), Complex III (Cytochrome bc1 oxidoreductase) and Complex IV (cytochrome c oxidase) as well as two mobile electron carriers ubiquinone, and cytochrome c (reviewed in [131]). Succinate dehydrogenase is also an enzyme within the TCA cycle. Electrons stripped from reducing equivalents, NADH and $FADH_2$ are funneled through the electron transport chain, resulting in protons being pumped into the intermembrane space of the mitochondria. This generates a membrane potential, which is used by ATP synthase to generates ATP, a process that consumes oxygen.

Complex I (NADH:ubiquinone oxidoreductase) is the largest complex and consists of 45 subunits, seven are encoded by mitochondrial DNA and 38 from nuclear DNA. 14 core subunits have been described that are responsible for the main energy transduction functions of complex

I; 7 hydrophobic (within the mitochondrial inner membrane) and 7 hydrophilic subunits (extending into the mitochondrial matrix). Proper assembly of each of these subunits in a stepwise fashion relies on protein chaperones [132]. Complex I oxidizes NADH produced primarily from the TCA cycle and Fatty acid β-oxidation, resulting in two electrons stripped and 4 protons eventually being translocated to the inner mitochondrial membrane, contributing to a proton gradient. In doing so, complex I contributes to the NAD+ pool in the mitochondria. NADH is oxidized by the flavin mononucleotide within the hydrophilic arm of complex I and then two electrons then travel along 7 FeS clusters, to the final FeS cluster (called N2), that is adjacent to the ubiquinone binding site, where it reduces ubiquinone (Coenzyme Q, CoQ) to ubiquinol (thought to occur one electron at a time producing a semiquinone) [133]. The mechanism by which protons are pumped into the inter membrane space by complex I was poorly understood for some time. Recent work by Kampjut and Sazanov elucidated that proton transfer occurs on the membrane arm, and depends on a conformational change at the junction of the hydrophobic and hydrophilic arms, that leads to a water wire that translocate protons across the membrane arm, upon quinone binding to the binding pocket [134].

The electrons are next transferred from ubiquinol ($CoQH_2$) to complex II. Complex II is another entry point for electrons, into the ETC. Electron transport through complex II is not accompanied by the translocation of protons. Electrons from complex II-mediated oxidation of $FADH_2$ are then shuttled to CoQ reducing it to $CoQH_2$. Complex III then catalyzes the transfer of electrons from reduced CoQH2 to cytochrome c for transport to complex IV, with four protons pumped into the intermembrane space. Two protons are pumped into the membrane space at complex IV, and the electrons reduce O_2 to water. Finally, ATP synthase, utilizes this electrochemical gradient, translocating protons back to the matrix, to capture energy via ATP. Importantly, the transfer of electrons is not 100% efficient, resulting in electron leakage. (See Figure 1.3).

1.4.2 Redox balance overview

Oxidation and reduction (redox) reactions encompass all reactions where electrons are transferred to an electron acceptor from an electron donor. In physiological states, these reactions are held in balance within cells, such that the production of reactive oxygen species (ROS) and reactive nitrogen species (RNS) are counteracted appropriately with cellular antioxidant mechanisms. Redox balance is dynamic and fundamental to maintain cellular homeostasis [135]. The following two sections explore key concepts of ROS and scavengers [136].

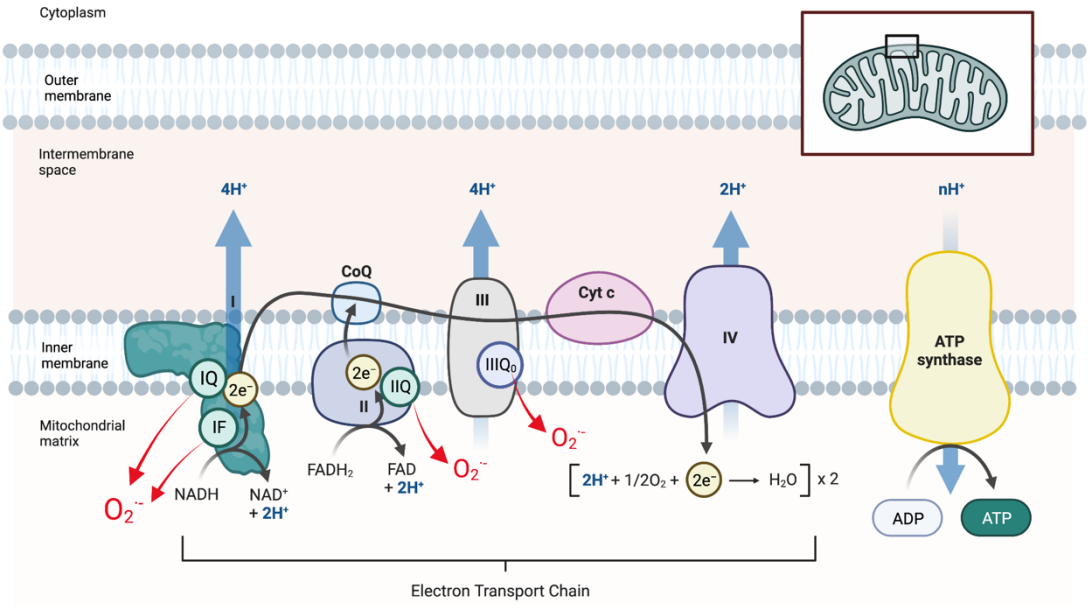

Figure 1.3: Electron transport chain
Electrons stripped from NADH and $FADH_2$ are funneled through the electron transport chain, resulting in protons being pumped into the intermembrane space of the mitochondria. Complex I oxidizes NADH resulting in two electrons stripped and four protons translocated to the inner mitochondrial space, contributing to a proton gradient. The electrons are next transferred to CoQ, producing $CoQH_2$. Complex II is another entry point for electrons. Complex II oxidation of $FADH_2$ results in electrons that are then shuttled to CoQ. Complex III catalyzes the transfer of electrons from reduced $CoQH_2$ to cytochrome c for transport to complex IV. Electrons from complex IV combine with O_2 to produce H_2O. ATP synthase then uses the proton gradient to generate ATP. Mitochondrial ETC is a major source of cellular ROS, caused from leakage of electrons that interact with oxygen to form superoxide. The main complexes where superoxide leaks from are complexes I, II and III. IQ/IIQ/Q_o: the ubiquinone-binding sites in complex I/complex II/complex III; IF: the flavin site; ETC: Electron transport chain; CoQ: ubiquinone; $CoQH_2$ ubiquinol. Adapted from (Mazat et al., 2020) (Nolfi-Donegan et al., 2020). **Created with** BioRender.com

1.4.2.1 Reactive oxygen species overview

Reactive oxygen species is a collective term used to describe any molecule or chemical species that is reactive and derived from molecular oxygen. ROS includes radical species like superoxide ($O_2^{\bullet-}$), and hydroxyl radical (•OH), as well as non-radicals, like hydrogen peroxide (H_2O_2), organic hydroxyperoxides (ROOH), ozone (O_3), hypochlorous acid (HOCl) [137] [137] and hypobromous acid (HOBr) [135]. Superoxide, discovered by Pauling and Neuman in 1934 [138, 139], is a precursor to more stable reactive oxygen species, such as H_2O_2, by superoxide dismutase enzymes (SODs) [140, 141]. H_2O_2 is relatively more stable than radical species, owing to its O-O bond, however less stable than O_2. As such, H_2O_2 has more time to react with molecules in the cells. H_2O_2 reacts with free iron (Fe^{2+}) to generate highly reactive and damaging hydroxyl radicals, producing (Fe^{3+}), known as the Fenton reaction and is thought to be a main mechanism of ROS production [142]. Superoxide can also react with H_2O_2 to

generate hydroxyl radical, hydroxide and molecular oxygen, known as the Haber Weiss Reaction [143]. The formation and transformation of ROS is summarized in Figure 1.4. ROS radicals are particularly unstable and highly reactive, given that they have one or more unpaired electrons. This reactivity results in the removal of electrons from other molecules, generating new radicals, and amplifying ROS.

ROS are constantly generated within cells. Mitochondrial ETCs are a major source of ROS in many cells, caused from leakage of electrons that interact with oxygen to form superoxide and eventually H_2O_2. The main complexes where superoxide leaks from are complex I and III. Under disease states, leakage from complex II has also been identified [144, 145]. In particular, several lines of evidence point to complex I being the major source of superoxide production [146]. In particular specific sites within complex I have been proposed as being responsible for electron leakage and ROS generation, the ubiquinone-binding sites in complex I (site IQ) and the flavin site (site IF); depending on the presence of a proton-motive force [147-150] (See Figure 1.3). Furthermore, ROS can be generated by reverse electron transport (RET), where complex I can reduce NAD+ to NADH from electrons received from reduced CoQ, which can occur when CoQ becomes overly-reduced [151]. There is evidence that superoxide production at Complex I is influenced by NAD+ and NADH levels in the cells, whereby increased NAD+ (for a constant NADH) suppresses ROS production [152]. Other major endogenous sources are the NADPH oxidases (Nox), xanthine oxidoreductase, endoplasmic reticulum and peroxisomes. NOX family members are found in many cell types, including neutrophils and macrophages, and along with myeloperoxidase (MPO) contribute to the respiratory burst, which targets both pathogens, infected host cells and tumor cells, alike [153-155]. There are also exogenous sources of ROS, caused by cell exposure to certain chemical compounds, to hypoxia/hyperoxia, or to ionizing radiation. Importantly, different compartments and organelles of the cell can be maintained at different redox states [156].

The main mechanism of physiologic redox signaling is through the reversible modification of thiol groups, on cysteine, within target proteins and peptides. More specifically, H_2O_2 can react with a target protein cysteine thiolate (-S) to form the sulfenic acid (-SO) [157], which can lead to a reversible change in protein structure and/or function, or to other reactions such as intramolecular or intermolecular disulfide (-S-S-) formation. Higher levels of cellular ROS leads to further oxidation of sulfenic acid to sulfinic ($-SO_2H$) or sulfonic ($-SO_3H$) acid, which are considered essentially irreversible protein modifications, and as such are markers of oxidative stress. Nitric oxide (NO) can cause S-nitrosylation of cysteine residues. $O_2^{\bullet-}$ reacts with Fe–S clusters in proteins to alter their function. A classic example of this is aconitase.

Nitration of tyrosine residues by peroxynitrite ($ONOO^-$) formed by $O_2^{\bullet-}$ and nitric oxide (NO) is another ROS/RNS mediated alteration, a classic example of this is nitration of tyrosine-34 of superoxide dismutase 2 (SOD2) causing its inactivation [158].

ROS have been shown to play direct roles in signaling transduction pathways by influencing tyrosine and serine/threonine kinases alike, including activation of Epidermal growth factor receptor [15], inhibition of AKT2, and both activation and inactivation of SRC, depending on the model [159-161]. Additionally, serine/ threonine phosphatases such as protein tyrosine phosphatase 1B (PTP1B) and PTEN, have been shown to be inhibited by cysteine oxidation. More specifically, H_2O_2 was shown to oxidize and inactivate PTEN through disulfide bond formation between the catalytic domain cysteine-124 and cysteine-71 residues [162].

"Oxidative eustress" is a term to describe the oxidative challenge that benefits cells. Whereas, a supraphysiological oxidative challenge resulting from imbalances from excessive ROS generation and limited antioxidant defenses, is referred to as "oxidative stress" [163]. Excessive ROS can damage cellular macromolecules leading to uncontrolled protein oxidation, such as protein carbonylation, that forms reactive aldehyde or ketone residues on proteins [164, 165], peroxidation and oxidation of lipids [166], as well as oxidative damage to nucleic acids, such as 8-oxoguanine (8-oxo-dG) [167]. Accumulation of this damage, and indeed ROS overproduction has been implicated in many pathologies. Accumulated oxidative damage can ultimately lead to cell death [168, 169]. This will be further discussed in section below on ROS in cancer.

1.4.2.2 ROS Scavengers overview

Elimination of ROS can occur through multiple mechanisms in the cell, including by enzymatic and non-enzymatic ROS scavengers (antioxidants). Enzymatic ROS scavengers include superoxide dismutase (SOD), catalase (CAT), glutathione peroxidase (GPX), glutathione reductase (GR), thioredoxin reductase (TXNRD), and peroxidoredoxins. Non-enzymatic scavengers include glutathione (GSH), thioredoxin (TXN), coenzyme Q, Vitamin C and E and others. Glutathione will be discussed in more detail in the next section.

ROS scavengers are reducing agents that donate electrons. Superoxide dismutases (SODs) catalyse the reaction of 2 $O_2^{\bullet-}$ with each other to form H_2O_2. There are 3 forms of superoxide dismutase (SOD) enzymes SOD1 is a copper/zinc isoform that is found in the cytosol; SOD2 is a manganese isoform is found in mitochondria; and SOD3 a copper/zinc form found in the extracellular space [15]. Catalase is an oxidoreductase that is mainly located in peroxisomes and converts H_2O_2 into H_2O and O_2 [170]. Additional antioxidants, such as

glutathione peroxidases and peroxiredoxins convert H_2O_2 into H_2O. Glutathione peroxidases (of which there are 8 currently known, GPX 1-8) require GSH and cofactors, many are selenoproteins meaning they contain a selenocysteine amino acid residue in their catalytic centre [171]. Peroxiredoxins not only serve as an antioxidant system, but recent findings suggest that they may also regulate peroxide-mediated signal transduction [172]. Thioredoxin 1 (TXN1) is primarily found in the cytosol and nucleus, whereas thioredoxin 2 (TXN2) is primarily found in mitochondria and can reduce oxidized cysteine residues and perform denitrosylation of proteins [173] [174]. TXNs are recycled to their reduced state by thioredoxin reductase, which is dependent on NADPH as a co-factor [175].

The master regulator of ROS scavenging is the nuclear factor E2-related factor 2 (NRF2) transcription factor that responds to oxidative stress by binding to antioxidant response elements (ARE) in genes that encode several antioxidant enzymes. The mechanism of NRF2 response is elegant and elucidates quite nicely the concept of redox-controlled molecular switches. In low ROS states, Kelch-like erythroid cell-derived protein with CNC homology [ECH]-associated protein 1 (KEAP1) promotes NRF2 targeted ubiquitylation and degradation [176]. Yet, under higher ROS states, KEAP1 cysteine residues, including cysteine-151, cysteine-273 and cysteine-288 are oxidized, leading to a conformational change in KEAP1, the stabilization of NRF2 and its translocation within the nucleus, where it binds to ARE elements to promote transcription of several ROS scavengers [177]. The exact mechanisms of NRF2 stabilization remains to be clarified [178]. NRF2- target genes include glutathione reductase-1, NAD(P)H:quinone oxidoreductase1 (NQO1) and two subunits that constitute glutamate-cysteine ligase (GCL) (previously known as γ-glutamylcysteine synthetase), which is the first enzyme in the biosynthesis of glutathione, and others [179, 180]. (See Figure 1.4)

1.4.2.3 Glutathione overview

Glutathione is recognized as a master cellular antioxidant. It was first described by de Rey-Pailhade in 1888, as a substance in yeast that reacts with sulfur to make hydrogen sulfide, that he called “philothion” (meaning “love” and “sulfur” in Greek) [181]. Several sequential studies helped elucidate the structure and function of what is now referred to as glutathione [reviewed in [181]]. Glutathione is a tripeptide of cysteine, glutamate, and glycine. Glutathione exists in 2 states, either the reduced form (GSH) or the oxidized form (GSSG). GSH can function directly as an antioxidant, as a cysteine-containing peptide, glutathione can be easily oxidized. When GSH donates an electron to ROS, GSH becomes reactive to thiols, and given that GSH is the most abundant thiol in the cell, a disulphide bridge forms between two

glutathione molecules, resulting in the formation of GSSG [182]. GSH can also be used as a substrate by GPx. The redox status of cells can be expressed as the ratio of GSH/GSSG. In addition to the cytoplasm, GSH is also found in in the endoplasmic reticulum, nucleus, peroxisomes and mitochondria [183, 184]. Interestingly, SLC25A39 was recently identified as a mitochondria carrier important for glutathione uptake [185]

Glutathione can either be synthesized *de novo,* which occurs in the cytosol, or through salvage pathways. The first step in *de novo* synthesis is the rate limiting step by glutamate-cysteine ligase (GCL) (previously called γ-glutamylcysteine synthase) is a heterodimer, made of a catalytic subunit a modulatory subunit (GCLM) and a catalytic subunit (GCLC). GCL forms a bond between glutamate and cysteine, resulting in γ-glutamylcysteine, in an ATP-dependent manner. The second step also requires ATP wherein glycine is added to γ-glutamylcysteine by glutathione synthetase (GS), (a homodimer), forming GSH [186, 187]. GSH can also be

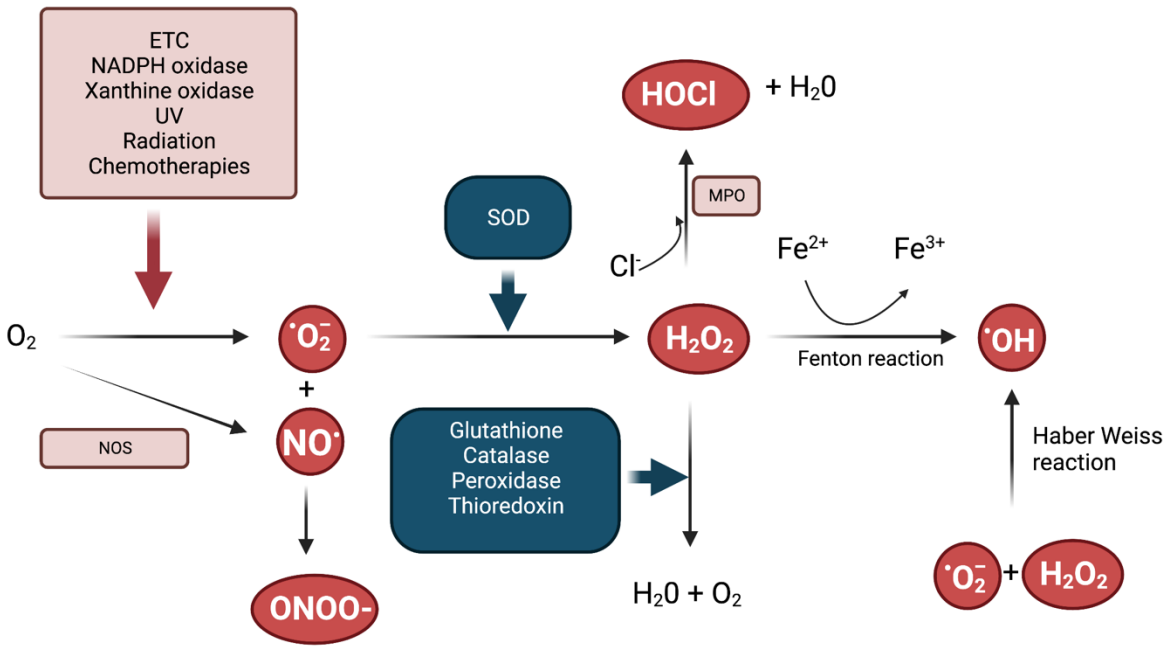

Figure 1.4: Formation and transformation of important ROS and RNS species.
There are several sources of $O_2^{\cdot-}$ including the ETC, NADPH oxidases, and extrinsic sources like radiation and UV. Superoxide can then be dismutated by the SOD family of enzymes, to H_2O_2. Alternatively, ;$O_2^{\cdot-}$; and NO can combine to form $ONOO^-$. H_2O_2 can be converted into H_2O_2 into H_2O and O_2 by several scavengers such as glutathione and catalase. H_2O_2 can alternatively be converted to HOCl by MPO; or be converted to the ·OH through the Fenton reaction. $O_2^{\cdot-}$; ·OH: hydroxyl radical, H_2O_2: hydrogen peroxide; HOCl: hypochlorous acid; $ONOO^-$: peroxinitrite; NO: nitric oxide; ETC: Electron transport chain; SOD: superoxide dismutase; UV: ultraviolet; MPO: Myeloperoxidase. Figure adapted from (Emanuele, D'Anneo et al. 2018). **Created with** BioRender.com

regenerated from the oxidized GSSG by glutathione reductase (GR) which required NADPH as a cofactor [188].

1.4.3 Normal breast metabolism

Metabolic pathways adapt to the changing needs of cells, and the state of the organism. As mentioned above, breasts are dynamic organs, with metabolic demands that correspondingly vary throughout the lifecycle, during puberty, the menstrual cycle, the tissue undergoes various changes, milk production and also involution [189]. Characterization of normal breast metabolism is quintessential to the search for targetable breast cancer-specific vulnerabilities. Recent transcriptome analysis comparing mammary glands from lactating mice to those in late-pregnancy, reveals interesting differences, including increases GLUT-1 and SLC5a1, as well as expected increases in lactose and fatty acid synthesis after parturition [190].

Given the cellular complexity of the breast, metabolically characterizing different cell types within the normal breast tissue is necessary. Recent work highlighted that luminal progenitor ($CD49f^{+}CD90(THY1)^{-}EpCAM^{+}MUC1^{+}$) cells contain more mitochondria and can tolerate higher levels of ROS than basal cells ($CD49f^{+}CD90(THY1)^{+}EpCAM^{-/low}MUC1^{-}$). Whereas basal cells are more reliant on glutathione than luminal progenitors [191]. More recently, using single-cell transcriptomic and proteomic analyses of normal mammary epithelial cells from human reduction mammoplasties, Mahendralingam et al., describe that basal cells, luminal progenitors and mature luminal lineages have distinct metabolic programs [192]. More specifically, while cellular ROS levels are similar between the 3 lineages, basal cells and mature luminal cells have higher baseline mitochondrial ROS. They also find enrichment of metabolic pathways related to OXPHOS in luminal cells, and that of glycolysis in basal cells, which they corroborated with functional inhibitor studies [192].

While opportunities remain to further characterize normal breast tissue metabolism, these studies shed light into the metabolic complexity of the breast. Distinct lineage-specific metabolic phenotypes in normal breast lineages may have important implications for distinct breast cancer subtypes, depending on their cell of origin.

1.5 Tumor metabolism overview

"**Dysregulating cellular metabolism**", is now recognized as one of the hallmarks of cancer, which describes the orchestration of certain metabolic pathways in cancer cells compared to normal cells, wherein these altered pathways contribute to cancer progression

[86]. To meet the biosynthetic, bioenergetic and redox balance demands of tumorigenesis and metastasis, cancer cells rely on the integration of metabolic pathways [reviewed in [193]].

The classical understanding of altered tumor metabolism is the Warburg effect, which describes the propensity of cancer cells to increase glucose uptake and perform aerobic glycolysis [194]. This observation was incorrectly postulated to be due to defective mitochondria and was solely attributed to a cancer's energy requirements. Increase in glycolysis in many tumors types is not simply for energy production, but also allows for the generation of necessary biomass and reducing equivalents from glycolytic intermediates [reviewed in [195]]. Activation of the pentose phosphate pathway (PPP) in glycolytic tumors to scavenge excessive ROS and for biosynthesis [196] [reviewed in [197]]. The fact that many tumors upregulate glycolysis forms the basis of ^{18}F-fluorodeoxyglucose positron-emission tomography (^{18}FDG-PET) imaging, used for cancer detection and monitoring [198, 199].

It is also now widely accepted that in addition to glycolysis, many tumor cells also heavily rely on their mitochondria for energy generation, biosynthesis and reducing equivalents, and have different metabolic dependencies [reviewed in [200, 201]]. Many intermediates in the TCA cycle are anabolic precursors, used by various cancers, such as citrate for lipid synthesis, malate for gluconeogenesis, pyruvate for NADH production; and oxaloacetate for aspartate which can be used for nucleotide and amino acid synthesis [reviewed in[202, 203]].

Many tumors increase metabolism, in the case of glutamine replete conditions. Glutamine is the most abundant amino acid in circulation [reviewed [204]]. Glutamine serves many functions in the cell, including supplying metabolites to support energy generation, as well as, acting as a source of non-essential amino acids, purines, pyrimidines and even lipids for cellular division [205, 206]. Glutamine is synthesized from glutamine synthetase in a two-step reaction. Glutamine can also be converted to glutamate by glutaminase (GLS or GLS2) and used as an essential building block for glutathione; or it can be converted into α-ketoglutarate by either glutamate dehydrogenase (GLUD) or aminotransferases. α-ketoglutarate can then enter the TCA and undergo oxidation for ATP and NADH generation. Alternatively, α-ketoglutarate can be converted into isocitrate by isocitrate dehydrogenases, IDH1 (in the cytosol) or IDH2 (in mitochondria), through a process called reverse carboxylation (or reductive glutamine metabolism). This eventually produces citrate, which is primarily used for fatty acid synthesis [207]. An increased α-ketoglutarate to citrate ratio favours reductive glutamine metabolism [208]. Many oncogenes and loss of tumor suppressors promote glutamine metabolism and even glutamine dependence in many tumor types. Interestingly, cancer cells with defective ETCs have been shown to be dependent on reductive glutamine metabolism [209]. Additionally,

reductive carboxylation supports NADPH generation and resistance to elevated mitochondrial ROS levels generated during anchorage-independent growth [128]. (See Figure 1.5).

Two characteristics of many tumors that are important to consider are *metabolic heterogeneity* and *metabolic flexibility*. Metabolic heterogeneity is continually appreciated in cancers. This heterogeneity is seen in metabolic profiles and dependencies between tumors; between primary tumors and their metastases; as well as between cancer cells of distinct areas of a single tumor [200, 210-212]. Metabolic flexibility (or metabolic plasticity) is the propensity of some cancer cells to dynamically adapt to changing metabolic conditions, including low nutrient and oxygen conditions, and periods of increased redox stress throughout cancer progression, metastasis and even with treatment. This includes the redirection of metabolic intermediates into pathways for antioxidant generation, which will be discussed more in detail in the section

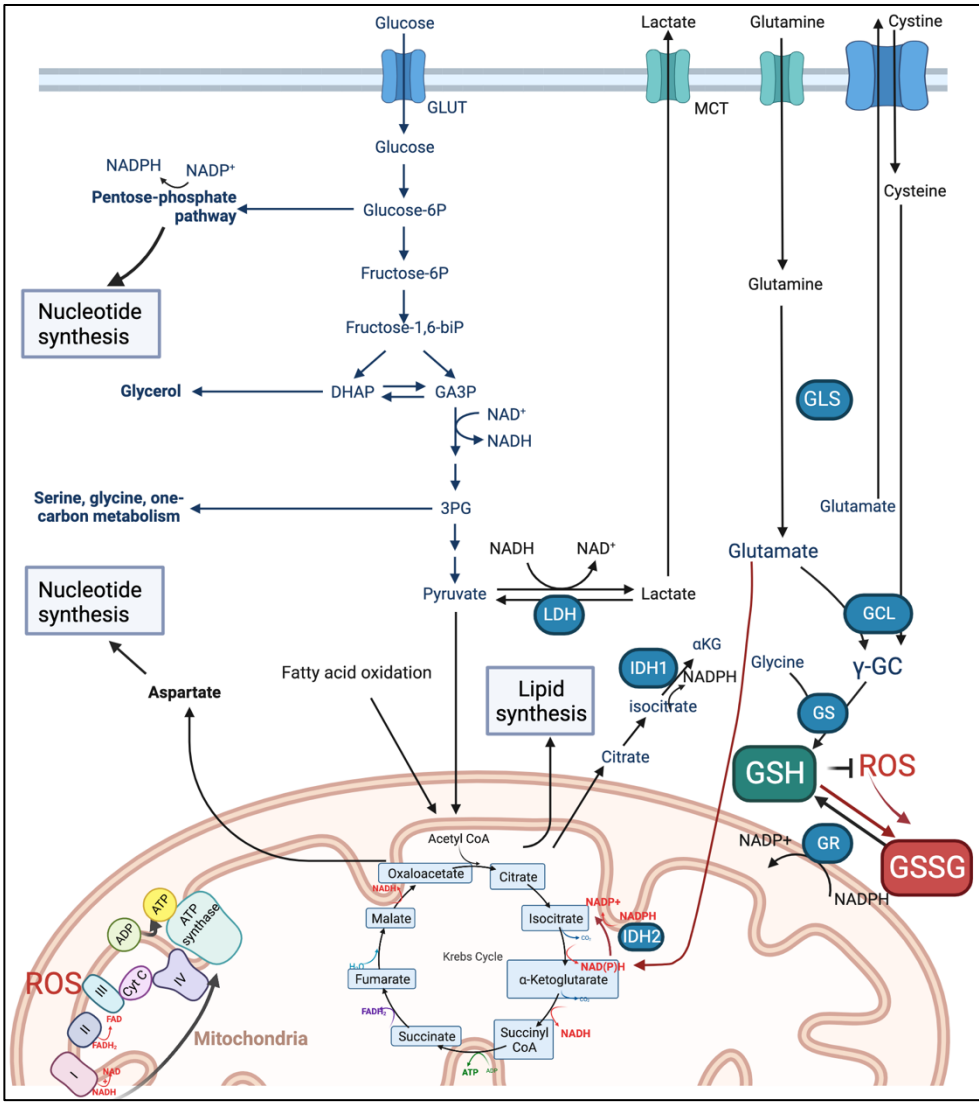

Figure 1.5 Overview of major metabolic pathways in breast cancer
Schematic of metabolic pathways in breast cancers. Glutamine, glucose and fatty acid oxidation are used for ATP generation, biosynthesis and redox control. Glucose is converted to pyruvate, which in turn is either converted to acetyl-coA that can enter the TCA cycle; or to lactate. Glycolysis intermediates can be used in other pathways. 1) glucose-6-phosphate can enter the pentose phosphate pathway to generate NADPH and nucleotide precursors 2) DHAP can be used for lipid metabolism 3) 3PG can be used in serine, glycine and one-carbon metabolism. Glutamine can be converted to α-ketoglutarate and undergo either forward oxidation to succinyl-coA, or be converted to isocitrate (reductive carboxylation) to produce citrate, used in lipid synthesis. Glutamine is also important for glutathione production. Cystine is imported into the cell, and is reduced to cysteine. Glutamate, cysteine and glycine can be used to make glutathione by a two step enzymatic process 1) rate limiting step by GCL, glutamate and cysteine form γ-GC 2) glycine is then added to γ-GC by GS forming GSH. GSH can also be regenerated from GSSG by GR, requiring NADPH. TCA cycle reactions generate cofactors NADH and $FADH_2$. GSH: reduced glutathione; GSSG:oxidized glutathione; GCL: glutamate-cysteine ligase; GS: glutathione synthase; GR: glutathione reductase, 3PG: 3-phosphoglycerate DHAP: dihydroxyacetone phosphate; γ-GC: γ-glutamylcysteine. Adapted from (Deberardinis and Chandel, 2016), (Wang et al. 2020) and (Dias et al., 2019). **Created with** BioRender.com

below. Metabolic flexibility is associated with therapeutic resistance and the propensity of cancer cells to metastasize in many cancer types, including breast cancer [213, 214] [215].

Tumors have different degrees of plasticity and uncovering the specific molecular drivers of this flexibility can guide therapeutic strategies. Many tumor suppressors and oncogenes influence tumor metabolism, including MYC family of transcription factors [reviewed in [216] and [197]]. Oncogenic MYC coordinates many aspects of cancer metabolic reprogramming including promoting glycolysis, glutamine metabolism, fatty acid synthesis and nucleotide synthesis [reviewed in [217]]. Furthermore, central signaling pathways in tumor metabolism include PI3K/AKT/mTORC1 and LKB1-AMP kinase pathways, both with relevance to breast cancer. The phosphoinositide 3-kinase (PI3K) /AKT signaling network plays an essential role in promoting growth and survival and is activated downstream of receptor tyrosine kinases (RTKs) (including insulin receptor) and cytokine receptors [218, 219]. Briefly, activated class I PI3K (heterodimer of regulatory p85, and catalytic p110 subunits) converts its phospholipid substrate, phosphatidylinositol 4,5-bisphosphate (PIP_2) into its secondary messenger, phosphatidylinositol 3,4,5-triphosphhate (PIP_3). PIP_3 can then accumulate at the plasma membrane, creating docking sites for downstream effectors, such as the serine/threonine kinase AKT, which can then be activated by phosphorylation at its Threonine-308 site. Full activation with a second phosphorylation site Serine-473 via either itself or other kinases such as mTORC2. Mammalian/mechanistic target of rapamycin is a serine threonine kinase, which is the catalytic subunit of two multi-protein complexes called mTORC1 and mTORC2 [220]. AKT can activate several downstream substrates, including mTORC1, which upon activation can then perform its effector roles in energy, nutrient and redox sensing, and as a central regulator of mRNA translation [reviewed in [221]].

5'-AMP-activated protein kinase (AMPK) is a heterotrimeric enzyme made of α catalytic subunit, as well as β and γ regulatory subunits [222]. AMPK is a key cellular energy sensor that plays a fundamental role as a regulator of energy homeostasis. Activated by depletion of energy and nutrient levels as well as hypoxia, AMPK coordinates metabolic pathways in order to balance catabolism [reviewed in[223]]. ADP and AMP bind to γ subunit, leading to Thr172 phosphorylation in the activation loop of the α subunit, by upstream kinases, such as liver kinase-B1 (LKB1). A conformational change upon binding of ADP or AMP to the γ subunit of AMPK also protects the Thr172 site from phosphatases [224]. AMPK activation promotes catabolic pathways to generate ATP and inhibits anabolic ATP-consuming processes including mRNA translation by inhibiting mTORC1. AMPK increases insulin receptor signaling, enhances

translocation of glucose receptors to cell surface, inhibits fatty acid synthesis and increases β oxidation [reviewed in [225]].

Other metabolic sensors such as hypoxia-inducible factor (HIF) and peroxisome proliferator-activated receptor gamma coactivator 1 alpha (PGC-1α) deserve mention given their central roles in metabolism, though an in-depth review is beyond the scope of this literature review. HIF is an important transcription factor, made of an α subunit that is sensitive to oxygen levels, and a β subunit that is constitutively expressed. Under normoxic conditions, the HIF1-α subunit is degraded, yet under low oxygen conditions, HIF1-α is stabilized and then can dimerize with the β subunit to form the active transcription factor, which can then bind to Hypoxia response elements (HRE) near the promoter of target genes. The HIF transcriptional program promotes growth and angiogenesis under low oxygen conditions by upregulating glycolysis and limiting OXPHOS. For example, it activates pyruvate dehydrogenase kinase 1 (PDK1) which inactivates pyruvate dehydrogenase (PDH), inhibiting pyruvate conversion to acetyl-coA [226] [reviewed in [227]]. Additionally, HIF1-α promotes mitophagy [228].

PGC-1α is a member of the PGC1 family, that interacts with transcription factors, as well as nuclear receptors to promote adaptive thermogenesis, gluconeogenesis, as well as mitochondrial biogenesis and oxidative metabolism [reviewed in [229]]. Given its central role in promoting mitochondrial respiration and that mitochondria are major sites of ROS production, PGC-1α has been shown to have an accompanying role in increasing ROS scavengers including SOD2 and GPX1 [230]. Breast cancer metabolism will be addressed in more detail in the section below.

Improving our understanding of the metabolic phenotypes, dependencies and flexibility of tumors is motivated by the potential that this may allow for the development of improved therapeutic strategies. The field of tumor metabolism is continually expanding. For this body of work, we will address breast cancer metabolic reprogramming and ROS in cancer. Furthermore, given the relevance to this project, we will review biguanides and other complex I inhibitors.

1.5.1 Impact of ROS in cancer, good vs bad

Many cancers are characterized by higher levels of ROS compared to normal cells [231][reviewed in [232]]. ROS play contradictory pro- and anti-tumorigenic roles in cancer. Elevated ROS levels were initially presumed to promote tumorigenesis by favoring DNA damage, that if mis-repaired favored further genetic perturbations [reviewed in [233]]. Yet, it is currently understood that low to moderately elevated levels of ROS, that do not induce DNA

damage, promote cancer cell proliferation and survival through stimulating cell signaling pathways such as PI3K/Akt, primarily through oxidizing critical cysteine residues on negative regulators, phosphatases, PTEN and PTP1B [162, 234]. ROS can also promote MAPK/ERK signaling, primarily by inactivating MAPK phosphatases [235]. ROS oxidation of prolyl hydroxylase domain protein 2 (PHD2) leads to the stabilization of HIF-1α, to promote angiogenesis, cell survival and metastasis [236] [reviewed in [237]. Additionally, ROS is an inflammatory mediator, downstream of cytokine and growth factor signaling, including IFNγ and TNF [238]. ROS also promotes inflammation through tumor necrosis factor -tumor necrosis factor receptor (TNF-TNFR) signaling. TNF is a proinflammatory cytokine that plays key roles in cellular homeostasis and immunity, including activating the transcription factor, nuclear factor kappa-light chain-enhancer of activate B cell (NF-κB). Activated NF-κB can translocate to the nucleus and lead to the upregulation of transcription of proinflammatory, anti-apoptotic, and antioxidant genes [239]. However, high ROS levels can also inhibit NF-κB signaling, decreasing cell survival signaling and promoting cell death, as well [reviewed in [240]]. NF-κB signaling will be discussed more in the *Inflammation overview* section below. In addition to cancer cell-intrinsic ROS, cells of the TME also contribute to ROS production and are influenced by ROS. Activated immune cells, such as myeloid cells, are a source of ROS in tumors [241]. Mitochondrial ROS production has been shown to be important for the activation of T cells [242]. Yet, T cells were shown to require the antioxidant GSH to protect from high ROS levels [243].

As described above, beyond a critical threshold, ROS without appropriate compensatory scavenging mechanisms results in irreversible damage to proteins, lipids and DNA, as well as promotes cell death pathways [reviewed in [244]]. ROS can generate DNA adducts, for example between the sugar-phosphate backbone ultimately leading to double-strand breaks. 8-oxoguanine (8-oxoG) and its nucleotide 8-oxo-2′-deoxyguanosine (8-oxodG) are ROS mediated DNA damage lesions that can be used as biomarkers of oxidative stress. 8-oxoguanine DNA glycosylase (OGG1) repairs 8-oxo-G and prevents mutagenesis since 8-oxo-G may pair with adenine instead of cytosine. PARP inhibitors reduce the capacity to repair ROS-induced DNA damage [reviewed in [245]]. Mitochondrial DNA is particularly susceptible to ROS damage, given its lack of histones and mitochondrial nucleotide excision repair [246]. Lipid peroxidation can alter the structure and function of cell membranes. Lipid oxidation generates highly reactive aldehydes, such as 4-hydroxy-2,3-nonenal and malondialdehyde, that generate free radicals, impacting mitochondrial and cell membrane integrity [reviewed in [247]]. High levels of ROS can trigger cell cycle arrest, senescence and cancer cell death [reviewed in [248-250].

As addressed above, cells have evolved ROS scavenging mechanisms to counteract the harmful effects of high ROS levels. To maintain redox balance, tumors increase antioxidant levels, for example through transcription factor activation including the master regulator of the antioxidant response, NRF2, leading to upregulation of its target genes, including NQO1, GCLC, GCLM, GSR, XCT, IDH1, TXN1 PRDX1, ME1, G6PD, among others [reviewed in [248, 251, 252]]. Additionally, tumors rewire metabolic pathways to generate redox cofactors, such as NADPH and NADH [reviewed in [248, 251, 252]]. These pathways are reviewed in the *Tumor metabolism overview* section. Finally, there is accumulating evidence that certain cancers depend on particular ROS scavengers and pathways [253]. See sections above for more details on ROS scavengers.

Early evidence implicating elevated ROS/loss of ROS scavengers in promoting transformation and tumorigenesis led researchers to study whether antioxidants could protect against carcinogenesis [254, 255] [256]. These findings and others stimulated interest in exploring antioxidants as cancer treatment [reviewed in [248]. However, clinical trials and further pre-clinical yielded controversial results. On the one hand, a randomized control trial revealed decreased total mortality, cancer-related mortality and liver cancer, with vitamin E and selenium [257]. However, several pre-clinical studies supported that antioxidant treatment can promote tumorigenesis and metastasis in mouse models [137, 258]. Furthermore, other clinical trials showed that antioxidants such as Vitamin A and Vitamin E could increase cancer risk [259, 260] [reviewed in [251]]. A meta-analysis revealed antioxidant use to be associated with increased all-cause mortality [261]. Given this, treatment with antioxidants has fallen out of favour.

The role of ROS in cancer initiation, progression, metastasis, and response to therapies is complex and is continually being elucidated [reviewed in [248]]. Mitochondrial superoxide promotes cancer cell migration and invasion [262] [263]. To survive, cancer cells must adapt to variations in ROS levels throughout tumorigenesis. Labuschagne et al. recently showed that cancer cells in circulation that experience elevated ROS could cope by clumping together. This cancer cell clustering generates hypoxic stress that induces HIF-1α, which enhances mitochondrial autophagy and decreases oxidative stress [264].

Given their altered redox environment, cancer cells are vulnerable to increased ROS and/or inhibitors of the scavenging potential of tumor cells compared to normal cells [232, 248, 251]. Therapies that tip the balance beyond a critical ROS threshold are promising therapeutic strategies [reviewed in [251, 265]]. Indeed many chemotherapies such as doxorubicin, and cisplatin have been shown to alter redox balance in cancer cells, induce ROS and lead to oxidative damage [198]. Radiation induces free radical generation [266]. However, cancer cells

can increase their antioxidant capacity to resist these therapies. In 1988, Kramer et al. elucidated the role of increased GSH redox capacity in contributing to multi-drug resistance in several preclinical cancer models, including the MCF7 cell line [267]. With these ROS-scavenging mechanisms intact, some tumors exploit elevated ROS levels to potentiate HIF-1α signaling, leading to the development of chemo-resistant breast cancers [268, 269]. Increased expression of GCL was shown to be sufficient to induce tamoxifen resistance in MCF7 cells [270]. Melanomas that acquire resistance to BRAF inhibitors were also shown to have high NRF2-activation, with increased GSH levels [271]. Given that increased antioxidant levels are associated with chemotherapy and radiation resistance, targeting these therapeutic resistance mechanisms with inhibitors of ROS scavenging mechanisms is a promising therapeutic strategy [251].

Inhibiting antioxidants is not a new concept. In 1982, Arrick et al. showed that inhibiting glutathione with buthionine sulfoximine (BSO), sensitizes tumors to activated macrophage and granulocyte oxidative burst [272]. BSO inhibits GCL, the rate-limiting enzyme in glutathione *de novo* synthesis [273]. Reducing GSH levels in breast and ovarian cancer cells was shown to promote apoptosis [274]. The fact that elevated levels of glutathione (GSH) have been shown to confer resistance to chemotherapy and radiation in multiple cancer models lead several groups to explore the impact of inhibiting GSH on tumor cell viability and growth [reviewed in [275]]. For example, inhibiting GSH synthesis re-sensitized cisplatin-resistant breast cancer cells [276]. Inhibiting GSH also re-sensitizes ovarian cancer models to radiation [277]. These data support combining ROS-generating treatments with inhibitors of ROS scavenging mechanisms as a worthwhile therapeutic strategy to explore [278].

Additional examples are explored in the *Breast cancer metabolic reprogramming* section below. Phase I trials with BSO and melphalan showed limited toxicity [279, 280]; however this was not pursued further. Another example of GSH targeting therapy is NOV-002, which mimics GSSG, and causes disbalance in the GSH/GSSG ratio that showed efficacy in combination with chemotherapy [281].

An additional concept to consider is the possibility of some cancer cells relying on multiple antioxidant mechanisms. For example, Harris et al. recently showed that cancer cells shown to be resistant to GSH depletion with BSO had “functional redundancy” in other antioxidant systems, in particular, the thioredoxin system. They showed that inhibiting both GSH and TXN/TXNRD inhibition causes synergistic cell death in breast cancer models [282]. A small molecule inhibitor of TXN, PX-12, was shown to be tolerated in a phase I clinical trial for several solid cancers, but in phase II trials for individuals with advanced pancreatic cancer, trials were

ended early [283]. Much of the focus has been on inhibiting GSH, given its central role in maintaining redox balance, however other antioxidants should be considered [reviewed in [251]]. Further characterization of the ROS scavenging landscape and dependencies of cancer cells is warranted. The contextual relevance of additional ROS scavengers, such as NQO1 and TXN, could likely guide the development of additional therapeutic strategies. NQO1 will be explored more in the section below.

1.5.2 NQO1

Central to this thesis is the NQO1 scavenger; as such it will be reviewed in more detail here. NAD(P)H:quinone oxidoreductase (NQO1) is an obligatory 2-electron reductase. The first description of NAD(P)H: Quinone oxidoreductase (NQO1) is largely recognized to be by Lars Ernster and Navazio in 1958, who briefly described a diaphorase in the soluble fraction of the rat liver homogenates [284]. It was named DT-diaphorase based on its reduction of NADH and NADPH, which at that time were known as DPNH and TPNH [284]. Ernster and Navazio then isolated and characterized what is now referred to as NQO1 [285]. NQO2 is distantly related, and it uses dihydro-nicotinamide riboside (NRH) as an electron donor cofactor instead of NADH and NADPH (as NQO1), and recent evidence implicating it instead as a toxifying agent [reviewed in [286]].

NQO1 is primarily located in the cytosol, though lower levels have been found within the nucleus and even in mitochondria [287]. More recently, NQO1 was shown to also localize to the mitotic spindles during mitosis in multiple human cell lines, non-transformed, immortalized, as well as a model of pancreatic cancer [288].

NQO1 contains an (antioxidant response element) ARE in its promoter region and is an NRF2 target gene that is classically induced upon oxidative stress [289]. NQO1 is also regulated by the Aryl hydrocarbon receptor (AhR) through one of its xenobiotic response element (XRE) elements, XRE 1 [290, 291]. NQO1 functions as a homodimer and requires a tightly bound FAD cofactor. The first step involves FAD being reduced by NADH or NADPH to $FADH_2$, and the resulting NAD+ or NADP+ leaves the active site. Subsequently, the second substrate, such as quinones, are reduced by $FADH_2$ [292] [293, 294]. The detoxification of many quinones to stable hydroquinone by NQO1 is owed to this direct 2-electron reduction, bypassing semiquinone radical and ROS formation that otherwise could be formed by 1 electron reduction [295]. NQO1 can also directly act as a superoxide reductase [296, 297]. In addition, NQO1 maintains reduced Coenzyme Q, which is widely found in lipid membranes and participates in the ETC and also as an antioxidant [298] [reviewed in [299]]. NQO1 also has non-enzymatic

functions stabilizing p53 and preventing E6-mediated degradation [300-302]]. NQO1 has also been shown to protect PGC1α from 20s proteasomal degradation [303]. Similarly, NQO1 was found to stabilize HIF-1α, by directly binding to its oxygen-dependent domain and inhibiting proteasomal degradation [304]. Finally, there is evidence that during mitochondrial inhibition, NQO1 binds to SIRT1 and supports its ability to regulate gene-expression [305].

NQO1 C609T (rs1800566, Pro187Ser) polymorphism in exon 6 of the human NQO1 gene has been shown to destabilize the protein and is associated with loss of NQO1 enzyme activity, and rapid degradation through ubiquitination and proteasomal degradation [306]. The half-life of NQO1 protein is greater than 18 hours, whereas NQO1 C609T polymorphism is 1.2 hours [307]. AKT has been reported to phosphorylate Threonine-128 on NQO1, leading to its polyubiquitination and proteasomal degradation in a model of Parkinson's disease [308].

NQO1 has been shown to have both anti-tumorigenic and pro-tumorigenic roles largely depending on the stage of tumorigenesis [reviewed in [294] and [309]]. Firstly, NQO1 loss has been shown to increase cancer susceptibility owed to its roles in scavenging ROS, detoxifying quinone, and stabilizing p53. NQO1-/- mice that are exposed to γ-radiation were found to develop lymphoma and lung adenocarcinoma at significantly higher rates than WT mice [310]. NQO1 protects against quinone-induced toxicity and oxidative stress, as NQO1-/- mice in another study were found to be very sensitive to menadione treatment, where 70% of mice died compared to none in the wild-type group [311]. Furthermore, NQO1-/- mice had increased carcinogen-induced carcinomas, associated with decreased p53 levels [312]. Additionally, two meta-analyses found that NQO1 C609T polymorphism was associated with increased breast cancer susceptibility in Caucasian but not in Asian nor Arab females [313, 314].

Yet, in many established cancers, NQO1 is commonly overexpressed compared to normal tissue, including cervical cancer, melanoma, and breast cancer, among others [315-317]. Increased NQO1 levels are associated with poorer prognosis in many tumor types. NQO1 protein levels are higher in IBC, than in DCIS and adjacent non-tumor tissue, and associated with decreased disease-free survival and inferior overall survival for individuals with breast cancer [318]. High NQO1 expression was shown to be associated with poorer overall survival in patients with pancreatic adenocarcinoma, cervical cancer, gastric adenocarcinoma, and serous ovarian cancers [319-321]. In MCF7 breast cancer cells, NQO1 was shown to be sufficient to cause resistance to tamoxifen [270]. Furthermore, AMPK activation by oxygen and glucose deprivation was NQO1-dependent in thyroid cancer and breast cancer cell models [322].

In addition to tumor intrinsic NQO1, Kimura et al. found that NQO1 specifically in macrophages suppresses toll-like receptor innate immune responses, by interacting with IκB-ζ

and promoting its ubiquitin-dependent degradation [291]. However, our understanding of tumor-extrinsic NQO1 roles, remains limited.

Given the high expression of NQO1 and its multiple pro-tumorigenic roles in established tumors, it continues to be explored as a targetable protein for anti-cancer therapy [reviewed in [294]]. NQO1 mediated 2-electron reduction of certain quinones such as β-lapachone and Mitomycin C, results in the generation of redox reactive or reactive alkylating species, respectfully [323]. This is appropriately referred to as a bioactivations. Given the high levels of NQO1 in cancer cells, these compounds mechanism of preferentially targeting tumor cells and sparing normal cells. More specifically, as an example to illustrate this, NQO1 promotes redox cycling of quinone β-lapachone, causing cytotoxicity in several cancer models, including breast cancer [170, 324]. ARQ-761 is a β-lapachone analogue inhibitor of NQO1-mediated ROS scavenging for which phase I clinical trial data in advanced solid tumors are available, showing modest activity as a single agent and tolerable adverse event profile, with stable disease in 12 patients and 6 patients with tumor reduction out of 42 total. In this study as could be expected, improved response was associated with higher NQO1 expression [325]. Additionally, in a recent single arm phase 1/1b clinical trial, 53% of individuals with advanced pancreatic cancer treated with ARQ-761 in combination with gemcitabine and nanoparticle albumin bound-paclitaxel had stable disease, with acceptable adverse-event profiles [Abstract [326]].

1.5.3 Breast cancer metabolic reprogramming

Many breast tumors upregulate glycolysis and the PPP for NADPH production [reviewed in [327]]. Mitochondrial metabolism also plays a central role in many breast cancers, including for energy generation through glutaminolysis and FAO; for redox balance; as well as amino acid and nucleotide synthesis [reviewed [328]]. While accumulating evidence supports breast cancer subtype-specific metabolic phenotypes, breast cancer is a heterogenous disease, and the diversity of its metabolic phenotypes is no exception. For example, TNBC cell lines have been shown to be less dependent on oxidative phosphorylation and more dependent on glycolysis than the ER-positive cell lines tested [212, 329]. Yet, OXPHOS was also shown to be upregulated in TNBC compared to matched normal cells [330]. Several HER2+ models have been shown to have increased lipid metabolism that is linked to increased aerobic glycolysis [331] [332], which corroborated findings showing that HER2-expression promotes *FASN* (gene that encodes fatty acid synthase) phosphorylation and activity [333].

Different breast cancer subtypes maintain different levels of ROS, as well. Several lines of evidence support higher ROS levels in many TNBCs. TNBC cells were shown to maintain

increased ROS levels in in comparison to a luminal ER-positive cell line and non-transformed cells. Furthermore, TNBC models were shown to be dependent on these elevated ROS levels [334]. Basal B tumor cell lines Hs578T, MDA-MD-231, MDA-MB-436 and CAL120, were found to be dependent on glutaminase-1 (GLS1), for both TCA anaplerosis and glutathione production; and as such were sensitive to GLS1 inhibition [335]. Glutamine metabolism is seen across molecular subtypes of breast cancer, however, a subset of TNBCs that were glutamine-addicted required the xCT transporter for cystine import for glutathione production to control ROS levels [336] [reviewed in[337]]. PGC-1α supports glutamine metabolism in some HER2-positive cancers. Additionally, increased glutamine metabolism gene expression is associated with poorer outcomes for individuals with HER2-positive cancers [338].

Although there are some dependencies that are common in molecular subtypes of breast cancer, the influence of cross-talk from cells of the tumor microenvironment on metabolism, is continually appreciated [339] [reviewed in [340]]. Furthermore, emerging evidence supports that metabolic phenotypes and dependencies evolve throughout different stages of tumorigenesis, as metabolically flexible cancer cells have a survival advantage when challenged by various nutrient and oxygen availability as well as different cellular stresses throughout initiation, progression, and various stages of the metastatic cascade [reviewed in [341] and [342]]. In 2009, Schafer et al., showed in HER2-positive breast cancer MCF10A acini models, that detachment from the extracellular matrix leads to decreased glycolysis and decreased flux through the PPP resulting in lower NADPH levels. Detached cells consequently had elevated ROS levels, which they found inhibited fatty acid oxidation. NAC treatment could rescue this and promote cancer cell survival [343]. OXPHOS upregulation in patient pre-treatment biopsies with TNBC, was associated with poorer outcomes [344]. Recent characterizations of PDX models of metastatic TNBC breast tumors revealed that OXPHOS is a top pathway upregulated during metastatic seeding, and that by inhibiting the electron transport chain in these models, metastasis was functionally abrogated [345]. Furthermore, there is recent evidence that depending on metastatic sites, breast cancer cells develop different metabolic phenotypes, such as those in the liver develop a more glycolytic phenotype with higher HIF-1α activity and expression of its target PDK1, than bone and lung metastases that instead elevated OXPHOS [346].

Both OXPHOS and increased ROS scavenging are emerging as important factors in promoting breast cancer metastasis and resistance to therapies. High OXPHOS levels have been reported in many tumor types to be associated with resistance to standard treatment regimens [347-351]. Metabolic reprogramming for redox balance impacts sensitivity to

chemotherapy, targeted therapies, and radiation in breast cancer. Tamoxifen-induces oxidative stress in breast cancer cells, resulting in increased Nrf2 activation and expression of target genes [352]. The group studied 176 primary breast cancers and found that high levels of NRF2 and NQO1 at the time of diagnosis, were prognostic of poor survival after tamoxifen therapy [352]. Lapatinib (dual EGFR and HER2 inhibitor) resistance in HER2-positive is mediated by ERRα-dependent increased glutamine flux and increased ROS scavenging potential [353]. Additionally, in TNBC models, glutathione levels are increased through a HIF-1α-dependent mechanism in response to paclitaxel, of which is a proposed mechanism of resistance by inducing breast cancer stem cells [354]. Cancer stem cells (CSCs) from the MMTV-Wnt1 tumors have decreased ROS levels associated with increased expression of antioxidant genes involved in GSH biosynthesis; in compared to more mature tumor cells [269]. Indeed, this group went on to demonstrate that targeting glutathione synthesis with the inhibitor BSO, can sensitize CSCs to radiation [269]. While metabolically flexibility augments the ROS scavenging potential of breast cancer cells, providing them with a survival advantage and acquired resistance to certain standard therapies, this does not preclude that these adaptive pathways cannot be successfully targeted. (See Figure 1.5).

1.5.4 Biguanides in cancer therapy

Biguanides are a class of anti-hyperglycemic agents that stemmed from the active ingredient guanidine isolated from the French lilac [reviewed in [355]]. The concept of repurposing of biguanides for cancer treatment, such as phenformin (N-phenethylbiguanide), and metformin (dimethylbiguanide) the latter of which is a widely used anti-hyperglycemic drug for the management of Type-II diabetes mellitus, stemmed from epidemiological evidence. The first was from Evans et al. in 2005, reporting that in individuals with diabetes, metformin use was associated with reduced rates of several types of cancer compared to other diabetic therapies [356].

Several epidemiological studies that followed associated metformin use with decreased incidence of cancer and even with reduced mortality among diabetic individuals (reviewed in [357]) [358]. Individuals known for diabetes and breast cancer receiving neoadjuvant chemotherapy and who were also on metformin, had higher pathological complete response than those not taking metformin (24% vs 8%) [359]. Yet, conflicting results also arose from epidemiological studies, including a cohort study of women with TNBC treated with adjuvant chemotherapy, including those with diabetes treated with and without metformin as well as non-diabetic individuals, wherein metformin use did not impact overall survival rates [360]. These

studies and their methodological limitations were explored by Dowling et al., such as the data being obtained retrospectively from clinical and hospital registries possibly introducing selection bias, as well as other confounding variables like severity of disease in patients that can receive metformin, and exposures to many treatments in addition to metformin [361]. Furthermore, these retrospective studies were limited in exploring metformin use in diabetic individuals. Extrapolating these findings to non-diabetic individuals was not ensured, as it is plausible that cancer biology is altered when they develop in the context of diabetes (including exposure to elevated glucose levels, ROS and insulin resistance) compared with that of a non-diabetic individual.

The anti-tumor properties of biguanides are attributed to both direct effects on the tumor cells and indirect systemic effects, such as lowering circulating glucose levels and insulin levels [362]. Metformin's role in glycemic control is owed to its effects on the liver, by inhibiting gluconeogenesis, it also increases glucose uptake through increasing GLUT-1 translocation, insulin receptor activation and stimulation of glycolysis [363-366]. Additionally, in skeletal muscles metformin increases insulin-mediated glucose uptake through GLUT-4 as well as increased tyrosine kinase activity of the insulin receptor [reviewed in [367]]. These systemic effects result in lower circulating glucose levels and insulin levels; contributing to its anti-tumorigenic effects, as well [reviewed in [368] and [369].

The main cellular mechanism of action of metformin and other biguanides, such as phenformin is inhibiting complex I of the electron transport chain [120, 370]. Metformin and phenformin reversibly inhibit complex I of the electron transport chain, reducing NADH oxidation, leading to reduced proton gradient and consequently decreased ATP production, and increased AMP and ADP, which activates AMPK [220, 371, 372]. Anti-tumor effects involve AMPK-dependent inhibition of the mTORC1 signaling [220]. AMPK phosphorylates and inhibits regulator-associated protein of mTOR (Raptor); and phosphorylates and activates a negative regulator of mTORC, tuberous sclerosis complex 2 (TSC2) [373]. Independent of AMPK, metformin can inhibit mTORC1 through Rag GTPases [374]. mTORC inhibition leads to reduced activation of its downstream effectors, ribosomal protein S6 (S6Ks) and the eukaryotic initiation factor 4E-binding proteins (4E-BPs), ultimately resulting in decreased protein synthesis and growth inhibition of tumor cells [220, 375]. Direct tumor effects of metformin were also shown to elicit decreases in citrate production and lipid biosynthesis from both glucose and glutamine in tumor cells, independent of AMPK and LKB1 [376]. In Her2/neu transgenic and transplantable breast cancer mouse models, metformin delayed the onset of mammary tumors, and inhibited tumor growth [377]. (See Figure 1.6).

Initial prospective trials of metformin in cancer, offered valuable insight into the potential of biguanides in the clinical setting, substantiating the indirect effects of biguanides in non-diabetic patients, including decreasing circulating insulin and glucose, decreasing insulin receptor levels and phosphorylated AKT, as well as variable effects on the proliferation marker, ki67 [378-382] [383]. Yet outcomes such as progression-free survival, pathological complete response and overall survival were largely unaffected by metformin treatment in combination with chemotherapy, including in advanced pancreas cancer (chemotherapy and Epidermal Growth factor receptor (EGFR) inhibitor) [384], rectal cancer (chemotherapy and radiotherapy) [385], in metastatic breast cancer (chemotherapy) [386]. Individuals with diabetes with the minor *C* allele of non-coding SNP *rs11212617,* located near the ATM gene is associated with improved response to metformin in type II diabetes. This prompted Cuyàs et al. to investigate the impact of this SNP in individuals with HER2-positive breast cancer on response to neoadjuvant metformin in combination with anthracycline/taxane-based chemotherapy and trastuzumab (the METTEN study). They found that metformin increased pathological complete response compared to chemotherapy alone in individuals with at least one copy of the *rs11212617* C allele [387]. Most recently, in a phase III double blind randomized control trial (MA.32 study) with 5 year treatment of non-diabetic individuals with high-risk non-metastatic breast cancer (stratified based on HR-positivity and HER2-positive status), that underwent surgical resection, and then treated with adjuvant metformin compared to placebo (in addition to other adjuvant therapies), found that metformin does not significantly improve overall survival, distant relapse-free survival and breast cancer-free intervals [388]. In secondary analyses, metformin treatment in individuals with HER2-positive tumors, was associate with longer overall survival (0.78 deaths per 100 patient-years) compared to placebo (1.43 deaths per 100 patient-years in placebo; HR, 0.54; 95% CI, 0.30-0.98; $P = .04$.) and disease free survival (1.93 events per 100 patient-years in metformin group compared to 3.05 events per 100 patient-years in the placebo group; HR, 0.64; 95% CI, 0.43-0.95; $P = .03$). The benefit was found in individuals with HER2-positive tumors, with any *C* allele of the rs11212617 SNV (*CC, AC* genotype). These findings suggested that metformin positively influences outcomes in a subset of HER2-positive patients with C allele rs11212617 SNV and should be repeated. However, while metformin may impact tumors, these impacts are not sufficient to influence overall outcomes in most individuals with breast cancer.

Metformin pharmacokinetic experiments in healthy volunteers, using ^{11}C metformin demonstrate that it was primarily taken up kidneys, urinary bladder, and liver and to a lesser extent in the salivary glands, skeletal muscle, and intestines. There was no elimination of ^{11}C

metformin through bile and was primary excreted in the urine [389]. Metformin depends on transporters for entry into the cell including solute carrier family 22 member (SLC22A) 1 and 4 (also referred to as organic cation transporters (OCT1 and OCTN1)); the plasma amine membrane transporter hENT4 (PMAT); as well as multi-drug and toxin extrusion protein (MATE) [367]. Given their positive charge, biguanides accumulate in the mitochondrial matrix in a voltage-dependent manner [372] [390]. Yet, a major limitation of translating metformin to the clinic is that the concentration used in many preclinical *in vitro* and *in vivo* mouse studies, well above what can be safely achieved in humans (daily dose of 1,000–2,550 mg) [391]. Route of administration of metformin and phenformin may lead to different tissue accumulation. Also, different tissues display different uptake of these two biguanides, and different accumulation within the mitochondria [392].

The initial focus of metformin as opposed to a related biguanide phenformin can be in part be attributed to metformin's current approval, widespread and well-tolerated use as part of the long-term management for type II diabetes (and more recently for other conditions like polycystic ovary syndrome (PCOS). This is in comparison to phenformin that had comparatively higher rates of lactic acidosis in certain diabetic individuals, especially those with existing renal and hepatic disease [393]. Yet, there is compelling literature to support that phenformin is instead the more suitable biguanide for oncology. While metformin and phenformin are both complex I inhibitors that have overlap in their anti-tumor mechanisms as addressed above, phenformin does not rely on OCT transporters for entry into the cell, is a more potent inhibitor of complex I at lower concentrations, and has increased anti-tumor effects, including in breast cancer stem cell populations [394, 395], [396], [397], [398], [399],[400]). The binding site of the biguanide IM1092 that is a derivative of phenformin, was recently described to be the quinone binding channel of complex I, by Bridges et al. [preprint [401]]. Additional mechanisms of action of phenformin have been proposed, including phenformin inhibiting medulloblastoma growth through a redox-dependent mechanism whereby it inhibits mitochondrial glycerophosphate dehydrogenase leading to increased NADH levels [402]. Phenformin and metformin deplete the tricarboxylic acid cycle and glycolytic intermediates in early transformed cells [198, 397]. In contrast, in breast cancer stem cells, these two biguanides deplete nucleotide triphosphates while only modestly decreasing glycolytic and TCA cycle intermediates [198, 397], supporting the notion that these complex I inhibitors have different anti-tumor effects on cells at different stages of tumorigenesis. Inhibition of complex I of the ETC with phenformin, not only decreases mitochondrial ATP production, but has been shown to have an underappreciated role in increasing levels of reactive oxygen species [372, 403].

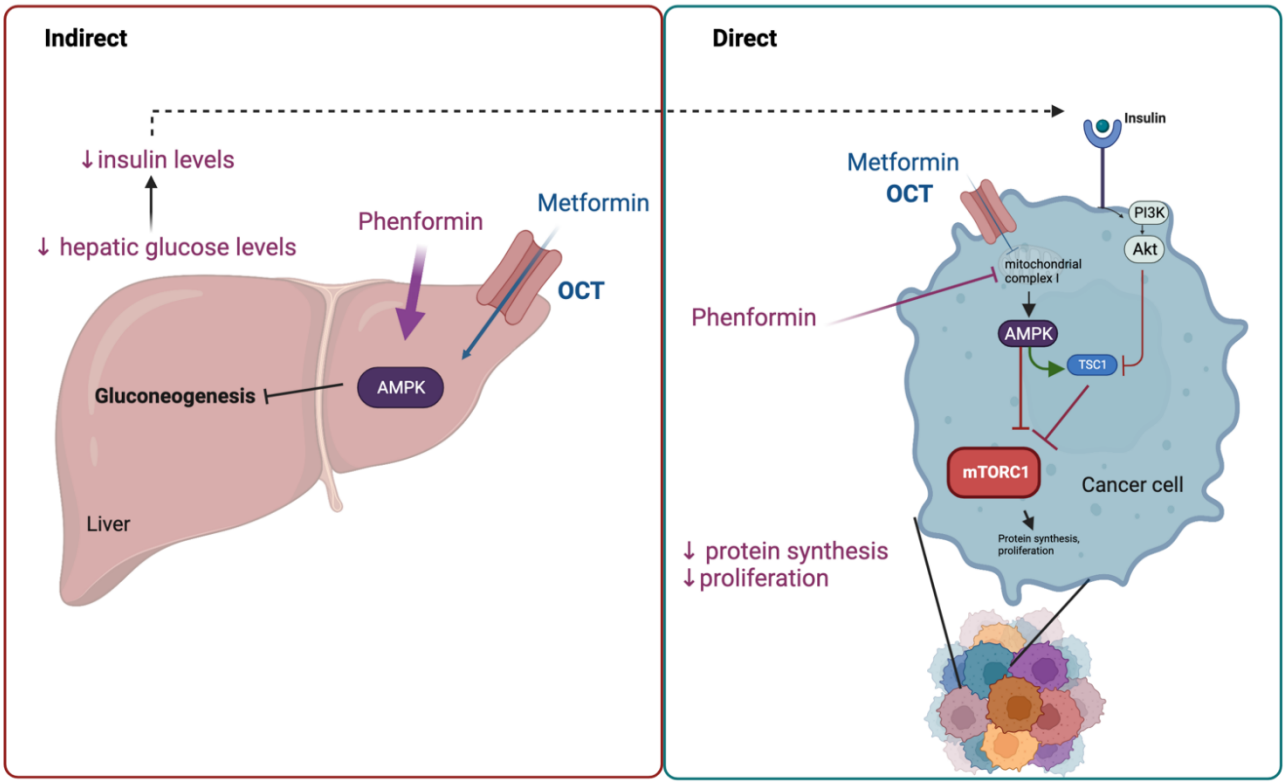

Figure 1.6: Classical mechanisms of action of biguanides, phenformin and metformin
Simplified representation of the direct and indirect anti-tumor effects of biguanides. Indirect actions of biguanides on the liver cause activation of AMPK and inhibition of gluconeogenesis, resulting in decreased circulating glucose and consequently decreased circulating insulin. Decreased insulin can reduce activation of the PI3K/AKT/mTOR signalling in cancer cells. The direct insulin-independent effects of biguanids are mediated by mitochondrial complex I inhibition, leading to activation of AMPK, reducing mTOR signalling (either through activating TSC1, inhibiting Raptor) or through AMPK-independent mechanisms (not shown). This reduction in mTORC1 signaling decreases protein synthesis and proliferation. Phenformin can passively enter cells, whereas metformin requires transporters such as OCT1. OCT: Organic cation transporter. Adapted from (Dowling et al., 2011). **Created with** BioRender.com

Given the metabolic flexibility of many cancers, it is likely that single agent phenformin will have limited success clinically. Indeed, accumulating evidence supports rational combination anti-tumor strategies with phenformin. Influences of phenformin and metformin on cells of the tumor microenvironment have recently been appreciated, including enhancing CD8+ T cell infiltration and augmenting anti-PD1 therapy [404, 405]. Availability of certain metabolites in the tumor microenvironment has been shown to alter sensitivity to biguanides [406] [407]. Studying these liabilities can offer insight into particular rational combination therapies [403] [408]. Reductive carboxylation of glutamine to generate citrate is a pathway used by cancer cells with dysfunctional mitochondria to produce necessary TCA cycle intermediates for growth [209]. Combining phenformin with a glutaminase inhibitor (GSL1) inhibitor (inhibits conversion of glutamine to glutamate) effectively induces apoptosis in *in vitro* and *in vivo* models of esophageal squamous cell carcinoma [87]. Furthermore, synthesis of non-essential amino acids such as aspartate, which is a precursor for purine and pyrimidine synthesis, depends on a functional election transport chain. Upon complex I inhibition, glutamic-oxaloacetic transaminase

(GOT1) is required for aspartate synthesis [202]. Additionally, kinase inhibitors selectively sensitize tumor cells to phenformin, partly through inhibiting mTORC1/4E-BP axis regulation of non-essential amino acid aspartate, asparagine, and serine synthesis, as well as through favouring their reliance on oxidative phosphorylation [408, 409]. Along this line, phenformin is currently in a phase I clinical trial in combination with Dabrafenib and Trametinib for individuals with metastatic BRAF-mutated melanoma (NCT03026517), the results of which anticipated as this may enable future rational combination trials.

1.5.4.1 Other complex I inhibitors

Several other complex I inhibitors have been explored as anti-cancer therapies [410]. The ones included in this section are non-exhaustive. The small molecule complex I inhibitor AG311 was shown to competitively inhibit complex I at its ubiquinone site, induce superoxide production and reduce tumor growth, including in breast cancer models [411, 412]. Recently, another small molecule complex I inhibitor, IACS-010759 was extensively characterized and found to decrease proliferation and induce apoptosis in brain and AML models and show that IACS-010759 increases mitochondrial ROS [413]. Recent evidence suggests that IACS-010759 binds to the middle of the ND1 subunit of complex I, inducing structural changes at the quinone-binding pocket [414]. The small molecule IACS-010759 was in two phase I clinical trials; for relapsed/refractory acute myeloid leukemia, (NCT02882321); and for solid cancers (NCT03291938), they found that in both studies, the concentrations used had unfavourable side effect profile with elevated lactate levels (none fatal), and lactic acidosis in 47% of the patients in the AML trial (but none in the solid tumor trial) and peripheral neuropathy being the most common adverse events. In the solid tumor group, 1/23 had a partial response and 8/23 had stable disease, however in the AML trial, no patient responded, and studies were terminated early given adverse events [415]. IM156 is a biguanide derivative that was in phase I clinical trials for individuals with unselected solid tumors. Stable disease was observed in 32% of patients with manageable adverse events, and recommended phase 2 dose was determined [416]. Neoadjuvant ME344 was shown to decrease tumor Ki67 levels when in combination with bevacizumab, compared to bevacizumab alone in early HER2-negative breast cancer [417]. EVT-701 was shown recently to have anti-tumor effects in multiple cancer cell lines, including breast cancer and a pre-clinical mouse model of Non-Hodgkin lymphoma and non-small cell lung cancer, however the exact mechanism binding site remains unknown [418]. Considering the metabolic flexibility of many tumors and currently available clinical trial evidence, rational combination therapies with complex I inhibitors may be more suitable and promising therapeutic

strategies in comparison to using these as single agents; allowing for decreased therapeutic concentrations and possibly reduced adverse events.

1.6 Inflammation overview

Our understanding of inflammation continues to evolve from the first recorded descriptions by Aulus Cornelius Celsus who characterized inflammation in terms of physical signs of redness, swelling, heat and pain [reviewed in [419]]. Inflammation can be broadly defined as the immune system's defence against tissue injury responding to pathogens, or non-infectious causes like physical, chemical and ischemic damage. Acute inflammation is a rapid complex biological response that occurs immediately after injury lasting hours to days and sometimes weeks, after which it is normally resolved. The acute inflammatory process is initiated by the release of damage associated molecular patterns (DAMPs) (such as high mobility group box-1, or ATP) by injured cells, that in turn can bind to DAMP receptors such as Toll-like receptors (TLR2, TLR4) or receptor for advanced glycation end products (RAGE), on resident immune cells including immature antigen-presenting cells, inducing their maturation to professional APCs [reviewed in [420] and [421]]. Similarly, in the case of infectious agents, pathogen associated molecular patterns (PAMPs) (such as lipids from bacteria walls, or nucleic acids) are released and can also bind retinoic acid-inducible gene I (RIG-I)-like receptors (RLRs), the cytosolic DNA sensor cyclic GMP-AMP synthase (cGAS), and particular TLRs on resident innate immune cells [reviewed in [422]]. (TLR3 signaling will be discussed in more detail below). PAMPs/DAMPs binding to their receptors leads to downstream signaling, that activates transcription factors such as NF-κB and interferon regulatory factor-3 (IRF3) in turn activating transcriptional programs, and later secretion of inflammatory mediators by these innate immune cells necessary for the remaining stages of the inflammatory cascade [reviewed in [423]].

Activated resident innate immune cells also cause release of inflammatory mediators that increase permeability of nearby blood vessels [reviewed in [424]]. Proinflammatory cytokines and chemokines promote the margination and chemotaxis of neutrophils, the most abundant leukocyte in circulation, to the site of injury where they perform effector roles in phagocytosis, ROS production and neutrophil extracellular traps [reviewed in [425]]. Monocytes are next to migrate to the site of injury, where they differentiate into macrophages and dendritic cells. Professional Antigen presenting cells (APCs) can then process antigens and transport them to nearby lymph nodes to present them via major histocompatibility complex (MHC) class II molecules to immature CD4+ and MHC class I to CD8+ T cells, and with co-stimulatory

signals. This leads to clonal proliferation and activation of antigen-specific T cells and B cells thereby bridging the innate and adaptive immune system. The activation of cells of the adaptive immune system, including B cells and T cell subtypes, enables recognition of a diversity of pathogens well beyond that of the innate immune system. Activated T lymphocytes, either T helper cell subtypes (such as Th1 subtype) can then migrate to the site of injury and act to maximize immunity against the offending stimulus [reviewed in [426]].

Key inflammatory mediators include histamine, platelet activating factor, leukotrienes and prostaglandins, vasoactive peptides (kinins), complement proteins (C3a, C5a), ROS and cytokines (interleukins (IL-12, IL-6, IL-8), tumor necrosis factor alpha (TNFα) and interferons [reviewed in [427]]. Interferons are pleiotropic cytokines, recognized for their immunomodulatory, antiviral and antitumor roles. They are separated into three major types; Type I IFN, main members are IFNα and IFNβ; type II interferon, with the sole member, IFNγ; and Type III, which consists of IFNλ1-4 [428]. Given its relevance to this project, IFNγ will be discussed in more detail in sections below.

Resolution of inflammation involves neutrophil apoptosis after fulfilling their effector roles, macrophage phagocytosis of neutrophil apoptotic contents, and switch of macrophage phenotype to that of pro-resolution [reviewed in [429]]. Additionally, T helper subsets, such as Tregs, normally also contribute to resolving acute inflammatory and immune responses, as well as promoting tissue repair [reviewed in [429, 430]]. Proinflammatory cytokines are balanced by compounds that have classically anti-inflammatory effects like IL-10, transforming growth factor beta (TGF-β), as well as specialized pro-resolving mediators (lipoxins, E-series and D-series resolvins, protectins and maresins) that help control inflammation, promote immune cell apoptosis, halt further leukocyte migration and promote tissue healing at the end of a normal acute inflammatory response [reviewed in [431, 432]]. Additionally, “immune checkpoints”, such as PD-1, cytotoxic T lymphocyte-associated protein 4 (CTLA-4), T-cell immunoglobulin and mucin domain 3 (TIM-3) on the surface of T cells bind to their ligands on APCs, acting as inhibitor stimuli to terminate the T cell response [reviewed in [433]].

The TLR family consists of 10 members in humans, which are either expressed on the cell surface or intracellularly and recognize distinct DAMPs, PAMPs or microbial components [reviewed in [421] [434, 435]. For example, TLR4 recognized bacterial lipopolysaccharide (LPS) and TLR3 recognizes viral double stranded RNA (dsRNA) from viruses. Of particular relevance to this project, TLR3 is expressed on the surface of macrophages, dendritic cells, NK cells and tumor cells, including breast cancer cells [reviewed in [436]]. Double stranded RNA or mimetics like polyIC bind and activate TLR3 that are then internalized within endosomes.

Activated TLR3s dimerize, and then signal through the adaptor protein TIR domain-containing adaptor inducing IFNβ (TRIF) [437, 438]. TRIF can recruit tumor necrosis factor receptor (TNFR)-associated factor-3 (TRAF3) and then Tank-binding kinase TBK1/ IKKε which phosphorylates interferon regulatory factor 3 (IRF-3). IRF-3 phosphorylation leads to its dimerization and function as a transcription factor, promoting Type I IFN production [439]. Alternatively, TLR3 signaling can lead to NF-κB signaling. NF-κB is a family of transcription factors, made of hetero- or homo-dimers, including the canonical p50/relA dimer [reviewed in[440]]. NF-κB dimers are usually sequestered by a family of inhibitor proteins such as the IκBα. Upon activation of TLR (and others, such as TNF receptor), TRIF adaptor can recruit and activate TRAF6 (E3 ubiquitin ligase) which self ubiquitinates, recruits and activates downstream kinases, transforming growth factor β-activated kinase (TAK1) complex, which in turn activates the IκB-kinase (IKK) complex (made of catalytic subunits IKKα, IKKβ and a regulatory subunit named NF-κB essential modulator (NEMO) or IKKγ). The activated IKK complex phosphorylates IκBα, leading to its ubiquitination and degradation, which releases NF-κB. NF-κB can then function as a transcription factor leading to the expression of various inflammatory cytokines and chemokines, in this context [reviewed in [441]]. TLR3 activation with dsRNA mimetics, like polyIC have been explored as a vaccine adjuvant and in immunotherapy [442, 443]. In addition to activated TLR3, polyIC has also been shown to activate RLR on NK cells to promote IFNγ production [444].

Importantly, if the acute inflammatory response does not resolve properly, chronic inflammation will ensue [reviewed in [445]]. Chronic inflammation can last months to even years and results in tissue damage, fibrosis, and necrosis; and contributes to the development of many pathologies, including autoimmune and inflammatory diseases; atherosclerosis; some neurodegenerative diseases, as well as initiate and promote cancer. Tumor-intrinsic and tumor-extrinsic inflammation both with paradoxical pro- and anti-tumor roles will be briefly addressed in the following two sections.

1.6.1.1 Tumor extrinsic inflammation overview

Inflammation plays paradoxical roles in cancer, often depending on whether it is acute or chronic inflammation, and the mediators involved. Effective acute inflammation is necessary for tumor immunosurveillance mechanisms that prevent the initiation of tumors. Immunosurveillance involves the elimination of neoplastic cells before they develop into clinically detectable tumors [446]. Main players in anti-tumor immunity include activated NK

cells, CD8+ T cells, CD4+ Th1 cells and macrophages with pro-inflammatory phenotype, referred to as M1 [reviewed in [447]]. Established tumors occur when initial cancer cells escape immunosurveillance mechanisms [reviewed in [448, 449]]. Evidence supports that overcoming immunosurveillance in metastatic sites, is also necessary for metastatic disease progression [reviewed in [450]]. Cancer cells that manage to evade immune surveillance do so through multiple mechanisms including upregulating immune checkpoints, decreasing antigen presentation MHC class I molecules, and promoting immune suppression [reviewed in [451]].

Chronic inflammation promotes tumorigenesis, through multiple mechanisms including immunosuppression, genetic changes, as well as cell signaling resulting in proliferation, inhibition of apoptosis and even therapeutic resistance [reviewed in [445, 452]]. Indeed, "**tumor promoting inflammation"** is recognized as a hallmark of cancer as mentioned above. Classic examples of chronic inflammation promoting cancer include inflammatory bowel disease (colon cancer), *Helicobacter*-induced gastritis (gastric cancer) and chronic hepatitis (liver cancer) [reviewed in [453]]. It is now understood that tumor-intrinsic inflammatory signaling can also promote tumorigenesis. Inflammation can predispose to cancer, but also promote tumor progression, immune suppression, and metastasis [reviewed in [427, 445, 454]]. Some of the main tumor extrinsic players in chronic inflammation include myeloid derived suppressor cells (MDSCs), tumor associated neutrophils (TAN) particularly the N2-polarized immunosuppressive phenotype, and T regulatory cells (Tregs) [reviewed in [447, 455, 456]]. Tumor associated macrophages (TAMs) in early stages of tumorigenesis are thought to be M1 phenotype (TAM1) secreting proinflammatory cytokines among others, IL-1, IL-6, TNF and iNOS. TAMs undergo a polarization to an anti-inflammatory phenotype, M2 macrophages (TAM2) secreting anti-inflammatory cytokines[reviewed in [447]]. In addition to dysregulated anti-tumor immune responses, chronic inflammation can also stem from other tumor extrinsic sources such as chemical exposures, obesity and as well as by signaling in other cells of the tumor microenvironment, such as fibroblasts. Indeed, cancer associated fibroblasts (CAFs) have been shown to mediate tumor-promoting inflammation [457].

Reinstating effective acute inflammatory signaling is a requirement of several immune therapies that are under continued investigation; such as immunogenic cell death, where certain chemotherapies and radiotherapy cause release of DAMPs; treatment with PAMP mimetics, such as polyIC that activate TLRs; or oncolytic viruses that induce local inflammation [reviewed in [458] and [432, 459]].

1.6.1.2 Tumor intrinsic inflammation overview

Inflammatory signaling in cancer cells can play both pro-tumorigenic and anti-tumorigenic roles. Oncogene activation, tumor suppressor loss and tyrosine kinase signaling can promote tumor-intrinsic inflammatory signaling [reviewed in[460]. Chronic unresolved inflammation can also promote tumor development and metastasis through tumor intrinsic inflammatory signaling. Additionally, there is significant cross talk between tumors and their microenvironments, just as cancer cells can influence and promote a pro-inflammatory TME, the TME can also promote tumor intrinsic inflammation through inflammatory mediators [461]. Some of the key inflammatory pathways within tumor cells include, IFN-JAK-STAT, cGAS-stimulator of interferon genes [8] and TLR signaling [462]. Each of these pathways has been reported to play dual roles in breast cancers and other cancers, either pro or anti-tumorigenic [463, 464] [reviewed in [465]]. As an example that is particularly relevant to this work, TLR3 expression in breast cancers was associated with increased metastasis in a cohort of breast cancer patients [466]. Yet, there is accumulating evidence that activation of TLR3 instead has anti-tumor effects. For example, the TLR3 mimetic polyAU was shown to decrease the risk of metastatic relapse in TLR3-positive human breast cancers [467]. Furthermore, TLR3 activation also leads to breast cancer apoptosis *in vitro* [436]. Additionally, tumors can produce inflammatory mediators, like ROS, TGF-β, TNF-α, interleukins, and various chemokines, with both tumor promoting and anti-tumorigenic roles [reviewed in [468] [248, 460, 469]]. Considering the central role of IFNγ-JAK-STAT signaling in this project, it will be discussed in more detail in sections below.

1.6.2.1 Interferon gamma overview

Interferon gamma (IFNγ) is a pro-inflammatory cytokine that is classically recognized to play diverse roles in both the innate and adaptive immune responses against intracellular pathogens and cancers [reviewed in [470] and [471]]. IFNγ was first described in 1965, by Wheelock et al., as an interferon-like viral inhibitor [472]. IFNγ is mainly produced by activated natural killer (NK), $\gamma\delta$T cells and natural killer T cells (NKT) (in the innate immune system); as well as activated CD8+ and CD4+ Th1 T cells (in the adaptive immune system) [reviewed in [473]]. IFNγ production by these cell types is stimulated primarily by IL-12, IL-15, IL-18, type I IFNs and PAMPs [reviewed in [474-476]]. IFNγ binds its cell surface receptors, consisting of heterodimers of IFNGR1 and IFNGR2 subunits, which leads to activation of the JAK-STAT1 (Signal transducer and activator of transcription 1). IFNGR1 and IFNGR2 are widely expressed on nucleated cells, including endothelial, epithelial, immune and tumor cells [477, 478]. IFNγ-signaling orchestrates a broad collection of transcriptional responses with expression changes

in hundreds of genes with vast roles, including transcriptional activators, inflammatory molecules, antigen presentation, cell death pathways, apoptosis, cell survival with new target genes that continue to be identified in different cell types [479, 480] [reviewed in [481, 482]]. IFNγ-STAT1 signaling will be described in more detail below.

Our understanding of IFNγ-signaling in the immune system stemmed from pivotal initial studies in mice engineered to lack expression of IFNγ or its receptor [483, 484]; as well as a series of sequential experiments with these models [reviewed in[485]]. These mouse models subsequently led to the understanding of IFNγ's potent immunostimulatory and immunomodulatory roles, that are critical for effective anti-tumor immunity, including natural killer (NK), macrophages and cytotoxic T lymphocyte (CD8+) action [reviewed in [470]]. IFNγ also induces superoxide generation during the respiratory burst of phagocytic cells, which occurs through the donation of electrons to O_2 using NADPH as an electron donor [486]. IFNγ also plays dual and opposing roles in cancer, both tumor cell-intrinsic and extrinsic effects, which will be explored in the next section.

1.6.2.2 Interferon gamma in cancer

IFNγ plays key roles in anti-tumor immunity in several immune tumor types, through effects within both immune cells and tumor cells [reviewed in [487]]. IFNγ is required for activation of key cellular players in immune surveillance, include CTLs, CD4+ Th1 and NK cells. IFNγ and lymphocytes protect mice against the development of carcinogen-induced adenocarcinomas and sarcomas [488]. IFNγ also promotes recruitment of immune cells into the TME, through regulating expression of chemokines CXCL9, CXCL10 and CXCL11, as well as their receptors CXCR3 and CCR5 on immune and tumor cells [489] [reviewed in [487]]. IFNγ upregulates MHC class I expression on tumors cells, increasing tumor processing and presentation to improve CTL mediated recognition and tumor cell death [488].

In addition to playing key orchestrating roles in anti-tumor immunity, recombinant IFNγ was shown to have direct anti-proliferative and pro-apoptotic effects on cancer cells (reviewed in [490]. Recently, IFNγ was reported to induce NOX4, NOX1 expression, DNA damage response and senescence in HeLa cells [491]. In HT-29 colon cancer cells, IFNγ was shown to sensitize cancer cells to apoptotic signals, in a p53-independent manner [492]. IFNγ was shown to be growth inhibitory in breast cancer cell lines MDA-MB-231 and MCF7 [493]. IFNγ has also been reported to induce oxidative stress, DNA damage and tumor cell senescence in a B16 murine melanoma model [491]. When combined, IFNγ and TNFα were shown to drive human

melanoma cell lines, rhabdomyosarcoma, as well as mammary tumor cells isolated from the PyMT (poliomavirus middle T model), into senescence [494, 495].

IFNγ has also been shown to have tumor promoting roles [reviewed in [471, 496]]. Additionally, IFNγ increases expression of indoleamine 2,3- dioxygenase (IDO), which catalyzes the breakdown of tryptophan, an amino acid that is required for proper CTL functioning, thereby leading to immunosuppression and also increased number of T regulatory cells [497, 498]. Given that IFNγ primarily signals through STAT1, more details of IFNγ/STAT1 axis in cancer will be described in the STAT1 sections below. Additionally, recent roles for IFNγ/STAT1 axis in metabolism will also be addressed separately below [499].

1.6.3.1 STAT1 signaling overview

Signal transducer and activator of transcription (STATs) are activated downstream of binding of ligand-binding to growth factor, cytokine and hormone receptors [reviewed in [500]]. They comprise a family of 7 signal transducers and activators of transcription [reviewed in [500]]. For this thesis, the next few sections will focus on STAT1. STAT1 is a transcription factor that is activated in response to interferons and other cytokines and that plays important and diverse roles in the immune cells and tumors alike [501][reviewed in [7, 481, 502]]. Canonically, STAT1 is activated by IFNγ, IFNα or IFNβ. More specifically, STAT1 signaling results from binding of IFNγ, to pairs of its receptor dimers, on the surface of immune and non-immune cells, which results in auto- and trans-phosphorylation of Janus kinases (JAK1 and JAK2) [503, 504]. Activated JAKs then phosphorylate the tyrosine-440 (Y440) residue of IFNGR1, which creates a docking site for STAT1 via its Src-homology 2 (SH2) domain [505]. STAT1 is then phosphorylated at tyrosine-701 (Y701) by the JAKs, leading to its activation and dimerization [506]. STAT1 homodimers can then undergo nuclear translocation and activate transcription through binding gamma-activated sequence (GAS) elements in primary response genes, increasing transcription of transcription factors such as interferon-regulatory factor-1 (IRF1) and STAT1 [507]. IRF1 then binds to interferon-stimulated response elements (ISRE) leading to increased transcription of secondary response genes [reviewed in [508]]. A second phosphorylation event in the cytoplasm on STAT1 serine-727, dependent on JAK2 and PYK2 kinases has been shown to lead to full transcriptional activation [509]. Importantly, STAT1 can also be activated by IFNα/IFNβ, through binding to the IFNAR (interferon-alpha receptor), resulting in JAK1 and TYK2 auto- and trans-phosphorylation [510, 511]. Activated JAK1 and TYK2 can then phosphorylate tyrosine-466 of the IFNAR1[512]. Which in turn allows for docking and the phosphorylation of STAT1 (at position tyrosine-701) and STAT2 (at tyrosine-660), which

can then heterodimerize, or heterotrimerize with the addition of IRF9 that can then also lead to transcriptional activation [513, 514]. A major negative feedback regulator of the STAT1 signaling pathway is the suppressor of cytokine signaling molecules (SOCS), particularly SOCS1 which inhibits JAK1, JAK2 and Tyk2 [515, 516] [reviewed in [517]] (See Figure 1.7). STAT1's role in cancer is explored below.

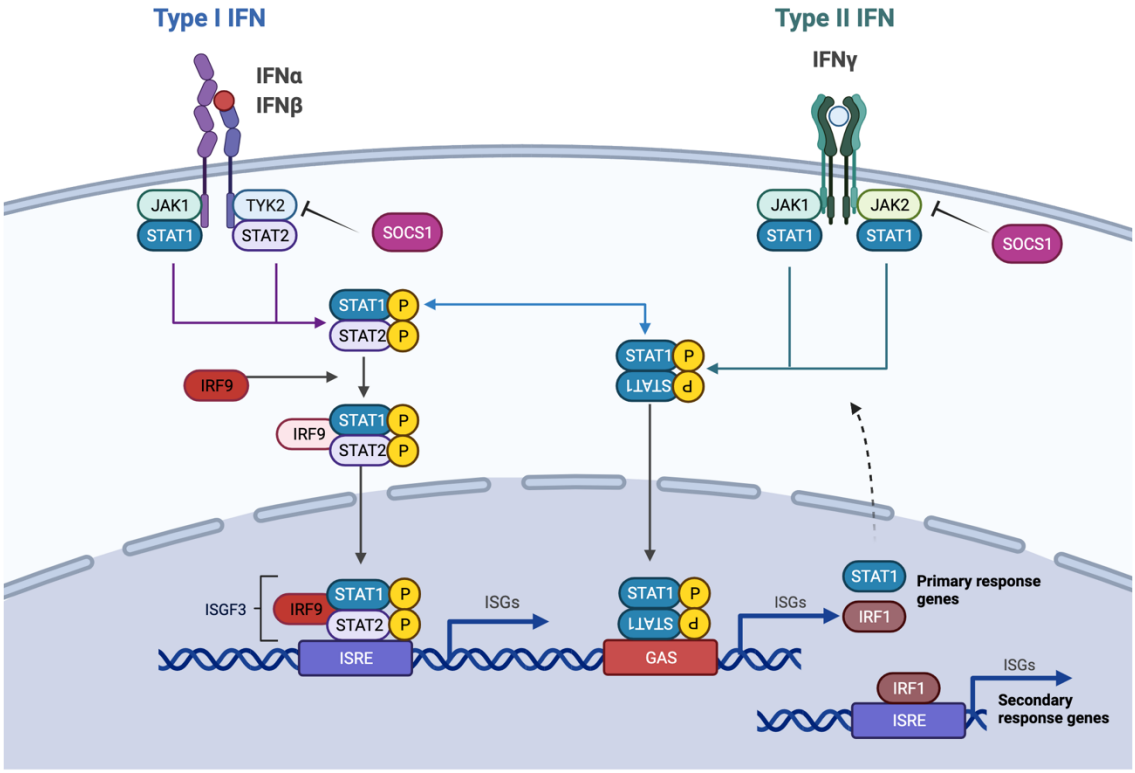

Figure 1.7: Canonical STAT1 signaling downstream of Type I and Type II interferons.
Binding of IFNγ to its receptors IFNGR1 and IFNGR2 results in activation and trans-phosphorylation of JAK1 and JAK2. Activated JAKs then phosphorylate the Y440 residue of IFNGR1, creating a docking site for STAT1. JAKs then phosphorylate STAT1 at Y701 leading to its activation and dimerization, allowing for entry into the nucleus. STAT1 homodimers then activate transcription through binding GAS elements in primary response genes, thereby increasing transcription of transcription factors such as IRF1 and STAT1. IRF1 protein can then bind to ISRE leading to increase transcription of secondary response genes. Importantly, STAT1 can also be activated by IFNα/IFNβ, through binding to the IFNARs, resulting in JAK1 and TYK2 auto- and trans-phosphorylation. Activated JAK1 and TYK2 can then phosphorylate Y466 of the IFNAR1 permitting docking and phosphorylation of STAT1 Y701 and STAT2 Y660. These can then heterodimerize or heterotrimerize, with the addition of IRF9; also lead to transcriptional activation by binding to ISRE. SOCS1 is an important negative feedback regulator of the STAT1 signaling by inhibiting JAK1, JAK2 and TYK2. JAK: Janus kinase; Y: Tyrosine; GAS: gamma-activated sequence; IRF: interferon-regulatory factor-1; ISRE: interferon-stimulated response elements. Adapted from (Castro, Cardoso et al. 2018) and (Platanias 2005). **Created with** BioRender.com

1.6.3.2 STAT1 in cancer overview

STAT1 expression has been associated with both good and poor prognosis in human cancer. Gross staining of human tumors, reveals that higher STAT1 levels are largely associated with improved outcomes in multiple cancer types, including breast cancer, pancreas, rectal cancer, esophageal cancer and high grade serous ovarian cancers, among others [518-521]. In breast cancer specifically, women with tumors with higher STAT1 activation, have longer overall and relapse free survival [522]. In PDX models of breast cancer, IFN/STAT1 pathway predicts response to adriamycin and cyclophosphamide treatment of ER-negative tumors [523]. However, contradictory findings have been found, where elevated nuclear levels of STAT family of transcription factors, including STAT1 were reported in human breast carcinoma compared to normal breast tissue [524]. Additionally, in premenopausal women, phosphorylated STAT1 is related to advanced stage and worse survival, yet postmenopausal women with phosphorylated STAT1/ER-positive or PR-positive tumors had longer disease-free survival than those with less than 1% of pSTAT1-positive cells [525]. The complexity of STAT1's role in cancer is continually appreciated. An important concept to consider is that gross tumor sample analyses in these studies prevents discernment of the influence of STAT1 expression levels in different cells within the tumor microenvironment. Indeed, Chan et al., showed that despite low or lost STAT1 expression in the neoplastic cells in a subset of human breast cancer samples in their cohort, STAT1 expression remained elevated in tumor infiltrating lymphocytes [526]. It is now understood that STAT1 in both tumor cells (tumor intrinsic) and cells of the tumor microenvironment (tumor extrinsic) can play both tumor promoting and anti-tumor roles and these will be addressed below.

1.6.3.3 STAT1 in the tumor microenvironment

STAT1 expression in cells of the TME is understood to play key anti-tumor roles, yet recent evidence suggests certain tumor-promoting roles as well. STAT1's central roles in innate and adaptive immunity, were established by Meraz et al., with their generation and characterization of *Stat1*-deficient mice [527]. The tumor suppressor functions of STAT1 primarily through promoting anti-tumor immunity, in many tumor types is well established [reviewed in [528]]. STAT1 plays central roles in proper NK and T cells function [527, 529]. Some key lines of evidence in breast cancer specifically, include *Stat1*-/- mice have increased spontaneous mammary tumor development in multiparous mice [530]. Furthermore, orthotopic transplantation of spontaneous mammary tumors into *Stat1*-/- mice had accelerated growth compared to wild-type mice, in part due to impaired CTL-mediated tumor immunosurveillance

[530]. Stat1 expression in stromal compartment suppresses Erbb2/neu driven-tumorigenesis [531]. Stat1 expression in the TME has been shown to have anti-tumor roles in other tumor types, models of renal cell carcinoma and mesothelioma, where the STAT1 in NK cells has been shown to sensitize pre-clinical models to ICB [532]. STAT1 expression in the immune compartment, particularly in NK cells, inhibits melanoma growth in mouse models [533]. In addition to the immune compartment, Stat1 expression in endothelial cells has been shown to play anti-angiogenic roles [534].

On the other hand, pro-tumor functions for STAT1-signaling in cells of the tumor microenvironment have also been identified. Overexpression of STAT1 and activation of STAT1 in tumor-associated macrophages (TAMs) was associated with poorer overall survival in patients with follicular lymphoma [535]. STAT1 signaling in TAMs was shown to be responsible for TAM-mediated T cell suppression in a lymphoma model [536]. Knockdown of STAT1 in cancer associated fibroblasts reduced breast cancer progression in mouse mammary tumor models [537]. Tumor-intrinsic STAT1 can also lead to immune suppression by multiple mechanisms, which will be explored below.

1.6.3.4 Tumor-intrinsic STAT1

Tumor-intrinsic STAT1-signaling has been shown to have both tumor suppressor and tumor promoting roles, including coordinating many downstream actions of IFNs, including IFNγ that were addressed above. STAT1 has proapoptotic roles, including inhibiting the expression of antiapoptotic genes including Bcl-2 and upregulating pro-apoptotic proteins such as certain caspases [538-540]. STAT1 was shown to also sensitize tumors to cell death receptor such as FAS and TRAIL [541-543]. MHC class I upregulation by IFNγ in a STAT1-dependent manner was required for adaptive tumor immune surveillance in preventing carcinogen-induced mouse tumors [544]. Yet, loss of STAT1 in a leukemia model was shown to lead to downregulation of MHC class I and consequent increased killing by NK cells [545]. In breast cancer, primary mammary cells from *Stat1*-/- mice have increased cell growth rate and loss of structured acini formation in 3D-cultures [530]. Klover et al. showed that *Stat1* deletion specifically from mammary epithelium of transgenic mice that express the neu oncogene under the control of the mouse mammary tumor virus long terminal repeat [107] (MMTV-neu-IRES-cre [NIC]) led to early tumor onset supporting a tumor intrinsic role for STAT1 in suppressing tumor onset [546].

In certain contexts, STAT1 can also promote tumorigenesis and treatment resistance [547]. The phosphorylation status of STAT1 was implicated in its function as a tumor suppressor, where unphosphorylated STAT1 instead promotes tumorigenesis by repressing

Fas-mediated apoptosis and promoting immune escape [548]. Tumor-intrinsic expression of Stat1 has been shown to promote myeloid-derived suppressor cell recruitment and promote tumor growth [549]. Tumor-intrinsic STAT1-signaling can also increase PD-L1 expression favouring immune suppression, in several tumor types including endometrial, melanoma and breast cancer models [550-552].

1.6.3.5 IFN-STAT1 axis and metabolism

More recently, STAT1's roles in modulating metabolism in both immune and tumor cells have gained attention. Evidence supports a bidirectional relationship of IFNγ-STAT1 axis being affected by metabolic signaling and IFNγ-STAT1 affecting metabolic signaling in different cell types. Most of the work to date has been in immune cells, particular effector T cell populations. For instance, there is evidence that IFNγ expression is enhanced by metabolic signaling, including lactate dehydrogenase A (LDHA) that maintains high levels of histone acetylation and transcription of *Ifng* in CD4 T cells of mice, and in low glucose conditions, GAPDH binds to *Ifng* 3'UTR to suppress translation [553, 554]. IFNγ's ability to modulate metabolism has also gained attention. For example, IFNγ was shown to cause activated M1 macrophages to switch to aerobic glycolysis [555]. More broadly, IFNγ-induced metabolic rewiring is postulated to favor "anti-viral" state to limit viral replication, such as in a recent report where IFNγ treatment of host cells decrease glycolysis and glucose uptake [556]. IFNγ suppresses mTORC1 signaling activity, with suppressed eukaryotic translation initiation factor 4E-binding protein 1 (4EBP1) and (S6 kinase) S6K phosphorylation and impacts the translatome of multiple metabolic processes, including purine synthesis in human primary macrophages [557].

In 2019, Wang et al. showed that IFNγ produced by activated CD8+ T cells sensitizes melanoma and sarcoma models to ferroptosis, by decreasing the expression of SLC3A2 (4F2hc) and SLC7A11 (xCT) subunits of the glutamate-cystine antiporter system xc^- that promotes lipid peroxidation [66, 558]. The cystine/glutamate antiporter system Xc^-or the trans-sulfuration pathway involves a regulatory subunit, solute carrier family 3 member 2 (SLC3A2), and a catalytic subunit, solute carrier family 7 member 11 (SLC7A11) (reference). It promotes the exchange of extracellular cystine and intracellular glutamate across the plasma membrane. Cystine in the cell is then reduced to cysteine, which is required for the production of GSH [559]. In human monocytes, IFNγ was found to increase NAD+ biosynthesis and increase oxygen consumption [560]. One report found that treatment of a colon cancer model with IFNγ increased ROS levels, and also decreased mitochondrial pyruvate carrier (MPC) levels, which the authors proposed is a compensatory action, given that overexpression of MPC promotes

increased ROS production, sensitizing cells to apoptosis [561]. Recent evidence supports metabolic cross-talk wherein CAFs produce glutathione and cysteine to decrease ovarian cancer sensitivity to carboplatin. This effect could be reversed upon IFNγ-STAT1 signaling, which promotes GSH extracellular degradation, through gamma-glutamyl transferase (GGT) activation, and downregulation of the xCT system to decrease cystine in CAFs, re-sensitizing tumors to platinum-based therapy. Interestingly, IFNγ treatment of tumor cells did not result in changes in cystine uptake, nor in GGT expression levels [562].

STAT1 activation downstream of IFNγ increases indoleamine 2,3-dioxygenase (IDO), which can contribute to T cell suppression. However, STAT1 activation in cells of the tumor and immune compartments, have also been shown to sensitize tumors to immune checkpoint blockage [532, 552]. More recently, STAT1 activation in both squamous cell carcinoma models and mesenchymal cells has been shown to increase glycolysis [563, 564]. Using transcriptomic and proteomic analysis of knock-down of STAT1 in squamous cell carcinoma of the oral tongue models, led to concordant downregulation at both the protein and RNA level of 16 of 22 total concordant genes in gluconeogenesis and glycolysis [563]. IFNγ and STAT1-driven classical M1 macrophage activation on the upregulation of not only inflammatory genes but also glycolysis. Recently, it was shown that the rate limiting enzyme in NAD+ salvage pathway, nicotinamide phosphoribosyltransferase (NAMPT) was shown to be upregulated in macrophages, upon IFNγ treatment. In this system, STAT1 occupies a previously unknown region within the *Nampt* first intron, *Nampt* Regulatory Element-1. Furthermore, that NAMPT enzymatic functions is required for IFNγ-induced glycolysis in Macrophages M1 phenotype [565].

In viral infection models, Type I IFN-signalling through STAT1 causes decreased SOD1 levels in hepatocytes, leading to oxidative stress and liver damage [566].
Furthermore, silencing STAT1 leads to increased levels of MnSOD, catalase, NQO1 at both the protein and mRNA levels in murine podocyte cell line, in both high glucose and normal glucose conditions [567]. Yet, the role of STAT1 in redox regulation and metabolism within cancer cells remains unclear.

1.7 Rationale

Breast cancer is a group of heterogeneous diseases. An improved understanding of breast cancer biology has led to the development of targeted therapies for several subtypes, which have improved the survival of many women with breast cancer. Despite this fact, there remains a subset of women who either experience distant metastases of their disease, most frequently those with HER2+ (25%) and triple-negative breast (23%) subtypes, and those with local disease recurrence, representing 7.5% of patient with HER2+ tumors and 7% of patients with triple-negative tumors [1]. Triple-negative breast cancers lack targeted therapies, and given their molecular heterogeneity remain poorly characterized. The mainstay of treatment for these tumors remains chemotherapy. These difficult to treat breast cancers underscore the need to identify therapeutic approaches that elicit durable responses with minimal toxicity to normal cells. Given that cancer cells rely on diverse metabolic pathways to meet the energetic, biosynthetic demands and redox balance required for tumor progression, identifying possible cancer-specific metabolic dependencies could represent a promising targetable vulnerability [211, 568].

A hallmark of many breast cancers is metabolic flexibility. Tyrosine kinase inhibitors were found to reduce the metabolic flexibility of cancer cells, sensitizing them to biguanides [569]. This project stemmed from previous work showing that increased metabolic flexibility associated with increasing receptor tyrosine kinase signaling requires the ShcA adaptor protein [409]. More specifically, loss of phospho-tyrosine-dependent ShcA signaling (Y239F/Y240F/Y313F mutant) makes breast cancer cells more reliant on mitochondrial metabolism and thus more sensitive to phenformin [409]. More specifically, cells that were unable to phosphorylate ShcA at site Y313 were sensitize to phenformin. Previous observations made by our team, that these ShcA Y313F cells have increased baseline STAT1 expression, a transcription factor that is induced in response to inflammatory stimuli [570]. My PhD thesis explored whether STAT1 function and/or inflammatory cytokines was required for increased sensitivity of breast cancer cells to phenformin.

1.7.1 Hypothesis and aims

We **hypothesize** that strategies that increased IFNγ-STAT1 signaling sensitizes cancer cells to the mitochondrial complex I inhibitor phenformin, and that elucidating the mechanism of cooperation will reveal metabolic vulnerabilities that can be targeted to eradicate difficult to treat breast cancers.

Aim 1: Elucidate the mechanism of cooperation between IFNγ and phenformin combination in decreasing breast tumor growth.

Aim 2: Test if IFNγ and phenformin is relevant to other *in vitro* and *in vivo* models of breast cancer.

Aim 3: Characterize how IFNγ and phenformin combination influences breast cancer metabolism.

Aim 4: Address if the mechanism of cooperation can be translated into effective rational combination treatment strategies that sensitize more clinically relevant models of breast cancer and to other mitochondrial complex I inhibitors, while sparing non-transformed cells.

Chapter 2: Methodology

2.1 Cell culture

Human breast cancer lines were either grown in Dulbecco's Modified Eagle's Medium (DMEM, Wisent: MCF7, BT474, MDA-MB-231, BT20, MDA-MB-436, Hs578t, BT549) or Roswell Park Memorial Institute 1640 Medium (RPMI, Wisent: HCC1954) supplemented with 10% fetal bovine serum (FBS), 1x penicillin/streptomycin (Wisent), and 1x gentamycin (Wisent). Murine breast cancer cell lines MT4788 and MT864; MT6737 and MT6738 ShcA313F mutant cells lines; MT4788-VC, MT864-VC and their STAT1$^{-/-}$ counterparts (generated with CRISPR/Cas9, as previously described [570]), were all grown in DMEM media, 2.5 % FBS, mammary epithelial growth supplement (MEGS: 5 mg/ml insulin, 3 ng/ml human epidermal growth factor, 0.5 mg/ml hydrocortisone and 0.4% v/v bovine pituitary extract) and penicillin/streptomycin and gentamycin. The NIC cell line was generated as previously described [571] cultured in DMEM supplemented with 5% FBS and MEGS, Penicillin/Streptomycin and Gentamycin. NMuMG parental and ErbB2-transformed murine counterparts, NT2197 were previously described [571] and grown in DMEM supplemented with 10% FBS, 10 µg/ml insulin, 10 mmol/L HEPES, penicillin/streptomycin and gentamycin. NOP6, NOP23 (graciously provided by Dr. Brad Nelson) were described in [572] and cultured in DMEM, 5% FBS, 1x ITSS (insulin, transferrin, sodium selinite) (Sigma), with penicillin/streptomycin and gentamycin. 4T1-537 cells, generated as previously described [573], were cultured in DMEM, supplemented with 10% FBS, HEPES 10 mmol/L, penicillin/streptomycin and gentamycin.

Cell lines were generated from patient-derived xenografts established at McGill University and the Jewish General Hospital. Patients generously donated tumor tissue for breast cancer research and provided informed consent. Specifically, PDX cell lines GCRC2080, GCRC1735, GCRC1971, GCRC1986 and GCRC1963 were previously described [574] (see sections below for more details). These PDX cell lines were grown in F media: 3:1 DMEM (Wisent): F12 Nutrient Mixture (Wisent), 5% fetal bovine serum, hydrocortisone 25ng/mL, insulin 5 µg/mL, cholera toxin 8.4ng/mL (Sigma), epidermal growth factor (Invitrogen) 0.125ng/ml, gentamycin 50 µg/mL, Y-27632 (Enzo Life Sciences) 10 µmol/L. PDX CRC-132 was grown in 66% DMEM high glucose, 25% F12 nutrient mixture (Gibco), 7.5% FBS, 10 µM Rock inhibitor, 10 ng/ml EGF, 8.4 ng/ml cholera toxin, 5 µg/ml insulin, 0.4 µg/ml hydrocortisone, 1.48 mM L-glutamine, penicillin/streptomycin. All cell lines were grown in 37°C, 5% CO_2 and screened for mycoplasma infection at minimum monthly or 24 hours prior to any *in vivo* injection using the MycoAlert ^{TM} mycoplasma detection kit (Lonza), as per manufacturer's protocol.

2.2 Patient-derived cell line generation

Patient-derived xenografts (PDX) were developed in accordance with the McGill University Health Center research and Jewish General Hospital ethics boards (SUR-99-780, 05-006) and the McGill University Animal Care Committee (2014-7514) guidelines. Studies were performed in NOD SCID gamma (NSG) mice. Breast cancer PDXs were derived from different HER2+ and TNBC tumors as previously reported [574, 575]. For the Goodman Cancer Research Centre (GCRC) PDXs, (GCRC2080, GCRC1735, GCRC1915, GCRC1963, GCRC1986) tumour fragments taken from mice were minced and digested in a rotator shaker at 37ºC for 1 hour with an enzymatic mix of one part Collagenase-IV, 9 parts of Digestion Media (DMEM, FBS, HEPES, Gentamicin). Tissue was later digested with Trypsin 0.25% and a mix of DNaseI (10 µl)/Dispase (1ml). Murine cells were removed using a Mouse Cell Depletion Kit (Miltenyi), and single-human epithelial cancer cells were culture in their respective F-Media described above. For CRC-132, tumor fragments from PDX-132 were incubated with a mix of Collagenase/Hyaluronidase and Dispase (STEMCELL Technologies) for 1 hr at 37°C on oscillator to perform tissue dissociation. After centrifugation at 1100 rpm for 5 min and resuspension in DMEM 10%FBS, cells were filtered through a 70 µM cell strainer, centrifuged at 1100 rpm for 5 min, and resuspended in F-medium. Cells were then transferred to a T25 flask containing lethally irradiated 3T3-J2 cells ($1x10^6$ cells). After 5 passages, co-culture with irradiated 3T3-J2 cells was suspended, murine cells were removed using a Mouse Cell Depletion Kit (Miltenyi), and cells were grown in conditioned medium (3 part of conditioned medium for 1 part of fresh medium) for another 10 passages and then maintained in F-medium.

2.3 Animal models

Nulliparous FVB, SCID-beige and BALB/c female mice (6-9 weeks old) were purchased from Charles River Laboratories (Quebec, Canada) and used for mammary fat pad injection studies. $IFN\gamma^{-/-}$ and $CD8^{-/-}$ were previously backcrossed onto an FVB background as previously described [570] and maintained. All mice had *ad libitum* access to food and water and housed within the animal facilities of the Lady Davis Institute, on a 12h light day cycle, mean temperature 22.5°C ± 1.5 °C. All studies were approved by the Animal Resource Centre at McGill University and comply with guidelines set by the Canadian Council of Animal Care.

2.4 *In vivo* experiments

For Mammary Fat Pad injections, cells were trypsinized, washed 2 times in PBS, and counted, such that, 0.05 $x10^6$ (4T1-537); 0.5 $x10^6$ (MT4788); or 1 $x10^6$ cells (MDA-MB-231) cells were injected into the 4^{th} mammary fat pads (MFP) of anesthetized mice (volume 50 µl), through

a small skin incision. For MDA-MB-231 and 4T1-537 injections, as well as for the oncolytic virus study, cells were re-suspended in a 1:1 PBS and Matrigel (Corning) mixture. Otherwise, cells were resuspended and injected in sterile PBS.

For the procedure, mice were given two doses of Carprofen, one pre-op and one 24 hours post-op, as well as Lidocaine-bupivacaine mixture at surgical site, and monitored as per Animal ethical protocol. A small clip was placed at the incision site and removed between 7-9 days post MFP injection. After implantation and palpation, tumors were measured by digital caliper every 2 days. Tumor volume was calculated using the following equation: volume=4/3 × (3.14159) × (length/2) × (width/2)^2. All drug treatment studies were initiated when tumors reached an initial volume of ~100-200mm^3, see Figure legends for starting details on starting tumor volumes and treatments.

2.5 Drug preparation and treatments

Phenformin hydrochloride (Cayman chemicals) powder (stored at -20°C) was resuspended in PBS, filter sterilized with a 0.22 μM syringe filter, and stored for a maximum of 4 weeks at 4 °C. For *in vitro* experiments, phenformin was used at a final concentration ranging from 20 μM-500 μM (see Figures and Figure legends). For the *in vivo* studies, phenformin was administered intraperitoneally at a concentration of 50 mg/kg daily (unless otherwise specified in Figure legends), the concentration was based on previous studies (Im et al. 2018, Hulea et al. 2018), in a 100 μl volume for a 25g mouse.

Small molecule complex I inhibitor, IACS-010759 (ChemieTek) was diluted to 10 mM in Dimethyl sulfoxide (DMSO) and stored at -80 °C . For *in vitro* experiments this stock was further diluted in DMSO 1/100 (5 μl aliquots + 495 μl), and cells were treated at a final concentration of 50 nM [413].

Metformin hydrochloride (Cayman Chemicals) powder (stored at -20°C) was resuspended in filter-sterilized PBS and stored for 4 weeks at 4 °C.

β-lapachone (Cayman chemicals) stock solution was dissolved in DMSO at a concentration of 100 μM (24.27 mg/ml) and frozen at -80°C for up to 4 months. For the *in vitro* experiments, β-lapachone was used at a final concentration of 0.5 μM-4 μM (see Figure legends) and DMSO served as the vehicle control.

For *in vivo* experiments, *β*-lapachone was dissolved in in 225 mg/ml hydroxypropyl-β-cyclodextrin (HPβCD) (Cayman Chemicals) in sterile PBS, protected from light, and heated to 70 °C for 3x 10 mins. *β*-lapachone/HPβCD was stored at room temperature, protected from light, for up to two weeks [576]. Mice were treated with either 5 mg/kg β-lapachone-HPβCD or

with 225 mg/ml HPβCD/PBS (vehicle control), every 2 days, intraperitoneally. For *in vivo* studies, β-lapachone-HPβCD and HPβCD/PBS control treatment were started two days prior to start of phenformin (or PBS) treatment.

Buthionine sulfoximine (BSO) (Cayman chemicals) was resuspended in PBS to 40 mg/ml and heated at 37°C to dissolve. BSO stocks were stored at -20°C for 3 months and thawed to 37°C prior to use.

MitoTEMPO (Sigma) stock was either prepared in DMSO (allowing for longer storage) or in PBS (2 weeks maximum storage at 4°C), see figure legends. For the *in vitro* studies, MitoTEMPO was used at final concentration ranging from 5-10 μM. Cells were pre-treated with MitoTEMPO for 24 hours prior to the start of drug treatments and MitoTEMPO-containing media was changed every 24 hours thereafter. For the *in vivo* experiment, mice were treated with 3 mg/kg MitoTEMPO (or PBS control), in combination with polyIC and phenformin or with PBS as a control.

Mouse and human recombinant interferon gamma (IFNγ) (R&D systems) were resuspended in PBS and stored at -80°C. Prior to use, aliquots were thawed at room temperature and diluted. Final concentration of IFNγ was 1 ng/ml unless otherwise specified in the figure legends.

Polyinosinic-polycytidylic acid (polyIC) high molecular weight form (InvivoGen) was prepared as per manufacturer's protocol and stored at -20°C. Single use aliquots were prepared to avoid freeze/thaw cycles. For the *in vivo* experiments, mice were treated with 50 μg of polyIC per mouse, every 2 days, intraperitoneally, (50 μl), or with saline control. PolyIC treatment was started two days prior to start of phenformin treatment. This dose of polyIC was selected based on a previous report [577]. Treatment was started two days prior to the start of phenformin (or PBS) treatment.

For the immune checkpoint inhibitor studies, 100 μg of neutralizing anti-PD1 antibody (clone RMP1-14, BioXCell) was injected intraperitoneally every 3 days. Isotype control IgG (InVivoMAb Rat IgG2a, clone 2A3, BioXCell) was injected using a similar dosing schedule for control groups.

For the oncolytic virus VSV (MΔ51) studies, the viral preparation was administered through two consecutive intra-tumoral injections of $1x10^7$ particle forming units (PFU) per tumor in total volume of 50 μl PBS, administered 24 hours apart. Sterile PBS was injected intra-tumorally as the control.

2.6 *In vitro* viability counts

Cell lines were plated in 24 well plates at a density of 2.0-6.0 x10^4 per well. After 24 hours, cells were incubated with drugs (as described above) and/or with media containing different concentrations of glutamine and glucose (described below) for the indicated time periods (see Figure legends). After incubation, cells were washed in PBS, adherent cells were trypsinized and resuspended in media and live cells were quantified by trypan blue exclusion using a hemocytometer.

2.7 Glucose and glutamine deprivation

Cells were incubated with treatments in either glucose-free DMEM media (supplemented with sodium pyruvate to 1mM), or glutamine-free DMEM combined with complete DMEM media to attain final percent concentrations of glucose and glutamine, respectively (see Figure legends); each base media was supplemented with 2.5 % FBS, MEGS, penicillin/streptomycin and gentamycin, as described in cell culture section above. Cells were then treated with IFNγ or PBS control for 48 hours, after which viability was determined.

2.8 Immunohistochemistry

Tumor pieces were fixed in 10% neutral buffered formalin immediately after euthanasia for 18-24 hours at room temperature, and then washed and stored in 70% ethanol at 4°C until paraffin embedding at the Lady Davis Institute Pathology Core. Paraffin-embedded sections (5 µm) were made with a microtome and mounted on glass microscope slides and left to dry overnight at room temperature. Antigen retrieval was performed in 10mM Sodium Citrate buffer in distilled water, pH adjusted to 6.0 with 1N HCl, supplemented with 0.05% Tween 20) in a pressure cooker for 12 minutes, and cooled on ice for 30 minutes. Slides were then washed 2 x 5-minutes with TBST (TBS/0.05% Tween 20), rinsed 2x in TBS and blocked for 10 mins each with unconjugated Avidin followed by unconjugated Biotin (Biolegend). After another 5 min TBST wash, slides were blocked with 10% BSA/TBS and then incubated with primary antibody in 2% BSA/TBS overnight at 4ºC. Details of the primary antibodies used can be found in Table 2.1. Slides were subsequently washed in TBST (3 x 5 mins), blocked with freshly diluted 3% Hydrogen peroxide, washed 2x 5 mins and incubated with the appropriate biotinylated secondary antibody in 2% BSA/TBS for one hour at room temperature. Slides were again washed in TBST (3x 5 mins), rinsed 1x TBS, and incubated for 30 mins with avidin/biotinylated complex reagent (Vectastain®, Vector Laboratories). This was followed by timed incubation with

DAB reagent (Vector Laboratories) for development which was stopped with tap water. For the mouse antibody 8 oxo-dG antibody there was no antigen retrieval step, and the slides were instead stained using Mouse on Mouse polymer kit (Abcam), as per manufacturer's protocol. All slides were then dehydrated, counterstained with 20% hematoxylin Fisher Scientific and mounted with ClearMount™ media (StatLab). Slides were then scanned with a ScanScope XT Digital Slide Scanner (Aperio). Images were analysed with the ImageScope software (Aperio) using positive pixel count or IHC nuclear algorithms.

Table 2.1 Antibody information used for immunohistochemical staining of paraffin-embedded sections

Antibody	Company	Identifier	Dilution	Antigen retrieval buffer
STAT1 p84/p91 (E-23)	Santa Cruz	Sc346	1:750	Citrate
Ki67	Abcam	ab15580	1:500	Citrate
Cleaved Caspase-3 (Asp175)	Cell Signaling	9661	1:250	Citrate
8 oxo-dG[1]	Trevigen	4354-MC-050	1:2000	No retrieval
Phosphorylated-AMPK α (Thr172)	Cell Signaling	2535	1:100	Citrate
Anti-Granzyme B	Abcam	ab4059	1:300	Citrate
Biotinylated anti-Rabbit [58]	Vector Laboratories	BA-1100	1:1000	N/A

[1] Mouse on Mouse polymer kit used instead of secondary anti-Rabbit

Table 2.2 Antibody conditions used for immunoblot analysis

Antibody	Company	Identifier	Dilution
Anti-STAT1 (D4Y6Z)	New England Biolabs	14995S	1:1000
Anti-phosphoY701- STAT1 (58D6)	New England Biolabs	9167S	1:1000
Anti-Tubulin	Sigma	T5168	1:10000
Anti-Actin (H-6)	Santa Cruz Biotechnology	sc-376421	1:10000
Anti-NQO1 for human (clone: A180) (anti-mouse)	Santa Cruz Biotechnology	sc-32793	1:500
WB:Anti-NQO1 (for Mouse)	Abcam	ab34173	1:1000

2.9 Immunoblot

2.9.1 Tumor lysates of lung cancer brain metastases

PDX models of lung cancer brain metastases were established as previously described [578, 579]. Fresh surgically resected brain metastasis patient material was received from the neurosurgery operating room at the Montreal Neurological Institute Hospital. Tumor fragments were expanded as patient-derived xenografts in the subcutaneous flank of NSG mice (The Jackson Laboratories, Strain # 005557). Once tumors reached a size of >250 mm^3, mice were euthanized, and tumors were flash frozen in liquid nitrogen. Flash frozen tumor pieces from GCRC PDX models of lung cancer brain metastases were crushed in liquid nitrogen and then lysed in 200ul to 500uL RIPA buffer (10 mM Na phosphate [pH 7.0], NaCl 150 mM, NP-40 1.0%, SDS 0.1%, Na Deoxycholate 1.0%, NaF 10 mM, EDTA 2 mM, 5 mM $NaVO_4$, PIN: 1 µg/ml Chymostatin, 2 µg/ml Antipain, 2 µg/ml Leupeptin, 1 µg/ml Pepstatin, 2 µg/ml Aprotinin.), and mixed by pipetting multiple times.

2.9.2 Whole cell lysates

After washing cells with PBS, whole cell lysates were prepared on ice by lysing cells with PLCγ buffer (50 mM HEPES [pH 7.5], 150 mM NaCl, 10% glycerol, 1% Triton X-100, 1 mM EGTA [pH 8.0], 1.5 mM MgCl2, 5 mM $NaVO_4$, 5 mM NaF, and PIN: 1 µg/ml Chymostatin, 2 µg/ml Antipain, 2 µg/ml Leupeptin, 1 µg/ml Pepstatin, 2 µg/ml Aprotinin) for 10 minutes on ice, unless otherwise specified.

Both whole cell and tumor lysates were centrifuged at 16,000 x g, at 4ºC for 10 min. Protein concentration was measured by Biorad Protein assay, colorimetric assay and the Synergy Hybrid plate reader. Lysates were then separated by SDS-PAGE and transferred onto polyvinylidene difluoride (PVDF) membranes. Membranes were then blocked in 3% Bovine Serum Albumin (Bioshop) or 5% milk in TBST and probed with antibodies as listed in Table 2.2. Secondary antibodies conjugated to horseradish peroxidase (1:10,000) and ECL (Thermo Fisher) or Luminata Forte HRP substrate (Millipore Sigma) were used for protein detection. Densitometric quantification of the immunoblots was performed with the Image J software.

2.10 Flow cytometry

Cells were plated in 60 mm dishes, (0.5 or $1.0x10^6$ cells) and treated with various drug combinations (see Figure legends). Cells were rinsed with PBS and then trypsinized and counted. After the specific staining protocol outlined below, cells were analyzed with the BD LSR Fortessa. Appropriate single stained and unstained controls were used for each experiment. Analysis was performed with Flow Jo Software Version 10.

2.10.1 MitoSOX™ Red Mitochondrial superoxide indicator

On the day of the experiment, MitoSOX™ (Invitrogen) was prepared in DMSO to make a 5mM stock, protected from light. This was then diluted in PBS to make 2 µM working stock, as determined by titration experiments for MDAMB231 and MT4788 cells.

After the indicated treatment time, cells from each condition were washed in PBS, gently trypsinized, and then counted. 5×10^5 cells in suspension were distributed in individual labelled falcon tubes and then were centrifuged at 100 g for 3 minutes at room temperature. PBS was gently aspirated, and cell pellets were each gently resuspended in 1 ml MitoSOX working stock with 1 ml of working stock of MitoSOX™ for 10 mins at 37 °C and protected from light. Cells were then washed with PBS, stained with a final concentration of 2.5 µg/ml DAPI (Vector laboratories) prepared in PBS in 100 µl volume, for at least 10 minutes, protected from light, prior to timely flow cytometric analysis with the BD LSRFortessa. MitoSOX fluorescence was detected by excited cells with the blue (488 nm) laser and detected with the 585/42 bandpass filter with the 550-LP dichroic mirror; whereas DAPI was detected by exciting cells with the violet (405 nm) laser and detected with the 450/50 bandpass filter. Cells heated at 65 °C for 3 mins were used as the positive control for DAPI staining, and H_2O_2 treated cells were used as MitoSOX positive controls. Gating strategy can be found in Figure 2.1a.

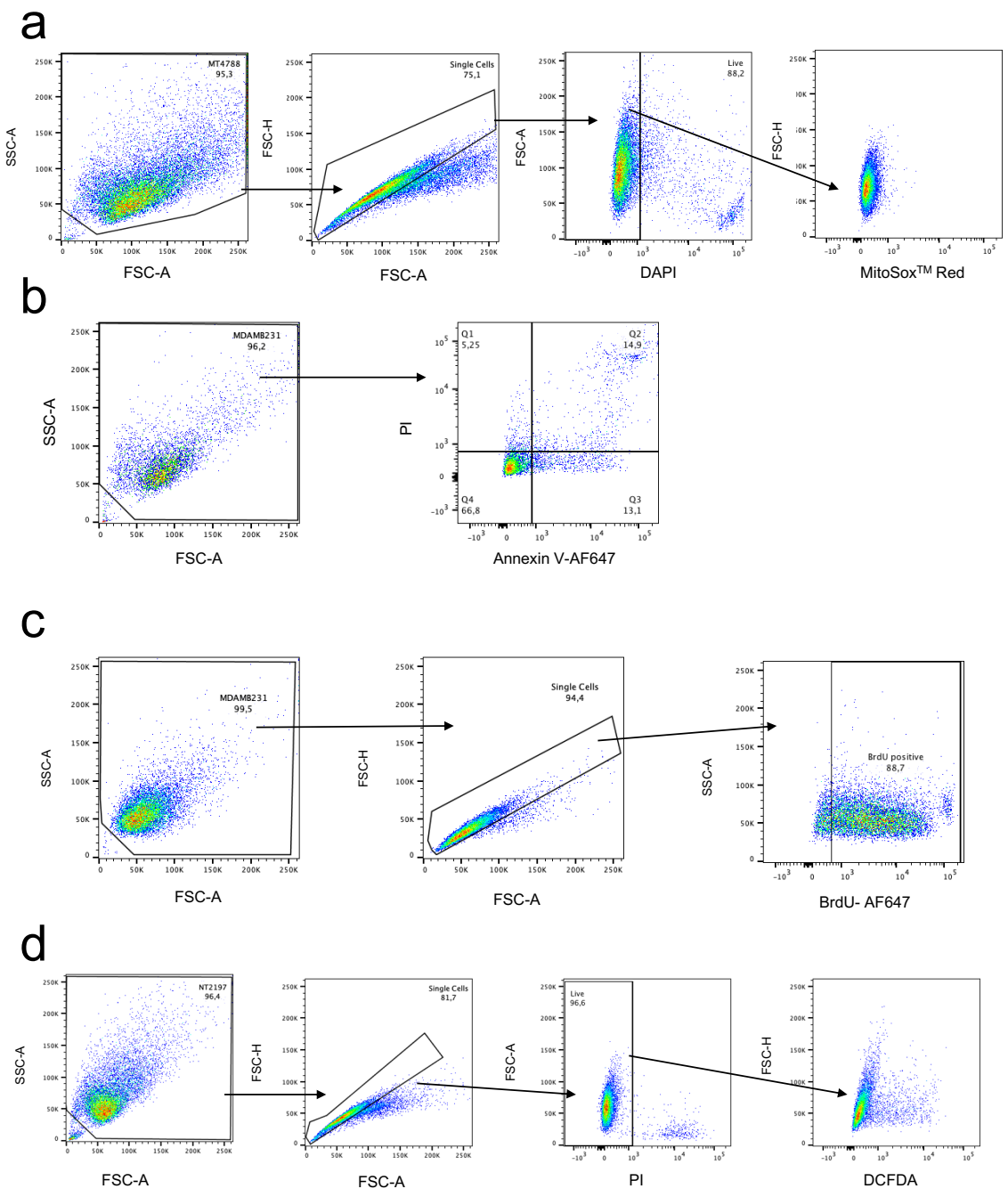

Figure 2.1: Gating strategies for flow cytometry experiments

(a) Gating strategy for *MitoSOX™ Red Mitochondrial superoxide indicator* experiments (Figures 3.8a, 3.8b)

(b) Gating strategy for Annexin V and PI experiments (Figures 3.11f, 3.11g, 3.16d)

(c) Gating strategy for BrdU incorporation assay gating was performed (Figures 3.11h, 3.16e)

(d) Gating strategy for DCFDA experiments (Figures 3.8c, 3.8d, 3.8e, 3.12 b, 3.18a; 3.19b)

2.10.2 Apoptosis assay

Cells from each treatment group were first washed in PBS, trypsinized and counted. After centrifugation, cell pellets were resuspended in Annexin V binding buffer (BD Pharmingen) at 1x 10^5 cells/100 µl. 100 µl of this cell suspension was stained with 5 µL of Annexin V-Alexa Fluor®-647 (AF647) (Biolegend) antibody for 15 mins and then 0.25 µg/ml propidium iodide (PI) (BD Biosciences) was added to each flow cytometry tube and incubated in the dark for 15 mins. Samples were then analyzed by flow cytometry with BD LSR Fortessa. Annexin V-AF647 fluorescence was detected with excitation with the red (633 nm) laser and detection with the 670/14 bandpass filter. PI fluorescence was detected with excitation with the yellow-green (561 nm) laser and detection with the 610/20 bandpass filter. Gating strategy can be found in Figure 2.1b.

2.10.3 Proliferation assay

Cells from each condition were cultured with 0.5 µl/ml of media 5-bromo-2'-deoxyuridine (BrdU) for 18 hours prior to the end of the experiment. Cells were rinsed with PBS, trypsinized and then washed twice with PBS. Cells were then stained as per the Phase-flow BrdU proliferation kit for Flow Cytometry (Biolegend) manufacturer's protocol. Specifically, cell suspensions were centrifuged at 200 g, supernatant was removed, and cell pellet was fixed by gently resuspending in 100ul Buffer A at 4 ºC for 20 mins, and then cells were washed with 3% BSA/PBS. After being centrifuged at 200 g, cell pellets were resuspended in 1 ml of 90% FBS-10% DMSO, and then stored at -80 °C for maximum 1 week, until the day of flow staining and analysis. Cells were then thawed at 37 ºC, counted, and 1x10^6 cells were aliquoted and washed with 2 ml of 1x Buffer B and centrifuged for 5 minutes at 200 g. This wash was carefully aspirated, leaving approximately 50 µl of liquid in each tube. Cell pellets were then permeabilized by resuspending in 100 µl of Buffer C and incubating at room temperature for 10 minutes. A repeated wash step with 1 ml 1x Buffer B was performed. Cell pellets were then fixed a second time by gently resuspending cells in 100 µl of Buffer A and incubating for 5 mins at room temperature. The wash step was repeated as above, and the supernatant was discarded. Cells were next incubated with 50 µl of DNAse (400 µg/ml stock) at 37 ºC for 1 hour and then stained with an anti-BrdU antibody-AF647 (included in kit), for 15 mins at room temperature in the dark, and then washed as above. Finally, cell pellets were resuspended in 100 µl of PBS and samples were analyzed promptly with the BD LSR Fortessa flow cytometer.

BrdU-AF647 fluorescence was determined with excitation with the red (633 nm) laser and detection with the 670/14 bandpass filter. Gating strategy can be found in Figure 2.1c.

2.10.4 General oxidative stress indicator

On the day of the experiment, CM-H2DCFDA (Invitrogen) was prepared in DMSO to make a 2mM stock, protected from light. This was then diluted further in PBS to make working stocks, such that cells would be incubated in appropriate final concentrations of CM-H2DCFDA, as determined by titration experiments: 0.5 μM (BT474); 2.5 μM (MDA-MB-231); 5 μM (MT4788); 1 μM for NT2197 and NMuMG.

After trypsinizing and counting treated cells, 1 x 10^6 cells of each condition in PBS were distributed in separate 15 ml labeled falcon tubes, and then centrifuged for 3 minutes at 100 g, at room temperature. PBS was then carefully aspirated, and the cell pellet was gently resuspended in 1 ml of working stock of CM-H2DCFDA (Invitrogen), as outlined above for individual cell lines. Cells were incubated with the CM-H2DCFDA probe for 30 mins at 37°C in the cell incubator and protected from light. Cells were then washed with PBS, and the pellet was resuspended in 100 μl volume of 0.25 μg/ml propidium iodide (PI) (BD Biosciences) in PBS, for at least 15 min, protected from light, prior to timely flow cytometry analysis with the BD LSR Fortessa.

DCFDA fluorescence was determined, with excitation with the blue (488 nm) laser and detection with the 530/30 nm bandpass filter (505LP dichroic filter); PI fluorescence was determined with excitation by the yellow-green (561 nm) laser and detection with the 610/20 bandpass filter. Cells heated at 65 °C for 3 mins were used as positive control for PI staining, and H_2O_2 treated cells were used as DCFDA positive controls. Gating strategy can be found in Figure 2.1d.

2.11 Seahorse real-time metabolic analysis

MT4788 STAT1-WT and MT4788 STAT1-KO cells were seeded at 15 000 cells in a Seahorse XF24 cell culture microplate (Agilent, ON, Canada). The next day, cells were treated for 24 hours with IFNγ (1ng/ml) or PBS (for MT4788 STAT1-WT, MT4788 STAT1-KO cells); or parental MT4788 cells were treated for 24 hours with IFNγ (1ng/ml), phenformin (500μM), either alone, or in combination, and PBS was used as the control (See Figure legends for treatment details). The Extracellular Acidification Rate (ECAR) and the Oxygen Consumption Rate (OCR) were determined using the Seahorse XFe24 Analyzer and Wave Desktop Software (Agilent), according to the manufacturer's instructions.

The sensor cartridge was incubated at 37°C with calibrant, overnight. On the day of the assay, cells were washed twice with PBS, and then incubated with supplemented Seahorse XF base medium (Agilent, ON, Canada) [Glucose (25mM), L-Glutamine (4mM) and Sodium pyruvate (1mM), adjusted to pH 7.4 and filter-sterilized 0.2μM], with appropriate treatments in a CO_2-free incubator at 37°C for 1 hour. During this incubation time, Oligomycin, FCCP, Rotenone/Antimycin and Monensin were pipetted into the injection ports of the sensor cartridge to obtain desired final concentrations. The cell culture plate and with the sensor cartridge were combined and loaded in the XFe24 Analyzer. OCR and ECAR were determined at baseline and following the sequential injection of 1 mM Oligomycin, 1 mM FCCP (Fluoro-Carbonyl Cyanide Phenylhydrazone), 0.5 mM Rotenone/Antimycin A and 20 mM Monensin, (Sigma-aldrich). Readings were taking over 3 minutes, after 3 mins of mixing and 3 minutes of pause.
The rates of ATP production (by glycolysis, J_{ATP} glycolysis, and by OXPHOS, J_{ATP} oxidative) were calculated by adding monensin, as described in [580]. All measurements were normalized to the number of cells, as determined by parallel cell counts for each treatment on the day of each biological repeat.

2.12 Gas Chromatography-Mass Spectrometry (GC-MS)

MT4788 STAT1-WT (vector control) and MT-STAT1-KO cells; or MT4788 parental cells were seeded in 6-well plates and incubated overnight. The following day, cells were treated with either IFNγ (1ng/ml), phenformin (500 μM), or the two in combination, or PBS (control) for 36 hours. To extract metabolites, at approximately 80% confluency, the cells were washed twice in cold saline solution (NaCl, 0.9g/L) and then were quenched with 600 mL of 80% iced methanol on dry ice. Following 10 minutes of sonication on slurry ice using a bath sonicator (Biorupter) with the cycling 30 seconds on/off at the highest settings, the homogenates were centrifuged at 14,000g at 4°C for 10 minutes. Supernatants were collected and supplemented with 750 ng of myristic acid-D_{27} (an internal standard; Sigma-Aldrich) and dried overnight in cold vacuum centrifuge (Labconco). The dried samples were reconstituted with 30 mL of methoxyamine-HCl (10 mg/mL dissolved in pyridine; Sigma-Aldrich) and incubated for 30 minutes at room temperature. Next, the samples were derivatized with MTBSTFA (Sigma-Aldrich). Following a 1-hour incubation at 70°C, 1 μL of each derivatized sample was then injected into the GC-MS instrument (5975C, Agilent). Data were acquired in Scan mode and analyzed with MassHunter software (Agilent) as described previously [409, 581]. The level of each metabolite was normalized by the intensity of myristic acid-D27 and average cell number of the 3 independent

wells per treatment that were ran in parallel on the day of each separate biological repeat experiment.

2.13 Liquid Chromatography-Mass Spectrometry (LC-MS)

MT4788 STAT1-WT (vector control) and MT-STAT1-KO cells were seeded in 6-well plate and were treated with IFNγ (1ng/ml) and phenformin (500 μM) alone or in combination; or PBS (control) for 36 hours. At about 80% confluency, cells were washed three times with 150 mM ice cold ammonium formate and scrapped on dry ice using two different conditions.

For GSH & GSSG extraction, cells were scraped followed by the addition of 50% HPLC-grade methanol, 220 mL of ice-cold Acetonitrile (Fisher) were added to the slurry and then homogenized using the beat beater. After bead beating, 600 mL of ice-cold dichloromethane (Fisher) and 300 mL of HPLC-grade water were then added to the homogenates, following by 10 minutes centrifugation at 1500 x g at 1°C. The upper aqueous phase was transferred to a new tube and left to dry overnight by vacuum centrifugation with sample temperature controlled at -4^{o}C (Labconco).

For NADH/NAD^{+}/NADPH/NADP^{+} extraction, cells were scraped into 600 mL 80% HPLC grade methanol and allowed to rest at -80 °C overnight. Samples were then homogenized by bead beating. A volume of 600 mL of ice-cold dichloromethane (Fisher) and 300 mL of HPLC-grade water were then added to the homogenates, followed by 10 minutes centrifugation at 1500 x g at 1°C. The upper aqueous phase was transferred to a new tube and left to dry overnight as above.

All targeted analyses were carried out on an Agilent 6430 Triple quadrupole QQQ; 1290 Infinity ultra-performance LC System equipped with a Scherzo SM-C18 column 3 μm, 3.0×150 mm (Imtakt Corp, JAPAN) at 10^{o}C. Multiple reaction monitoring (MRM) transitions were optimized on authentic standards. Data were quantified by integrating the area under the curve of each compound using MassHunter Quant (Agilent Technologies). Relative concentrations were determined from external calibration curves prepared in water. No additional corrections were made for ion suppression or enhancement, thus relative metabolite responses are presented. Data were analyzed using MassHunter Quant (Agilent Technologies)

For GSH & GSSG measurements, dried samples were then solubilized in 35 mL HPLC-grade H_2O and 25x dilutions prepared. A volume of 5 mL injected into LC-MS where GSH and GSSG were chromatographically separated at a flow rate of 0.4 ml/min by starting with 100% solvent A (0.2% formic acid in water) for two minutes. The gradient was then increased to 80% solvent B (0.2% formic acid in methanol) over a period of 6 min. Solvent B was increased to

100% for column washing for 5 min then re-equilibrated to 100% A for 6 min before the next injection. The electrospray ionization (ESI) source and samples were analyzed in positive ionization mode. MRM transitions quantifier and qualifier ions were respectively 308.1 → 179.0 and 308.1 → 76.0 for reduced glutathione, and 613.2 → 355.1 and 613.2 → 231.0 for oxidized glutathione. Ion source gas temperature and flow were set at 350°C and 10 L/min respectively, nebulizer pressure was set at 40 psi and capillary voltage was set at 3500V.

For NAD, NADH, NADP and NADPH measurements, chromatographic separation was achieved using a chromatographic gradient started at 100% mobile phase A (50 mM ammonium acetate / 50 mM NH_4OH : 9/1, pH 8.6) for 2 min followed by a 8 min gradient to 40% B (100 mM ammonium acetate / 100 mM NH_4OH : 9/1, pH 8.6) / ACN : 80/20) at a flow rate of 0.4 mL/min. This was followed by a 5 min hold time at 100% mobile phase B and a subsequent re-equilibration time (6 min) before next injection. For these analyses, individual samples were re-suspended and run immediately to minimize loss of NADH and NADPH. A sample volume of 10 µL was injected. The mass spectrometer was equipped with an electrospray ionization (ESI) source and samples were analyzed in positive ionization mode. MRM transitions quantifier and qualifier ions were respectively 664.1 → 135.9 and 664.1 → 428.1 for NAD, 666.1 → 514.0 and 666.1 → 136.0 for NADH. Ion source gas temperature and flow were set at 350°C and 10 l/min respectively, nebulizer pressure was set at 40 psi and capillary voltage was set at 3500V.

2.14 *NQO1* knock-down and overexpression

HEK293T were seeded in 6 cm culture dishes, and at 80% confluency were transfected with 2 µg shRNA constructs targeting mouse *Nqo1* or human NQO1 or non-Mammalian shRNA control plasmid DNA (pLKO.1 or pLKO.5) and 2 µg packaging plasmids PsPAX2, PMD2.G (Addgene) using calcium phosphate precipitation. See Table 2.3 for nucleotide sequences of shRNAs. shRNA-containing plasmids were obtained through McGill's Genetic Perturbation Service. For Figure 3.15c and d, pooled human (#1-5) and mouse (#1-3) shRNAs were used with pLKO.1 as the control. For Figure 3.15e, f Human shRNA #1 and #2 were separately used, with pLKO.5 as the control. Media was replaced after 24 hours and then after 12hours, virus containing media was collected and filtered through a 0.45uM syringe filter. After replenishing the media, the virus containing media was collected again 12 hours later and filtered. MT4788, BT474 and MDA-MB-231 cells were plated in 6 cm culture dishes, and incubated with shRNA lentiviral supernatant, 1 in 2 dilution with fresh media with Polybrene (4 µg/ml) (Sigma). After 12-16 hours, lentiviral supernatant was then replaced by fresh media and then selected with

Puromycin 2 μg/ml (Thermo Fisher Scientific). Transduced cells were promptly used for both RT-qPCR confirmation of knockdown and for cell counts in parallel.

For the overexpression studies, the mouse NQO1 cDNA was PCR amplified from NQO1 cDNA ORF Clone expression plasmid (Sino Biological) and inserted into pQCXIP plasmid (Clontech) via NotI and EcoRI sites added during the amplification. See Table 2.3 for sequences. Phoenix cells were transfected with this construct or pQCXIP vector also using calcium phosphate precipitation. MT4788 cells were then transduced with the retroviral supernatant, as described above.

2.15 Reverse transcription quantitative real-time PCR (RT-qPCR)

Total RNA for RT-qPCR analysis was isolated from cell lines grown in 6 well plates, using TRIzol reagent (Invitrogen) according to the manufacturer's protocol. RNA concentration was determined using a Synergy Hybrid plate reader. With the same input RNA concentration among all samples, complementary DNA was synthesized with SSII (Life technologies) as per the manufacturer's protocol, using Random Primers (New England Biolabs). Quantitative RT-PCR was performed with EvaGreen 2x qPCR mixture (Diamed) and primers listed in Table 2.3. For Figure 3.1c, Taqman MasterMix 2x (Life Technologies) including tap1 primers were used. For Figure 3.14 with 5X All-in One RT MasterMix (Applied Biological Materials Inc).

2.16 RNA sequencing

MT864 and MT4788 (STAT1-WT and STAT1-KO) cell lines were cultured for 24 hours with IFNγ (1ng /ml). Total RNA was extracted using RNeasy Midi Kits (QIAGEN). RNA sequencing was performed at the McGill University and Genome Quebec Innovation Centre. RNA quality was assessed by Agilent 2100 Bioanalyzer (Agilent Technologies). Libraries for RNAseq were prepared according to strand-specific Illumina TruSeq protocols. Samples were multiplexed at four samples per lane and sequenced on an Illumina HiSeq 2500 PE125 instrument.

Raw reads were trimmed using Trimmomatic v0.32 [582]. First, adaptors and other Illumina-specific sequences from each read were removed using palindrome mode. Then, a four-nucleotide sliding window removes the bases once the average quality within the window falls below 30. Next, the first four bases at the start of each read were removed. Finally, reads shorter than 30 base pairs were dropped. Cleaned reads were aligned to the mouse reference genome build mm10 using STAR v2.3.0e [583] with default settings. Reads

mapping to more than 10 locations in the genome (MAPQ < 1) were discarded. Gene expression levels were estimated by quantifying uniquely mapped reads to exonic regions (the maximal genomic locus of each gene and its known isoforms) using featureCounts [584] (v1.4.4) and the Ensembl gene annotation set. Normalization (mean of ratios) and variance-stabilized transformation of the data was performed using DESeq2 [585] (v1.14.1). Multiple control metrics were obtained using FASTQC (v0.11.2), samtools [586] (v0.1.20), BEDtools [587] (v2.17.0) and custom scripts.

Table 2.3 Nucleotide sequences of primers used for RT-qPCR, ChIP-PCR analysis and subcloning, and sequences shRNAs.

Application	Gene	Species	Sequence	Identification number
RT-PCR	*β-ACTIN*	Human	Forward: TGCTATCCCTGTACGCCTCT Reverse: TAATGTCACGCACGATTTCC	
RT-PCR	*IRF7*	Human	Forward: TACCATCTACCTGGGCTTCG Reverse: AGGGTTCCAGCTTCACCA	
RT-PCR	*NQO1*	Human	Forward: GGGATCCACGGGGACATGAATG Reverse: ATTTGAATTCGGGCGTCTGCTG	
RT-PCR	*CXCL9*	Human	Forward: GAGTGCAAGGAACCCCAGTAGT Reverse: TTGTAGGTGGATAGTCCCTTGGTT	
RT-PCR	*STAT1*	Human	Forward: CGGCTGAATTTCGGCACCT Reverse: CAGTAACGATGAGAGGACCCT	
RT-PCR	*GAPDH*	Human	Forward: TGCACCACCAACTGCTTAGC	

			Reverse : GGCATGGACTGTGGTCATGAG	
RT-PCR	*β-Actin*	Mouse	Forward: GGCTGTATTCCCCTCCATCG Reverse: CCAGTTGGTAACAATGCCATGT	
RT-PCR	*Erap1*	Mouse	Forward: TAATGGAGACTCATTCCCTTGGA Reverse: AAAGTCAGAGTGCTGAGGTTTG	
RT-PCR	*Gapdh*	Mouse	Forward: AACGACCCCTTCATTGAC Reverse: TCCACGACATACTCAGCAC	
RT-PCR	*Irf9*	Mouse	Forward: GCCGAGTGGTGGGTAAGAC Reverse: GCCGAGTGGTGGGTAAGAC	
RT-PCR	*Nqo1*	Mouse	Forward: TTCTGTGGCTTCCAGGTCTT Reverse: AGGCTGCTTGGAGCAAAATA	
RT-PCR	*Psmb8*	Mouse	Forward: GTGCAGGTTGTATTATCTTCGGA Reverse: CGAGTCCCATTGTCATCTACG	
RT-PCR	*β2m*	Mouse	Forward: TGGTCTTTCTGGTGCTTGTCT Reverse: ATTTTTTTCCCGTTCTTCAGC	
RT-PCR	*Tap1*	Mouse	Mm00443188_m1 (ThermoFisher Scientific)	

shRNA	*Nqo1*	Mouse	(Gene ID: 18104) #1: CCGGCCATCAAGATTCGTTGTCTATCTC GAGATAGACAACGAATCTTGATGGTTTT TG	TRCN0000 041863
shRNA	*Nqo1*	Mouse	(Gene ID: 18104) #2: CCGGCCGAGTCATCTCTAGCATATACT CGAGTATATGCTAGAGATGACTCGGTT TTTG	TRCN0000 041864
shRNA	*Nqo1*	Mouse	(Gene ID: 18104) #3: CCGGCCCATTCAGAGAAGACATCATCT CGAGATGATGTCTTCTCTGAATGGGTTT TTG	TRCN0000 041867
shRNA	*NQO1*	Human	(Gene ID:18104) #1: CCGGTGGAAGAAACGCCTGGAGAATCT CGAGATTCTCCAGGCGTTTCTTCCATTT TTG	TRCN0000 350361
shRNA	*NQO1*	Human	Gene ID:18104) #2: CCGGTGGAAGAAACGCCTGGAGAATCT CGAGATTCTCCAGGCGTTTCTTCCATTT TT	TRCN0000 003768
shRNA	*NQO1*	Human	(Gene ID:18104) #3: CCGGAGACCTTGTGATATTCCAGTTCT CGAGAACTGGAATATCACAAGGTCTTTT TT	TRCN0000 003769
shRNA	*NQO1*	Human	(Gene ID:18104) #4: CCGGAGAAAGGACATCACAGGTAAACT CGAGTTTACCTGTGATGTCCTTTCTTTT TT	TRCN0000 003766
shRNA	*NQO1*	Human	(Gene ID:18104) #5: CCGGCATGTTATCAAATCTGGGTATCTC GAGATACCCAGATTTGATAACATGTTTT T	TRCN0000 003770
shRNA	-	Non-mammalian	MISSION® PLKO.1-Puro Non-Mammalian shRNA control plasmid DNA	SHC002

shRNA	-	Non-mammalian	MISSION®PLKO.5-Puro Non-mammalian shRNA control plasmid DNA	SHC202
ChIP-PCR	*Irf1* Promoter	Mouse	Forward: CTTAACAGCAGGGGAAACCA Reverse: CACCCACTCCAATCCAGTCT	
ChIP-PCR	*Irf1* TSS	Mouse	Forward: CAGTCTAAGCCGAACCGAAC Reverse: GAAAGATGCCCGAGATGCT	
ChIP-PCR	*Nqo1* Intron1	Mouse	Forward: TGAGTCCACCACAGCCATAA Reverse: CAGAGGCAAAGCACACAGAA	
ChIP-PCR	*Nqo1* Promoter	Mouse	Forward: CCAAGACCTCCTGGGTACAA Reverse: CACGGCTGAGTGAGGACTAA	
ChIP-PCR	*Nqo1* TSS	Mouse	Forward: AGGGAGTGGCAGCTCTGTTA Reverse: ATTCTGCAGCCCAAGTTCAC	
ChIP-PCR	*NQO1* TSS	Human	Forward: CCTGAGGTCAGGAGTTCGAG Reverse: TCCCGAGTAGCTGGGACTTA	
ChIP-PCR	*NQO1* Promoter	Human	Forward: CCTGAGGTCAGGAGTTCGAG Reverse: TCCCGAGTAGCTGGGACTTA	
ChIP-PCR	*NQO1* Intron1	Human	Forward: AGAGCGAATTGCCAGAGAAA Reverse: GTTGCAGATGCCTTCTCTCC	
ChIP-PCR	*NQO1* TSS	Human	Forward: TTCCCTTTGTGGGTTTTGAG Reverse: GTCGTCTCTCGAGCACTGGT	
Subcloning	*NQO1 cDNAORF*		Forward: AAAGCGGCCGCATGGCGGCGAGAA Reverse: CCCCCCCGAATTCTTATTTTCTAGCTTTGATCTGGTTG	

shRNAs were obtained from McGill University's Genetic Perturbation Service and Dr. Sidong Huang

MISSION® shRNA library available through Sigma-Aldrich.

2.17 Chromatin immunoprecipitation and quantitative PCR (ChIP-qPCR)

MT4788, MDA-MB-231 and MDA-MB-436 cells grown in 15 cm dishes treated with PBS, or IFNγ (10 ng/ml) for 1 hour or 24 hours, such that at 70-80% confluency cells were fixed 10 minutes in 4% formaldehyde and stored at -80 °C. The pellets were subsequently resuspended in 1 ml of ChIP-buffer [0.25% NP-40, 0.25% Triton X-100, 0.25% Sodium Deoxycholate, 0.005% SDS, 50nM Tris (pH8), 100mM NaCl, 5mM EDTA, 1X PMSF, 2mM NaF, 1X P8340 Cocktail Inhibitor (Roche)] and sonicated with a probe sonicator (Fisher Scientific Sonic Dismembrator Model 500) using the following cycles: 5 cycles at 20% power, 5 cycles at 25% power, and 5 cycles at 30% power. Each cycle was 10 seconds, and the samples were kept on ice between each cycle to avoid overheating. Next, the samples were spun at high speed in a microcentrifuge for 30 minutes. Lysates were then collected and protein concentration was measured using the Bradford assay. Based on protein concentrations, samples were diluted to 2 mg/ml proteins in ChIP-buffer and 50 µl/ml of Protein G Plus-Agarose Suspension Beads (Calbiochem, IP04-1.5ML) were added for 3h to preclear. 2% of the sample was collected as input and kept at -20 °C until DNA purification. Immunoprecipitation was carried out at 4°C overnight with 1 ml of sample, 60 µl of beads and primary STAT1 antibody (CAT#14995S, see Table 2.2) or IgG control. The beads were then washed once with Wash1, Wash2, Wash3 [0.10% SDS, 1% Triton X-100, 2mM EDTA, 20mM Tris (pH 8), 150/200/500mM NaCl for Wash 1,2,3 respectively], Wash LiCl [0.25M LiCl, 1% NP-40, 1% Sodium Deoxycholate, 1mM EDTA, 10mM Tris (pH8)] and twice with TE buffer [10mM Tris (pH8), 1mM EDTA]. Then, beads were resuspended in elution buffer [1% SDS, 0.1M $NaHCO_3$]. The samples were decrosslinked overnight at 65 °C. 20 µg of Proteinase K (Sigma, # 39450-01-6) was added for 1 hour at 42 °C. Then, DNA was purified using BioBasic DNA collection column (BioBasic, #SD5005). Final ChIP-product was diluted in 60 µl of DNAse-free water. qPCR was performed with the ChIP product following the manufacturer protocol (GoTaq qPCR MasterMix 2X, Promega, #A600A). 2-ΔΔCT formula was used for quantification, normalized on a 2% chromatin input of each sample, and then compared between sites and conditions. Primer sequences used for DNA amplification can be found in Table 2.3.

2.18 Statistical Analysis and figure generation

Statistical analyses and generation of graphs were performed in GraphPad Prism 9 software, or Microsoft Excel, see details on statistical tests performed in Figure legends. Figures were combined in Microsoft Excel. Flow Cytometry analyses and statistics (Geometric fluorescent mean and percentages) were determined with FlowJo Software 10. Figure in

Chapter 1 were created with Biorender.com Premium account. Figure 1.3 was adapted from the *Electron Transport* template, Figure 1.7 was adapted from *Interferon Pathway* template Figure 1.5 was adapted from *Warburg Effect* template. See Figure legends for additional references.

Chapter 3: Results

3.1 Introduction to results

Cancer recurrence, either locally, regionally or distally, remains the leading cause of death for individuals with breast cancer and a clinical challenge [1, 2] [3]. The current treatments options for individuals with recurrent breast cancer are ineffective and limited, and therefore, there is an ongoing need to identify therapeutic strategies that elicit durable responses with minimal toxicity.

Cancer cells depend on the integration of diverse catabolic and anabolic pathways to meet energetic and biosynthetic requirements, as well as maintain redox balance, despite variations in the microenvironment including nutrient and oxygen availabilities. Most tumors rely on mitochondrial metabolism and oxidative phosphorylation, including many breast cancers. Given this, there is an ongoing interest in anti-tumor mechanisms of biguanides, that have been studied in various pre-clinical cancer models, resulting more recently in clinical trials for individuals with several cancer types. Biguanides such as metformin and phenformin function primarily by inhibiting complex I of the electron transport chain [372, 588]. Accordingly, they suppress oxidative phosphorylation, have been shown to activate AMPK (5' AMP-activated protein kinase), inhibit mTORC1 (mammalian target of rapamycin complex 1) signaling and translation in pre-clinical models [375], [589], [590],[591]. In spite of promising pre-clinical results, metformin had limited effects on progression free survival and pathologic response, in clinical trials [384, 385, 592]. There is accumulating evidence that phenformin is more suitable in oncology than metformin. Phenformin is a more potent complex I inhibitor than metformin, is more lipophilic than metformin, and does not requiring the organic cationic transport (OCT) to enter cells, unlike metformin [394, 395, 403]. Considering the metabolic flexibility of many tumors, rational combination therapies with complex I inhibitors are likely to be more effective in comparison to using these as single agents and may also allow for decreased concentrations of biguanides to be used [193, 593].

There is recent evidence that biguanides also promote antitumor immunity. Metformin was shown to increase CD8 positive tumor infiltrating lymphocyte (TIL) numbers and activation [594]. Phenformin treatment was shown to inhibit myeloid-derived suppressor cells and improve tumor sensitivity to PD1 blockade [405]. Further evidence highlighting the importance of the interplay between metabolism and immunology derives from literature on JAK/STAT signaling. Signal transducer and activator of transcription 1 (STAT1) is a transcription factor that is activated in response to interferons, and plays important and diverse roles in the immune cells

and tumors alike, including sensitizing tumors to immune checkpoint blockage [528], [532, 552]. More recently, STAT1's roles in modulating metabolism in both immune and tumor cells have gained attention. STAT1 activation in both tumor and mesenchymal cells has been shown to increase glycolysis [563, 564]. Yet, the role of STAT1 in metabolic regulation remains unclear.

With these concepts in mind, we decided to pursue an interesting finding that indicated that the pro-inflammatory cytokine IFNγ sensitizes multiple breast cancer cell lines to phenformin. This led us to explore a previously underappreciated role of phenformin in generating reactive oxygen species.

3.2 IFNγ-drive STAT1 activation sensitizes multiple breast cancer cell models to phenformin *in vitro*

Biguanides such as metformin and phenformin induce energetic stress in cancer cells by inhibiting complex I of the electron transport chain [588, 595, 596]. Previous work demonstrated that tyrosine kinase inhibitors reduce metabolic flexibility of cancer cells, sensitizing them to biguanides [569]. We recently showed that in breast cancers, tyrosine kinases-associated metabolic flexibility requires the ShcA adaptor protein [409]. Furthermore, breast cancer models with loss of phospho-tyrosine-dependent ShcA signaling (Y239F/Y240F/Y313F mutant), have an increased reliance on mitochondrial metabolism, revealing a susceptibility to phenformin [409]. Using cell lines established from polyoma virus Middle T-driven mammary tumors, cells with the non-phosphorylatable ShcA mutant (Y313F) are specifically sensitized to phenformin in comparison to ShcA WT cell lines (Figure 3.1a). Coupling this finding with previous observations that loss of pY313-dependent ShcA signaling increases STAT1 expression in breast cancer cells [570], we developed the hypothesis that tumors with elevated STAT1 signaling have increased sensitivity to phenformin treatment. We first confirmed that MT/Shc$^{313F/313F}$ breast cancer cells (MT6737 and MT6738) have basally elevated STAT1 levels compared to the ShcA$^{+/+}$ MT4788 and MT864 cell lines (Figure 3.1b).

IFNγ is an inflammatory cytokine that activates the STAT1 pathway both in tumor and immune cells [597]. While STAT1 levels are basally low in MT/ShcA$^{+/+}$ cells, IFNγ treatment increases STAT1 expression in these cells to levels comparable to that of MT/Shc$^{313F/313F}$ cells (Figure 3.1b). Given that high doses of IFNγ (100 ng/ml) elicit anti-proliferative responses in breast cancer cells [598], we selected a lower concentration of IFNγ (1 ng/ml) that induces STAT1 transcriptional responses, including *β2M* and *Tap1* (Figure 3.1c), but does not impair the growth of breast cancer cells alone (Figure 3.2a).

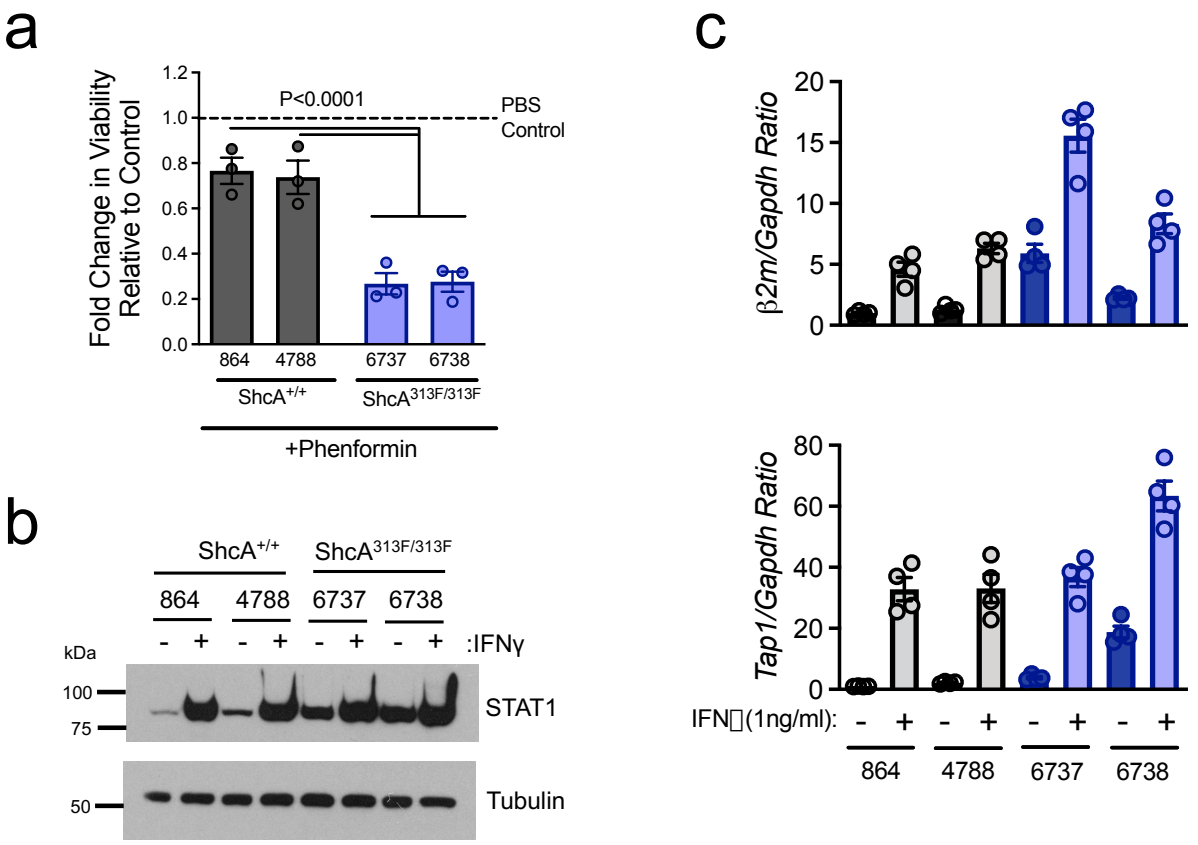

Figure 3.1: ShcA313F cell lines have increased sensitivity to phenformin and express higher baseline STAT1, compared to ShcA wild-type counterparts

(a) Viability of ShcA wild-type ($^{+/+}$) and ShcA313F cells treated with phenformin (500 μM) for 48 hours. Data is presented as fold change in viability compared to PBS-treated controls and is representative of *n*=3 independent (mean of means ± SEM).

(b) STAT1 immunoblot analysis of control and IFNγ-treated ShcA wild-type and ShcA313F cells. Tubulin is the loading control. Blot is representative of *n*=3 independent experiments.

(c) IFNγ target gene expression levels determined by RT-qPCR analysis in the indicated cell lines compared to PBS control, with *n*=4 technical repeats/condition. The data is reported as a ratio to GAPDH loading control (mean ± SD).

P values were calculated using one-way ANOVA with a Tukey's posthoc test (panel a).

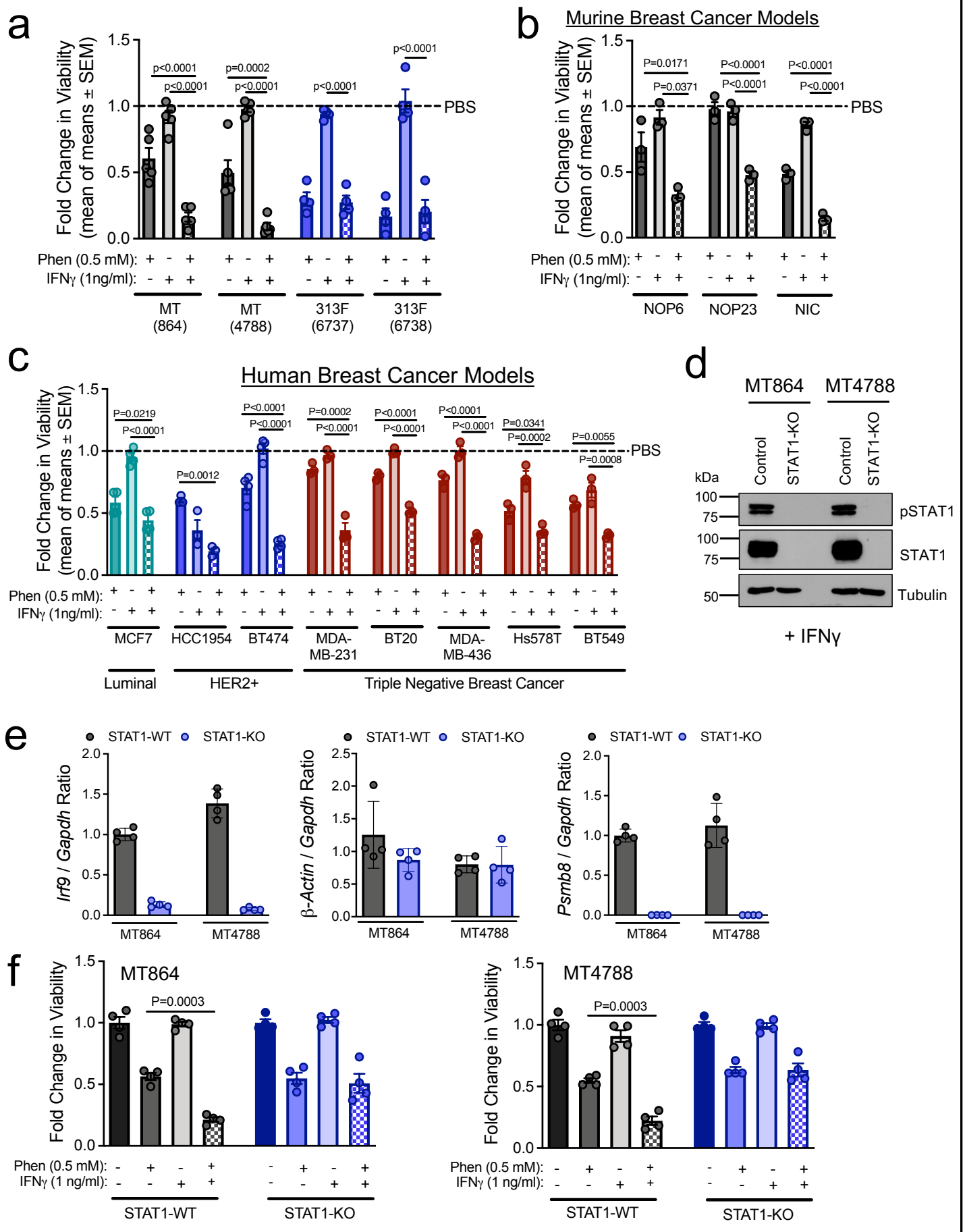
a
Fold Change in Viability (mean of means ± SEM)
PBS
p<0.0001
p<0.0001
p=0.0002
p<0.0001
p<0.0001
p<0.0001
Phen (0.5 mM):
IFNγ (1ng/ml):
MT (864)
MT (4788)
313F (6737)
313F (6738)
b
Murine Breast Cancer Models
P=0.0171
P=0.0371
P<0.0001
P<0.0001
P<0.0001
P<0.0001
NOP6
NOP23
NIC
c
Human Breast Cancer Models
P=0.0219
P<0.0001
P=0.0012
P<0.0001
P<0.0001
P=0.0002
P<0.0001
P<0.0001
P<0.0001
P=0.0341
P=0.0002
P=0.0055
P=0.0008
MCF7
HCC1954
BT474
MDA-MB-231
BT20
MDA-MB-436
Hs578T
BT549
Luminal
HER2+
Triple Negative Breast Cancer
d
MT864
MT4788
Control
STAT1-KO
kDa
100
75
pSTAT1
STAT1
50
Tubulin
+ IFNγ
e
STAT1-WT
STAT1-KO
Irf9 / Gapdh Ratio
β-Actin / Gapdh Ratio
Psmb8 / Gapdh Ratio
MT864
MT4788
f
MT864
MT4788
P=0.0003
Fold Change in Viability
Phen (0.5 mM):
IFNγ (1 ng/ml):
STAT1-WT
STAT1-KO

Figure 3.2: IFNγ-driven STAT1 activation sensitizes breast cancer cells to phenformin

(a-c) Viability of breast cancer cell lines after treatment with phenformin (500 μM) and IFNγ (1 ng/ml) alone or in combination, for 48 hours. Data is shown as a fold change in viability compared to PBS controls, (mean of means ± SEM) of independent experiments as follows: **(a)** Murine cell lines MT864, MT4788, *n*=5 independent experiments and ShcA313F cell lines: 6737 and 6738, *n*=4 independent experiments; **(b)** NOP6, NOP23, NIC, *n*=3 independent experiments **(c)** human breast cancer cell lines: MCF7 and BT474: *n*=4 independent experiments; HCC1954, MDA-MD-231, BT20, MDA-MB-436, Hs578T and BT549, *n*=3 independent experiments, (mean of means ± SEM).
(d) STAT1 and Y701-phosphorylated STAT1 immunoblot analysis of IFNγ-treated STAT1-WT and STAT1-KO cells, representative blot of *n*=3 independent experiments is shown.
(e) IFNγ target gene expression levels determined by RT-qPCR in indicated STAT1-WT and STAT1-KO cell lines, treated with IFNγ, *n*=4 technical repeats/condition. The data is shown as ratio with GAPDH used as loading control (mean ± SD).
(f) Viability of MT864 and MT4788 STAT1-WT and STAT1-KO cells treated with phenformin (500 μM), IFNγ (1 ng/ml) or PBS, alone or in combination, for 48 hours. Data is represented as a fold change in cell viability compared to respective PBS controls. Data is representative of 2 independent experiments, *n*=4 technical replicates each (mean ± SD).
P values were calculated using two-way ANOVA with a Tukey's posthoc test (panels a, b, c, f).

We observed that IFNγ treatment cooperates with phenformin to reduce the viability of MT breast cancer cells *in vitro* (Figure 3.2a). MT/ShcA313F cells. overexpressing STAT1, show increased phenformin sensitivity that is strikingly not further potentiated by IFNγ co-treatment (Figure 3.2a). We next explored the efficacy of this IFNγ and phenformin combination treatment in other breast cancer cells lines spanning the various molecular subtypes. We observed IFNγ and phenformin cooperatively elicit anti-tumorigenic responses in multiple murine ErbB2+ (NOP6, NOP23 and NIC) (Figure 3.2b) and human breast cancer cell lines representative of luminal (MCF7), HER2+ (HCC1954, BT474) and triple negative (MDA-MB-231, BT20, MDA-MB-436, Hs578T, BT549) disease (Figure 3.2c).

To address whether STAT1 was required for this increased sensitivity to IFNγ/phenformin combination treatment, we used STAT1-deficient MT cell lines (MT864, MT4788) previously generated by our group using Crispr/Cas9 genomic editing [570]. We first confirmed that IFNγ-stimulated, STAT1-deficient (STAT1-KO) cells are unable to induce STAT1 target genes, *Irf9* and *Psmb8*, in comparison to the vector control (STAT1-WT) counterparts (Figure 3.2e). We then compared phenformin and IFNγ combination treatment of STAT1-KO and STAT1-WT cell lines and found that STAT1 is required for IFNγ to sensitize breast cancer cells to the anti-tumorigenic effects of phenformin (Figure 3.2f). Taking together, these data demonstrate that IFNγ sensitizes multiple breast cancer cell lines, spanning distinct molecular subtypes, to phenformin in a STAT1-dependent manner.

3.3 In a STAT1-dependent manner, IFNγ and polyIC sensitize breast tumors to the tumoricidal effects of phenformin *in vivo*

We next addressed if IFNγ also sensitizes mammary tumors to the anti-neoplastic effects of phenformin in *in vivo* models of breast cancer. To address this, we first injected MT4788 cells into the mammary fat pads (MFP) of $IFN\gamma^{+/+}$ and $IFN\gamma^{-/-}$ mice, both on a pure FVB background [570]. When tumors reached 150 mm^3, mice were injected intraperitoneally with 50 mg/kg phenformin daily or PBS as the vehicle control, and tumor size was measured. Indeed, phenformin led to a 30% reduction in tumor size in $IFN\gamma^{+/+}$ an effect that was not observed in $IFN\gamma^{-/-}$ mice (Figure 3.3a). Given these findings and that IFNγ is required for immune surveillance of tumors, we aimed to clarify the relative importance of CD8-positive T lymphocytes in conferring increased sensitivity to phenformin. To do so, MT4788 breast cancer cells were injected into the mammary fat pads of $CD8^{+/+}$ or $CD8^{-/-}$ mice (also on a pure FVB background), and tumor-bearing mice were then treated with daily phenformin or PBS. $CD8^{-/-}$ mice lack cytotoxic T cell-mediated immunity, yet only a partial decrease in response of tumors to phenformin was observed compared to $CD8^{+/+}$ controls (Figure 3.3b). These results support that while IFNγ is required for tumor sensitivity to phenformin, CD8+ T cell immunity is insufficient to fully sensitize tumors to phenformin *in vivo*.

We next explored the ability of phenformin to enhance the efficacy of immune-based therapies that alleviate immune suppression. Immunocompetent MT4788 tumor-bearing mice were treated with phenformin and a PD1 neutralizing antibody (or isotype control), alone or in combination. Both phenformin and the anti-PD1 antibody single treatments inhibited tumor growth by 30%. However, only an additive effect of each on tumor size was observed in the combination treatment group (Figure 3.3c). VSV-M-(Δ51) is an oncolytic virus, which

selectively kills tumor cells, and does so in part, by augmenting anti-tumor immune responses [599]. Similarly, while VSV-M-(Δ51) and phenformin treatment alone elicited anti-tumor effects, there was no further decrease in tumor growth the combination treatment (Figure 3.3d). These data in the context of our *in vitro* findings, suggest that the ability of IFNγ to sensitize tumors to phenformin does not predominantly rely on the ability of the combination treatment to relieve immune suppression.

We therefore considered the possibility that therapies that induce STAT1-mediated inflammatory responses may increase the therapeutic efficacy of phenformin in breast cancer. Polyinosinic:polycytidylic acid (polyIC), a synthetic double stranded RNA analogue,is a toll-like receptor 3 (TLR3) and retinoic acid inducible gene I (RIG-I) receptor agonist [600]. Given that polyIC also induces IFN-driven STAT1 activation [601-603] we sought to assess whether polyIC treatment could sensitize breast tumors to phenformin. Employing the same MT4788 tumor models, we found that while polyIC treatment alone had no impact on MT4788 tumor growth, co-administration of polyIC with phenformin impaired the tumor growth (Figure 3.3e).

To address whether polyIC-driven sensitization to phenformin depends on STAT1 *in vivo*, we compared the growth of MT4788 STAT1-WT and STAT1-KO tumors upon treatment. Phenformin and polyIC combination treatment attenuated STAT1-WT tumors growth, however, had no effect against STAT1-KO tumors (Figure 3.3 f, g). This supports the notion that polyIC-driven sensitization of breast tumors to phenformin requires tumor-intrinsic STAT1 function. As a preliminary read-out of the toxicity of these treatment combinations, we weighed mice throughout the experiment. There were no significant changes in weights between treatment groups (Figure 3.3h).

We performed immunohistochemical (IHC) analysis and found that polyIC-treated tumors have increased STAT1 levels (Figure 3.4a) and phenformin-treated tumors elevated phospho-AMPK levels (Figure 3.4b). However, polyIC did not further increase AMPK phosphorylation (T172) and phenformin did not induce STAT1 expression in tumors treated with this drug combination (Figure 3.4a, b). Low infiltration of Granzyme B+ cells support the concept that the anti-tumor effects of combination treatment do not result from improved mobilization or augmented action of NK or T cell cytotoxic cell responses (Figure 3.4c). Finally, we observed no significant changes in Ki67 staining between control and treatment groups, suggesting similar proliferative rates (Figure 3.4d). However, combination treated-tumors (polyIC and phenformin) had increased cleaved caspase-3 levels relative to tumors treated with each drug individually or PBS control (Figure 3.4e). Combined, these findings suggest that polyIC treatment cooperates with phenformin by inducing STAT1-dependent breast cancer cell apoptosis.

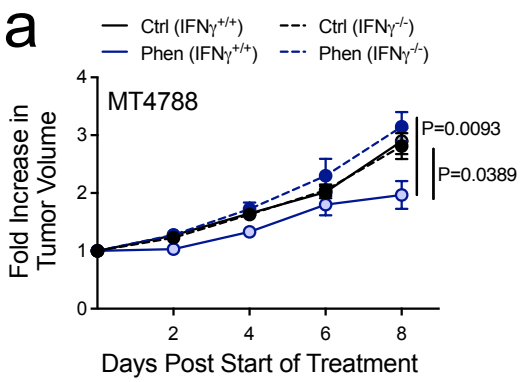
a
Ctrl (IFNγ+/+)
Phen (IFNγ+/+)
Ctrl (IFNγ-/-)
Phen (IFNγ-/-)
MT4788
P=0.0093
P=0.0389
Fold Increase in Tumor Volume
Days Post Start of Treatment

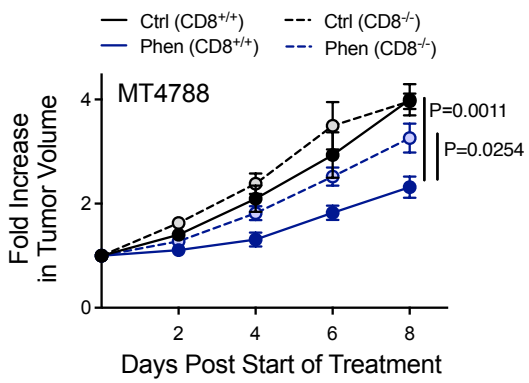
b
Ctrl (CD8+/+)
Phen (CD8+/+)
Ctrl (CD8-/-)
Phen (CD8-/-)
MT4788
P=0.0011
P=0.0254
Fold Increase in Tumor Volume
Days Post Start of Treatment

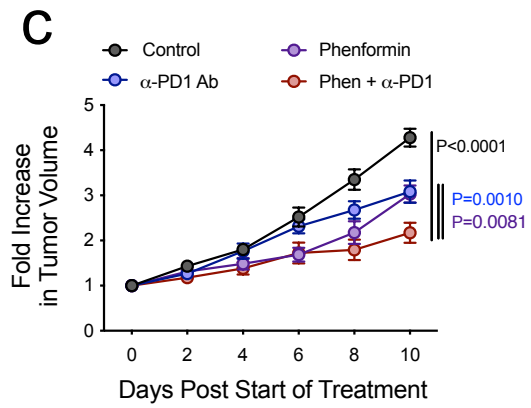
c
Control
α-PD1 Ab
Phenformin
Phen + α-PD1
P<0.0001
P=0.0010
P=0.0081
Fold Increase in Tumor Volume
Days Post Start of Treatment

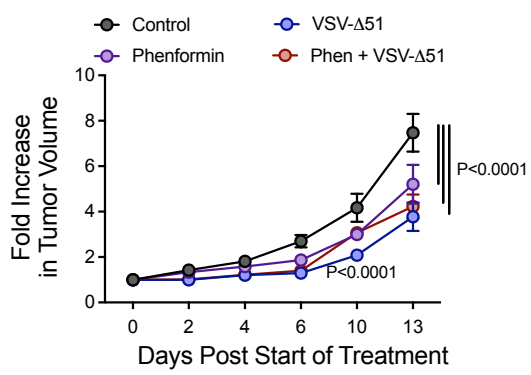
d
Control
Phenformin
VSV-Δ51
Phen + VSV-Δ51
P<0.0001
P<0.0001
Fold Increase in Tumor Volume
Days Post Start of Treatment

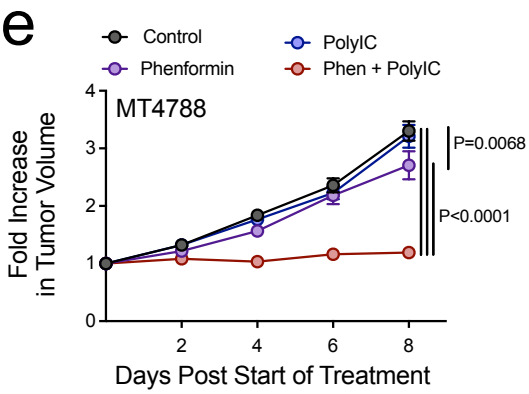
e
Control
Phenformin
PolyIC
Phen + PolyIC
MT4788
P=0.0068
P<0.0001
Fold Increase in Tumor Volume
Days Post Start of Treatment

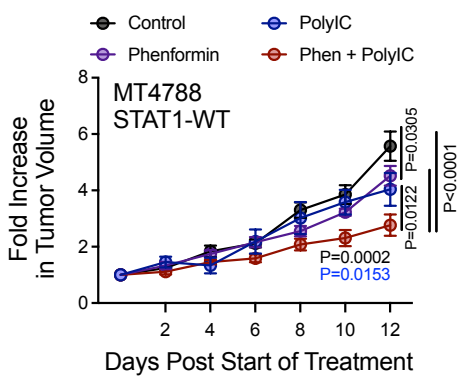
f
Control
Phenformin
PolyIC
Phen + PolyIC
MT4788
STAT1-WT
P=0.0305
P=0.0122
P<0.0001
P=0.0002
P=0.0153
Fold Increase in Tumor Volume
Days Post Start of Treatment

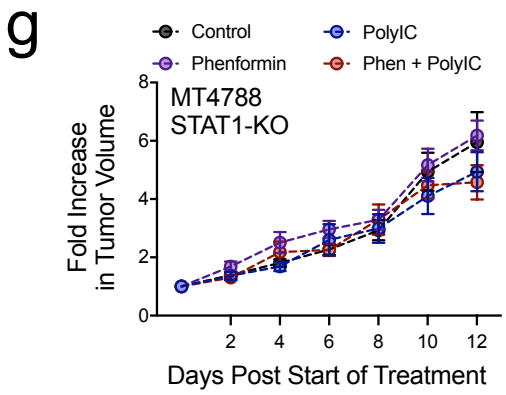
g
Control
Phenformin
PolyIC
Phen + PolyIC
MT4788
STAT1-KO
Fold Increase in Tumor Volume
Days Post Start of Treatment

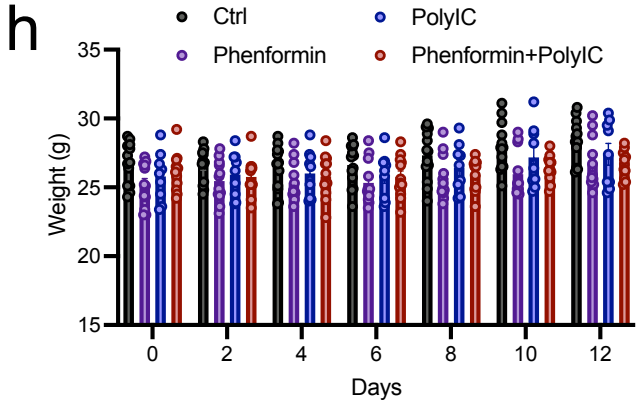
h
Ctrl
Phenformin
PolyIC
Phenformin+PolyIC
Weight (g)
Days

Figure 3.3: PolyIC sensitizes breast tumors to phenformin *in vivo* in a STAT1-dependent manner

(a, b) MT4788 breast cancer cells were injected into the mammary fat pads (MFP) of immunocompetent (FVB) mice or **(a)** IFNγ$^{-/-}$ or **(b)** CD8$^{-/-}$ animals. Mice were treated with phenformin (50 mg/kg daily) or equivalent volume of PBS. Panel a: Tumor volumes at start of treatment: PBS-treated IFNγ$^{-/-}$: 207.0 mm^3, SD: 26.5 mm^3; PBS-treated IFNγ$^{+/+}$: 209.1 mm^3 SD: 21.2 mm^3; phenformin-treated IFNγ$^{-/-}$: 141.5 mm^3, SD: 35.0 mm^3; phenformin-treated IFNγ$^{+/+}$: 169.6 mm^3 SD: 55.1 mm^3. PBS-treated IFNγ$^{-/-}$ and IFNγ$^{+/+}$: *n*=7, phenformin-treated IFNγ$^{-/-}$ and IFNγ$^{+/+}$: *n*=8 tumors/group; Panel b: Tumor volumes at start of treatment: PBS-treated CD8$^{-/-}$: 118.0 mm^3, SD: 33.8 mm^3; PBS-Treated CD8$^{+/+}$ 100.2 mm^3, SD: 25.5 mm^3 ; phenformin-treated CD8$^{-/-}$: 112.5 mm^3, SD: 22.0 mm^3; phenformin-treated CD8$^{+/+}$: 120.6 mm^3, SD: 29.7 mm^3 . PBS-treated CD8$^{-/-}$ (Ctrl): *n*=12; phenformin-treated CD8$^{-/-}$: *n*=11; PBS-Treated CD8$^{+/+}$ (Ctrl): *n*=5; phenformin-treated CD8$^{+/+}$ *n*=8 tumors.

(c) MT4788 breast cancer cells were injected into the MFP of FVB mice. Tumor bearing mice were randomized and injected intraperitoneally with phenformin (50 mg/kg daily), 100 µg anti-PD1 antibody (every 3 days), either alone or in combination. Tumor volumes at start of treatment: Control: 103.3 mm^3, SD: 24.7 mm^3; anti-PD1: 106.8 mm^3, SD: 21.0 mm^3; phenformin: 108.3 mm^3, SD: 15.9 mm^3; anti-PD1+phenformin: 127.6 mm^3, SD: 41.9 mm^3. Isotype control IgG antibodies (100 µg every 3 days) were injected for the control and phenformin alone treatment groups. Control: *n*=9; anti-PD1: *n*=10; phenformin: *n*=6; anti-PD1+phenformin: *n*=6 tumors/group. P value <0.0001 for Control; P value=0.0081 (purple) for phenformin and P value P=0.0010 [483] for anti-PD1, each compared to phenformin + anti-PD1 group.

(d) MT4788 breast cancer cells were injected into the MFP of FVB mice. Tumor bearing mice were randomized and treated intraperitoneally with phenformin (50 mg/kg daily) or oncolytic virus VSV MΔ51 (two intra-tumoral injections of 1x10^7 PFU administered 24 hours apart), alone or in combination. PBS was administered both intraperitoneally and/or intra-tumorally for the control groups. Tumor volumes at start of treatment: Control: 133.0 mm^3, SD: 55.3 mm^3; phenformin: 182.6 mm^3, SD: 91.8 mm^3 ; VSV MΔ51: 127.2 mm^3, SD: 36.3 mm^3; VSV MΔ51+phenformin: 170.8 mm^3, SD: 57.9 mm^3. Control: *n*=8; phenformin: *n*=7; VSV MΔ51: *n*=8; VSV MΔ51+phenformin: *n*=8 tumors/group. P<0.0001 (black) controls compared to VSV MΔ51 treated group. Other comparisons are indicated in Figure.

(e) MT4788 breast cancer cells were injected into the MFP of FVB mice. Treatment with polyIC (50 µg, every 2 days) or saline was initiated at ~100-150 mm^3. Two days later, phenformin (50 mg/kg, daily) (or PBS) treatment was started, in combination with polyIC or saline (every 2

days). Initial tumor volumes: Control: 168.6 mm^3, SD: 44.6 mm^3; phenformin: 140.2 mm^3, SD: 47.6; polyIC 161.3 mm^3, SD: 43.1 mm^3; phenformin + polyIC: 132.7 mm^3, SD: 26.0 mm^3. Control: *n*=18; phenformin: *n*=20; polyIC: *n*=17; phenformin + polyIC: *n*=17 tumors. **(f-h)** MFP injection of (f) MT4788 STAT1-WT or (g) STAT1-KO cells into FVB mice. At ~90mm^3 tumor volume, mice were treated with polyIC or saline. Two days later, phenformin (50 mg/kg, daily) or PBS treatment was started, in combination with polyIC or saline (every 2 days). Tumor volumes at start of treatment: (f) STAT1-WT Control: 93.2 mm^3, SD: 33.0 mm^3; phenformin: 109.5 mm^3, SD: 29.5 mm^3 ; polyIC: 94.0 mm^3, SD: 33.7 mm^3 ; phenformin+ polyIC: 83.8 mm^3, SD: 26.6 mm^3 . (g) Control: STAT1-KO Control: 106.7 mm^3, SD: 53.2 mm^3 ; phenformin: 96.1 mm^3, SD: 50.0 mm^3 ; polyIC: 103.2 mm^3, SD: 57.6 mm^3 ; phenformin+ polyIC: 129.2 mm^3, SD: 64.6 mm^3. Panel f: *n*=11 and panel g: *n*=10; phenformin: panels f, g: *n*=7; polyIC: panel f: *n*=6 and panel g: *n*=8; phenformin and polyIC: panels f *n*=8, g: *n*=9 tumors. P=0.0002 (black) for control compared to phenformin + polyIC; P=0.0153 for polyIC compared to phenformin + polyIC in STAT1-WT tumors. Other comparisons indicated in Figure. **(h)** Weights of mice FVB treated as in panels f-g mice. The data are presented as the mean fold change in tumor volume relative to the start of treatment (± SEM). P values were calculated using two-way ANOVA with a Tukey's posthoc test.

We next sought to determine the generalizability of these observations by measuring the effects of combined polyIC and phenformin treatment in independent pre-clinical models of murine and human breast cancer. These include 4T1-537 cells, a lung metastatic variant that is syngeneic in immunocompetent Balb/c mice [604] as well as a human model of triple negative breast cancer (MDA-MB-231) that forms tumors in immunodeficient (SCID-Beige) animals. PolyIC and phenformin combination treatment also impaired 4T1-537 and MDA-MB-231 tumor growth in contrast to each drug as a monotherapy, which minimally impacted disease progression (Figure 3.4f and g). PolyIC and phenformin cooperative growth suppression of MDA-MB-231 tumors in immunodeficient mice, reinforces the previous data suggesting that an adaptive immune response likely does not contribute significantly to the mechanism of action (Figure 3.4g). Instead, this data suggests that inflammatory responses likely underpin increased sensitivity of tumors to the polyIC and phenformin drug combination.

We next asked whether polyIC treatment could sensitize tumors to lower doses of phenformin that would be more readily achievable and associated with reduced toxicity in breast cancer patients [605, 606]. Employing the same MT4788 MFP tumor model, we found that combination treatment of polyIC with a five-fold decreased dose of phenformin (10 mg/kg) elicited comparable tumor growth suppression than with phenformin (50 mg/kg) (Figure 3.4h). Taken together, these findings support that polyIC-driven inflammation sensitizes tumors to the tumoricidal effects of phenformin in multiple preclinical breast cancer models, an effect that is also achieved with lower more clinically relevant phenformin concentrations.

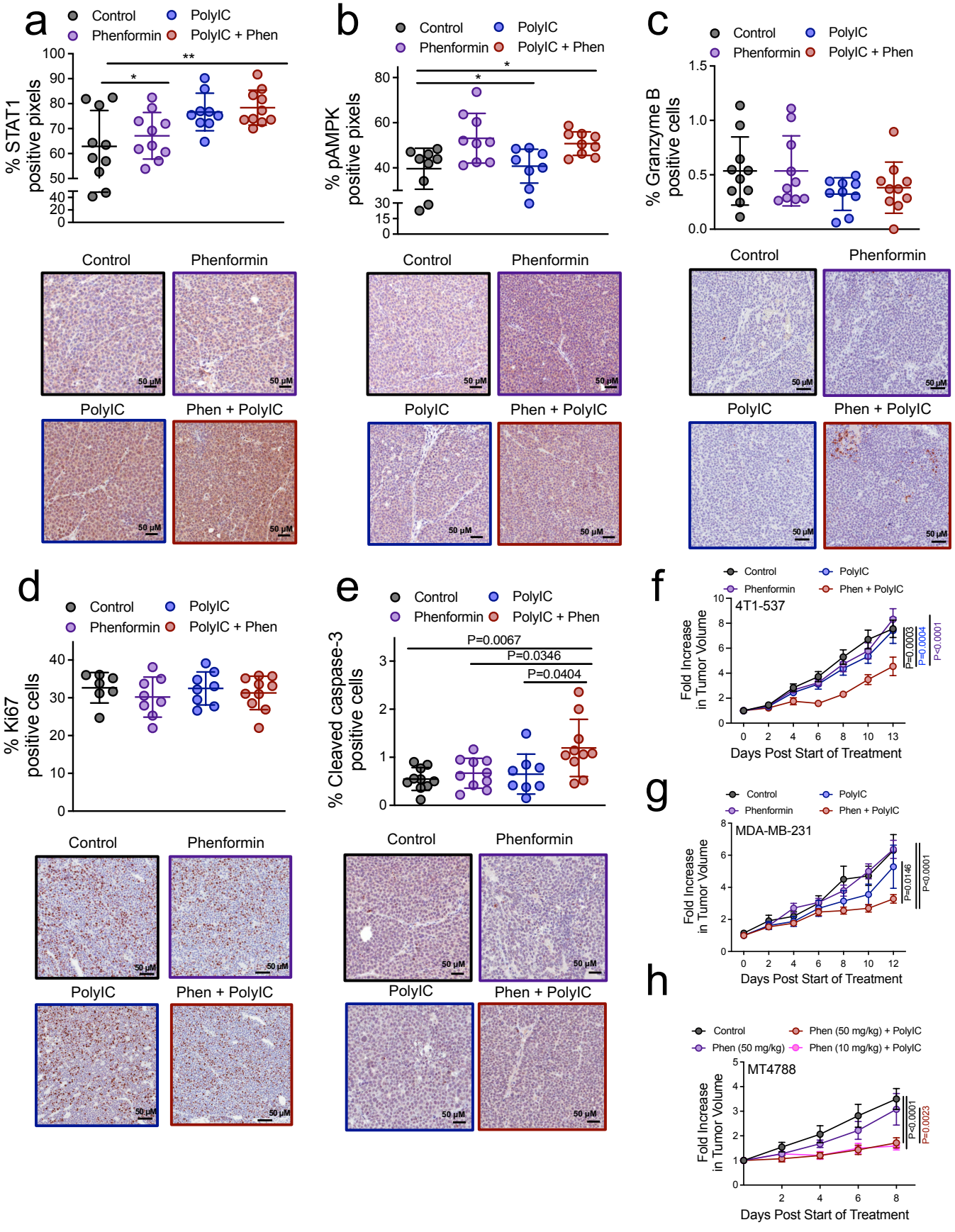
a
Control
PolyIC
Phenformin
PolyIC + Phen
% STAT1 positive pixels
b
% pAMPK positive pixels
c
% Granzyme B positive cells
Control
Phenformin
PolyIC
Phen + PolyIC
50 µM
d
% Ki67 positive cells
e
% Cleaved caspase-3 positive cells
P=0.0067
P=0.0346
P=0.0404
f
4T1-537
Fold Increase in Tumor Volume
Days Post Start of Treatment
P=0.0003
P=0.0004
P<0.0001
g
MDA-MB-231
P=0.0146
P<0.0001
h
Phen (50 mg/kg)
Phen (10 mg/kg) + PolyIC
MT4788
P<0.0001
P=0.0023

Figure 3.4: PolyIC-induced STAT1 activation sensitizes breast tumors to the tumoricidal effects of phenformin *in vivo*

(a-e) Immunohistochemical analysis of mammary tumors described in Figure 3.3e using **(a)** STAT1, **(b)** T172-phosphorylated AMPK (pAMPK) and **(c)** Granzyme B-specific antibodies **(d)** Ki67 **(e)** cleaved caspase-3-specific antibody. The data is shown as the mean percent of positive pixels for panels a, b; and percent of positive cells for panels c-e (±SEM). Panels a, c: *n*=10 tumors/group, except polyIC: *n*=9 tumors; panel b: *n*=9 tumors/group, except polyIC: *n*=8 tumors; panel d: control: *n*=7; polyIC: *n*=8; phenformin: *n*=8; phenformin + polyIC: *n*=10; panel e: *n*=10 except polyIC: *n*=8 tumors. Representative images are shown, scale bar = 50 μm.
(f, g) MFP injection of **(f)** 4T1-537 cells into Balb/c mice and **(g)** MDA-MB-231 cells into SCID-Beige mice. Mice were treated as described in figure 3.3 e. Tumor volumes at start of treatment: Panel f: Control: 61.2 mm^3, SD: 18.4 mm^3; phenfomin: 62.0 mm^3, SD: 24.0 mm^3; polyIC: 60.0 mm^3, SD: 21.4 mm^3; phenformin+ polyIC: 66.8 mm^3, SD: 17.6 mm^3. Panel g: Control: 84.8 mm^3, SD: 59.4 mm^3; phenfomin: 63.3 mm^3, SD: 19.6 mm^3; polyIC: 78.0 mm^3, SD: 29.4 mm^3; phenformin+ polyIC: 69.8 mm^3, SD: 16.0 mm^3. Panel f: Control: *n*=8; phenformin, PolyIC: *n*=9; phenformin+ polyIC: *n*=10 tumors; panel g: Control: *n*=12; phenformin: *n*=10; polyIC: *n*=9; phenformin+ polyIC: *n*=13 tumors/group. The data are presented as the mean fold change in tumor volume relative to the start of treatment (± SEM).
(h) MT4788 breast cancer cells were injected into the MFP of FVB mice. At tumor volumes of approximately 100 mm^3, treatment with polyIC (50 μg, every 2 days) or saline control was started. Then mice were either treated with one of two concentrations of phenformin (10 mg/kg or 50 mg/kg, daily) in combination polyIC (50 μg, every 2 days), or phenformin alone (50 mg/kg, daily), or PBS control. Initial tumor volumes at start of treatment: Control: 106.7 mm^3, SD: 30.4 mm^3; phenfomin: 128.0 mm^3, SD: 64.5 mm^3; polyIC: 127.7 mm^3, SD: 32.7 mm^3; phenformin+ polyIC: 121.0, SD: 53.9 mm^3. *n*=8 tumors/group except phenformin (10mg/kg) + polyIC: *n*=9. Data is presented as the mean fold change in tumor volume relative to the start of treatment (± SEM).
P values were calculated using one-way ANOVA using Tukey's posthoc test panels a-e, or using a two-way ANOVA with a Tukey's post hoc test panels f-h.

3.4 IFNγ minimally impacts phenformin-induced energetic stress and steady state metabolite levels in breast cancer cells

Recall that in combination treatment groups, polyIC did not further increase AMPK phosphorylation (T172), and that phenformin did not induce further higher STAT1 expression in tumors (Figure 3.4a, b). These data suggest that the mechanism of cooperativity of polyIC and phenformin is separate from simply amplifying energetic stress and/or anti-tumor immune responses. Yet, given that a central mechanism of biguanides, such as metformin and phenformin, is by causing energetic and biosynthetic stress in breast cancer, we next formally addressed if IFNγ influences tumor cell bioenergetics, and more specifically, if energetic stress underlies IFNγ-induced sensitivity of tumors to phenformin. We measured the impact of IFNγ and phenformin single and combination treatment on the bioenergetics of breast cancer cells. As expected from the literature, phenformin abolishes oxygen consumption rate (OCR) (Figure 3.5a-g) [595, 596, 607]. Interestingly, IFNγ treatment alone induced a decrease in the maximal respiration rate of breast cancer cells (Figure 3.5c), and this effect was found to be STAT1-dependent (Figure 3.5h,i). As expected, phenformin treatment increases breast cancer cell extracellular acidification rate (ECAR), yet no significant differences were measured when compared to co-treatment with phenformin and IFNγ (Figure 3.5j), suggesting that the mechanism of cooperation was not increased dependence on glycolysis. Previous studies support STAT1 activation increasing glycolysis [563, 564]. In accordance with this, MT4788 STAT1 proficient cells treated with IFNγ have increased pyruvate and lactate levels as well as an increase lactate/pyruvate ratio in comparison to PBS treated controls (Figure 3.6a,b), an effect that was not observed in MT4788 STAT1 deficient cells. MT4788 breast cancer cells co-treated with IFNγ and phenformin modestly increased pyruvate and lactate steady state levels above that of phenformin treatment alone (Figure 3.6c). However, while the lactate/pyruvate ratio was elevated upon both phenformin and combination treatment, there were no significant differences in cells from the two treatment groups (Figure 3.6d). To functionally assess whether IFNγ alters the glucose dependency of breast cancer cells, we performed glucose deprivation experiments. Upon glucose withdrawal, IFNγ treatment did not impact breast cancer cell viability compared to PBS control (Figure 3.6e).

While IFNγ treatment alone modestly decreases the metabolic flexibility of MT4788 breast cancer cells in STAT1 proficient cells; when combined with phenformin, IFNγ does not further disrupt breast cancer oxidative energy metabolism beyond that of phenformin treatment alone (Figure 3.6f, g). Moreover, IFNγ treatment led to a reduction in the bioenergetic capacity of breast cancer cells (Figure 3.6h). Albeit modest, decreases in both metabolic flexibility and

bioenergetic capacity of MT4788 breast cancer cells upon IFNγ-treatment were found to be STAT1-dependent (Figure 3.7a, c).

These results suggest that IFNγ-STAT1 axis reduces the bioenergetic capacity and flexibility of breast cancer cells. However, IFNγ and phenformin does not significantly alter breast cancer cell bioenergetics above the profound effects observed in the phenformin single treatment group, suggesting that the efficacy of IFNγ and phenformin treatment is likely independent of the individual effects of these agents in inducing energetic stress.

IFNγ further increases phenformin-induced α-ketoglutarate levels in breast cancer cells (from 4.7 fold to 5.8 fold above PBS controls) (Figure 3.7d). An increase in the α-ketoglutarate/citrate ratio was also observed in both the phenformin single and combination treated breast cancer cells, however there was no significant difference between the two groups (Figure 3.7e). The steady state increase in both the α-ketoglutarate levels (1.4 fold) and the α-ketoglutarate/citrate ratio in IFNγ-treated cells (1.6 fold), occurs in a STAT1-dependent manner (Figure 3.7f, g). An increased α-ketoglutarate/citrate ratio suggests increased reductive carboxylation of glutamine metabolism, as previously reported in tumors treated with ETC inhibitors [209, 608].

Along this line, we next sought to clarify whether IFNγ treatment causes breast cancer cells to be more reliant on glutamine. Upon partial glutamine withdrawal (4 mM, 0.4 mM, 0 mM), IFNγ treatment actually increases breast cancer cell viability by 14% in response to a 10-fold reduction in glutamine levels, an effect that was lost in media completely deplete of glutamine (Figure 3.7h), suggesting that the ability of IFNγ to alter glutamine metabolism cannot explain the increased cytotoxicity of combined IFNγ/phenformin treatment.

Taken together, these results support that IFNγ-STAT1 axis reduces the bioenergetic capacity and flexibility of breast cancer cells. Yet, in combination-treated cells, the additional impact of IFNγ treatment on bioenergetics and steady state metabolites is minimal, given the potent phenformin-induced energetic and biosynthetic stress, suggesting that another mechanism is responsible for IFNγ-induced sensitization of breast cancer cells to phenformin.

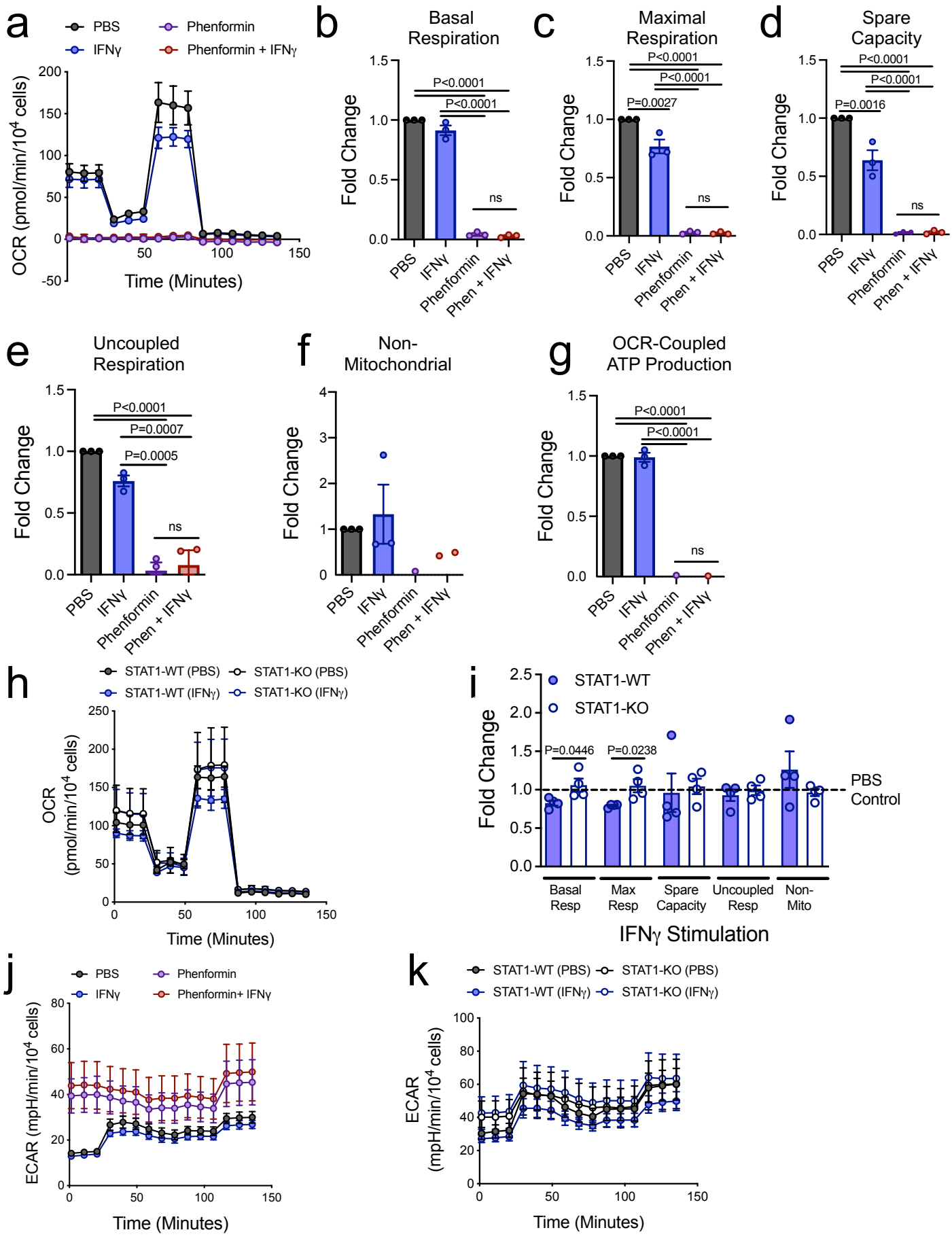
a
PBS
IFNγ
Phenformin
Phenformin + IFNγ
OCR (pmol/min/10^4 cells)
Time (Minutes)
b
Basal Respiration
c
Maximal Respiration
d
Spare Capacity
Fold Change
P<0.0001
P=0.0027
P=0.0016
ns
PBS
IFNγ
Phenformin
Phen + IFNγ
e
Uncoupled Respiration
P=0.0007
P=0.0005
f
Non-Mitochondrial
g
OCR-Coupled ATP Production
h
STAT1-WT (PBS)
STAT1-KO (PBS)
STAT1-WT (IFNγ)
STAT1-KO (IFNγ)
OCR (pmol/min/10^4 cells)
Time (Minutes)
i
STAT1-WT
STAT1-KO
P=0.0446
P=0.0238
PBS Control
Basal Resp
Max Resp
Spare Capacity
Uncoupled Resp
Non-Mito
IFNγ Stimulation
j
Phenformin+ IFNγ
ECAR (mpH/min/10^4 cells)
Time (Minutes)
k
ECAR (mpH/min/10^4 cells)
Time (Minutes)

Figure 3.5: IFNγ induces moderate energetic stress in breast cancer cells

(a-k) MT4788 cells were treated with IFNγ (1 ng/ml), phenformin (500 μM), alone or in combination, or with PBS treatment as control. The Seahorse real time metabolic analyzer was then used to determine **(a)** Oxygen consumption rate (OCR) and (b-g) fold change in the rates of **(b)** basal respiration, **(c)** maximal respiration, **(d)** spare capacity **(e)** uncoupled respiration **(f)** non-mitochondrial respiration **(g)** OCR-coupled ATP production, **(j)** the extracellular acidification rate (ECAR) of the same cells.
(h,i, k) STAT1-WT and STAT1-KO MT4788 cells were treated with IFNγ (1 ng/ml) or PBS. The Seahorse real-time metabolic analyzer was used to determine **(h)** Oxygen consumption rate (OCR) and **(i)** Fold change in the rates of basal respiration, maximal respiration, spare capacity, uncoupled respiration, and non-mitochondrial respiration from samples, relative to their PBS controls **k)** Seahorse measurements of the extracellular acidification rate (ECAR) of the same cells.
The data represent *n*=3-4 independent experiments (mean of means ±SEM). P values were calculated using a two-way ANOVA with a Tukey's posthoc tests, panels a-g, j. P values were calculated using two-tailed unpaired t-tests for panel h,i,k.

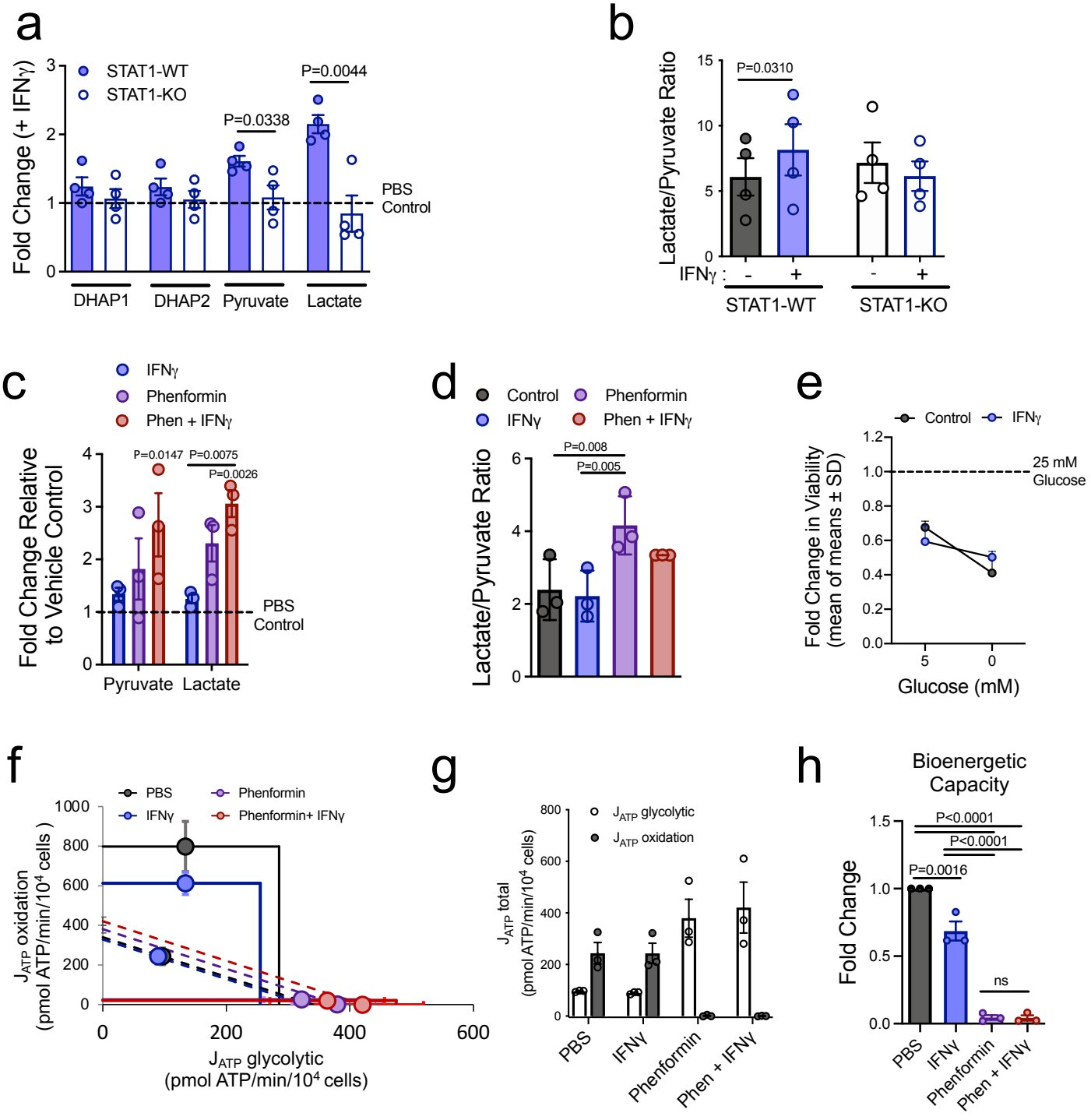
a
Fold Change (+ IFNγ)
STAT1-WT
STAT1-KO
P=0.0338
P=0.0044
PBS Control
DHAP1
DHAP2
Pyruvate
Lactate
b
Lactate/Pyruvate Ratio
P=0.0310
IFNγ : - + - +
STAT1-WT
STAT1-KO
c
IFNγ
Phenformin
Phen + IFNγ
Fold Change Relative to Vehicle Control
P=0.0147
P=0.0075
P=0.0026
PBS Control
Pyruvate
Lactate
d
Control
Phenformin
IFNγ
Phen + IFNγ
Lactate/Pyruvate Ratio
P=0.008
P=0.005
e
Control
IFNγ
Fold Change in Viability (mean of means ± SD)
25 mM Glucose
Glucose (mM)
f
PBS
IFNγ
Phenformin
Phenformin+ IFNγ
JATP oxidation (pmol ATP/min/10^4 cells)
JATP glycolytic (pmol ATP/min/10^4 cells)
g
JATP glycolytic
JATP oxidation
JATP total (pmol ATP/min/10^4 cells)
PBS
IFNγ
Phenformin
Phen + IFNγ
h
Bioenergetic Capacity
Fold Change
P<0.0001
P<0.0001
P=0.0016
ns
PBS
IFNγ
Phenformin
Phen + IFNγ

Figure 3.6: IFNγ minimally impacts phenformin-induced energetic stress and steady state glycolytic metabolite levels in breast cancer cells

(a, b) STAT1-WT and STAT1-KO MT4788 cells were treated IFNγ (1 ng/ml) or PBS for 36 hours, *n*=4 independent experiments were performed **(a)** Fold change in steady state levels of glycolytic metabolites were determined by GC-MS, (mean of means, ±SEM). **(b)** The lactate/pyruvate ratio was determined (mean ±SD).
(c, d) MT4788 cells were treated with IFNγ (1 ng/ml), phenformin (500 μM), alone or in combination, or with PBS treatment as control, for 36 hours, *n*=3 independent experiments were performed **(c)** Fold change in steady state levels of glycolytic metabolites were determined by GC-MS. Pyruvate levels: P=0.0147 and lactate levels: P=0.0026 both compares phenformin+ IFNγ treatment to control. **(d)** The lactate/pyruvate ratio was determined (mean ±SD).
(e) Viability of MT4788 cells treated with IFNγ (1 ng/ml) or PBS treatment upon glucose withdrawal (48 hours). Data is expressed as a fold change relative to their own treated controls in 25 mM glucose media, *n*=3 independent experiments (mean of means ±SEM).
(f) The total bioenergetic capacity and flexibility of breast cancer cells from (c-d) was determined by calculating the basal (point on dotted line) and maximal rates (point on solid line) of ATP production from glycolysis (J_{ATP} Glycolytic) and oxidative phosphorylation (J_{ATP} Oxidation)
(g) ATP production from glycolysis (J_{ATP} Glycolytic) (white) and oxidative phosphorylation (J_{ATP} Oxidation) (grey), from breast cancer cells from panels (c-d) **(h)** Bioenergetic capacity was calculated and represented as a fold change to that of respective PBS controls, from breast cancer cells from panels (c-d).
The data represent *n*=3-4 independent experiments (mean of means ±SEM). P values were calculated using two-tailed unpaired t-tests for panels a, b, e; and using a two-way ANOVA with a Tukey's posthoc tests, panels c, d, f-h.

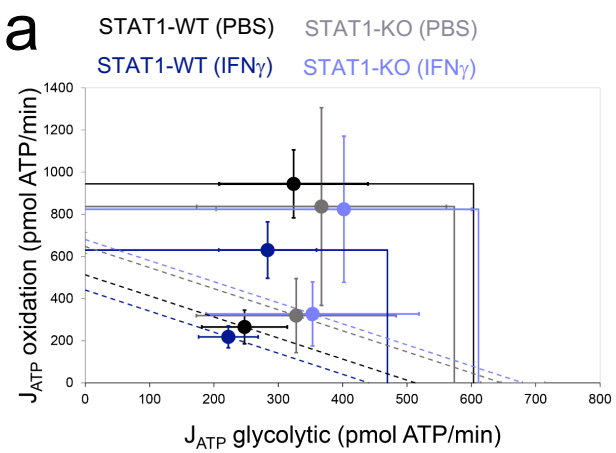
a
STAT1-WT (PBS)
STAT1-KO (PBS)
STAT1-WT (IFNγ)
STAT1-KO (IFNγ)
J_ATP oxidation (pmol ATP/min)
J_ATP glycolytic (pmol ATP/min)

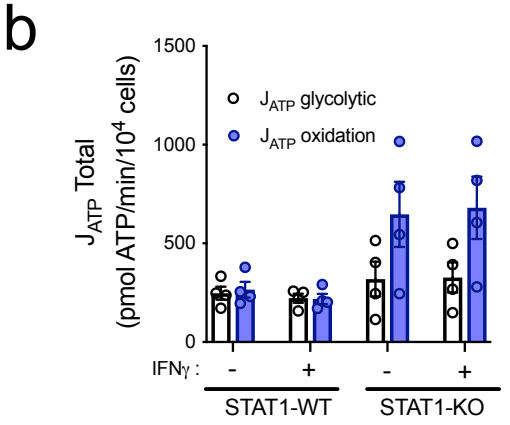
b
J_ATP glycolytic
J_ATP oxidation
J_ATP Total (pmol ATP/min/10^4 cells)
IFNγ :
STAT1-WT
STAT1-KO

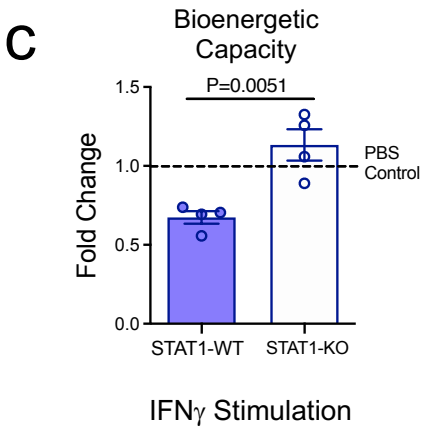
c
Bioenergetic Capacity
P=0.0051
Fold Change
PBS Control
STAT1-WT
STAT1-KO
IFNγ Stimulation

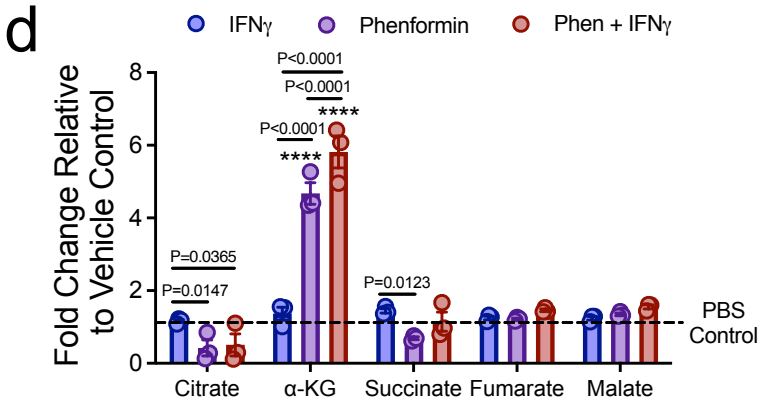
d
IFNγ
Phenformin
Phen + IFNγ
Fold Change Relative to Vehicle Control
P<0.0001
P<0.0001
P<0.0001
****
****
P=0.0365
P=0.0147
P=0.0123
PBS Control
Citrate
α-KG
Succinate
Fumarate
Malate

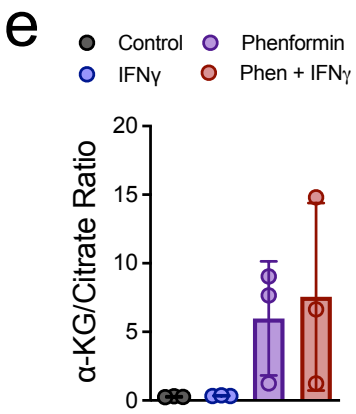
e
Control
IFNγ
Phenformin
Phen + IFNγ
α-KG/Citrate Ratio

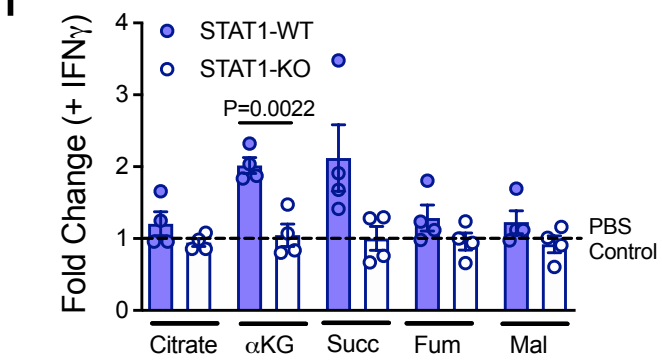
f
STAT1-WT
STAT1-KO
P=0.0022
Fold Change (+ IFNγ)
PBS Control
Citrate
αKG
Succ
Fum
Mal

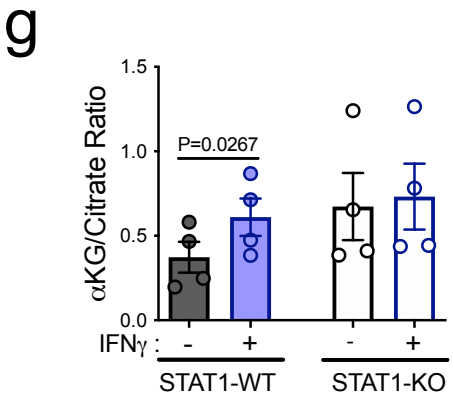
g
P=0.0267
αKG/Citrate Ratio
IFNγ :
STAT1-WT
STAT1-KO

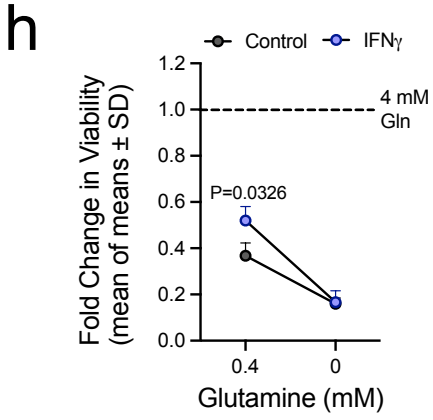
h
Control
IFNγ
4 mM Gln
P=0.0326
Fold Change in Viability (mean of means ± SD)
Glutamine (mM)

Figure 3.7: IFNγ increases cellular α-ketoglutarate/citrate ratio in a STAT1-dependent manner

(a-c) STAT1-WT and STAT1-KO MT4788 cells were treated with IFNγ (1 ng/ml) or PBS. The Seahorse real time metabolic analyzer was used to determine **(**a**)** The total metabolic capacity and flexibility of these same breast cancer cells was determined by calculating the basal (point on dotted line) and maximal rates (point on solid line) of ATP production from glycolysis (J_{ATP} Glycolytic) and oxidative phosphorylation (J_{ATP} Oxidation), **(b)** ATP production from glycolysis (J_{ATP} Glycolytic) (white) and oxidative phosphorylation (J_{ATP} Oxidation) [483], **(c)** Bioenergetic capacity was calculated and represented as a fold change relative to that of respective PBS controls. The data represents *n*=4 independent experiments (mean of means ±SEM).
(d-e) MT4788 cells were treated with IFNγ (1 ng/ml), phenformin (500 μM), alone or in combination, or with PBS treatment as control, for 36 hours, *n*=3 independent experiments were performed, same cells from Figure 3.6 c-d. **(d)** Fold change in steady state levels of citric acid cycle metabolites determined by GC-MS, (mean of means ±SEM). ****P<0.0001 compared to PBS Control. Other P values are indicated in the Figure. **(e)** α-ketoglutarate/citrate ratio, of these same cells (mean of means ±SEM).
(f) Fold change in steady state levels of citric acid cycle metabolites of the cells in Figure 3.6 panels a and b.
(g) α-ketoglutarate/citrate ratio was determined from the cells in Figure 3.6 panels a and b, (mean of means ±SEM).
(h) Viability of MT4788 cells with IFNγ (1 ng/ml) or PBS treatment upon glutamine withdrawal (48 hours). Data is expressed as a fold change relative to their own treated controls in 4 mM glutamine and is representative of *n*=3 independent experiments (mean of means ±SEM).
P values were calculated using two-tailed unpaired t-tests for panels a-c. f, g, h; and using a two-way ANOVA with a Tukey's posthoc test for panels d, e.

3.5 IFNγ and polyIC-induced phenformin sensitivity requires mitochondrial ROS

By inhibiting complex I of the electron transport chain, phenformin hinders cellular respiration and has also been shown to increase the production of mitochondrial reactive oxygen species (ROS) [403, 596]. Indeed, using the MitoSOX fluorescent probe, we found phenformin profoundly increases mitochondrial ROS production (1.7 fold and 3.6 fold) in MT4788 and MDA-MB-231 cell, respectively (Figure 3.8 a, b). This phenformin-induced increase in total ROS levels was further corroborated with CM-H2DCFDA staining, in MT4788, MDA-MD-231 and BT474 cells (Figure 3.8c-e). IFNγ treatment alone did not increase total ROS nor mitochondrial ROS levels in breast cancer cells (Figures 3.8a-e). Furthermore, IFNγ did not further increase ROS levels above that of phenformin in the combination-treated cells (Figures 3.8a-e).

Many tumor cells maintain elevated ROS levels compared to their non-transformed counterparts, as moderately elevated ROS levels in cancer cells are understood to promote tumor growth and metastasis through multiple mechanisms [609]. The therapeutic potential of exploiting ROS-induced oxidative damage to selectively kill cancer cells has been explored [610]. We hypothesized that IFNγ stimulation sensitizes breast tumors to phenformin-induced ROS production. To functionally test this, we employed MitoTEMPO, a mitochondrial ROS scavenger. We found that MitoTEMPO reverses the cytotoxic effects of IFNγ and phenformin combination treatment in three independent breast cancer models (MT4788, MDA-MB-231, BT474) (Figures 3.8f-h). Furthermore, MitoTEMPO treatment of mice restores the growth potential of MT4788 tumors treated with polyIC and phenformin combination therapy (Figure 3.9a). Consistent with these observations, MDA-MB-231 tumors co-treated with phenformin and polyIC showed an increase in oxidative DNA damage (1.6 fold), as assessed by 8-oxo-dG IHC (Figure 3.9b). These findings support that oxidative stress underlies IFNγ-driven sensitization of breast cancer cells to phenformin. Combined with the observation that IFNγ treatment does not further increase breast cancer cell ROS levels above that of phenformin treatment alone, these data led us to develop the hypothesis that IFNγ perturbs their ROS scavenging potential.

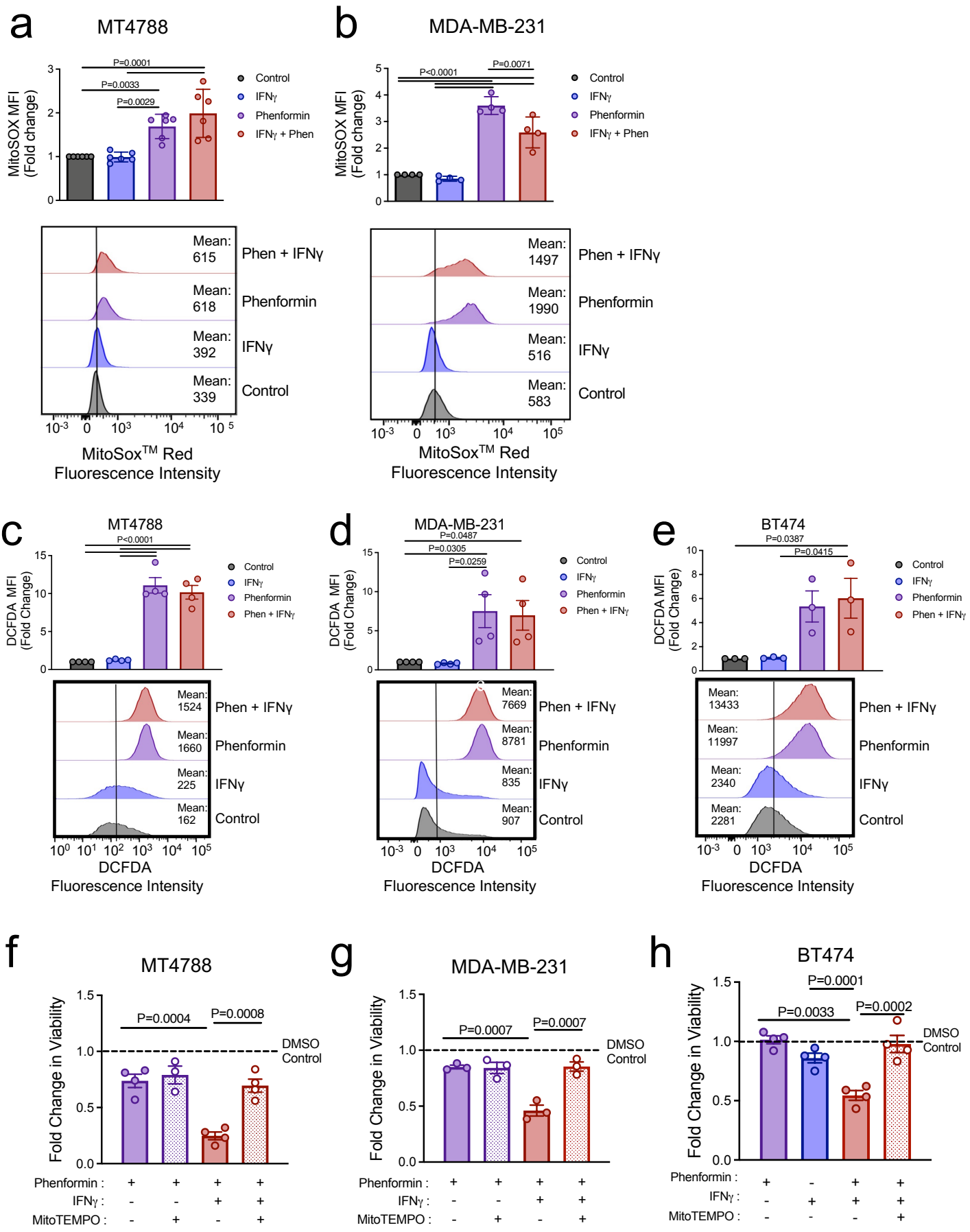
a
MT4788
MitoSOX MFI (Fold change)
P=0.0001
P=0.0033
P=0.0029
Control
IFNγ
Phenformin
IFNγ + Phen
Mean: 615
Mean: 618
Mean: 392
Mean: 339
Phen + IFNγ
Phenformin
IFNγ
Control
MitoSox™ Red Fluorescence Intensity
b
MDA-MB-231
MitoSOX MFI (Fold change)
P<0.0001
P=0.0071
Mean: 1497
Mean: 1990
Mean: 516
Mean: 583
MitoSox™ Red Fluorescence Intensity
c
MT4788
DCFDA MFI (Fold Change)
P<0.0001
Mean: 1524
Mean: 1660
Mean: 225
Mean: 162
DCFDA Fluorescence Intensity
d
MDA-MB-231
P=0.0487
P=0.0305
P=0.0259
Mean: 7669
Mean: 8781
Mean: 835
Mean: 907
e
BT474
P=0.0387
P=0.0415
Mean: 13433
Mean: 11997
Mean: 2340
Mean: 2281
f
MT4788
Fold Change in Viability
P=0.0004
P=0.0008
DMSO Control
Phenformin :
IFNγ :
MitoTEMPO :
g
MDA-MB-231
P=0.0007
P=0.0007
h
BT474
P=0.0001
P=0.0033
P=0.0002

Figure 3.8: IFNγ-induced phenformin sensitivity requires mitochondrial ROS

(a, b) Mitochondrial ROS levels, assessed by flow cytometry with MitoSOX (a) MT4788 and (b) MDA-MB-231 cells treated with IFNγ (1 ng/ml) and phenformin (500 μM), alone or in combination, for 24 hours. The data is shown as mean fold change in geometric mean fluorescence intensity (MFI) compared to PBS controls (±SEM) and representative histograms are shown. Panel a: MT4788: *n*=6/group; Panel b: MDA-MB-231: *n*=4/group.
(c-e) Total ROS levels, assessed by flow cytometry with DCFDA **(c)** MT4788, **(d)** MDA-MB-231 and **(e)** BT474 cells treated with IFNγ (1 ng/ml), phenformin (500 μM), for 24hours. The data represents the mean fold change in the DCFDA geometric MFI relative to PBS treated controls (±SEM) from panel c, d: *n*=4 or panel e *n*=3 independent experiments. Representative histograms are shown.
(f-h) Viability of **(f)** MT4788 **(g)** MDA-MB-231 and **(h)** BT474 cells treated for 48 hours with IFNγ (1 ng/ml) and/or phenformin (500 μM), either with 10 μM MitoTEMPO or with DMSO control. Data is expressed as a fold change relative to DMSO control, (mean of means ±SEM), *n*=4 independent experiments for panels f, h or of *n*=3 for panel g.
For panels a-e, see Figure 2.1a and d in methods section for gating strategy.
P values were calculated using a two-way ANOVA with a Tukey's posthoc test and are shown in the Figure.

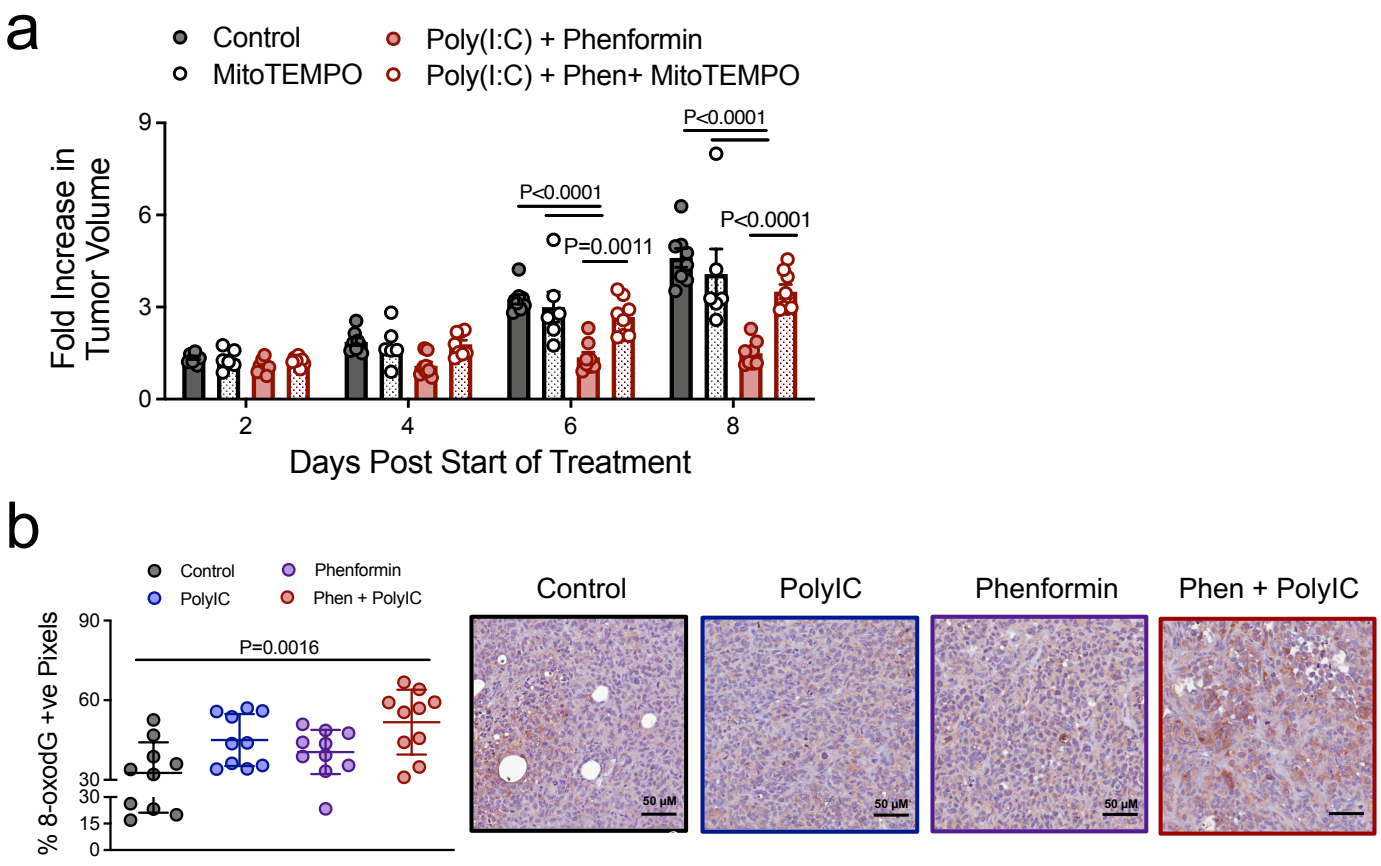

Figure 3.9: PolyIC-induced phenformin sensitivity in *vivo* requires mitochondrial ROS

(a) MT4788 breast cancer cells into the mammary fat pads (MFP) of FVB mice. At ~100 mm^3, mice were treated with polyIC (50 µg, every two days) or saline control, two days later phenformin (50 mg/kg, daily) or PBS treatment was initiated, with or without MitoTEMPO (3 mg/kg). Tumor volumes at start of treatment: Control: 97.0 mm^3, SD: 60.9 mm^3; MitoTEMPO: 100.7 mm^3, SD: 61.2 mm^3; polyIC+phenformin: 116.9 mm^3, SD: 37.6 mm^3; polyIC+phenformin+MitoTEMPO: 100.2 mm^3, SD: 23.1 mm^3. Data is represented as mean fold increase in tumor volume relative to the start of combination treatment (± SEM). Control: *n*=8; MitoTempo: *n*=6; Phenformin + polyIC: *n*=8; Phenformin + polyIC + MitoTempo: *n*=8 tumors.
(b) Immunohistochemical 8-oxo-dG staining of paraffin-embedded MDA-MB-231 treated-tumors from Figure 3.4f. The data is represented as mean of the percent of positive pixels, ±SD (*n*=10 independent tumors/group). Representative images are also shown.
P values were calculated using a two-way ANOVA with a Tukey's posthoc test.

3.6 Inhibiting glutathione synthesis sensitizes breast cancer cells to phenformin

Reduced glutathione (GSH) is a major ROS scavenger in cells. Once GSH provides reducing equivalents to deactivate ROS in cells, it is itself oxidized to glutathione disulfide (GSSG). Healthy cells predominantly maintain glutathione in its reduced form (90-95%), by either synthesizing new GSH or recycling the reduced form of GSSG back to GSH using NADPH is an essential co-factor and electron donor [187]. A decreased GSH/GSSG ratio indicates oxidative stress. A previous study suggested that IFNγ may decrease glutathione levels in ovarian cancer cells [611]. We first assessed whether IFNγ or phenformin treatment, alone and in combination, altered glutathione levels in breast cancer cells. Phenformin treatment reduced GSH levels and decreased the GSH/GSSG ratio in MT4788 cells (Figure 3.10a), which is consistent with its ROS-inducing properties (Figure 3.8a-e). However, IFNγ treatment, alone or combined with phenformin, did not further decrease glutathione levels or the GSH/GSSG ratio (Figure 3.10a). Moreover, similar trends in glutathione regulation were observed in STAT1-deficient cells (Figure 3.10b). Finally, phenformin increases the NADH/NAD+ ratio in breast cancer cells, which is reflective of its role as a complex I inhibitor (Figure 3.10c). Although AMPK activation has previously been shown to reduce NAPDH consumption [612], IFNγ and/or phenformin treatment did not alter the NADPH/NADP+ ratio in MT4788 breast cancer cells (Figure 3.10d). Moreover, IFNγ treatment of MT4788 breast cancer cells does not change the steady state levels of amino acid constituents of glutathione (Glutamic acid, Cystein, Glycine) (Figure 3.10e). These results suggest that IFNγ-driven STAT1 activation does not impair the glutathione pathway to sensitize tumor to phenformin-generated ROS.

Yet, we were intrigued by the ability of phenformin to decrease the pool of reduced glutathione in breast cancer cells. Pharmacological inhibitors of glutathione synthesis were shown to re-sensitize tumors to ROS-inducing chemotherapies [613]. Therefore, we examined whether decreasing glutathione levels in breast cancer cells would sensitize them to the anti-tumorigenic effects of phenformin. We co-treated breast cancer cells with phenformin and buthionine sulfoximine [614], an inhibitor of the first step in glutathione synthesis. BSO treatment alone had no impact on cell viability, yet, it increased the sensitivity of MDA-MB-231 (4.6-fold) and BT474 (5.7-fold) cells to phenformin treatment (Figure 3.11a,b). Moreover, dose de-escalation experiments revealed that BSO co-treatment elicited comparable anti-tumorigenic effects in combination with a 5-fold (100 μM) and 25-fold (20 μM) reduction in phenformin levels in MDA-MB-231 and BT474 cells, respectively (Figures 3.11c,d).

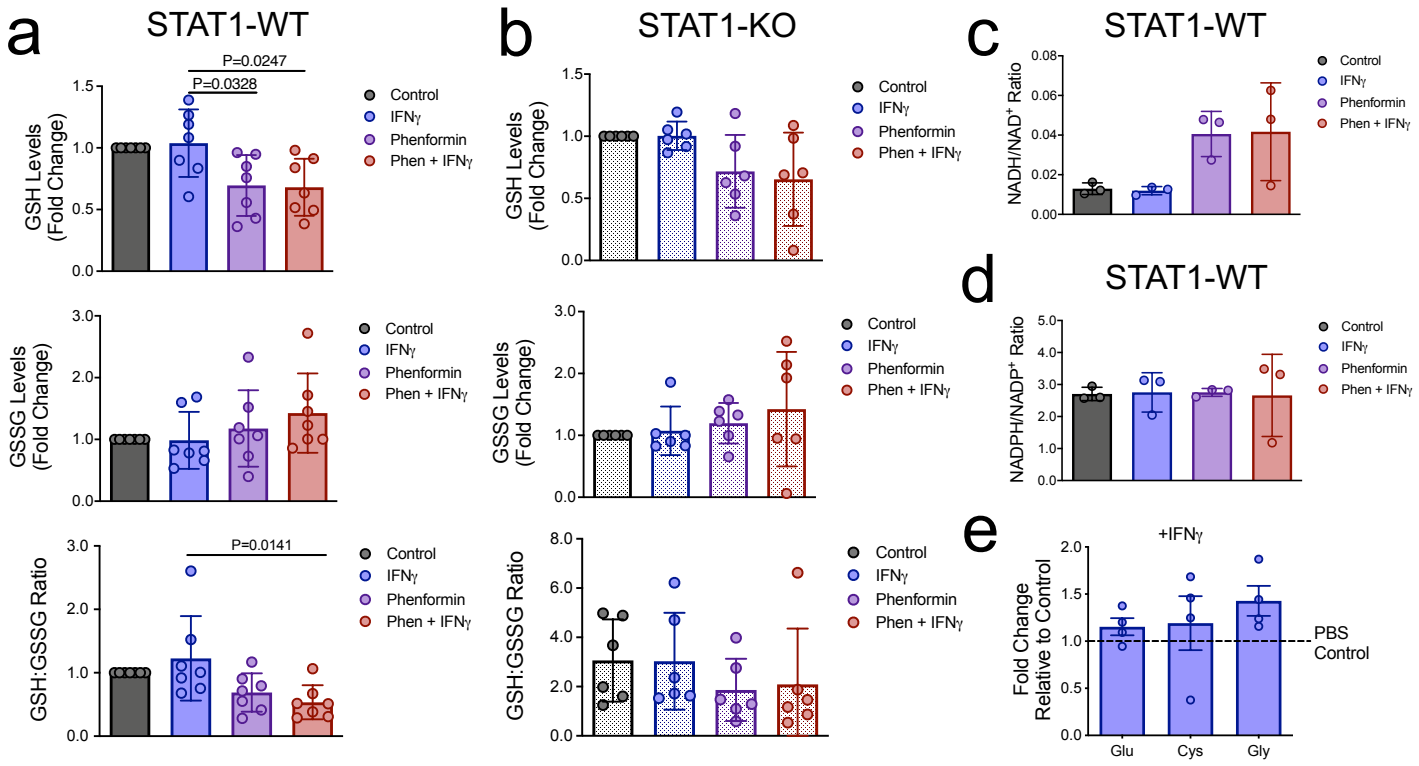

Figure 3.10: Phenformin minimally reduces glutathione levels in breast cancer cells

(a,b) GSH and GSSG levels, as well as the GSH/GSSG ratio was determined by LC-MS in **(a)** MT4788 STAT1-WT or **(b)** MT4788 STAT1-KO cells treated with phenformin (500 μM) and IFNγ (1 ng/ml) alone or in combination, for 36 hours. Data is shown as the average fold change in GSH or GSSG levels or by calculating the GSH/GSSG ratio compared to PBS controls from *n*=6 technical replicates over 2 independent experiments, (mean ±SD).

(c, d) Ratios of **(c)** NADH/NAD+ and **(d)** NADPH/NADP+ were determined in MT4788 cells treated with phenformin (500 μM), IFNγ (1 ng/ml), combination or PBS control. The data is representative of *n*=3 independent experiments, (mean of means ±SEM).

(e) Relative glutamic acid, cysteine, and glycine levels in MT4788 STAT1-WT and MT4788 STAT1-KO cells cultured either with IFNγ or PBS control for 24 hours. Data is representative of *n*=4 independent experiments (mean of means ± SEM).

P values were calculated using a two-way ANOVA with a Tukey's posthoc test.

Finally, MitoTEMPO rescued the viability of breast cancer cells treated with BSO and phenformin (Figure 3.11e). These results support that glutathione synthesis inhibitors sensitize breast cancer cells to phenformin by inducing oxidative stress. Although BSO and phenformin co-treatment induced a modest reduction in the number of BrdU+ cells (1.3-fold), we observed a robust increase in the frequency of Annexin V/propidium iodide+ cells (2.7-fold) in response to this combination treatment (Figure 3.11f-h). These data suggest that the tumoricidal effects of combined BSO and phenformin treatment are predominately a result of increased breast cancer cell apoptosis.

Phenformin is a more potent complex I inhibitor than metformin at lower concentrations in part because it does not require the organic cationic transport (OCT) to enter cells [395, 397, 596]. However, most studies in oncology have focused on the related family member, metformin [606], largely due to its approved use in the long-term management of diabetes mellitus, type 2 [615] and its lower rates of lactic acidosis, in comparison to phenformin in early studies [393]. We therefore assessed the relative ability of BSO to sensitize breast cancer cells to the cytotoxic effects of metformin versus phenformin. Low dose phenformin (100 μM) combines with BSO to reduce cancer cell viability, whereas metformin does not potentiate BSO-induced cancer cell death, even at 10-fold higher concentrations (1 mM) (Figure 3.12a). Unlike phenformin, metformin treatment does not stimulate ROS production in breast cancer cells at these concentrations (Figure 3.12b). These data demonstrate that co-treatment with phenformin and an inhibitor of glutathione synthesis causes in breast cancer apoptotic cell death.

3.7 Inhibition of NQO1 levels potentiates the ROS-dependent anti-tumorigenic effects of phenformin

These studies demonstrate the potential of combining an inhibitor of glutathione synthesis and phenformin in breast cancer treatment. However, they do not clarify how IFNγ-driven STAT1 activation potentiates the ROS-dependent, cytotoxic effects of phenformin. To address this, we performed genome-wide RNA sequencing analysis of STAT1-KO and STAT1-WT breast cancer cells (MT864, MT4788) following IFNγ treatment. We identified 1233 genes differentially expressed between MT4788-STAT1-WT and STAT1-KO cells and 573 genes differentially expressed between MT864-STAT1-WT and STAT1-KO cells (>100 reads, > 2 fold, FDR <0.05). GO term analysis identified numerous biological processes that were STAT1-dependent (Figure 3.13a), including the top upregulated genes, which were related to immune system processes, anti-viral responses and antigen processing and presentation (Figure 3.13b).

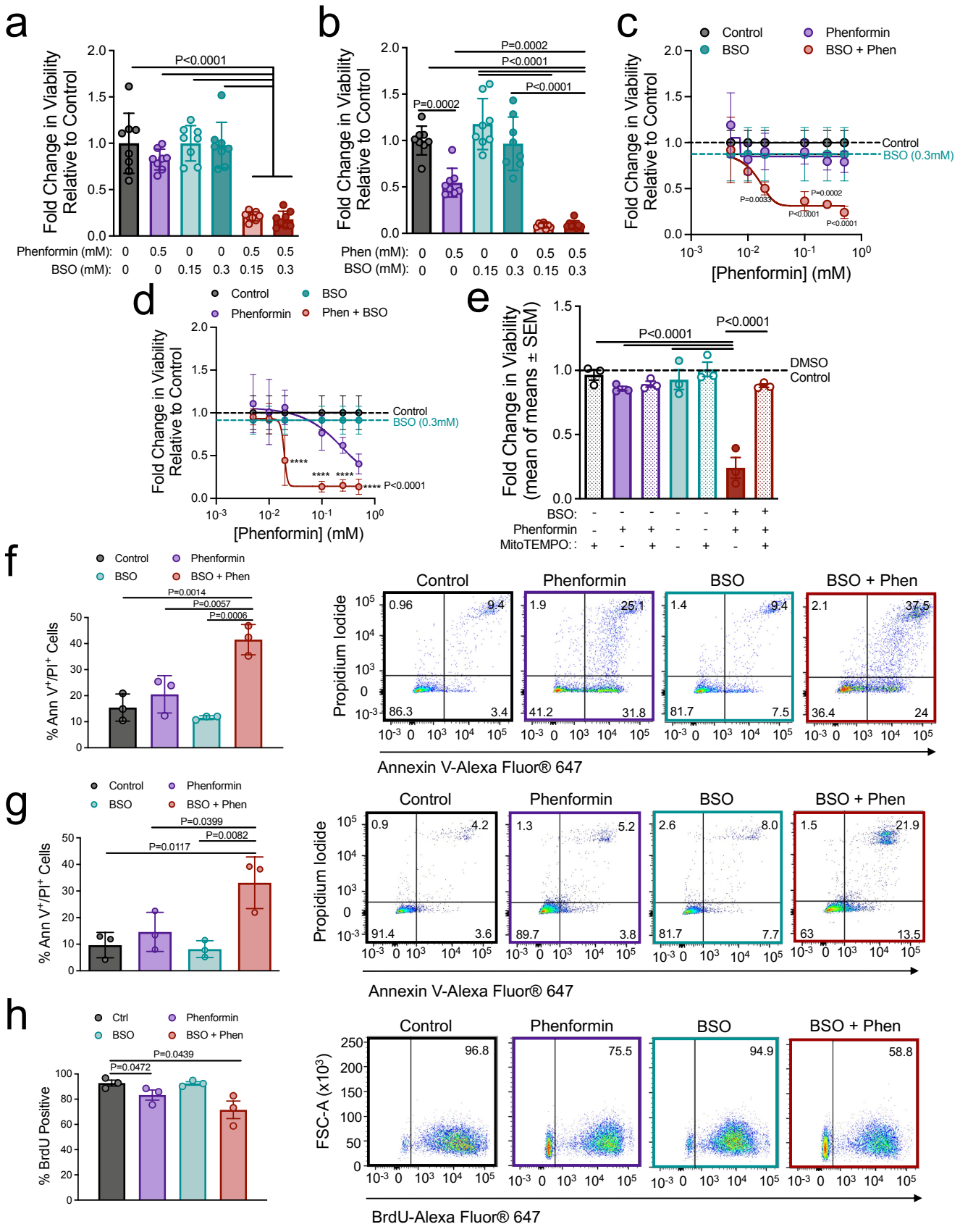
a
Fold Change in Viability Relative to Control
P<0.0001
Phenformin (mM): 0 0.5 0 0 0.5 0.5
BSO (mM): 0 0 0.15 0.3 0.15 0.3
b
Fold Change in Viability Relative to Control
P=0.0002
P<0.0001
P=0.0002
P<0.0001
Phen (mM): 0 0.5 0 0 0.5 0.5
BSO (mM): 0 0 0.15 0.3 0.15 0.3
c
Control
Phenformin
BSO
BSO + Phen
Fold Change in Viability Relative to Control
Control
BSO (0.3mM)
P=0.0033
P=0.0002
P<0.0001
P<0.0001
[Phenformin] (mM)
d
Control
BSO
Phenformin
Phen + BSO
Fold Change in Viability Relative to Control
Control
BSO (0.3mM)
P<0.0001
[Phenformin] (mM)
e
Fold Change in Viability (mean of means ± SEM)
P<0.0001
P<0.0001
DMSO Control
BSO:
Phenformin
MitoTEMPO:
f
Control
Phenformin
BSO
BSO + Phen
P=0.0014
P=0.0057
P=0.0006
% Ann V+/PI+ Cells
Control
Phenformin
BSO
BSO + Phen
Propidium Iodide
0.96
9.4
86.3
3.4
1.9
25.1
41.2
31.8
1.4
9.4
81.7
7.5
2.1
37.5
36.4
24
Annexin V-Alexa Fluor® 647
g
Control
Phenformin
BSO
BSO + Phen
P=0.0399
P=0.0082
P=0.0117
% Ann V+/PI+ Cells
Control
Phenformin
BSO
BSO + Phen
Propidium Iodide
0.9
4.2
91.4
3.6
1.3
5.2
89.7
3.8
2.6
8.0
81.7
7.7
1.5
21.9
63
13.5
Annexin V-Alexa Fluor® 647
h
Ctrl
Phenformin
BSO
BSO + Phen
P=0.0439
P=0.0472
% BrdU Positive
Control
Phenformin
BSO
BSO + Phen
FSC-A (x10³)
96.8
75.5
94.9
58.8
BrdU-Alexa Fluor® 647

Figure 3.11: Inhibiting glutathione synthesis sensitizes breast cancer cells to phenformin

(a) Viability of MDA-MB-231 cells treated for 48 hours with phenformin, buthionine sulfoximine (BSO), alone or in combination, or with PBS control, with varying concentrations of BSO. See Figure for concentrations.
(b) Viability of BT474 cells treated for 48 hours with phenformin, BSO, either alone or in combination, with varying concentrations of BSO. See Figure for concentrations.
(c) Viability of MDA-MB-231 cells were treated for 48 hours with phenformin, BSO, in combination, or with PBS control, with varying concentrations of phenformin as indicated in Figure.
(d) Viability of BT474 cells were treated for 48 hours with phenformin, BSO, either alone or in combination, with varying concentrations of phenformin as indicated.
(e) Viability of MDA-MB-231 pre-treated with 10 μM MitoTEMPO, and then treated with phenformin (500 μM) and BSO (300 μM), either alone or in combination, or with PBS control for 48 hours.
(f) Percent of Annexin V and propidium iodide (PI) double positive cells, as determined by flow cytometry, of MDA-MB-231 cells that were treated with and PBS control, phenformin (500 μM) and/or BSO (300 μM) for 40 hours. *n*=3 independent experiments.
(g) Percent of Annexin V and propidium iodide (PI) double positive cells, as determined by flow cytometry, of BT474 cells that were treated with PBS control, phenformin (500 μM) and/or BSO (300 μM) for 40 hours. *n*=3 independent experiments.
(h) Percentage of BrdU positive cells, as determined by flow cytometry, of MDA-MB-231 cell line that were treated PBS control, phenformin (500 μM) and/or BSO (300 μM) for 40 hours.
Panels a-d, the data is shown as fold change in viability compared to PBS control (mean ±SD), two independent experiments each, with n=4 technical repeats each. For panels e-h, *n*=3 independent experiments, (mean of means ±SEM). For panels f-h representative dot plots are also shown. For panels f, g, h, see Figure 2.1c for gating strategies used.
P values indicated in panels c and d compare combination of phenformin + BSO to treatment with respective concentration of phenformin alone, ****P<0.0001.
P values were calculated using a two-way ANOVA with a Tukey's posthoc test.

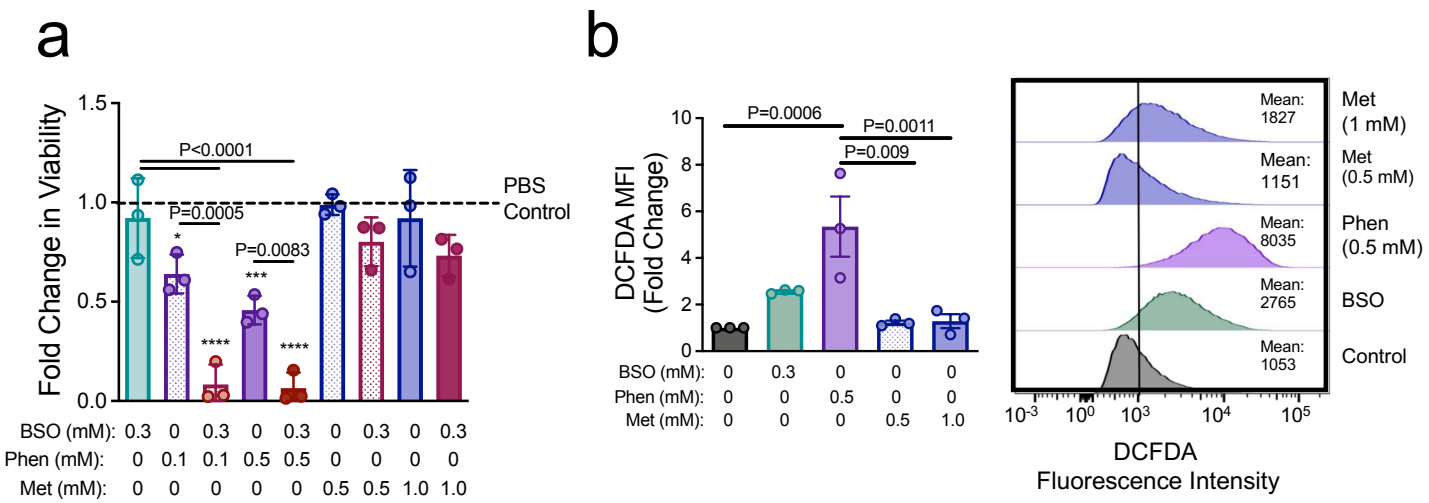

Figure 3.12: Phenformin is more potent than metformin in inducing ROS production and in sensitizing breast tumors to BSO treatment

(a) Viability of BT474 cells treated with BSO and varying concentrations of phenformin or metformin (as indicated), either alone or in combination for 48 hours. The data is shown as a fold change in cell viability compared to PBS control and is representative of *n*=3 independent experiments (mean of means ±SEM). *P values to control *P=0.0154, ***P=0.0006, ****P<0.0001. Otherwise, P value comparison is indicated with a line.

(b) Total ROS levels assessed by flow cytometry with DCFDA of BT474 cells treated with BSO, phenformin or metformin, or PBS control for 24hours. The data represents the average fold change in the DCFDA geometric mean fluorescence intensity (MFI) relative to PBS treated controls from *n*=3 independent experiments (mean of means ±SEM). Representative histograms are shown. See Figure 2.1d in methods section for gating strategy.

P values were calculated using a two-way ANOVA with a Tukey's posthoc test.

Given the evidence that oxidative stress is required for IFNγ and phenformin to elicit anti-tumorigenic effects (Figures 3.8f-h, 3.9a,b), we focused on differentially expressed genes that control redox homeostasis (Figure 3.13c). This included 10 genes (Nos2, Nox4, Txnip, Xdh, Bnip3, Noxo1, Ddit4, Duoxa1, Lrrk2, Duox1), encoding proteins with ROS-inducing properties that were overexpressed in $STAT1^{WT}$ cells compared to their STAT1-deficient counterparts (Figure 3.13c, d). However, as IFNγ is not sufficient to stimulate ROS production in breast cancer cells (Figure 3.8a-e), we focused on differentially expressed genes that function as ROS scavengers. Three such genes were identified, including PRDX4, SOD3 and NQO1 (Figure 3.13d). *Prdx4* mRNA levels were increased by IFNγ and *Sod3* mRNA levels were only repressed by IFNγ in MT4788 cells (Figure 3.13d). However, STAT1 activation reduced *Nqo1* levels in both MT864 and MT4788 cells in response to IFNγ stimulation (Figure 3.13d).

NQO1 encodes an NAD(P)H dehydrogenase that functions as a two-electron reductase with important roles in superoxide scavenging, quinone detoxification and the cellular stress response [294]. Moreover, NQO1 is frequently overexpressed in many tumor types, including lung and breast cancers [315, 616]. We first validated *Nqo1* as a STAT1 target gene whose expression decreases upon IFNγ treatment, specifically in STAT1-proficient MT4788 cells (Figure 3.13e). As a control, we confirmed a strong induction of *Erap1*, a known IFNγ responsive gene, in STAT1-proficient cells (Figure 3.13e). We also found that levels of *Nqo1* were also decreased in breast cancer cells that were co-treated with IFNγ and phenformin (Figure 3.13f). We sought to address whether IFNγ also decreased *NQO1* transcript levels in the panel of human breast cancer cells that were used in Figure 3.2c. *NQO1* levels did not decrease upon IFNγ treatment in the human cell lines tested, as assessed by RT-PCR (Figure 3.14a). We next interrogated these same cells for baseline NQO1 protein, as well as STAT1 total and pY701-STAT1 among these various subtypes. We did not observe a correlation between either STAT1 or pY701-STAT1 and NQO1 at baseline (Figure 3.14b). Considering this, we sought to understand whether IFNγ treatment in these same human cell lines led to decreased NQO1 protein. Indeed, IFNγ treatment decreased NQO1 protein levels in 3/5 TNBC cell lines tested, namely MDA-MB-231, Hs578t and MDA-MB-436, but not the other subtypes or cell lines. Increased STAT1 expression and Y701-STAT1 phosphorylation confirms IFNγ-driven STAT1 activation in these cells (Figure 3.14c). Immunoblot analysis of tumor lysates from 18 patient derived xenografts of lung cancer brain metastases confirmed this inverse correlation (Figure 3.14d).

With the aim of further clarifying IFNγ-STAT1 driven NQO1 regulation downregulation, we performed STAT1-CHIP experiments in both MT4788 and MDA-MB-231 cells at 1h and 24h following IFNγ treatment. We measured relative STAT1 binding to the promoter or transcriptional

start site (TSS) of NQO1 (along with intron 1 as a negative control). As a positive control, we included the promoter and TSS of IRF1, which is a known STAT1 target gene. While IRF1 showed STAT1 binding, we did not observe STAT1 binding to the promoter or TSS of *Nqo1/NQO1* in either mouse or human breast cancer cell lines. Thus, we cannot conclude that NQO1 is a direct STAT1 target gene. Rather, IFNγ-STAT1 signaling indirectly controls NQO1 gene expression through complex mechanisms, including both at transcriptional and post-transcriptional levels. These results suggest that NQO1 is a STAT1 target that is repressed in response to IFNγ treatment in some but not all breast cancers, and that the mechanism remains unclear and beyond the scope of this thesis.

To functionally test whether IFNγ-induced inhibition of NQO1 expression contributes to the observed cooperation between IFNγ and phenformin, we overexpressed NQO1 in MT4788 cells (Figure 3.15a). Increasing NQO1 protein levels rescued their viability in response to combined IFNγ and phenformin treatment to the level of phenformin treatment alone (Figure 3.15b). We also employed mouse and human shRNAs to silence *NQO1* expression levels in MT4788, MDA-MD-231 and BT474 breast cancer cell lines (Figure 3.15c*)*. Reducing *NQO1* expression impaired the viability of MT4788, BT474 and MDA-MB-231 cells in response to phenformin treatment alone and did so at the approximated reduction in viability observed with IFNγ/phenformin combination treatment in each cell line (Figure 3.15d). Additionally, breast cancer cells expressing NQO1 shRNAs are not further sensitized to IFNγ and phenformin co-treatment, compared to control shRNA, suggesting that NQO1 is an essential target gene that confers the anti-tumorigenic effects phenformin (Figure 3.15d). Finally, we examined whether IFNγ-mediated inhibition of *NQO1* expression sensitizes tumors to phenformin through an oxidative stress response. While shRNA-mediated *NQO1* knockdown increased the cytotoxic potential of phenformin in MDA-MB-231 cells, this was reversed by co-treatment with MitoTEMPO (Figure 3.15e, f). These findings are congruent with a previous study demonstrating that ROS-induced cytotoxicity of rotenone, another complex I inhibitor, could be reversed with Coenzyme Q (CoQ) in an NQO1-dependent manner [298]. Taken together, these results demonstrate that STAT1-dependent signaling inhibits NQO1 expression in some breast cancer cells sensitizing them to phenformin through inducing oxidative stress. Strikingly, directly silencing NQO1 sensitizes tumors to phenformin, independent of IFNγ treatment, revealing an important role for NQO1 in protecting tumor cells from phenformin-generate ROS.

a

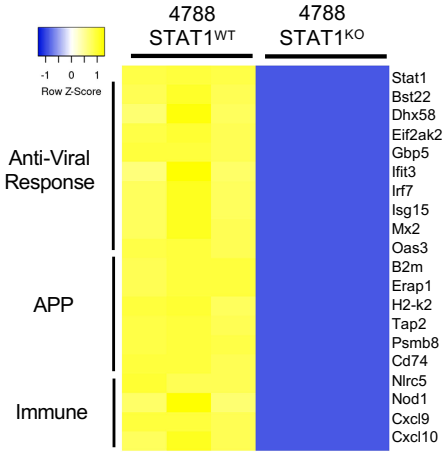

b

GO Term	# Genes	FDR	Fold Enrichment
immune system process	89	4.5E-27	3.667
anti-viral defense	45	1.66E-16	4.252
innate immune response	62	1.34E-10	2.446
antigen processing	20	3.21E-10	5.844
cell migration	36	5.51E-08	2.798
ossification	23	1.03E-07	3.780
IFNγ response	19	1.45E-07	4.409
inflammatory response	48	5.18E-07	2.202
wound healing	20	5.58E-06	3.357
response to hypoxia	30	1.13E-05	2.465
gene expression	49	1.42E-05	1.938
cell adhesion	55	3.84E-05	1.789
regulation of apoptosis	42	3.99E-05	1.978
ROS regulation	**11**	**9.21E-05**	**4.567**
cell chemotaxis	16	9.66E-05	3.237
regulation of proliferation	31	1.05E-04	2.155
angiogenesis	32	1.16E-04	2.113
circadian rhythm	19	1.42E-04	2.776
regulation of exocytosis	09	2.50E-04	5.072
ECM organization	19	2.86E-04	2.629
signal transduction	44	4.87E-04	1.736
glucose metabolism	06	7.01E-04	5.049
superoxide metabolism	**05**	**0.0289**	**4.152**

c

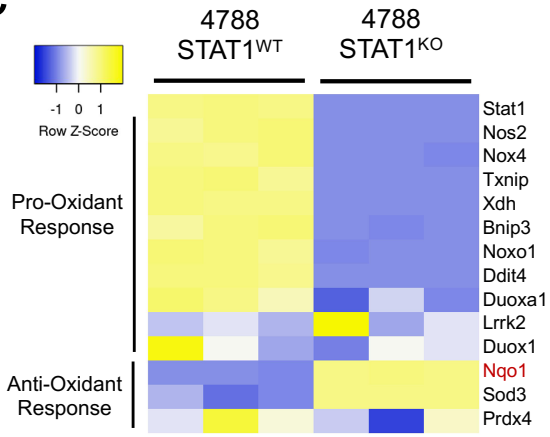

d

Gene	864 WT/KO*	864 FDR	4788 WT/KO8	4788 FDR	
STAT1	↑ 34 fold	0	↑ 77 fold	0	
NOS2	↑ 4.8 fold	1.23E-23	↑ 212 fold	8.7E-128	ROS Inducer
NOX4	no change	0.293	↑ 64 fold	4.68E-43	ROS Inducer
TXNIP	no change	0.516	↑ 8.6 fold	0	ROS Inducer
XDH	↑ 2.4 fold	7.5E-125	↑ 3.6 fold	0	ROS Inducer
BNIP3	↑ 1.4 fold	3.74E-07	↑ 3.1 fold	8.7E-110	ROS Inducer
NOXO1	↑ 1.2 fold	0.00046	↑ 3.0 fold	1.8E-161	ROS Inducer
DDIT4	↓ 1.4 fold	0.0292	↑ 2.6 fold	0	ROS Inducer
DUOXA1	↓ 2.1 fold	6.69E-61	↑ 1.3 fold	0.00026	ROS Inducer
LRRK2	↑ 3.5 fold	1.95E-33	no change	0.5257	ROS Inducer
DUOX1	↓ 3.2 fold	1.1E-97	no change	0.8522	ROS Inducer
NQO1	**↓ 1.5 fold**	**2.5E-09**	**↓ 3.9 fold**	**0**	ROS Scavenger
SOD3	no change	0.3472	↓ 2.6 fold	2.83E-10	ROS Scavenger
PRDX4	↑ 2.1 fold	3.9E-102	no change	0.1032	ROS Scavenger

***Fold change between STAT1WT and STAT1KO cells treated with IFNγ**

e

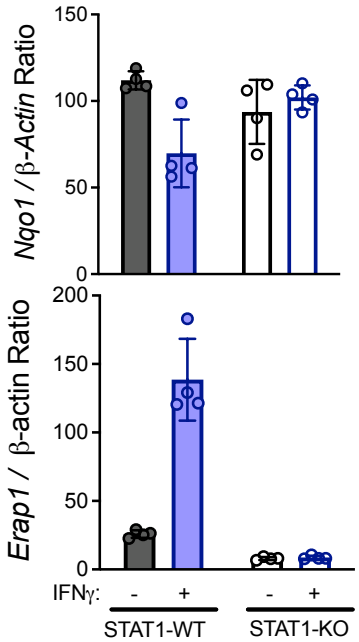

f

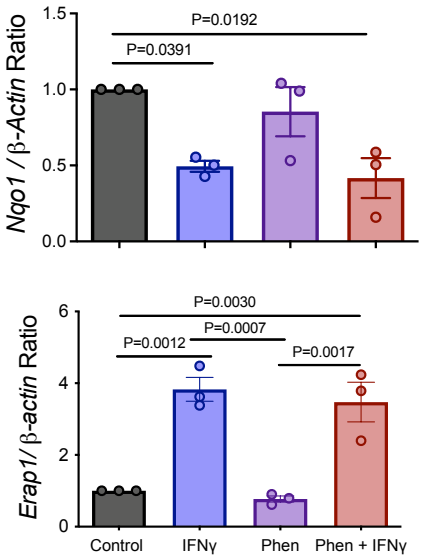

Figure 3.13: Nqo1 is identified as a ROS scavenger downstream of IFNγ-STAT1 axis in MT4788 and MT864 murine breast cancer cells

(a-d) RNAseq analysis of MT4788-WT and MT4788 STAT1-KO breast cancer cells stimulated with IFNγ for 24 hours.
(a) Heatmaps of the top differentially expressed genes (>2 fold; FDR <0.05) controlling known IFNγ-regulated pathways. *n*=3 biological repeats per condition.
(b) Gene Ontology (GO) terms that are most differentially expressed between IFNγ-treated MT4788 STAT1-WT and MT4788 STAT1-KO. The number of differentially expressed genes, false discovery rate (FDR) and fold enrichment for each GO term are shown.
(c) Heatmap of differentially expressed genes (>2 fold; FDR <0.05) associated with ROS metabolism, between IFNγ-treated MT4788 STAT1-WT and MT4788 STAT1-KO cells.
(d) Differentially regulated genes involved in redox control, including ROS inducers and ROS scavengers. The fold change in gene expression (WT/KO) and false discovery rate (FDR) for each gene is shown across both cell lines.
The data is representative of n=3 biological repeats per condition.
(e) *Nqo1* and *Erap1* expression by RT-qPCR analysis, in IFNγ-treated (1 ng/ml) or PBS-treated MT4788 STAT1-WT and STAT-KO cells, for 24 hours, *n*=4 technical repeats (mean ±SD), reported as a ratio to β -actin.
(f) *Nqo1* and *Erap1* expression by RT-qPCR analysis in PBS control, IFNγ (1 ng/ml), phenformin (500 μM), co-treated or single-treated MT4788 cells for 24 hours, *n*=3 independent experiments (mean of means ±SEM), reported as a ratio to β -actin. P values in were calculated using two-way ANOVA with a Tukey's posthoc test.

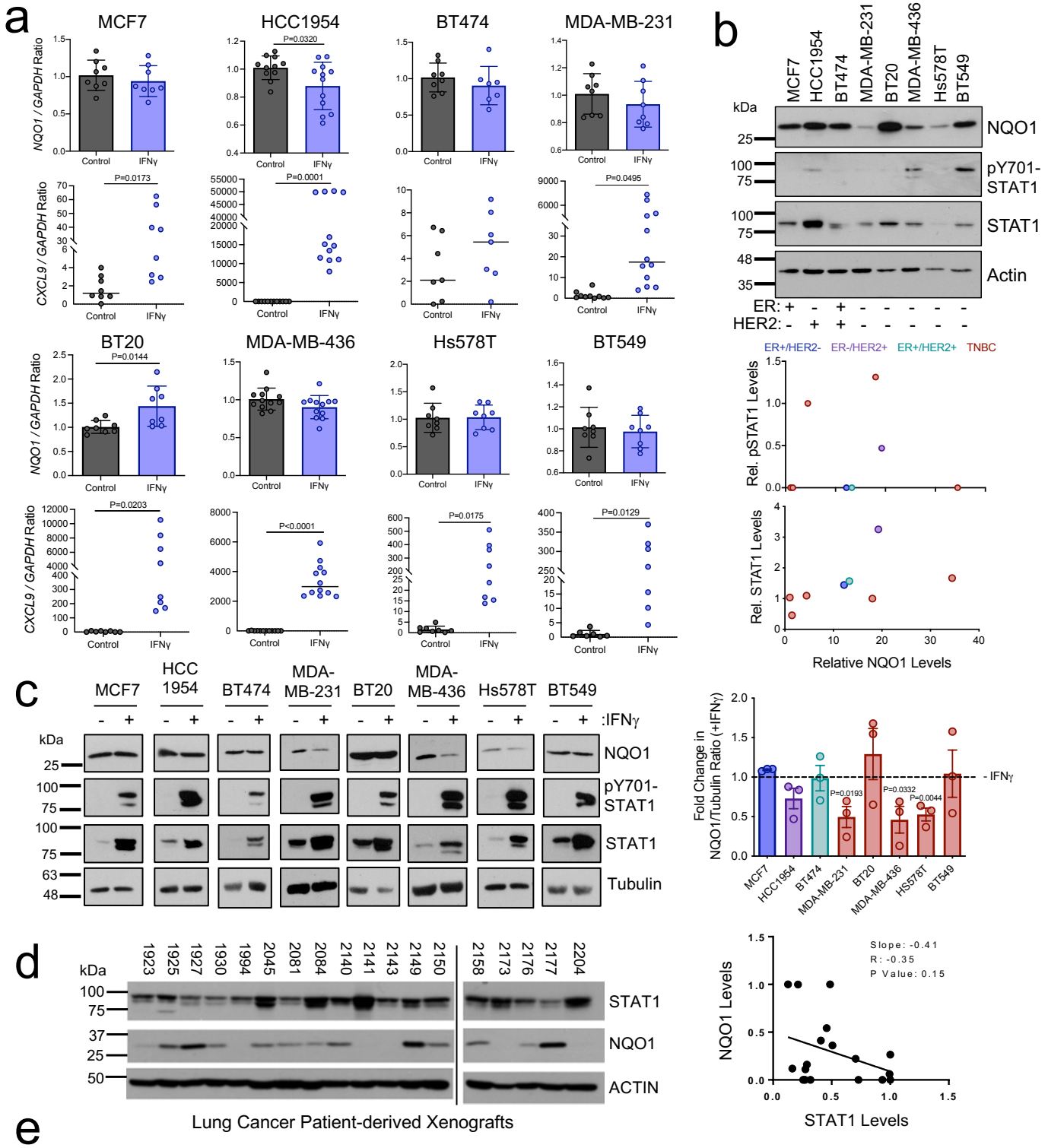
a
MCF7
HCC1954
BT474
MDA-MB-231
BT20
MDA-MB-436
Hs578T
BT549
NQO1 / GAPDH Ratio
CXCL9 / GAPDH Ratio
Control
IFNγ
P=0.0320
P=0.0173
P=0.0001
P=0.0495
P=0.0144
P=0.0203
P<0.0001
P=0.0175
P=0.0129
b
kDa
NQO1
pY701-STAT1
STAT1
Actin
ER: + - + - - - - -
HER2: - + + - - - - -
ER+/HER2-
ER-/HER2+
ER+/HER2+
TNBC
Rel. pSTAT1 Levels
Rel. STAT1 Levels
Relative NQO1 Levels
c
MCF7
HCC 1954
BT474
MDA-MB-231
BT20
MDA-MB-436
Hs578T
BT549
:IFNγ
kDa
NQO1
pY701-STAT1
STAT1
Tubulin
Fold Change in NQO1/Tubulin Ratio (+IFNγ)
- IFNγ
P=0.0193
P=0.0332
P=0.0044
d
kDa
1923 1925 1927 1930 1994 2045 2081 2084 2140 2141 2143 2149 2150 2158 2173 2176 2177 2204
STAT1
NQO1
ACTIN
Lung Cancer Patient-derived Xenografts
NQO1 Levels
STAT1 Levels
Slope: -0.41
R: -0.35
P Value: 0.15
e
MT4788
MDA-MB-231
MDA-MB-436
% input
mIRF1 Promoter
mIRF1 TSS
mNQO1 Promoter
mNQO1 TSS
mNQO1 Intron 1
hIRF1 Promoter
hIRF1 TSS
hNQO1 Promoter
hNQO1 TSS
hNQO1 Intron 1
IgG
Untreated
IFNγ 1h
IFNγ 24h

Figure 3.14: Nqo1 levels are inversely correlated with STAT1 transcriptional activity in MT4788 breast cancers and lung adenocarcinomas

(a) RT-qPCR analysis in PBS-treated or IFNγ-treated (10 ng/ml) for 24 hours, from human breast cancer cell lines from Figure 3.2c. MCF7: *n*=8; HCC1954: Control: *n*=11, IFNγ: *n*=12; BT474: Control: *n*=8, IFNγ: *n*=7; MDA-MB-231: *n*=8; BT20: *n*=8; MDA-MB-436: *n*=12; Hs578t: *n*=8; BT549: *n*=8; technical repeats over two independent experiments each, expressed as a ratio to GAPDH, mean ±SD.
(b) NQO1, Y701-phosphorylated STAT1 and STAT1 immunoblot analysis of human breast cancer cell lines. Relative NQO1 protein levels compared to pY701 STAT1 or total STAT1 levels were quantified, *n*=1 technical repeat. β-Actin was used as a loading control.
(c) NQO1, Y701-phosphorylated STAT1 and STAT1 immunoblot analysis of cell lines from panel b following 48-hour IFNγ (10 ng/ml) treatment. Fold change of the NQO1/Tubulin Ratio upon IFNγ treatment relative to PBS controls was quantified from *n*=3 independent experiments, (mean of means ±SEM). Tubulin is used as a loading control.
(d) NQO1 and STAT1 immunoblot analysis of tumor lysates from 18 independent lung cancer brain metastasis patient-derived xenografts. Densitometric quantification of the immunoblots shown, represented as relative NQO1 and STAT1 levels normalized to loading control, β-Actin.
(e) ChIP-PCR, with STAT1 antibody, and either murine or human primers for NQO1 promoter, transcription start site (TSS) or intron 1; in MT4788, MDA-MB-231 and MDA-MB436 breast cancer cell lines that were treated with PBS, or IFNγ (10 ng/ml) for 1 hour or 24 hours. Known STAT1 target gene, IRF1 primers was used as a positive control; IgG was used as a negative antibody control. *n*=1 independent repeats for each.
P values were calculated using unpaired two-sided t-tests for panel a, one-way ANOVA with a Tukey's posthoc test panel c. A Pearson's correlation (linear regression analysis) was used to calculate the relationship between NQO1 and STAT1 levels panel d.

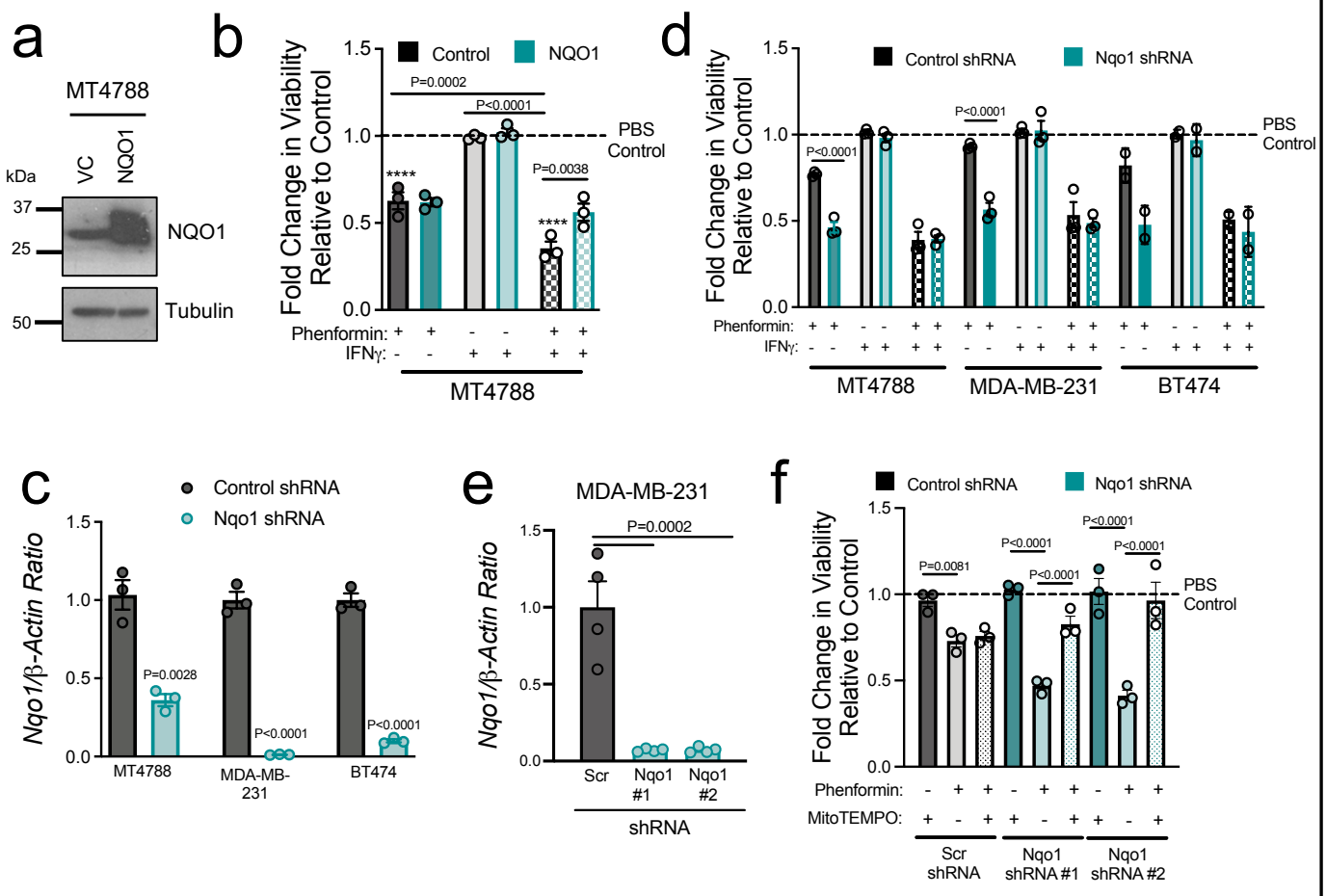

Figure 3.15: IFNγ-induced inhibition of NQO1 expression potentiates the anti-tumorigenic effects of phenformin

(a) NQO1 immunoblot analysis of MT4788-Vector control (VC) and NQO1-overexpressing MT4788 cells, *n*=3 biological repeats. Tubulin is used as a loading control. Representative blot is shown.

(b) Relative viability of cells described in panel a in response to phenformin (500 μM), IFNγ (1ng/ml) or PBS, alone or combination treatment for 48 hours. Data is shown as fold change in viability compared to PBS-treated controls, *n*=3 independent experiments (mean of means ±SEM).****P value<0.0001 comparing with PBS control. Other P values are indicated in Figure.

(c) RT-qPCR analysis of cell lines transduced with shRNAs targeting human NQO1 or mouse *Nqo1* or with a control non-mammalian shRNA, (mean of means ±SEM), *n*=3 biological repeats.

(d) Viability of cells in panel c treated with IFNγ (1 ng/ml) and/or phenformin (500 μM), for 48h. The data is shown as fold change in cell viability compared to PBS control and is representative of *n*=3 independent experiments (MT4788 and MDA-MB-231) (mean of means ±SEM), or *n*=2 independent experiments (BT474) (mean of means ±SD).
(e) RT-qPCR analysis of MDA-MB-231 cells engineered to individually express two shRNAs (1 and 2) targeting human *NQO1* or a control with non-mammalian targeting shRNA. *n*=4 biological repeats, (mean of means ±SEM).
(f) Viability of cells described in panel e treated with phenformin (500 μM) for 48h, either in the absence or presence of pre-treatment with 5 μM MitoTEMPO. Data is shown as fold change in viability compared to PBS controls, *n*=3 independent experiments, (mean of means ±SEM).
P values were calculated using unpaired two-sided t tests comparing panels c; a two-way ANOVA with a Tukey's posthoc test for panels b, d, f; and a one-way ANOVA with a Tukey's posthoc test for panel e.

3.8 β-lapachone, an NQO1-bioactivatable drug, sensitizes breast tumors to phenformin by inducing oxidative damage

NQO1 is a viable drug target in oncology [294] and is overexpressed in many tumors compared to normal tissues [617][617][617][617][617]. β-lapachone is a quinone-containing pro-drug that is bioactivated by NQO1 to undergo a futile redox cycle. In doing so, β-lapachone not only sequesters NQO1 from its endogenous substrates but also further potentiates superoxide generation in NQO1-expressing cells [576, 616, 618, 619]. We next tested whether combining β-lapachone could sensitize tumors to phenformin-induced ROS. At the concentrations tested, β-lapachone treatment alone minimally impacted cell viability (Figure 3.16a-c). Yet, β-lapachone profoundly sensitized all cell lines tested (MDA-MB-231, BT474 and BT549) to phenformin treatment in combination-treated cells (Figure 3.16a-c). Although β-lapachone and phenformin co-treatment did not appreciably alter apoptotic cell death (Figure 3.16d), this drug combination significantly decreased tumor cell proliferation (Figure 3.16e).

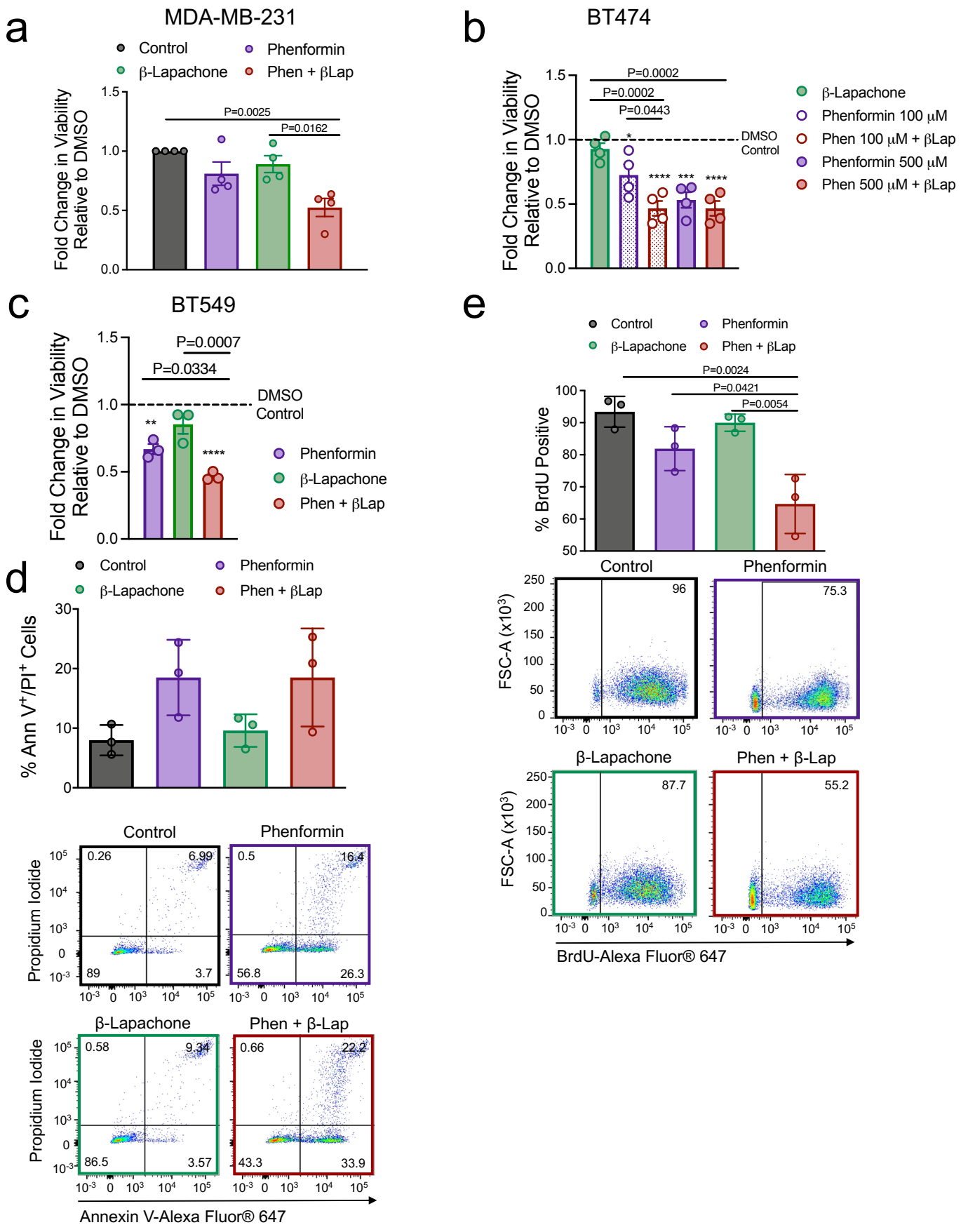
a
MDA-MB-231
Control
Phenformin
β-Lapachone
Phen + βLap
Fold Change in Viability Relative to DMSO
P=0.0025
P=0.0162
b
BT474
P=0.0002
P=0.0002
P=0.0443
DMSO Control
β-Lapachone
Phenformin 100 μM
Phen 100 μM + βLap
Phenformin 500 μM
Phen 500 μM + βLap
c
BT549
P=0.0007
P=0.0334
DMSO Control
Phenformin
β-Lapachone
Phen + βLap
d
% Ann V+/PI+ Cells
Control
Phenformin
β-Lapachone
Phen + βLap
Propidium Iodide
0.26
6.99
89
3.7
0.5
16.4
56.8
26.3
0.58
9.34
86.5
3.57
0.66
22.2
43.3
33.9
Annexin V-Alexa Fluor® 647
e
% BrdU Positive
P=0.0024
P=0.0421
P=0.0054
FSC-A (x10³)
96
75.3
87.7
55.2
BrdU-Alexa Fluor® 647

Figure 3.16: Breast cancer cells are sensitive to the anti-tumorigenic effects of β-lapachone and phenformin combination treatment

(a, b) Viability of **(a)** MDA-MB-231 **(b)** BT474 **(c)** BT549 cells treated with phenformin (100 μM or 500 μM), β-lapachone (panels a and c: 0.5 μM, panel b: 1 μM), or DMSO/PBS control alone or in combination, for 48 hours. Data is shown as the fold change in cell viability relative to DMSO control, panels a and b: *n*=4 independent experiments; panel c: *n*=3 independent experiments (mean of means ±SEM).
(d, e) Percent of **(d)** Annexin V/PI double positive **(e)** BrdU positive MDA-MB-231 cells that were treated with PBS control, phenformin (500 μM) and/or β-Lapachone (0.5 μM) for 48 hours, as assessed by flow cytometry. Data is expressed as the fold change in geometric MFI. The data is representative of *n*=3 experiments (±SEM). Representative dot plots are shown.
For panels d and e, see Figure 2.1b,c in methods section for gating strategy.
P values were calculated using a two-way ANOVA with a Tukey's posthoc test and are indicated in the figure.

We next sought to explore whether these findings could be extended *in vivo*. Using the MDA-MB-231 MFP model, we show that combined β-lapachone and phenformin treatment significantly impaired MDA-MB-231 mammary tumor growth (Figure 3.17a). Using IHC, we characterized these tumors. There were no steady state differences in the percentage of Ki67 and cleaved caspase 3 positive cells at the experimental endpoint (Figure 3.17b,c). However, combined treatment with phenformin and β-lapachone significantly increased oxidative damage in mammary tumors as assessed by 8-oxo-dG IHC staining (32.7% in control tumors vs 49.2% in β-lapachone/phenformin-treated tumors) (Figure 3.17d). These data demonstrate that β-lapachone sensitizes breast tumors to the anti-neoplastic effects of phenformin by inducing oxidative DNA damage.

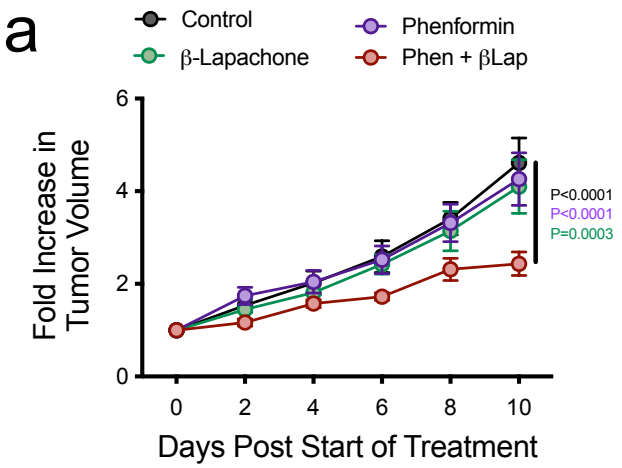
a
Control
Phenformin
β-Lapachone
Phen + βLap
Fold Increase in Tumor Volume
Days Post Start of Treatment
P<0.0001
P<0.0001
P=0.0003

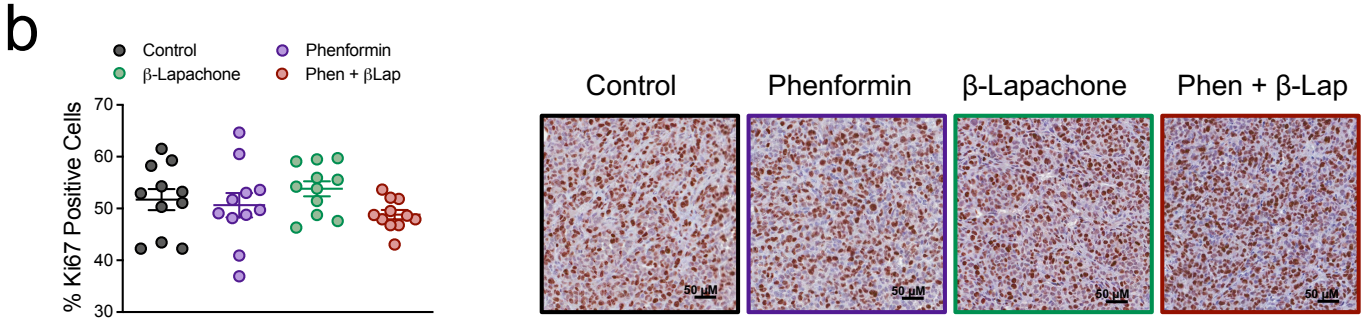
b
Control
Phenformin
β-Lapachone
Phen + βLap
% Ki67 Positive Cells
Control
Phenformin
β-Lapachone
Phen + β-Lap
50 μM

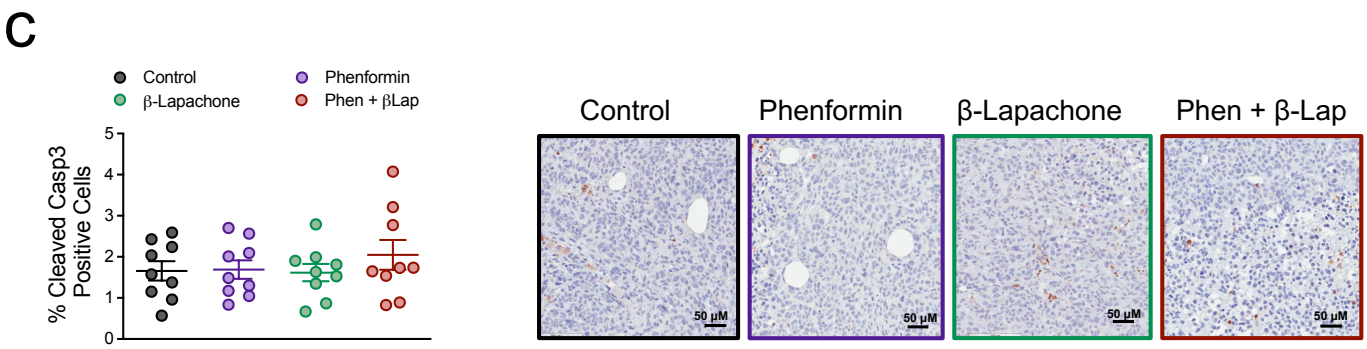
c
Control
Phenformin
β-Lapachone
Phen + βLap
% Cleaved Casp3 Positive Cells
Control
Phenformin
β-Lapachone
Phen + β-Lap
50 μM

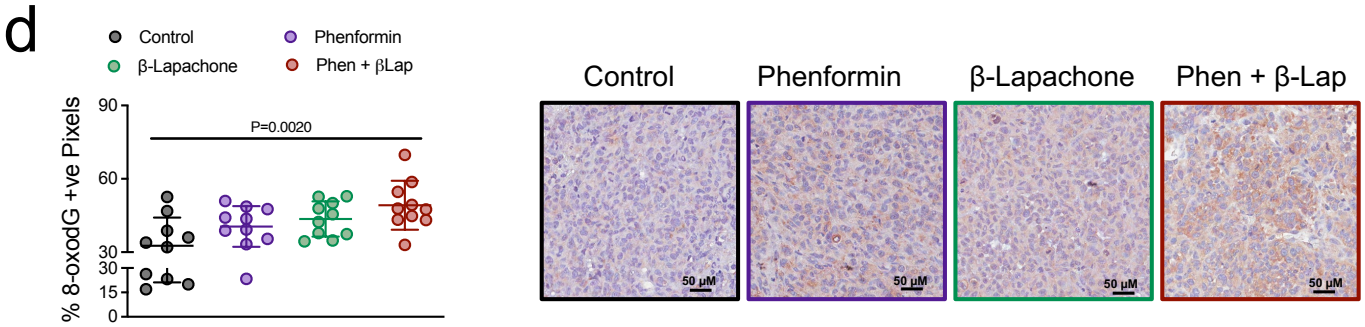
d
Control
Phenformin
β-Lapachone
Phen + βLap
% 8-oxodG +ve Pixels
P=0.0020
Control
Phenformin
β-Lapachone
Phen + β-Lap
50 μM

Figure 3.17: β-lapachone, an NQO1-bioactivatable drug, sensitizes breast tumors to phenformin by inducing oxidative damage

(a) MDA-MB-231 breast cancer cells were injected into the MFP of SCID-Beige mice. At tumor size of approximately 100 mm^3, β-lapachone/HPβCD (25 mg/kg, every 2 days) or (HPβCD/PBS, every 2 days) treatment was initiated. Two days later, phenformin (50 mg/kg, daily) (or PBS, daily) was initiated, in combination with vehicle (HPβCD/PBS) or β-lapachone/HPβCD. Tumor volumes at start of treatment: Control: 87.3 mm^3, SD: 30.2 mm^3; phenformin: 98.0 mm^3, SD: 38.1 mm^3; β-lapachone: 102.9 mm^3, SD: 25.0 mm^3; phenformin+ β-lapachone: 104.6 mm^3, SD: 30.0 mm^3. Data is represented as fold change in tumor volume relative to the start of combination treatment (±SEM), *n*=11 tumors/group; except β-lapachone/HPβCD, *n*=12 tumors/group. P values indicated in the Figure comparing combination treatment group to (black font): control; (purple font): to phenformin; (green font): to β-lapachone groups.
(b-d) Immunohistochemical analysis of mammary tumors described in panel a using **(b)** Ki67 *n*=11 tumors/group and **(c)** cleaved caspase-3-specific antibodies *n*=9 tumors/group. The data is shown as the mean percent positive cells (±SEM). Representative images are shown.
(d) 8-oxo-dG, mean percent positive pixels (±SEM) with *n*=10 tumors/group. Representative images are shown.
P values were calculated using a two-way ANOVA with a Tukey's posthoc test.

3.9 Inhibiting targetable ROS scavenging mechanisms selectively sensitize human breast cancers to multiple mitochondrial complex I inhibitors

Many tumors have elevated ROS in comparison to normal cells, which must be finely balanced with increased ROS scavenging mechanisms. This likely makes cancer cells more vulnerable to further ROS insults produced either by inducers of ROS or by inhibitors of ROS scavengers [620]. We next sought to test whether phenformin-induced ROS selectively inhibits the viability of transformed cells. We used immortalized NMuMG cells and an isogenic cell line that was transformed with NeuNT, an oncogenic variant of ErbB2 (NMuMG-NT) [571]. As expected, NMuMG cells generated lower ROS levels following phenformin treatment compared to their NeuNT-transformed counterparts (Figure 3.18a). Consistently, NMuMG cells were more resistant to the cytotoxic effects of phenformin when combined with BSO or β-lapachone,

whereas they decreased NMuMG-NT viability in a cooperative manner (Figure 3.18b). Collectively, these results suggest that cancer cells are selectively vulnerable the combination of phenformin and drugs such as BSO or β-lapachone that potentiate oxidative stress, while sparing non-transformed cells.

A novel small molecule complex I inhibitor, IACS-010759, was recently shown to have potent anti-tumorigenic effects in pre-clinical models of leukemias, and it is currently in clinical trials for leukemia and advanced cancer [413, 621]. We find that IACS-010759 also cooperates with β-lapachone to decrease the viability of MDA-MB-231 and BT474 cells (Figure 3.19a). In line with this, we find that β-lapachone and IACS-010759 co-treatment increases overall ROS levels compared to controls and either treatment alone (Figure 3.19b). These findings suggest that the anti-tumorigenic activity of several complex I inhibitors can be augmented by combining them with treatment strategies that augment oxidative stress.

We finally aimed to assess whether these findings translated to more clinically relevant models of breast cancer. We used cell lines from six patient-derived xenografts obtained from HER2+ (CRC-132, GCRC2080) and basal-like (GCRC1735, GCRC1915, GCRC1963, GCRC1986) breast cancers. Both HER2+ PDXs showed remarkable sensitivity to the cytotoxic effects of phenformin when combined either with BSO or β-lapachone (Figure 3.19c,d). Except for GCRC1963, all remaining basal-like PDXs displayed reduced viability in response to both BSO/phenformin and β-lapachone/phenformin combination treatments *in vitro* (Figure 3.19e). Although we do observe an inverse relationship between NQO1 and STAT1 in these breast cancer PDXs (Figure 3.19g,h) the NQO1/STAT1 baseline ratio is not sufficient to predict relative sensitivity to combined β-lapachone/phenformin treatment (Figure 3.19h) Indeed, we observed differences in the relative ability of BSO or β-lapachone to sensitize individual PDXs to phenformin treatment (Figure 3.19e, f), suggesting that breast tumors likely differ in their reliance on glutathione and/or NQO1 to maintain redox balance. Taken together, these results support the notion that targetable ROS scavenging mechanisms can be inhibited to selectively sensitize human breast cancers to mitochondrial complex I inhibitors.

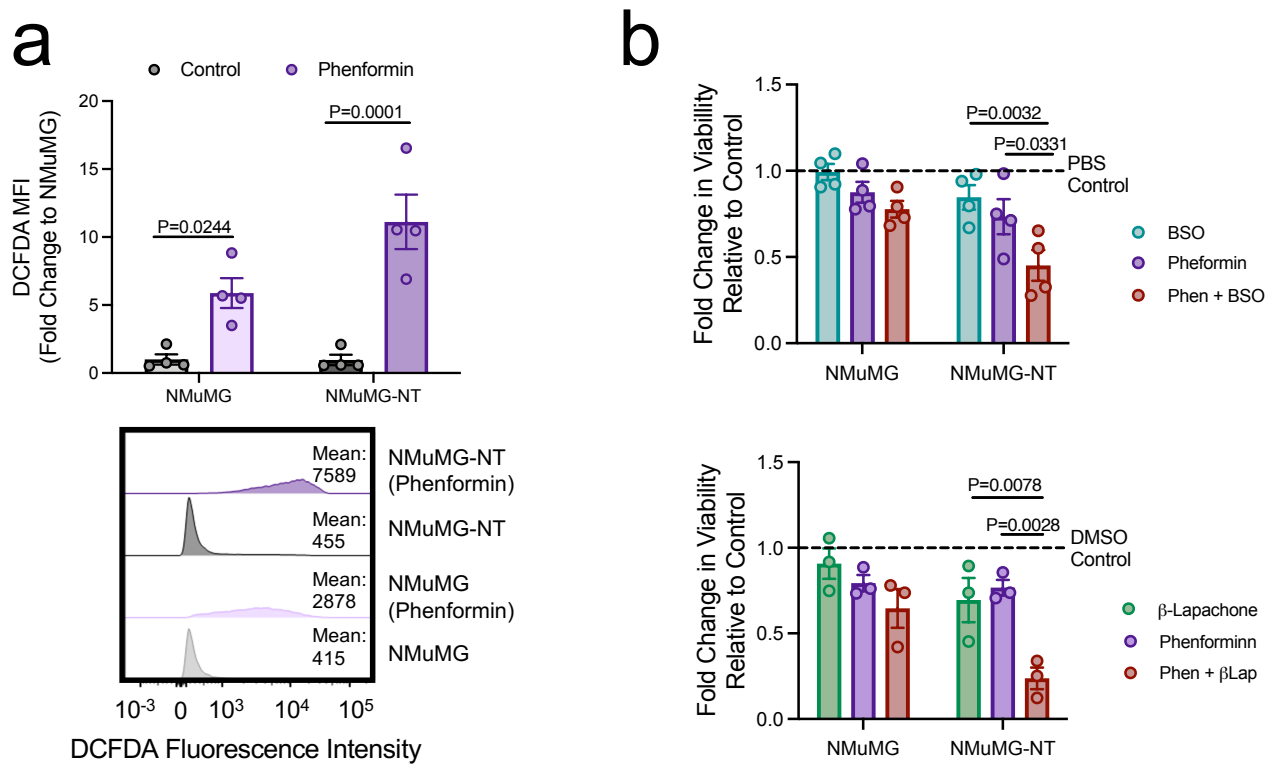

Figure 3.18: Phenformin in combination with β-lapachone or BSO selectively sensitize breast cancer cells, while sparing non-transformed cell models

(a) Total ROS, as assessed by flow cytometry with DCFDA of immortalized NMuMG and transformed NMuMG-NeuNT cells treated with PBS or phenformin (500 μM) for 24hours. The data is shown as fold change in mean fluorescence intensity compared to NMuMG cells and represents the mean of n=4 independent experiments (±SEM). Representative histograms are shown. See Figure 2.1d in methods section for gating strategy.

(b) Viability of cells described in panel a in response to phenformin (500 μM) and/or BSO (100μM) treatment (upper graph) or phenformin (500 μM) and/or β-lapachone (4μM) treatment (lower graph) for 48 hours. The data is shown as fold change in viability compared to PBS control and is representative of n=4 (upper graph) or n=3 independent experiments (lower graph), (mean of means ±SEM).

P values were calculated using a two-way ANOVA with a Tukey's posthoc test.

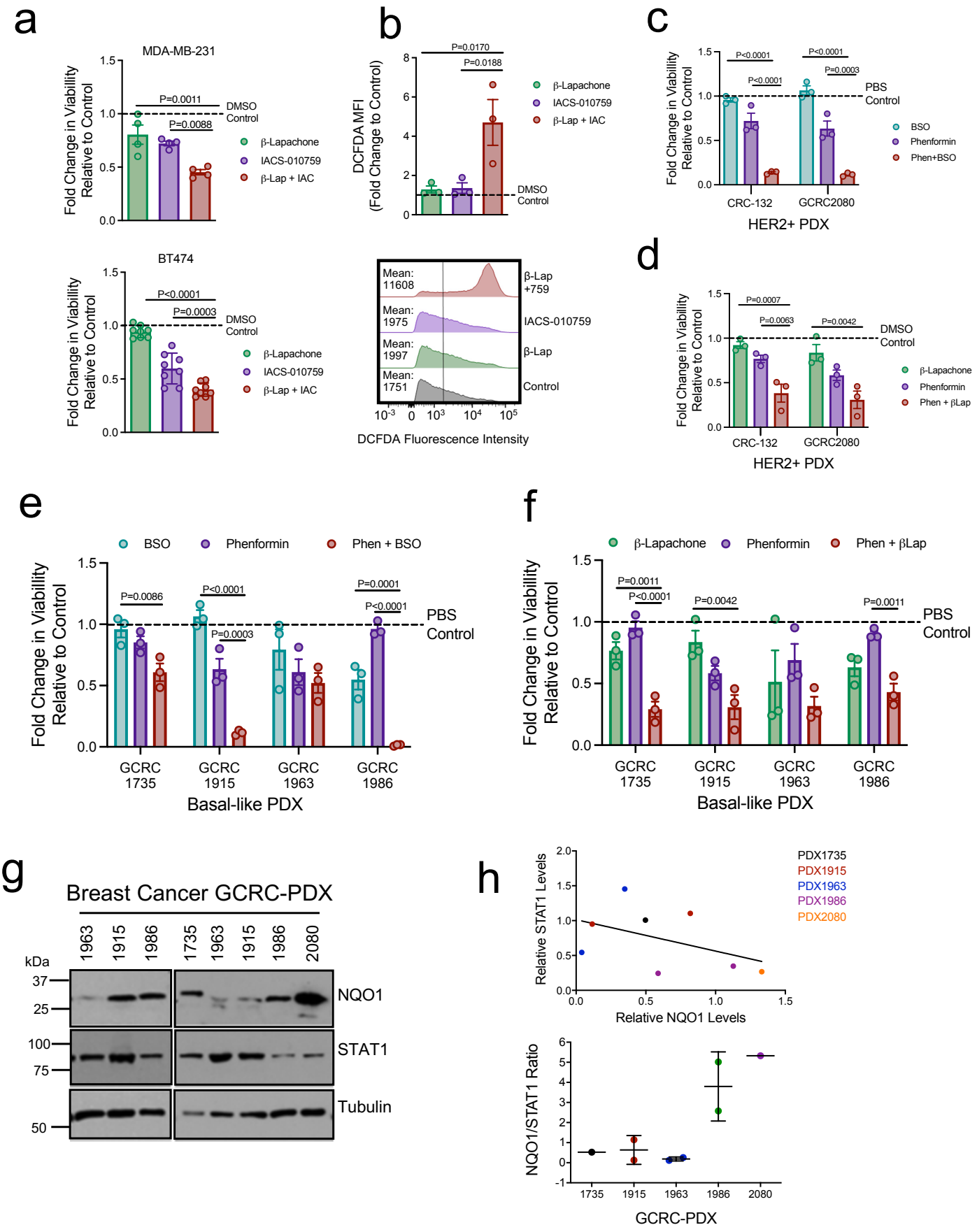
a
MDA-MB-231
Fold Change in Viability Relative to Control
P=0.0011
P=0.0088
DMSO Control
β-Lapachone
IACS-010759
β-Lap + IAC
BT474
P<0.0001
P=0.0003
b
DCFDA MFI (Fold Change to Control)
P=0.0170
P=0.0188
Mean: 11608
Mean: 1975
Mean: 1997
Mean: 1751
β-Lap +759
β-Lap
Control
DCFDA Fluorescence Intensity
c
P<0.0001
P=0.0003
PBS Control
BSO
Phenformin
Phen+BSO
CRC-132
GCRC2080
HER2+ PDX
d
P=0.0007
P=0.0063
P=0.0042
Phen + βLap
e
Phen + BSO
P=0.0086
P<0.0001
P=0.0003
P=0.0001
GCRC 1735
GCRC 1915
GCRC 1963
GCRC 1986
Basal-like PDX
f
g
Breast Cancer GCRC-PDX
kDa
37
25
100
75
50
NQO1
STAT1
Tubulin
h
Relative STAT1 Levels
Relative NQO1 Levels
PDX1735
PDX1915
PDX1963
PDX1986
PDX2080
NQO1/STAT1 Ratio
GCRC-PDX

Figure 3.19: Targetable ROS scavenging mechanisms sensitize human breast cancer models to multiple mitochondrial complex I inhibitors

(a) Viability of MDA-MB-231 and BT474 breast cancer cells treated with small molecule complex I inhibitor, IACS-010759 (50 nM) and/or β-lapachone (BT474: 1 μM and MDAMB231: 0.5 μM) for 48 hours. The data is shown as fold change in viability compared to DMSO control, *n*=4 independent experiments (mean of means ±SEM) for MDA-MB-231; or of *n*=8 technical replicates, over two independent experiments ±SD for BT474.
(b) Total ROS levels as assessed by flow cytometry with DCFDA of MDA-MB-231 cells treated with IACS-010759 (50 nM) and/or β-lapachone (0.5 μM), or DMSO control for 24 hours. The data is shown as fold change in MFI (±SEM) compared to DMSO control and is representative of *n*=3 independent experiments. See Figure 2.1d in methods section for gating strategy.
(c, d) Viability of HER2+ PDXs (CRC-132, GCRC2080) *in vitro* after treatment with phenformin (CRC-132, 100 μM; GCRC2080, 500 μM) and/or **(c)** BSO (300 μM); **(d)** β-lapachone (0.5 μM), for 48 hours. The data is shown as fold change in viability compared to vehicle (PBS for BSO and DMSO for β-lapachone) and is representative of *n*=3 independent experiments (mean of means ±SEM).
(e, f) Viability of basal-like PDXs (GCRC1735, GCRC1915, GCRC1963, GCRC1986) *in vitro* after treatment with phenformin (500 μM) and/or **(e)** BSO (300 μM); **(f)** β-lapachone (1 μM) for 48 hours. The data is shown as fold change in viability compared to vehicle and is representative of *n*=3 independent experiments (mean of means ±SEM).
(g) NQO1 and STAT1 immunoblot analysis of cell lysates from five independent breast tumor PDXs.
(h) Relative expression levels of STAT1 and NQO1 normalized to loading control Tubulin levels from quantifying immunoblots in panel g, were either plotted individually or the NQO1/STAT1 ratio for individual PDXs was also determined, GCRC1735, GCRC2080: *n*=1 sample; GCRC1915, GCRC1963, GCRC1986 *n*=2 biological repeats.
P values were calculated using a two-way ANOVA with a Tukey's posthoc test.

Chapter 4 Discussion

Taken together, the results of this body of work demonstrate the vulnerability of breast tumors across molecular subtypes to the combination of phenformin with inhibitors of ROS scavenging mechanisms. This treatment strategy concurrently exploits phenformin-induced energetic and oxidative stress (Figure 4.1).

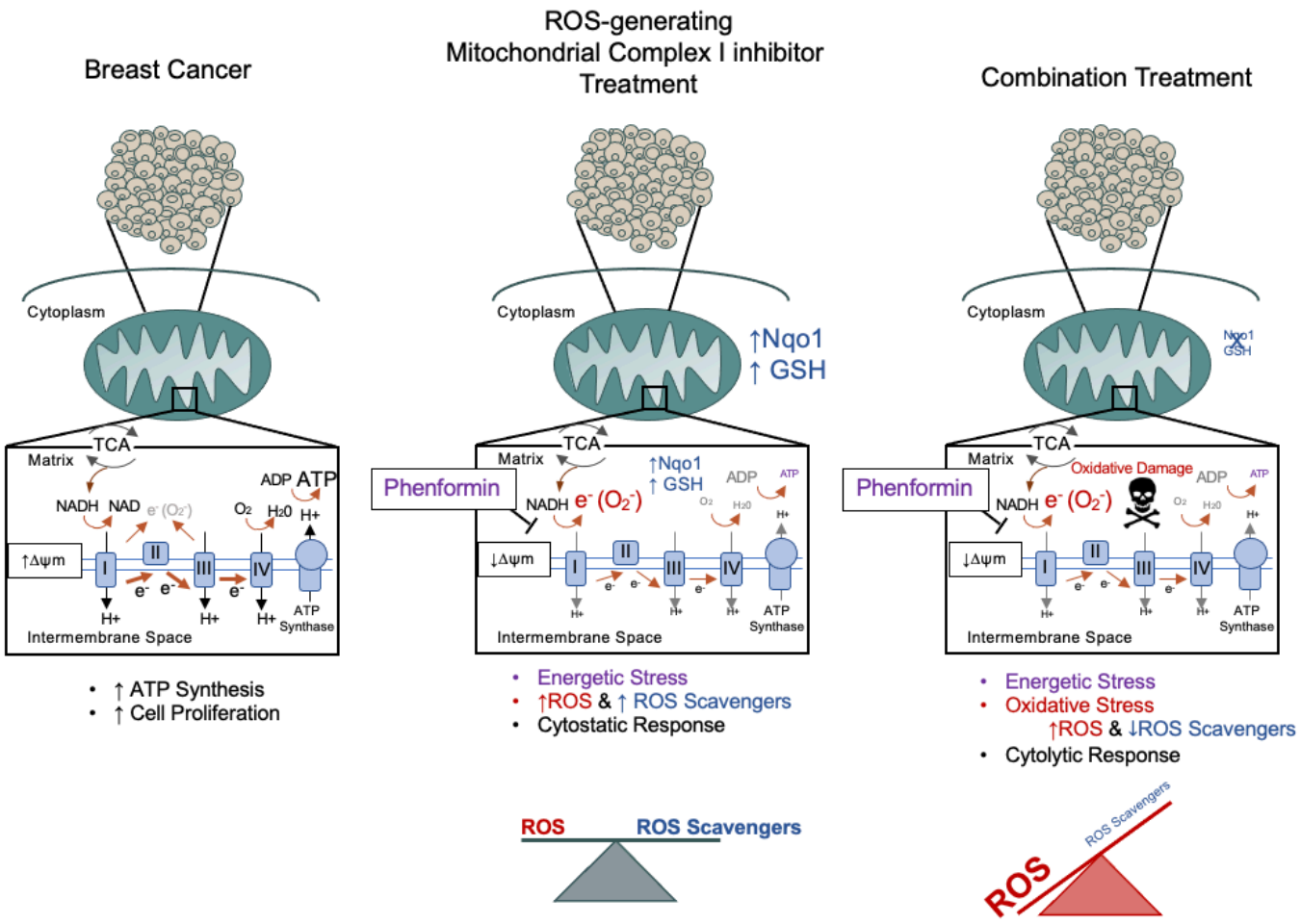

Figure 4.1: Human breast cancers are selectively sensitized to mitochondrial complex I inhibitors by disabling specific ROS scavenging mechanisms
Many breast cancers are characterized by higher levels of oxidative phosphorylation and consequently increased mitochondrial membrane potential, in comparison to normal epithelial cells. Phenformin preferentially accumulates in cells with actively respiring mitochondria. Phenformin treatment as monotherapy inhibits complex I of the electron transport chain and oxidative phosphorylation leading to energetic stress. By inhibiting complex I, phenformin also increases mitochondrial superoxide generation. Combination therapy with phenformin and simultaneously inhibiting tumor antioxidants, such as Nqo1 and glutathione, causes oxidative stress in addition to energetic stress, and is tumoricidal. Figure was adapted from Totten et al. 2021.

Despite improvement in therapies, women with IBC remain at risk of recurrence and/or progression to metastatic disease, from years to decades after their initial diagnosis [109, 110]. Breast cancer length of survival decreases if patients develop or present with distant metastases. Approximately 6-10% of individuals with breast cancer, are diagnosed with stage IV disease. Moreover, 20-30% of early-stage breast cancers will go on to develop metastatic disease [113]. Presently, metastatic disease is essentially incurable.

Mitochondrial metabolism and redox state of tumors have emerged as important factors in metastasis and resistance/residual disease, in breast cancer and other cancers alike [213, 214]. Specifically, high OXPHOS levels have been reported in many tumor types and are shown to predict resistance to standard treatments, as well as to be enriched in residual tumor cells [347-351]. OXPHOS upregulation in patient pre-treatment biopsies with TNBC, was associated with worse outcome [344]. Recent characterizations of PDX models of TNBC metastatic breast tumors revealed that OXPHOS is a top pathway upregulated during metastatic seeding, and that by inhibiting the electron transport chain in these models, metastasis was functionally abrogated [345]. Interestingly, metabolic phenotypes seem to differ between models that colonize specific organs, engaging either OXPHOS or glycolysis; versus cells that can seed multiple organs are, can engage both OXPHOS and glycolysis [215], highlighting the fact that metabolic plasticity is associated with progression to more aggressive disease.

Breast cancer metabolism is continually being understood, and there is evidence of common metabolic profiles and dependencies within molecular subtypes. For example, many HER2+ breast cancers demonstrate increased lipid metabolism [331-333]. TNBC metabolic heterogeneity is also appreciated. Some TNBC breast cancer cell lines have been shown to rely more heavily on glycolysis than ER positive cell lines tested, and others are instead more dependent on OXPHOS [329]. Basal B tumors have been shown to have increased levels and dependency on glutaminase [335]. Gong et al. recently described 3 metabolic-pathway based subtypes of TNBC: MSP1, the lipogenic subtype; MSP2, the glycolytic subtype; MSP3 the mixed type with different metabolite levels, metabolic gene expression, survival and sensitivities to metabolic inhibitors [330]. Importantly, even tumors that are found to primarily utilize glycolysis for energy generation, rely on mitochondrial respiration for biosynthesis and redox balance [622-624]. Furthermore, mitochondrial complex I inhibition not only hinders OXPHOS, but has also been shown to alter lipid metabolism, deplete TCA cycle intermediates and suppress nucleotide levels, thereby expanding their utility likely in oncology [202, 397]. Mirroring the diversity of molecular profiles, breast cancer metabolism is heterogeneous, with metabolic flexibility adding an additional layer of complexity to the classification of metabolic subtypes.

Given these different and likely dynamic metabolic phenotypes, it is not surprising that we and others have shown that breast cancer subtypes have variable sensitivities to phenformin as a monotherapy [398, 625, 626]. Yet, we find that the vulnerability of tumors to the combination of phenformin and co-targeting ROS scavenging mechanisms, is not subtype-restricted.

Many cancer types have been shown to maintain elevated levels of ROS, in comparison to normal cells, which can promote tumor growth and metastatic progression by favoring DNA damage and further genomic instability and also through promoting pro-growth signaling pathways [248, 334, 491, 627]. Tumor cells that concurrently increase antioxidant levels to maintain ROS at a pro-tumorigenic while preventing oxidative damage, have a survival advantage [248]. Considering this, mitochondrial complex I inhibitors, which simultaneously block OXPHOS and potentiate ROS production were predicted to be promising therapeutic agents for individuals with relapse and/or resistant disease [372, 628].

Therapy-induced ROS production also contributes to the cytotoxicity of chemotherapies and ionizing radiation. Resistant cancer cells have increased antioxidant levels [610]. Inhibitors of synthesis of a major cellular antioxidant, glutathione, have been shown to re-sensitize resistant tumors to chemotherapy and radiation [277, 629, 630]. Chemotherapy-resistant TNBC breast cancer cells have also been shown to have increased ROS levels above that of parental lines [631]. Increased OXPHOS and ROS scavenging mechanisms contribute to low response rates to standard therapies, as well as the development of residual disease [632, 633]. It is important to consider however, that for cancer cells that adapted by increasing ROS scavenging mechanisms, therapies that simply increasing ROS levels may not be sufficient. Instead, a more effective strategy will likely be to suppress the antioxidant mechanisms of these cells, representing key therapeutic vulnerabilities. Our results support a critical ROS threshold, even for TNBCs, where combination therapy effectively tips this balance by simultaneously increasing ROS and reducing antioxidant defences. We show that combining mitochondrial complex I inhibition and mitochondrial ROS generation by phenformin with co-treatments that hamper ROS scavenging mechanisms, targets important tumor resistance mechanisms by overpowering the already delicate balance between ROS and antioxidant capacity of the cell. Importantly, although we find that breast cancer subtypes had variable sensitivities to phenformin as a monotherapy, we observed that both HER2+ and TNBC subtypes, including cells derived from PDXs from each subtype, were sensitized to combinations with phenformin and inhibitors of important ROS scavengers. This could prove to be particularly relevant to TNBCs which lack targeted therapies and have a worse prognosis, in the recurrence and potentially even the neoadjuvant settings (for tumors that fail to achieve complete pathological

response with chemotherapy) [634, 635]. The sensitivity of breast cancers, across molecular subtypes, to this combination therapy is important given that many barriers remain to the widespread integration of genomic information to guide treatment decisions in the clinic [636].

Our findings set the foundation for further pre-clinical studies aimed at identifying the most effective combinations of mitochondrial complex I inhibitors and inhibitors of ROS scavengers that are suitable for treatment and that minimize toxicity to normal tissues. To date, most studies in oncology have focused on metformin as this biguanide is widely used for the long-term management of type II diabetes, is well-tolerated and has decreased risk of lactic acidosis [606]. Yet, the translating preclinical findings of metformin as an effective anti-tumor therapy into the clinic for cancer treatment, has been limited. One restricting factor for the use of metformin is the concentration that can be achieved in humans is at minimum 6-10 fold less than what has been used in preclinical animal cancer models [605, 607]. While pharmacokinetic studies with phenformin have been reported, ones that particularly compare plasma concentrations from intraperitoneal injections at doses used within animal models and corresponding tumor accumulation are needed [reviewed in[637]]. Pre-clinical evidence supports that phenformin has more effective anti-tumor effects in several cancers than metformin, and thus may be more suitable in oncology [397, 403, 638]. As addressed in the literature review, unlike metformin, phenformin does not require OCT transporters for cell entry, as such can accumulate to higher concentrations and can enter cells that decrease OCT expression; and phenformin is a more potent complex I inhibitor at lower concentrations [395, 397, 639-641]. Furthermore, herein, we find that combination treatment with phenformin with polyIC *in vivo*, is effective with decreased phenformin concentrations (10mg/kg), representing a 5-10 fold lower than the usual intraperitoneal dose used in pre-clinical animal models [405, 642, 643]. The result of an ongoing clinical trial is examining the safety of phenformin in combination with BRAF inhibitor and MEK inhibitor in melanoma (NT03026517) are awaited. We report that compared to metformin, phenformin is a more potent ROS inducer in tumor cells. This supports previous studies that demonstrated the ROS-generating properties of phenformin [372, 403]. Furthermore, pancreatic cancer stem cells were found to rely on OXPHOS, have reduced metabolic plasticity and are sensitive to mitochondrial complex I inhibition. Yet, these pancreatic stem cells developed resistance to metformin but not menadione, that combined ROS production with mitochondrial complex I inhibition [644]. We show that the molecular mechanism for the selective sensitivity of breast tumors to phenformin with therapies that target tumor ROS-scavenging mechanisms, is ROS-generation by phenformin. Taken together, our findings contribute to the body of literature that favours phenformin as the more effective biguanide for

use in oncology. There is a tendency in the literature to generalize findings from either metformin or phenformin, to biguanides; our results support that these compounds are not interchangeable and should be considered individually. In addition to phenformin, other complex I inhibitors such as IACS-010759, EVT-701 and IM156 may be worthwhile to explore in combination with inhibitors of antioxidant mechanisms [413, 418, 645]. Particularly, IACS-010759 is an attractive candidate, given its capacity to generate mitochondrial superoxide, as we and others have shown [413]. While we demonstrate the mechanism of cooperation to be oxidative stress, we cannot exclude that phenformin may also inhibit mitochondrial metabolism, independently of complex I, as it has been shown to also inhibit the activity of the mitochondrial glycerophosphate dehydrogenase enzyme, a key enzyme that connects oxidative phosphorylation and glycolysis, which increases NADH levels [402].

We find that NQO1 is repressed by IFNγ-driven STAT1 signaling in some breast cancers, building upon similar literature with inflammatory signals in other model systems [646, 647]. NQO1 is a classical Nrf2 target gene that catalyses the 2-electron reduction of quinones by utilizing NADH and NADPH as electron donors, preventing the development of ROS-generating unstable semi-quinones, that would otherwise be formed. In doing so, NQO1 modulates NAD(P)+/NAD(P)H pools. NQO1 also directly acts as a superoxide scavenger to maintain reduced forms of Coenzyme Q and Vitamin E derivatives [296, 648]. Furthermore, tamoxifen bound ERβ was shown to increase NQO1 expression, through ARE elements [649] and oxidative stress was shown to contribute to tamoxifen-induced breast cancer cytotoxicity [352]. IFNγ/STAT1 signaling decreases the expression of NQO1, thus reducing levels of an important ROS scavenger in breast cancer cells, facilitating phenformin-induced oxidative stress. The combination therapies with β-lapachone and phenformin or IACS-010759 further re-enforce these findings and provide pre-clinical evidence that this approach warrants further work to determine possible clinical translation. IFNγ/STAT1 downregulation of NQO1 at the transcriptional level in mouse cell lines tested, is in accordance with a previous report that IFNγ decreases NQO1 gene expression in human uterine microvascular endothelial cells [650]. We cannot exclude the possibility that IFNγ-stimulated STAT1 activation leads to transcriptional repression of NQO1 in a subset of cancers, although our data does not support that this is a major mechanism in human breast cancers. Instead, our data suggests that the mechanism of action is likely to be post-transcriptional in several human breast tumors. Elucidating the mechanism by which STAT1 controls NQO1 gene expression, while beyond the scope of this study, would be worthwhile to explore as it may have relevance to and beyond cancer. Additionally, it is possible that IFNγ-induced oxidative stress relies on additional mechanisms

that include but extend beyond decreasing NQO1 expression. Human breast cancer cell lines MCF7, HCC1954, BT474, BT20, BT549 are sensitive to combined IFNγ and phenformin treatment, however, NQO1 protein levels are not decreased in these cells with IFNγ treatment. Yet, functionally, BT474 sensitivity to IFNγ and phenformin combination treatment can be reversed with the mitochondrial ROS scavenger (MitoTEMPO). The elucidation of additional mechanisms through which IFNγ potentiates oxidative stress is interesting and worthwhile to explore in future work, given the important role of IFNγ in anti-tumor immune therapies. By demonstrating that STAT1 can repress NQO1 gene expression, this research provides evidence that STAT1 may potentiate oxidative stress by decreasing the ROS scavenging potential in cancer cells. Moreover, this finding exposed the vulnerability of breast cancers to the combination of ROS-inducing complex I inhibitors with inhibitors of antioxidant mechanisms. These findings support previous work showing that ROS-mediated protection of cells from the cytotoxic effects of rotenone, an irreversible and ROS-generating mitochondrial complex I inhibitor, requires NQO1 [298].

The findings herein identify NQO1 as an important scavenging molecule required for breast tumors to cope with phenformin-generated ROS. NQO1 is a promising target in cancer as it is frequently overexpressed in tumors compared to normal tissues, contributing to a therapeutic window. Furthermore, increased NQO1 levels are strongly associated with late-stage disease and worse survival [315, 616, 617] [316]. Single nucleotide polymorphisms (SNP) in the NQO1 gene are increasingly appreciated, including the well characterized C609T pathogenic variant, that has decreased enzymatic activity and has been associated with increased cancer risk [651, 652]. It is possible that tumors harboring NQO1 SNPs may display increased sensitivity to ROS-generating complex I inhibitors such as phenformin, either as a monotherapy or in combination with drugs that target the glutathione system. Additionally, ionizing radiation and chemotherapy lead to increased NQO1 levels in cancer cells [294]. NQO1 further protects PGC-1α from proteasomal degradation, which is a transcriptional co-activator and master regulator of genes that promote mitochondrial metabolism and ROS scavenging [302]. PGC-1α can be activated by oxidative damage and some chemotherapies, and it has been shown to promote resistance of breast cancer cells to complex I inhibitors [213]. We cannot exclude that IFNγ/STAT1-driven NQO1 suppression may also limit PGC-1α function. Addressing this would require further investigation. We also find that blocking glutathione synthesis with BSO sensitizes breast cancer cells to phenformin-generated ROS. Recent findings that a GLS1 inhibitor and phenformin effectively induce apoptosis in *in vitro* and *in vivo* models of esophageal squamous cell carcinoma. Although they observed synthetic lethality with

the GLS1 inhibitor and metformin as well, focusing on impacts on bioenergetics and did not study the influence of these combinations on redox balance [87]. The extent to which glutamine is used for glutathione production is not explored in this study, yet our results suggest that oxidative stress may be an additional mechanism of cooperation particularly with phenformin, which generates ROS.

IFNγ levels are a readout of how effective an immunotherapy is at re-engaging the anti-tumor response, in pre-clinical models and clinical trials, alike. IFNγ has potent immunostimulatory and immunomodulatory roles in both innate and adaptive immune responses, that are critical for effective anti-tumor immunity. IFNγ also induces superoxide generation during the respiratory burst of phagocytic cells [reviewed in [470]. In addition to its effects on immune cells, recombinant IFNγ was shown to have direct anti-proliferative and pro-apoptotic effects on cancer cells (reviewed in [490]). Recently, IFNγ was reported to induce NOX4, NOX1 expression, DNA damage response and senescence in HeLa cells [491]. IFNγ's ability to modulate metabolism in both immune and tumor cells, has also gained attention [555, 556]. Although not the mechanism of cooperation between IFNγ and phenformin, we find that in a STAT1-dependent manner, low dose IFNγ treatment (1ng/ml) reduces the maximal respiration and bioenergetic flexibility of breast cancer cells. IFNγ treatment also increases steady state levels of lactate, pyruvate, and the α-ketoglutarate levels, as well as the lactate/pyruvate and the α-ketoglutarate/citrate ratios in breast cancer cells. IFNγ's direct effects on tumor cell metabolism remain poorly understood, yet these findings highlight the need to elucidate the influences of cytokines within the microenvironment on tumor metabolism.

Although our data in the immunocompromised (SCID beige) model supports that phenformin and polyIC or β-lapachone combinations function by activating the innate inflammatory system and tumor intrinsic oxidative stress, our data does not exclude that these combinations may additionally function to potentiate anti-tumor immunity. In addition to favouring the metabolic reprogramming from naïve T cells that rely on generating ATP from OXPHOS to activated T cells that require glycolysis recent work has underscored that mitochondrial complex I inhibition can promote the functioning of the anti-tumor immune compartment [594, 653, 654]. Along this line, phenformin was recently shown to specifically sensitize tumors to PD1 inhibition [405]. Furthermore, there is evidence that β-lapachone also sensitizes tumors by re-engaging T cell anti-tumor immunity and overcoming resistance to immune checkpoint blockade [655]. It is likely that the combinations of phenformin/polyIC or phenformin/β-lapachone also stimulate the anti-tumor immune response, and we believe this is

worthwhile to explore. We hypothesize that the full value of phenformin in oncology could be exploited by combining phenformin, polyIC or β-lapachone (or its clinical formulation ARQ-761), with an immune checkpoint inhibitor.

In conclusion, this study positions NQO1 as an important ROS scavenger for breast tumors treated with phenformin, that can be suppressed to re-sensitize tumors to the ROS-generating complex inhibitor. As many cancers overexpress NQO1, our findings also supports that it represents a tumor-specific target that could selectively sensitize cancer cells to phenformin while sparing normal cells. Furthermore, we extend these findings to the novel small molecule complex I inhibitor, IACS-010759, which also cooperates with the NQO1 bioactivatable drug, β-lapachone. Thus, NQO1 is in attractive therapeutic target that can be repressed in oncology to sensitize tumors to multiple ROS-generating mitochondrial complex I inhibitors.

Chapter 5: Conclusion

5.1 Summary

The overall aims of this project were met as follows:

Aim 1: Elucidate the mechanism of cooperation between IFNγ and phenformin combination in decreasing breast tumor growth and Aim 2: Test if IFNγ and phenformin is relevant to other *in vitro* and *in vivo* models of breast cancer.

We find that multiple preclinical models of breast cancer, across molecular subtypes are sensitized to the anti-tumorigenic properties of phenformin upon co-treatment with the inflammatory signals driven by IFNγ *in vitro.* We extend our findings *in vivo* and find that combining polyIC and phenformin combine to inhibit tumor growth. Our functional experiments demonstrate that IFNγ and polyIC both sensitize tumors to phenformin-generated ROS, leading to oxidative stress. More specifically, through RNA sequencing we identify the ROS scavenger, NQO1 as a target that is decreased upon IFNγ treatment in a STAT1-dependent manner. Through genetic and pharmacological approaches, we establish NQO1 as a ROS scavenger important for breast cancer response to phenformin. Overall, we provide the first evidence that IFNγ-STAT1 signaling, at least in part through suppressing NQO1, sensitizes breast cancer cells to phenformin-generated mitochondrial ROS, inducing oxidative stress and cancer cell death.

Aim 3: Characterize how IFNγ and phenformin combination influence breast cancer bioenergetic and biosynthetic metabolism.

As addressed in aim 1 and aim 2, the mechanism of cooperation of IFNγ and phenformin depends on mitochondrial ROS. Yet, during out approach to elucidate this mechanism, we characterized the impact of single IFNγ treatment of breast cancer cells, through Seahorse real-time metabolic analysis, LC-MS and GC-MS. We establish that low dose IFNγ alone treatment alone modestly reduces the maximal respiration and bioenergetic flexibility of breast cancer cells in a STAT1-dependent manner. Additionally, to our knowledge we are the first to show that IFNγ-STAT1 signaling increases steady state levels of lactate, pyruvate, and the α-ketoglutarate levels, as well as increases the lactate/pyruvate and the α-ketoglutarate/citrate ratio in breast

cancer cells. This suggests that IFNγ treatment stimulates glycolytic metabolism and reductive carboxylation in breast cancer cells.

Aim 4: Address if the mechanism of cooperation can be translated into effective rational combination treatment strategies that sensitize more clinically-relevant models of breast cancer and to other mitochondrial complex I inhibitors, while sparing non-transformed cells.

We show that tumors can be successfully targeted upon co-treatment with phenformin and the NQO1-targeting drug β-lapachone or the glutathione inhibitor, BSO. We expand and find these treatment strategies are effective in more pertinent models of human breast cancer using cells from PDXs from women with breast cancers of HER2+ and basal-like subtypes. We also determine that breast cancer cells are comparatively more sensitive to combination treatment with complex I inhibitors and inhibitors of ROS scavenging mechanisms, than non-transformed counterparts. Overall, we show that therapeutic agents targeting multiple ROS scavengers potentiate oxidative stress thereby increasing the anti-neoplastic efficacy of ROS-generating mitochondrial complex I inhibitors, including phenformin, in breast cancers.

5.2 Implications of findings and future directions

Breast cancer recurrence and metastasis remains a reality for many individuals, and treatment options are limited in the recurrence setting. Deregulating cellular metabolism has emerged as a hallmark of cancer, and is implicated in tumor progression, response to therapies and recurrence/metastasis [86]. Characterizing breast cancer metabolism is ongoing, with the promise of identifying targetable vulnerabilities of cancer that distinguish them from normal cells. Mitochondrial complex I inhibitors have been explored in other cancer types and breast cancer, and most clinical trials have focused on the biguanide, metformin [reviewed in[656]]. We explored the underappreciated role and therapeutic implications of some mitochondrial complex I inhibitors in generating ROS [372]. Given metabolic flexibility and heterogeneity of many breast tumors, it is not surprising that we find responses to complex I inhibitors alone vary substantially across molecular subtypes and models tested. Our findings support the notion that combination strategies with mitochondrial complex I inhibitors that elicit both energetic and oxidative stress, are more effective than single treatment alone.

We establish that inflammatory signals through IFNγ and polyIC sensitize breast cancers to phenformin, by generating oxidative stress in tumor cells. In characterizing this mechanism of

cooperation, we revealed a vulnerability of many breast cancers to the combination of ROS-generating mitochondrial complex I inhibitors, such as phenformin, with inhibitors of antioxidants. Given that oxidative stress underlies the mechanism of cooperation, we also contribute to the accumulating evidence that phenformin, as a ROS-generating complex I inhibitor is more effective as an anti-tumor agent than metformin. We find that rational combination therapies that induce oxidative stress, are effective with lower doses of phenformin, which is relevant to translating these treatment strategies to the clinic and reducing toxic effects.

We find that while transformed cells are sensitized to combination therapy with phenformin and inhibitors of antioxidants, non-transformed cells are spared; supporting the notion that cancer cells are more vulnerable to and can be preferentially eliminated by ROS insults. We establish NQO1 a ROS-scavenger that is important for tumor cell response to phenformin treatment. Given that many tumor types increase NQO1 expression, it would be worthwhile to explore this in other cancers. While not mechanistically responsible for sensitising tumors to phenformin, our findings that low dose IFNγ has modest effects on the bioenergetics of breast cancer cells, contributes to the understanding of and highlights the need to better characterize the immune-metabolism interface.

Upregulation of ROS scavenging capacity has been associated with low response rates to standard therapies and residual disease [632, 633]. Our work supports hypotheses set forth by other groups, that effective strategies to eliminate cancer cells, can include suppressing these adaptable antioxidant mechanisms [251, 657]. Moreover, that cancer cells have a critical ROS threshold that can be surpassed [232, 620, 657]. The widespread susceptibility of various breast cancer models (that span molecular subtypes and vary in sensitivity to phenformin alone) to ROS-generating mitochondrial complex I inhibitors combined with inhibitors of antioxidants, warrants that this combination strategy be explored in metastatic breast cancer models prior to clinical trials. Additional considerations to translating these strategies to the clinic include studying the toxicities of these combinations, as well as the biodistribution of phenformin and antioxidant inhibitors, particular within metastatic sites, such as the brain.

Furthermore, our findings set the stage for pre-clinical and clinical trial-enabling studies, to select the best combinations of mitochondrial complex I inhibitors and inhibitors of antioxidants suitable for treatment of individuals with breast cancer, and likely other cancer types as well.

References

1. van Maaren, M.C., et al., *Ten-year recurrence rates for breast cancer subtypes in the Netherlands: A large population-based study.* Int J Cancer, 2019. **144**(2): p. 263-272.
2. Pan, H., et al., *20-Year Risks of Breast-Cancer Recurrence after Stopping Endocrine Therapy at 5 Years.* N Engl J Med, 2017. **377**(19): p. 1836-1846.
3. Colzani, E., et al., *Time-dependent risk of developing distant metastasis in breast cancer patients according to treatment, age and tumour characteristics.* Br J Cancer, 2014. **110**(5): p. 1378-84.
4. Cacho, N.T. and R.M. Lawrence, *Innate Immunity and Breast Milk.* Front Immunol, 2017. **8**: p. 584.
5. Cooper, A. and L. Lamar Soutter, *The anatomy and diseases of the breast.* 1845.
6. Medina, D., *The mammary gland: a unique organ for the study of development and tumorigenesis.* J Mammary Gland Biol Neoplasia, 1996. **1**(1): p. 5-19.
7. Meissl, K., et al., *The good and the bad faces of STAT1 in solid tumours.* Cytokine, 2017. **89**: p. 12-20.
8. Visvader, J.E. and J. Stingl, *Mammary stem cells and the differentiation hierarchy: current status and perspectives.* Genes Dev, 2014. **28**(11): p. 1143-58.
9. Nguyen, Q.H., et al., *Profiling human breast epithelial cells using single cell RNA sequencing identifies cell diversity.* Nature Communications, 2018. **9**(1): p. 2028.
10. Van Keymeulen, A., et al., *Distinct stem cells contribute to mammary gland development and maintenance.* Nature, 2011. **479**(7372): p. 189-193.
11. Lim, E., et al., *Aberrant luminal progenitors as the candidate target population for basal tumor development in BRCA1 mutation carriers.* Nat Med, 2009. **15**(8): p. 907-13.
12. Nicholson, B.T., J.A. Harvey, and M.A. Cohen, *Nipple-Areolar Complex: Normal Anatomy and Benign and Malignant Processes.* RadioGraphics, 2009. **29**(2): p. 509-523.
13. Polyak, K. and R. Kalluri, *The role of the microenvironment in mammary gland development and cancer.* Cold Spring Harb Perspect Biol, 2010. **2**(11): p. a003244.
14. Parmar, H. and G.R. Cunha, *Epithelial-stromal interactions in the mouse and human mammary gland in vivo.* Endocr Relat Cancer, 2004. **11**(3): p. 437-58.
15. Wang, Y., et al., *Superoxide dismutases: Dual roles in controlling ROS damage and regulating ROS signaling.* Journal of Cell Biology, 2018. **217**(6): p. 1915-1928.
16. Kleinberg, D.L., et al., *Growth hormone and insulin-like growth factor-I in the transition from normal mammary development to preneoplastic mammary lesions.* Endocr Rev, 2009. **30**(1): p. 51-74.
17. Brisken, C. and V. Scabia, *90 YEARS OF PROGESTERONE: Progesterone receptor signaling in the normal breast and its implications for cancer.* J Mol Endocrinol, 2020. **65**(1): p. T81-t94.
18. Vogel, P.M., et al., *The correlation of histologic changes in the human breast with the menstrual cycle.* Am J Pathol, 1981. **104**(1): p. 23-34.
19. Molina, P.E., *Endocrine physiology*. 2018, McGraw-Hill Education: [New York].
20. Estourgie, S.H., et al., *Lymphatic drainage patterns from the breast.* Ann Surg, 2004. **239**(2): p. 232-7.

21. Fisher, B., et al., *Five-year results of a randomized clinical trial comparing total mastectomy and segmental mastectomy with or without radiation in the treatment of breast cancer.* N Engl J Med, 1985. **312**(11): p. 665-73.
22. Board., W.C.o.T.E., *Breast tumours [Internet].* WHO classification of tumours series, 2019(5th ed, vol. 2).
23. Sung, H., et al., *Global Cancer Statistics 2020: GLOBOCAN Estimates of Incidence and Mortality Worldwide for 36 Cancers in 185 Countries.* CA: A Cancer Journal for Clinicians, 2021. **71**(3): p. 209-249.
24. Brenner, D.R., et al., *Projected estimates of cancer in Canada in 2022.* Canadian Medical Association Journal, 2022. **194**(17): p. E601-E607.
25. Committee., C.C.S.A., *Canadian Cancer Statistics 2022. .* Canadian Cancer Society, 2022.
26. MacMahon, B., et al., *Age at first birth and breast cancer risk.* Bull World Health Organ, 1970. **43**(2): p. 209-21.
27. Rosner, B., G.A. Colditz, and W.C. Willett, *Reproductive Risk Factors in a Prospective Study of Breast Cancer: The Nurses' Health Study.* American Journal of Epidemiology, 1994. **139**(8): p. 819-835.
28. de Blok, C.J.M., et al., *Breast cancer risk in transgender people receiving hormone treatment: nationwide cohort study in the Netherlands.* Bmj, 2019. **365**: p. l1652.
29. Antoniou, A., et al., *Average risks of breast and ovarian cancer associated with BRCA1 or BRCA2 mutations detected in case Series unselected for family history: a combined analysis of 22 studies.* Am J Hum Genet, 2003. **72**(5): p. 1117-30.
30. King, M.C., J.H. Marks, and J.B. Mandell, *Breast and ovarian cancer risks due to inherited mutations in BRCA1 and BRCA2.* Science, 2003. **302**(5645): p. 643-6.
31. Simard, J., et al., *Common origins of BRCA1 mutations in Canadian breast and ovarian cancer families.* Nat Genet, 1994. **8**(4): p. 392-8.
32. Bahcall, O., *Common variation and heritability estimates for breast, ovarian and prostate cancers.* Nature Genetics, 2013.
33. Richards, S., et al., *Standards and guidelines for the interpretation of sequence variants: a joint consensus recommendation of the American College of Medical Genetics and Genomics and the Association for Molecular Pathology.* Genetics in Medicine, 2015. **17**(5): p. 405-423.
34. Easton, D.F., et al., *Gene-panel sequencing and the prediction of breast-cancer risk.* N Engl J Med, 2015. **372**(23): p. 2243-57.
35. Michailidou, K., et al., *Association analysis identifies 65 new breast cancer risk loci.* Nature, 2017. **551**(7678): p. 92-94.
36. Mavaddat, N., et al., *Polygenic Risk Scores for Prediction of Breast Cancer and Breast Cancer Subtypes.* Am J Hum Genet, 2019. **104**(1): p. 21-34.
37. Li, C.I., D.J. Uribe, and J.R. Daling, *Clinical characteristics of different histologic types of breast cancer.* Br J Cancer, 2005. **93**(9): p. 1046-52.
38. Hammond, M.E., et al., *American Society of Clinical Oncology/College Of American Pathologists guideline recommendations for immunohistochemical testing of estrogen and progesterone receptors in breast cancer.* J Clin Oncol, 2010. **28**(16): p. 2784-95.

39. Beatson, G.T., *On the Treatment of Inoperable Cases of Carcinoma of the Mamma: Suggestions for a New Method of Treatment, with Illustrative Cases.* Trans Med Chir Soc Edinb, 1896. **15**: p. 153-179.
40. Leo McGuire, W., *Current status of estrogen receptors in human breast cancer.* Cancer, 1975. **36**(S2): p. 638-644.
41. Horwitz, K.B., et al., *PREDICTING RESPONSE TO ENDOCRINE THERAPY IN HUMAN BREAST-CANCER - HYPOTHESIS.* Science, 1975. **189**(4204): p. 726-727.
42. Clark, G.M., et al., *Progesterone Receptors as a Prognostic Factor in Stage II Breast Cancer.* New England Journal of Medicine, 1983. **309**(22): p. 1343-1347.
43. Kurozumi, S., et al., *Power of PgR expression as a prognostic factor for ER-positive/HER2-negative breast cancer patients at intermediate risk classified by the Ki67 labeling index.* BMC Cancer, 2017. **17**(1): p. 354.
44. Di Fiore, P.P., et al., *erbB-2 is a potent oncogene when overexpressed in NIH/3T3 cells.* Science, 1987. **237**(4811): p. 178-82.
45. Hudziak, R.M., J. Schlessinger, and A. Ullrich, *Increased expression of the putative growth factor receptor p185HER2 causes transformation and tumorigenesis of NIH 3T3 cells.* Proceedings of the National Academy of Sciences, 1987. **84**(20): p. 7159-7163.
46. Bargmann, C.I., M.C. Hung, and R.A. Weinberg, *The neu oncogene encodes an epidermal growth factor receptor-related protein.* Nature, 1986. **319**(6050): p. 226-30.
47. Slamon, D.J., et al., *Human breast cancer: correlation of relapse and survival with amplification of the HER-2/neu oncogene.* Science, 1987. **235**(4785): p. 177-82.
48. Yu, D. and M.C. Hung, *Overexpression of ErbB2 in cancer and ErbB2-targeting strategies.* Oncogene, 2000. **19**(53): p. 6115-21.
49. Hudziak, R.M., et al., *p185HER2 monoclonal antibody has antiproliferative effects in vitro and sensitizes human breast tumor cells to tumor necrosis factor.* Mol Cell Biol, 1989. **9**(3): p. 1165-72.
50. Shak, S., *Overview of the trastuzumab (Herceptin) anti-HER2 monoclonal antibody clinical program in HER2-overexpressing metastatic breast cancer. Herceptin Multinational Investigator Study Group.* Semin Oncol, 1999. **26**(4 Suppl 12): p. 71-7.
51. Slamon, D.J., et al., *Use of chemotherapy plus a monoclonal antibody against HER2 for metastatic breast cancer that overexpresses HER2.* N Engl J Med, 2001. **344**(11): p. 783-92.
52. O'Sullivan, C.C. and S.M. Swain, *Pertuzumab : evolving therapeutic strategies in the management of HER2-overexpressing breast cancer.* Expert Opin Biol Ther, 2013. **13**(5): p. 779-90.
53. Board, W.C.o.T.E., *Breast tumours [Internet].* WHO classification of tumours series, 5th ed.; vol. 2, 2019.
54. Bloom, H.J.G. and W.W. Richardson, *Histological Grading and Prognosis in Breast Cancer.* British Journal of Cancer, 1957. **11**(3): p. 359-377.
55. ELSTON, C.W. and I.O. ELLIS, *pathological prognostic factors in breast cancer. I. The value of histological grade in breast cancer: experience from a large study with long-term follow-up.* Histopathology, 1991. **19**(5): p. 403-410.
56. Cho, S.Y., et al., *Standardized pathology report for breast cancer.* J Pathol Transl Med, 2021. **55**(1): p. 1-15.

57. Perou, C.M., et al., *Molecular portraits of human breast tumours.* Nature, 2000. **406**(6797): p. 747-752.
58. Sørlie, T., et al., *Gene expression patterns of breast carcinomas distinguish tumor subclasses with clinical implications.* Proc Natl Acad Sci U S A, 2001. **98**(19): p. 10869-74.
59. Koboldt, D.C., et al., *Comprehensive molecular portraits of human breast tumours.* Nature, 2012. **490**(7418): p. 61-70.
60. Curtis, C., et al. *The genomic and transcriptomic architecture of 2,000 breast tumours reveals novel subgroups*. Nature, 2012. **486**, 346-352 DOI: 10.1038/nature10983.
61. Goldhirsch, A., et al., *Personalizing the treatment of women with early breast cancer: highlights of the St Gallen International Expert Consensus on the Primary Therapy of Early Breast Cancer 2013.* Ann Oncol, 2013. **24**(9): p. 2206-23.
62. Brenton, J.D., et al., *Molecular classification and molecular forecasting of breast cancer: ready for clinical application?* J Clin Oncol, 2005. **23**(29): p. 7350-60.
63. Herschkowitz, J.I., et al., *Identification of conserved gene expression features between murine mammary carcinoma models and human breast tumors.* Genome Biol, 2007. **8**(5): p. R76.
64. Prat, A., et al., *Phenotypic and molecular characterization of the claudin-low intrinsic subtype of breast cancer.* Breast Cancer Res, 2010. **12**(5): p. R68.
65. Dias, K., et al., *Claudin-Low Breast Cancer; Clinical & Pathological Characteristics.* PLoS One, 2017. **12**(1): p. e0168669.
66. Ahern, T.P., et al., *Metabolic Pathway Analysis and Effectiveness of Tamoxifen in Danish Breast Cancer Patients.* Cancer Epidemiol Biomarkers Prev, 2020. **29**(3): p. 582-590.
67. Lehmann, B.D., et al., *Multi-omics analysis identifies therapeutic vulnerabilities in triple-negative breast cancer subtypes.* Nature Communications, 2021. **12**(1): p. 6276.
68. Sotiriou, C. and L. Pusztai, *Gene-Expression Signatures in Breast Cancer.* New England Journal of Medicine, 2009. **360**(8): p. 790-800.
69. Cardoso, F., et al., *Early breast cancer: ESMO Clinical Practice Guidelines for diagnosis, treatment and follow-up†.* Annals of Oncology, 2019. **30**(8): p. 1194-1220.
70. Allred, D.C., S.K. Mohsin, and S.A. Fuqua, *Histological and biological evolution of human premalignant breast disease.* Endocr Relat Cancer, 2001. **8**(1): p. 47-61.
71. Fidler, I.J., *The pathogenesis of cancer metastasis: the 'seed and soil' hypothesis revisited.* Nat Rev Cancer, 2003. **3**(6): p. 453-8.
72. Soni, A., et al., *Breast Cancer Subtypes Predispose the Site of Distant Metastases.* American Journal of Clinical Pathology, 2015. **143**(4): p. 471-478.
73. Kennecke, H., et al., *Metastatic behavior of breast cancer subtypes.* J Clin Oncol, 2010. **28**(20): p. 3271-7.
74. Riggio, A.I., K.E. Varley, and A.L. Welm, *The lingering mysteries of metastatic recurrence in breast cancer.* British Journal of Cancer, 2021. **124**(1): p. 13-26.
75. Wu, Q., et al., *Breast cancer subtypes predict the preferential site of distant metastases: a SEER based study.* Oncotarget, 2017. **8**(17): p. 27990-27996.
76. Largillier, R., et al., *Prognostic factors in 1,038 women with metastatic breast cancer.* Ann Oncol, 2008. **19**(12): p. 2012-9.
77. Kreso, A. and J.E. Dick, *Evolution of the cancer stem cell model.* Cell Stem Cell, 2014. **14**(3): p. 275-91.

78. Vaillant, F., et al., *The mammary progenitor marker CD61/beta3 integrin identifies cancer stem cells in mouse models of mammary tumorigenesis.* Cancer Res, 2008. **68**(19): p. 7711-7.
79. Cristea, S. and K. Polyak, *Dissecting the mammary gland one cell at a time.* Nat Commun, 2018. **9**(1): p. 2473.
80. Visvader, J.E. and G.J. Lindeman, *The unmasking of novel unipotent stem cells in the mammary gland.* Embo j, 2011. **30**(24): p. 4858-9.
81. Visvader, J.E., *Keeping abreast of the mammary epithelial hierarchy and breast tumorigenesis.* Genes Dev, 2009. **23**(22): p. 2563-77.
82. Fu, N., G.J. Lindeman, and J.E. Visvader, *The mammary stem cell hierarchy.* Curr Top Dev Biol, 2014. **107**: p. 133-60.
83. Hu, L., et al., *Single-Cell RNA Sequencing Reveals the Cellular Origin and Evolution of Breast Cancer in BRCA1 Mutation Carriers.* Cancer Res, 2021. **81**(10): p. 2600-2611.
84. Shah, S.P., et al., *The clonal and mutational evolution spectrum of primary triple-negative breast cancers.* Nature, 2012. **486**(7403): p. 395-9.
85. *Comprehensive molecular portraits of human breast tumours.* Nature, 2012. **490**(7418): p. 61-70.
86. Hanahan, D., *Hallmarks of Cancer: New Dimensions.* Cancer Discovery, 2022. **12**(1): p. 31-46.
87. Qie, S., et al., *Targeting glutamine-addiction and overcoming CDK4/6 inhibitor resistance in human esophageal squamous cell carcinoma.* Nature communications, 2019. **10**(1): p. 1296-1296.
88. Paget, S., *The distribution of secondary growths in cancer of the breast. 1889.* Cancer Metastasis Rev, 1989. **8**(2): p. 98-101.
89. Hawsawi, N.M., et al., *Breast Carcinoma–Associated Fibroblasts and Their Counterparts Display Neoplastic-Specific Changes.* Cancer Research, 2008. **68**(8): p. 2717-2725.
90. Tan, Z., et al., *Mapping Breast Cancer Microenvironment Through Single-Cell Omics.* Front Immunol, 2022. **13**: p. 868813.
91. Ursini-Siegel, J. and M. Park, *It takes two to tango in the microenvironment!* Breast Cancer Research, 2013. **15**(2): p. 102.
92. Danenberg, E., et al., *Breast tumor microenvironment structures are associated with genomic features and clinical outcome.* Nature Genetics, 2022. **54**(5): p. 660-669.
93. Chen, F., et al., *Clinical Progress of PD-1/L1 Inhibitors in Breast Cancer Immunotherapy.* Frontiers in Oncology, 2022. **11**.
94. Loi, S., et al., *Tumor infiltrating lymphocytes are prognostic in triple negative breast cancer and predictive for trastuzumab benefit in early breast cancer: results from the FinHER trial.* Ann Oncol, 2014. **25**(8): p. 1544-50.
95. Denkert, C., et al., *Tumour-infiltrating lymphocytes and prognosis in different subtypes of breast cancer: a pooled analysis of 3771 patients treated with neoadjuvant therapy.* Lancet Oncol, 2018. **19**(1): p. 40-50.
96. Salgado, R., et al., *Tumor-Infiltrating Lymphocytes and Associations With Pathological Complete Response and Event-Free Survival in HER2-Positive Early-Stage Breast Cancer Treated With Lapatinib and Trastuzumab: A Secondary Analysis of the NeoALTTO Trial.* JAMA Oncol, 2015. **1**(4): p. 448-54.

97. Dieci, M.V., et al., *Update on tumor-infiltrating lymphocytes (TILs) in breast cancer, including recommendations to assess TILs in residual disease after neoadjuvant therapy and in carcinoma in situ: A report of the International Immuno-Oncology Biomarker Working Group on Breast Cancer.* Semin Cancer Biol, 2018. **52**(Pt 2): p. 16-25.
98. Gao, G., et al., *Prognostic value of tumor-infiltrating lymphocytes in patients with triple-negative breast cancer: a systematic review and meta-analysis.* BMC Cancer, 2020. **20**(1): p. 179.
99. Allen, M.D. and L.J. Jones, *The role of inflammation in progression of breast cancer: Friend or foe? (Review).* Int J Oncol, 2015. **47**(3): p. 797-805.
100. Halsted, W.S., *THE RESULTS OF RADICAL OPERATIONS FOR THE CURE OF CARCINOMA OF THE BREAST.*.* Annals of Surgery, 1907. **46**(1).
101. Fisher, B., et al., *Five-Year Results of a Randomized Clinical Trial Comparing Total Mastectomy and Segmental Mastectomy with or without Radiation in the Treatment of Breast Cancer.* New England Journal of Medicine, 1985. **312**(11): p. 665-673.
102. Cortazar, P., et al., *Pathological complete response and long-term clinical benefit in breast cancer: the CTNeoBC pooled analysis.* Lancet, 2014. **384**(9938): p. 164-72.
103. de Boer, M., et al., *Micrometastases or Isolated Tumor Cells and the Outcome of Breast Cancer.* New England Journal of Medicine, 2009. **361**(7): p. 653-663.
104. Peto, R., et al., *Comparisons between different polychemotherapy regimens for early breast cancer: meta-analyses of long-term outcome among 100,000 women in 123 randomised trials.* Lancet, 2012. **379**(9814): p. 432-44.
105. Paik, S., et al., *Gene expression and benefit of chemotherapy in women with node-negative, estrogen receptor-positive breast cancer.* J Clin Oncol, 2006. **24**(23): p. 3726-34.
106. Masuda, N., et al., *Adjuvant Capecitabine for Breast Cancer after Preoperative Chemotherapy.* New England Journal of Medicine, 2017. **376**(22): p. 2147-2159.
107. Marusyk, A., et al., *Non-cell-autonomous driving of tumour growth supports sub-clonal heterogeneity.* Nature, 2014. **514**(7520): p. 54-8.
108. Cleary, A.S., et al., *Tumour cell heterogeneity maintained by cooperating subclones in Wnt-driven mammary cancers.* Nature, 2014. **508**(7494): p. 113-7.
109. van Laar, C., et al., *Local recurrence following breast-conserving treatment in women aged 40 years or younger: trends in risk and the impact on prognosis in a population-based cohort of 1143 patients.* Eur J Cancer, 2013. **49**(15): p. 3093-101.
110. Wapnir, I.L., et al., *Prognosis after ipsilateral breast tumor recurrence and locoregional recurrences in five National Surgical Adjuvant Breast and Bowel Project node-positive adjuvant breast cancer trials.* J Clin Oncol, 2006. **24**(13): p. 2028-37.
111. Metzger-Filho, O., et al., *Patterns of Recurrence and Outcome According to Breast Cancer Subtypes in Lymph Node–Negative Disease: Results From International Breast Cancer Study Group Trials VIII and IX.* Journal of Clinical Oncology, 2013. **31**(25): p. 3083-3090.
112. Fallahpour, S., et al., *Breast cancer survival by molecular subtype: a population-based analysis of cancer registry data.* CMAJ Open, 2017. **5**(3): p. E734-e739.
113. Wang, R., et al., *The Clinicopathological features and survival outcomes of patients with different metastatic sites in stage IV breast cancer.* BMC Cancer, 2019. **19**(1): p. 1091.

114. Giaquinto, A.N., et al., *Breast Cancer Statistics, 2022.* CA: A Cancer Journal for Clinicians. **n/a**(n/a).
115. Tutt, A.N.J., et al., *Adjuvant Olaparib for Patients with BRCA1- or BRCA2-Mutated Breast Cancer.* N Engl J Med, 2021. **384**(25): p. 2394-2405.
116. Sharma, P., et al., *Results of a phase II randomized trial of cisplatin +/- veliparib in metastatic triple-negative breast cancer (TNBC) and/or germline BRCA-associated breast cancer (SWOG S1416).* Journal of Clinical Oncology, 2020. **38**(15_suppl): p. 1001-1001.
117. Bianchini, G., et al., *Treatment landscape of triple-negative breast cancer - expanded options, evolving needs.* Nat Rev Clin Oncol, 2022. **19**(2): p. 91-113.
118. Petersen, M.C. and G.I. Shulman, *Mechanisms of Insulin Action and Insulin Resistance.* Physiol Rev, 2018. **98**(4): p. 2133-2223.
119. Rix, I., et al., *Glucagon Physiology*, in *Endotext*, K.R. Feingold, et al., Editors. 2000, MDText.com, Inc.
Copyright © 2000-2022, MDText.com, Inc.: South Dartmouth (MA).
120. Lord, S.R., et al., *Integrated Pharmacodynamic Analysis Identifies Two Metabolic Adaption Pathways to Metformin in Breast Cancer.* Cell Metabolism, 2018. **28**(5): p. 679-688.e4.
121. Dunn, J. and M.H. Grider, *Physiology, Adenosine Triphosphate*, in *StatPearls*. 2022, StatPearls Publishing
Copyright © 2022, StatPearls Publishing LLC.: Treasure Island (FL).
122. Chandel, N.S., *Glycolysis.* Cold Spring Harb Perspect Biol, 2021. **13**(5).
123. Melkonian, E.A. and M.P. Schury, *Biochemistry, Anaerobic Glycolysis*, in *StatPearls*. 2022, StatPearls Publishing
Copyright © 2022, StatPearls Publishing LLC.: Treasure Island (FL).
124. Longo, N., M. Frigeni, and M. Pasquali, *Carnitine transport and fatty acid oxidation.* Biochim Biophys Acta, 2016. **1863**(10): p. 2422-35.
125. Stincone, A., et al., *The return of metabolism: biochemistry and physiology of the pentose phosphate pathway.* Biol Rev Camb Philos Soc, 2015. **90**(3): p. 927-63.
126. Plaitakis, A., et al., *The Glutamate Dehydrogenase Pathway and Its Roles in Cell and Tissue Biology in Health and Disease.* Biology (Basel), 2017. **6**(1).
127. Chandel, N.S., *NADPH-The Forgotten Reducing Equivalent.* Cold Spring Harb Perspect Biol, 2021. **13**(6).
128. Jiang, L., et al., *Reductive carboxylation supports redox homeostasis during anchorage-independent growth.* Nature, 2016. **532**(7598): p. 255-8.
129. Chini, C.C.S., et al., *Evolving concepts in NAD(+) metabolism.* Cell Metab, 2021. **33**(6): p. 1076-1087.
130. Navas, L.E. and A. Carnero, *NAD+ metabolism, stemness, the immune response, and cancer.* Signal Transduction and Targeted Therapy, 2021. **6**(1): p. 2.
131. Vercellino, I. and L.A. Sazanov, *The assembly, regulation and function of the mitochondrial respiratory chain.* Nature Reviews Molecular Cell Biology, 2022. **23**(2): p. 141-161.
132. Hirst, J., *Mitochondrial complex I.* Annu Rev Biochem, 2013. **82**: p. 551-75.
133. Barker, C.D., T. Reda, and J. Hirst, *The flavoprotein subcomplex of complex I (NADH:ubiquinone oxidoreductase) from bovine heart mitochondria: insights into the*

mechanisms of NADH oxidation and NAD+ reduction from protein film voltammetry. Biochemistry, 2007. **46**(11): p. 3454-64.
134. Kampjut, D. and L.A. Sazanov, *The coupling mechanism of mammalian respiratory complex I.* Science, 2020. **370**(6516).
135. Sies, H. and D.P. Jones, *Reactive oxygen species (ROS) as pleiotropic physiological signalling agents.* Nature Reviews Molecular Cell Biology, 2020. **21**(7): p. 363-383.
136. Sarsour, E.H., et al., *Redox control of the cell cycle in health and disease.* Antioxid Redox Signal, 2009. **11**(12): p. 2985-3011.
137. Piskounova, E., et al., *Oxidative stress inhibits distant metastasis by human melanoma cells.* Nature, 2015. **527**(7577): p. 186-91.
138. Neuman, E.W., *Potassium Superoxide and the Three-Electron Bond.* The Journal of Chemical Physics, 1934. **2**(1): p. 31-33.
139. Pauling, L., *The discovery of the superoxide radical.* Trends in Biochemical Sciences, 1979. **4**(11): p. N270-N271.
140. Hayyan, M., M.A. Hashim, and I.M. AlNashef, *Superoxide Ion: Generation and Chemical Implications.* Chemical Reviews, 2016. **116**(5): p. 3029-3085.
141. Hassan, H.M. and I. Fridovich, *Intracellular production of superoxide radical and of hydrogen peroxide by redox active compounds.* Arch Biochem Biophys, 1979. **196**(2): p. 385-95.
142. Winterbourn, C.C., *Toxicity of iron and hydrogen peroxide: the Fenton reaction.* Toxicology Letters, 1995. **82-83**: p. 969-974.
143. Kehrer, J.P., *The Haber-Weiss reaction and mechanisms of toxicity.* Toxicology, 2000. **149**(1): p. 43-50.
144. Mazat, J.-P., A. Devin, and S. Ransac, *Modelling mitochondrial ROS production by the respiratory chain.* Cellular and Molecular Life Sciences, 2020. **77**(3): p. 455-465.
145. Nolfi-Donegan, D., A. Braganza, and S. Shiva, *Mitochondrial electron transport chain: Oxidative phosphorylation, oxidant production, and methods of measurement.* Redox Biology, 2020. **37**: p. 101674.
146. Turrens, J.F. and A. Boveris, *Generation of superoxide anion by the NADH dehydrogenase of bovine heart mitochondria.* Biochem J, 1980. **191**(2): p. 421-7.
147. Hirst, J., M.S. King, and K.R. Pryde, *The production of reactive oxygen species by complex I.* Biochem Soc Trans, 2008. **36**(Pt 5): p. 976-80.
148. Brand, M.D., *Mitochondrial generation of superoxide and hydrogen peroxide as the source of mitochondrial redox signaling.* Free Radic Biol Med, 2016. **100**: p. 14-31.
149. Brand, M.D., *The sites and topology of mitochondrial superoxide production.* Exp Gerontol, 2010. **45**(7-8): p. 466-72.
150. Kussmaul, L. and J. Hirst, *The mechanism of superoxide production by NADH:ubiquinone oxidoreductase (complex I) from bovine heart mitochondria.* Proc Natl Acad Sci U S A, 2006. **103**(20): p. 7607-12.
151. Scialò, F., D.J. Fernández-Ayala, and A. Sanz, *Role of Mitochondrial Reverse Electron Transport in ROS Signaling: Potential Roles in Health and Disease.* Front Physiol, 2017. **8**: p. 428.
152. Starkov, A.A. and G. Fiskum, *Regulation of brain mitochondrial H2O2 production by membrane potential and NAD(P)H redox state.* J Neurochem, 2003. **86**(5): p. 1101-7.

153. Battelli, M.G., et al., *Xanthine Oxidoreductase-Derived Reactive Species: Physiological and Pathological Effects.* Oxid Med Cell Longev, 2016. **2016**: p. 3527579.
154. Bedard, K. and K.H. Krause, *The NOX family of ROS-generating NADPH oxidases: physiology and pathophysiology.* Physiol Rev, 2007. **87**(1): p. 245-313.
155. Clark, R.A. and S.J. Klebanoff, *Neutrophil-mediated tumor cell cytotoxicity: role of the peroxidase system.* J Exp Med, 1975. **141**(6): p. 1442-7.
156. Kietzmann, T., *Cellular Redox Compartments.* Antioxid Redox Signal, 2019. **30**(1): p. 1-4.
157. Beedle, A.E.M., S. Lynham, and S. Garcia-Manyes, *Protein S-sulfenylation is a fleeting molecular switch that regulates non-enzymatic oxidative folding.* Nature Communications, 2016. **7**(1): p. 12490.
158. Yamakura, F., et al., *Inactivation of Human Manganese-superoxide Dismutase by Peroxynitrite Is Caused by Exclusive Nitration of Tyrosine 34 to 3-Nitrotyrosine*.* Journal of Biological Chemistry, 1998. **273**(23): p. 14085-14089.
159. Giannoni, E., et al., *Intracellular reactive oxygen species activate Src tyrosine kinase during cell adhesion and anchorage-dependent cell growth.* Mol Cell Biol, 2005. **25**(15): p. 6391-403.
160. Truong, T.H., et al., *Molecular Basis for Redox Activation of Epidermal Growth Factor Receptor Kinase.* Cell Chem Biol, 2016. **23**(7): p. 837-848.
161. Kemble, D.J. and G. Sun, *Direct and specific inactivation of protein tyrosine kinases in the Src and FGFR families by reversible cysteine oxidation.* Proc Natl Acad Sci U S A, 2009. **106**(13): p. 5070-5.
162. Lee, S.R., et al., *Reversible inactivation of the tumor suppressor PTEN by H2O2.* J Biol Chem, 2002. **277**(23): p. 20336-42.
163. Sies, H., *Oxidative eustress: On constant alert for redox homeostasis.* Redox Biol, 2021. **41**: p. 101867.
164. Suzuki, Y.J., M. Carini, and D.A. Butterfield, *Protein carbonylation.* Antioxid Redox Signal, 2010. **12**(3): p. 323-5.
165. Stadtman, E.R. and R.L. Levine, *Protein oxidation.* Ann N Y Acad Sci, 2000. **899**: p. 191-208.
166. Ayala, A., M.F. Muñoz, and S. Argüelles, *Lipid peroxidation: production, metabolism, and signaling mechanisms of malondialdehyde and 4-hydroxy-2-nonenal.* Oxid Med Cell Longev, 2014. **2014**: p. 360438.
167. Hsu, G.W., et al., *Error-prone replication of oxidatively damaged DNA by a high-fidelity DNA polymerase.* Nature, 2004. **431**(7005): p. 217-221.
168. Zhao, R.Z., et al., *Mitochondrial electron transport chain, ROS generation and uncoupling (Review).* Int J Mol Med, 2019. **44**(1): p. 3-15.
169. David, S.S., V.L. O'Shea, and S. Kundu, *Base-excision repair of oxidative DNA damage.* Nature, 2007. **447**(7147): p. 941-950.
170. Glorieux, C. and P.B. Calderon, *Catalase, a remarkable enzyme: targeting the oldest antioxidant enzyme to find a new cancer treatment approach.* Biological Chemistry, 2017. **398**(10): p. 1095-1108.
171. Brigelius-Flohé, R. and M. Maiorino, *Glutathione peroxidases.* Biochim Biophys Acta, 2013. **1830**(5): p. 3289-303.

172. Wood, Z.A., L.B. Poole, and P.A. Karplus, *Peroxiredoxin evolution and the regulation of hydrogen peroxide signaling.* Science, 2003. **300**(5619): p. 650-3.
173. Powis, G. and W.R. Montfort, *Properties and Biological Activities of Thioredoxins.* Annual Review of Pharmacology and Toxicology, 2001. **41**(1): p. 261-295.
174. Benhar, M., et al., *Regulated protein denitrosylation by cytosolic and mitochondrial thioredoxins.* Science, 2008. **320**(5879): p. 1050-4.
175. Arnér, E.S., *Focus on mammalian thioredoxin reductases--important selenoproteins with versatile functions.* Biochim Biophys Acta, 2009. **1790**(6): p. 495-526.
176. Itoh, K., et al., *Keap1 represses nuclear activation of antioxidant responsive elements by Nrf2 through binding to the amino-terminal Neh2 domain.* Genes Dev, 1999. **13**(1): p. 76-86.
177. Nguyen, T., P. Nioi, and C.B. Pickett, *The Nrf2-antioxidant response element signaling pathway and its activation by oxidative stress.* J Biol Chem, 2009. **284**(20): p. 13291-5.
178. Kansanen, E., et al., *The Keap1-Nrf2 pathway: Mechanisms of activation and dysregulation in cancer.* Redox Biology, 2013. **1**(1): p. 45-49.
179. Rushmore, T.H., M.R. Morton, and C.B. Pickett, *The antioxidant responsive element. Activation by oxidative stress and identification of the DNA consensus sequence required for functional activity.* J Biol Chem, 1991. **266**(18): p. 11632-9.
180. Kawatani, Y., et al., *Nrf2 and selenoproteins are essential for maintaining oxidative homeostasis in erythrocytes and protecting against hemolytic anemia.* Blood, 2011. **117**(3): p. 986-96.
181. Meister, A., *On the discovery of glutathione.* Trends in Biochemical Sciences, 1988. **13**(5): p. 185-188.
182. Gilbert, H.F., *Catalysis of thiol/disulfide exchange: single-turnover reduction of protein disulfide-isomerase by glutathione and catalysis of peptide disulfide reduction.* Biochemistry, 1989. **28**(18): p. 7298-7305.
183. Pallardó, F.V., et al., *Role of nuclear glutathione as a key regulator of cell proliferation.* Mol Aspects Med, 2009. **30**(1-2): p. 77-85.
184. Hwang, C., A.J. Sinskey, and H.F. Lodish, *Oxidized redox state of glutathione in the endoplasmic reticulum.* Science, 1992. **257**(5076): p. 1496-502.
185. Wang, Y., et al., *SLC25A39 is necessary for mitochondrial glutathione import in mammalian cells.* Nature, 2021. **599**(7883): p. 136-140.
186. Anderson, M.E. and A. Meister, *Transport and direct utilization of gamma-glutamylcyst(e)ine for glutathione synthesis.* Proc Natl Acad Sci U S A, 1983. **80**(3): p. 707-11.
187. Lu, S.C., *Glutathione synthesis.* Biochim Biophys Acta, 2013. **1830**(5): p. 3143-53.
188. Couto, N., J. Wood, and J. Barber, *The role of glutathione reductase and related enzymes on cellular redox homoeostasis network.* Free radical biology & medicine, 2016. **95**: p. 27-42.
189. An, Y.S., et al., *Metabolic Activity of Normal Glandular Tissue on (18)F-Fluorodeoxyglucose Positron Emission Tomography/Computed Tomography: Correlation with Menstrual Cycles and Parenchymal Enhancements.* J Breast Cancer, 2017. **20**(4): p. 386-392.

190. Rudolph, M.C., et al., *Metabolic regulation in the lactating mammary gland: a lipid synthesizing machine.* Physiol Genomics, 2007. **28**(3): p. 323-36.
191. Kannan, N., et al., *Glutathione-dependent and -independent oxidative stress-control mechanisms distinguish normal human mammary epithelial cell subsets.* Proceedings of the National Academy of Sciences, 2014. **111**(21): p. 7789-7794.
192. Mahendralingam, M.J., et al., *Mammary epithelial cells have lineage-rooted metabolic identities.* Nat Metab, 2021. **3**(5): p. 665-681.
193. DeBerardinis, R.J. and N.S. Chandel, *Fundamentals of cancer metabolism.* Science Advances, 2016. **2**(5): p. e1600200.
194. Warburg, O., *On the origin of cancer cells.* Science, 1956. **123**(3191): p. 309-14.
195. Koppenol, W.H., P.L. Bounds, and C.V. Dang, *Otto Warburg's contributions to current concepts of cancer metabolism.* Nature Reviews Cancer, 2011. **11**(5): p. 325-337.
196. Patra, K.C. and N. Hay, *The pentose phosphate pathway and cancer.* Trends Biochem Sci, 2014. **39**(8): p. 347-54.
197. Cairns, R.A., I.S. Harris, and T.W. Mak, *Regulation of cancer cell metabolism.* Nature Reviews Cancer, 2011. **11**(2): p. 85-95.
198. Basit, F., et al., *Mitochondrial complex I inhibition triggers a mitophagy-dependent ROS increase leading to necroptosis and ferroptosis in melanoma cells.* Cell Death Dis, 2017. **8**(3): p. e2716.
199. Juweid, M.E. and B.D. Cheson, *Positron-emission tomography and assessment of cancer therapy.* N Engl J Med, 2006. **354**(5): p. 496-507.
200. DeBerardinis, R.J. and N.S. Chandel, *Fundamentals of cancer metabolism.* Sci Adv, 2016. **2**(5): p. e1600200.
201. Martínez-Reyes, I. and N.S. Chandel, *Mitochondrial TCA cycle metabolites control physiology and disease.* Nature Communications, 2020. **11**(1): p. 102.
202. Birsoy, K., et al., *An Essential Role of the Mitochondrial Electron Transport Chain in Cell Proliferation Is to Enable Aspartate Synthesis.* Cell, 2015. **162**(3): p. 540-51.
203. Vasan, K., M. Werner, and N.S. Chandel, *Mitochondrial Metabolism as a Target for Cancer Therapy.* Cell Metabolism, 2020. **32**(3): p. 341-352.
204. Spodenkiewicz, M., et al., *Minireview on Glutamine Synthetase Deficiency, an Ultra-Rare Inborn Error of Amino Acid Biosynthesis.* Biology (Basel), 2016. **5**(4).
205. Yang, L., S. Venneti, and D. Nagrath, *Glutaminolysis: A Hallmark of Cancer Metabolism.* Annual Review of Biomedical Engineering, 2017. **19**(1): p. 163-194.
206. Yoo, H.C., et al., *Glutamine reliance in cell metabolism.* Experimental & Molecular Medicine, 2020. **52**(9): p. 1496-1516.
207. Filipp, F.V., et al., *Reverse TCA cycle flux through isocitrate dehydrogenases 1 and 2 is required for lipogenesis in hypoxic melanoma cells.* Pigment Cell Melanoma Res, 2012. **25**(3): p. 375-83.
208. Fendt, S.M., et al., *Reductive glutamine metabolism is a function of the α-ketoglutarate to citrate ratio in cells.* Nat Commun, 2013. **4**: p. 2236.
209. Mullen, A.R., et al., *Reductive carboxylation supports growth in tumour cells with defective mitochondria.* Nature, 2011. **481**(7381): p. 385-8.

210. DeBerardinis, R.J., et al., *Beyond aerobic glycolysis: transformed cells can engage in glutamine metabolism that exceeds the requirement for protein and nucleotide synthesis.* Proc Natl Acad Sci U S A, 2007. **104**(49): p. 19345-50.
211. Vander Heiden, M.G. and R.J. DeBerardinis, *Understanding the Intersections between Metabolism and Cancer Biology.* Cell, 2017. **168**(4): p. 657-669.
212. Pelicano, H., et al., *Mitochondrial dysfunction in some triple-negative breast cancer cell lines: role of mTOR pathway and therapeutic potential.* Breast Cancer Research, 2014. **16**(5): p. 434.
213. Andrzejewski, S., et al., *PGC-1alpha Promotes Breast Cancer Metastasis and Confers Bioenergetic Flexibility against Metabolic Drugs.* Cell Metab, 2017. **26**(5): p. 778-787 e5.
214. Luo, M., et al., *Targeting Breast Cancer Stem Cell State Equilibrium through Modulation of Redox Signaling.* Cell Metab, 2018. **28**(1): p. 69-86 e6.
215. Dupuy, F., et al., *PDK1-Dependent Metabolic Reprogramming Dictates Metastatic Potential in Breast Cancer.* Cell Metab, 2015. **22**(4): p. 577-89.
216. Boroughs, L.K. and R.J. DeBerardinis, *Metabolic pathways promoting cancer cell survival and growth.* Nat Cell Biol, 2015. **17**(4): p. 351-9.
217. Dong, Y., et al., *Regulation of cancer cell metabolism: oncogenic MYC in the driver's seat.* Signal Transduction and Targeted Therapy, 2020. **5**(1): p. 124.
218. Hoxhaj, G. and B.D. Manning, *The PI3K–AKT network at the interface of oncogenic signalling and cancer metabolism.* Nature Reviews Cancer, 2020. **20**(2): p. 74-88.
219. Hopkins, B.D., M.D. Goncalves, and L.C. Cantley, *Insulin–PI3K signalling: an evolutionarily insulated metabolic driver of cancer.* Nature Reviews Endocrinology, 2020. **16**(5): p. 276-283.
220. Dowling, R.J., et al., *Metformin inhibits mammalian target of rapamycin-dependent translation initiation in breast cancer cells.* Cancer Res, 2007. **67**(22): p. 10804-12.
221. Valvezan, A.J. and B.D. Manning, *Molecular logic of mTORC1 signalling as a metabolic rheostat.* Nature Metabolism, 2019. **1**(3): p. 321-333.
222. Garcia, D. and R.J. Shaw, *AMPK: Mechanisms of Cellular Energy Sensing and Restoration of Metabolic Balance.* Mol Cell, 2017. **66**(6): p. 789-800.
223. Herzig, S. and R.J. Shaw, *AMPK: guardian of metabolism and mitochondrial homeostasis.* Nature Reviews Molecular Cell Biology, 2018. **19**(2): p. 121-135.
224. Shackelford, D.B. and R.J. Shaw, *The LKB1–AMPK pathway: metabolism and growth control in tumour suppression.* Nature Reviews Cancer, 2009. **9**(8): p. 563-575.
225. Mihaylova, M.M. and R.J. Shaw, *The AMPK signalling pathway coordinates cell growth, autophagy and metabolism.* Nature Cell Biology, 2011. **13**(9): p. 1016-1023.
226. Kim, J.W., et al., *HIF-1-mediated expression of pyruvate dehydrogenase kinase: a metabolic switch required for cellular adaptation to hypoxia.* Cell Metab, 2006. **3**(3): p. 177-85.
227. Weidemann, A. and R.S. Johnson, *Biology of HIF-1α.* Cell Death & Differentiation, 2008. **15**(4): p. 621-627.
228. Zhang, H., et al., *Mitochondrial autophagy is an HIF-1-dependent adaptive metabolic response to hypoxia.* J Biol Chem, 2008. **283**(16): p. 10892-903.

229. Austin, S. and J. St-Pierre, *PGC1α and mitochondrial metabolism – emerging concepts and relevance in ageing and neurodegenerative disorders.* Journal of Cell Science, 2012. **125**(21): p. 4963-4971.
230. St-Pierre, J., et al., *Suppression of reactive oxygen species and neurodegeneration by the PGC-1 transcriptional coactivators.* Cell, 2006. **127**(2): p. 397-408.
231. Szatrowski, T.P. and C.F. Nathan, *Production of large amounts of hydrogen peroxide by human tumor cells.* Cancer Res, 1991. **51**(3): p. 794-8.
232. Perillo, B., et al., *ROS in cancer therapy: the bright side of the moon.* Experimental & Molecular Medicine, 2020. **52**(2): p. 192-203.
233. Sullivan, L.B. and N.S. Chandel, *Mitochondrial reactive oxygen species and cancer.* Cancer & Metabolism, 2014. **2**(1): p. 17.
234. Salmeen, A., et al., *Redox regulation of protein tyrosine phosphatase 1B involves a sulphenyl-amide intermediate.* Nature, 2003. **423**(6941): p. 769-773.
235. Seth, D. and J. Rudolph, *Redox regulation of MAP kinase phosphatase 3.* Biochemistry, 2006. **45**(28): p. 8476-87.
236. Lee, G., et al., *Oxidative Dimerization of PHD2 is Responsible for its Inactivation and Contributes to Metabolic Reprogramming via HIF-1α Activation.* Scientific Reports, 2016. **6**(1): p. 18928.
237. Semenza, G.L., *Targeting HIF-1 for cancer therapy.* Nature Reviews Cancer, 2003. **3**(10): p. 721-732.
238. Tiku, M.L., J.B. Liesch, and F.M. Robertson, *Production of hydrogen peroxide by rabbit articular chondrocytes. Enhancement by cytokines.* J Immunol, 1990. **145**(2): p. 690-6.
239. Takada, Y., et al., *Hydrogen peroxide activates NF-kappa B through tyrosine phosphorylation of I kappa B alpha and serine phosphorylation of p65: evidence for the involvement of I kappa B alpha kinase and Syk protein-tyrosine kinase.* J Biol Chem, 2003. **278**(26): p. 24233-41.
240. Blaser, H., et al., *TNF and ROS Crosstalk in Inflammation.* Trends Cell Biol, 2016. **26**(4): p. 249-261.
241. Canli, Ö., et al., *Myeloid Cell-Derived Reactive Oxygen Species Induce Epithelial Mutagenesis.* Cancer Cell, 2017. **32**(6): p. 869-883.e5.
242. Sena, L.A., et al., *Mitochondria are required for antigen-specific T cell activation through reactive oxygen species signaling.* Immunity, 2013. **38**(2): p. 225-36.
243. Mak, T.W., et al., *Glutathione Primes T Cell Metabolism for Inflammation.* Immunity, 2017. **46**(4): p. 675-689.
244. Fiers, W., et al., *More than one way to die: apoptosis, necrosis and reactive oxygen damage.* Oncogene, 1999. **18**(54): p. 7719-7730.
245. Ba, X. and I. Boldogh, *8-Oxoguanine DNA glycosylase 1: Beyond repair of the oxidatively modified base lesions.* Redox Biol, 2018. **14**: p. 669-678.
246. Yakes, F.M. and B. Van Houten, *Mitochondrial DNA damage is more extensive and persists longer than nuclear DNA damage in human cells following oxidative stress.* Proc Natl Acad Sci U S A, 1997. **94**(2): p. 514-9.
247. Dalleau, S., et al., *Cell death and diseases related to oxidative stress:4-hydroxynonenal (HNE) in the balance.* Cell Death & Differentiation, 2013. **20**(12): p. 1615-1630.

248. Reczek, C.R. and N.S. Chandel, *The Two Faces of Reactive Oxygen Species in Cancer.* Annual Review of Cancer Biology, 2017. **1**(1): p. 79-98.
249. Circu, M.L. and T.Y. Aw, *Reactive oxygen species, cellular redox systems, and apoptosis.* Free Radic Biol Med, 2010. **48**(6): p. 749-62.
250. Moon, D.O., et al., *Butein induces G(2)/M phase arrest and apoptosis in human hepatoma cancer cells through ROS generation.* Cancer Lett, 2010. **288**(2): p. 204-13.
251. Gorrini, C., I.S. Harris, and T.W. Mak, *Modulation of oxidative stress as an anticancer strategy.* Nat Rev Drug Discov, 2013. **12**(12): p. 931-47.
252. Jaramillo, M.C. and D.D. Zhang, *The emerging role of the Nrf2-Keap1 signaling pathway in cancer.* Genes Dev, 2013. **27**(20): p. 2179-91.
253. Panieri, E. and M.M. Santoro, *ROS homeostasis and metabolism: a dangerous liason in cancer cells.* Cell Death & Disease, 2016. **7**(6): p. e2253-e2253.
254. St Clair, D.K., et al., *Suppression of radiation-induced neoplastic transformation by overexpression of mitochondrial superoxide dismutase.* Mol Carcinog, 1992. **6**(4): p. 238-42.
255. Safford, S.E., et al., *Suppression of fibrosarcoma metastasis by elevated expression of manganese superoxide dismutase.* Cancer Res, 1994. **54**(16): p. 4261-5.
256. Neumann, C.A., et al., *Essential role for the peroxiredoxin Prdx1 in erythrocyte antioxidant defence and tumour suppression.* Nature, 2003. **424**(6948): p. 561-5.
257. Blot, W.J., et al., *Nutrition intervention trials in Linxian, China: supplementation with specific vitamin/mineral combinations, cancer incidence, and disease-specific mortality in the general population.* J Natl Cancer Inst, 1993. **85**(18): p. 1483-92.
258. Sayin, V.I., et al., *Antioxidants accelerate lung cancer progression in mice.* Sci Transl Med, 2014. **6**(221): p. 221ra15.
259. Klein, E.A., et al., *Vitamin E and the risk of prostate cancer: the Selenium and Vitamin E Cancer Prevention Trial (SELECT).* Jama, 2011. **306**(14): p. 1549-56.
260. Omenn, G.S., et al., *Effects of a combination of beta carotene and vitamin A on lung cancer and cardiovascular disease.* N Engl J Med, 1996. **334**(18): p. 1150-5.
261. Bjelakovic, G., et al., *Mortality in randomized trials of antioxidant supplements for primary and secondary prevention: systematic review and meta-analysis.* Jama, 2007. **297**(8): p. 842-57.
262. Porporato, Paolo E., et al., *A Mitochondrial Switch Promotes Tumor Metastasis.* Cell Reports, 2014. **8**(3): p. 754-766.
263. Lewis, K., et al., *p66ShcA functions as a contextual promoter of breast cancer metastasis.* Breast Cancer Res, 2020. **22**(1): p. 7.
264. Labuschagne, C.F., et al., *Cell Clustering Promotes a Metabolic Switch that Supports Metastatic Colonization.* Cell Metab, 2019. **30**(4): p. 720-734.e5.
265. Postovit, L., et al., *Harnessing Oxidative Stress as an Innovative Target for Cancer Therapy.* Oxidative medicine and cellular longevity, 2018. **2018**: p. 6135739-6135739.
266. Riley, P.A., *Free radicals in biology: oxidative stress and the effects of ionizing radiation.* Int J Radiat Biol, 1994. **65**(1): p. 27-33.
267. Kramer, R.A., J. Zakher, and G. Kim, *Role of the glutathione redox cycle in acquired and de novo multidrug resistance.* Science, 1988. **241**(4866): p. 694-7.

268. Parekh, A., et al., *Multi-nucleated cells use ROS to induce breast cancer chemo-resistance in vitro and in vivo.* Oncogene, 2018. **37**(33): p. 4546-4561.
269. Diehn, M., et al., *Association of reactive oxygen species levels and radioresistance in cancer stem cells.* Nature, 2009. **458**(7239): p. 780-3.
270. Fiorillo, M., et al., *Mitochondrial "power" drives tamoxifen resistance: NQO1 and GCLC are new therapeutic targets in breast cancer.* Oncotarget, 2017. **8**(12): p. 20309-20327.
271. Khamari, R., et al., *Glucose metabolism and NRF2 coordinate the antioxidant response in melanoma resistant to MAPK inhibitors.* Cell Death & Disease, 2018. **9**(3): p. 325.
272. Arrick, B.A., et al., *Glutathione depletion sensitizes tumor cells to oxidative cytolysis.* J Biol Chem, 1982. **257**(3): p. 1231-7.
273. Griffith, O.W., *Mechanism of action, metabolism, and toxicity of buthionine sulfoximine and its higher homologs, potent inhibitors of glutathione synthesis.* J Biol Chem, 1982. **257**(22): p. 13704-12.
274. Lewis-Wambi, J.S., et al., *Buthionine sulfoximine sensitizes antihormone-resistant human breast cancer cells to estrogen-induced apoptosis.* Breast Cancer Res, 2008. **10**(6): p. R104.
275. Jiang, H., H. Wang, and M. De Ridder, *Targeting antioxidant enzymes as a radiosensitizing strategy.* Cancer Letters, 2018. **438**: p. 154-164.
276. Rudin, C.M., et al., *Inhibition of Glutathione Synthesis Reverses Bcl-2-mediated Cisplatin Resistance1.* Cancer Research, 2003. **63**(2): p. 312-318.
277. Britten, R.A., et al., *BSO-induced reduction of glutathione levels increases the cellular radiosensitivity of drug-resistant human tumor cells.* Int J Radiat Oncol Biol Phys, 1992. **22**(4): p. 769-72.
278. Shah, M.A. and H.A. Rogoff, *Implications of reactive oxygen species on cancer formation and its treatment.* Seminars in Oncology, 2021. **48**(3): p. 238-245.
279. O'Dwyer, P.J., et al., *Phase I trial of buthionine sulfoximine in combination with melphalan in patients with cancer.* J Clin Oncol, 1996. **14**(1): p. 249-56.
280. Bailey, H.H., et al., *Phase I clinical trial of intravenous L-buthionine sulfoximine and melphalan: an attempt at modulation of glutathione.* J Clin Oncol, 1994. **12**(1): p. 194-205.
281. Townsend, D.M., et al., *NOV-002, a glutathione disulfide mimetic, as a modulator of cellular redox balance.* Cancer Res, 2008. **68**(8): p. 2870-7.
282. Harris, Isaac S., et al., *Glutathione and Thioredoxin Antioxidant Pathways Synergize to Drive Cancer Initiation and Progression.* Cancer Cell, 2015. **27**(2): p. 211-222.
283. Ramanathan, R.K., et al., *A Phase I pharmacokinetic and pharmacodynamic study of PX-12, a novel inhibitor of thioredoxin-1, in patients with advanced solid tumors.* Clin Cancer Res, 2007. **13**(7): p. 2109-14.
284. Ernster, L.N., F *Soluble Diaphorase in Animal Tissues.* Proceedings of the Swedish Biochemical Society, 1958. **12**(3): p. 595-602.
285. Ernster, L., L. Danielson, and M. Ljunggren, *DT diaphorase. I. Purification from the soluble fraction of rat-liver cytoplasm, and properties.* Biochim Biophys Acta, 1962. **58**: p. 171-88.

286. Janda, E., et al., *Molecular Pharmacology of NRH:Quinone Oxidoreductase 2: A Detoxifying Enzyme Acting as an Undercover Toxifying Enzyme.* Molecular pharmacology, 2020. **98**(5): p. 620-633.
287. Winski, S.L., et al., *Subcellular localization of NAD(P)H:quinone oxidoreductase 1 in human cancer cells.* Cancer Res, 2002. **62**(5): p. 1420-4.
288. Siegel, D., J.K. Kepa, and D. Ross, *NAD(P)H:quinone oxidoreductase 1 (NQO1) localizes to the mitotic spindle in human cells.* PLoS One, 2012. **7**(9): p. e44861.
289. Kaspar, J.W. and A.K. Jaiswal, *Antioxidant-induced phosphorylation of tyrosine 486 leads to rapid nuclear export of Bach1 that allows Nrf2 to bind to the antioxidant response element and activate defensive gene expression.* J Biol Chem, 2010. **285**(1): p. 153-62.
290. Ma, Q., et al., *Induction of murine NAD(P)H:quinone oxidoreductase by 2,3,7,8-tetrachlorodibenzo-p-dioxin requires the CNC (cap 'n' collar) basic leucine zipper transcription factor Nrf2 (nuclear factor erythroid 2-related factor 2): cross-interaction between AhR (aryl hydrocarbon receptor) and Nrf2 signal transduction.* Biochem J, 2004. **377**(Pt 1): p. 205-13.
291. Kimura, A., et al., *NQO1 inhibits the TLR-dependent production of selective cytokines by promoting IκB-ζ degradation.* J Exp Med, 2018. **215**(8): p. 2197-2209.
292. Iyanagi, T. and I. Yamazaki, *One-electron-transfer reactions in biochemical systems. V. Difference in the mechanism of quinone reduction by the NADH dehydrogenase and the NAD(P)H dehydrogenase (DT-diaphorase).* Biochim Biophys Acta, 1970. **216**(2): p. 282-94.
293. Hosoda, S., W. Nakamura, and K. Hayashi, *Properties and reaction mechanism of DT diaphorase from rat liver.* J Biol Chem, 1974. **249**(20): p. 6416-23.
294. Oh, E.T. and H.J. Park, *Implications of NQO1 in cancer therapy.* BMB Rep, 2015. **48**(11): p. 609-17.
295. Bianchet, M.A., M. Faig, and L.M. Amzel, *Structure and mechanism of NAD[P]H:quinone acceptor oxidoreductases (NQO).* Methods Enzymol, 2004. **382**: p. 144-74.
296. Siegel, D., et al., *NAD(P)H:quinone oxidoreductase 1: role as a superoxide scavenger.* Mol Pharmacol, 2004. **65**(5): p. 1238-47.
297. Zhu, H., et al., *The highly expressed and inducible endogenous NAD(P)H:quinone oxidoreductase 1 in cardiovascular cells acts as a potential superoxide scavenger.* Cardiovasc Toxicol, 2007. **7**(3): p. 202-11.
298. Chan, T.S., et al., *Coenzyme Q cytoprotective mechanisms for mitochondrial complex I cytopathies involves NAD(P)H: quinone oxidoreductase 1(NQO1).* Free Radic Res, 2002. **36**(4): p. 421-7.
299. Ross, D. and D. Siegel, *Functions of NQO1 in Cellular Protection and CoQ(10) Metabolism and its Potential Role as a Redox Sensitive Molecular Switch.* Frontiers in physiology, 2017. **8**: p. 595-595.
300. Pey, A.L., C.F. Megarity, and D.J. Timson, *NAD(P)H quinone oxidoreductase (NQO1): an enzyme which needs just enough mobility, in just the right places.* Biosci Rep, 2019. **39**(1).
301. Asher, G., et al., *NQO1 stabilizes p53 through a distinct pathway.* Proc Natl Acad Sci U S A, 2002. **99**(5): p. 3099-104.

302. Adamovich, Y., et al., *The protein level of PGC-1alpha, a key metabolic regulator, is controlled by NADH-NQO1.* Mol Cell Biol, 2013. **33**(13): p. 2603-13.
303. Adamovich, Y., et al., *The protein level of PGC-1α, a key metabolic regulator, is controlled by NADH-NQO1.* Mol Cell Biol, 2013. **33**(13): p. 2603-13.
304. Oh, E.-T., et al., *NQO1 inhibits proteasome-mediated degradation of HIF-1α.* Nature Communications, 2016. **7**(1): p. 13593.
305. Tsvetkov, P., et al., *NQO1 binds and supports SIRT1 function.* bioRxiv, 2017: p. 139907.
306. Traver, R.D., et al., *Characterization of a polymorphism in NAD(P)H: quinone oxidoreductase (DT-diaphorase).* Br J Cancer, 1997. **75**(1): p. 69-75.
307. Siegel, D., et al., *Rapid polyubiquitination and proteasomal degradation of a mutant form of NAD(P)H:quinone oxidoreductase 1.* Mol Pharmacol, 2001. **59**(2): p. 263-8.
308. Luo, S., et al., *Akt Phosphorylates NQO1 and Triggers its Degradation, Abolishing Its Antioxidative Activities in Parkinson's Disease.* J Neurosci, 2019. **39**(37): p. 7291-7305.
309. Zhang, K., et al., *NAD(P)H:Quinone Oxidoreductase 1 (NQO1) as a Therapeutic and Diagnostic Target in Cancer.* Journal of Medicinal Chemistry, 2018. **61**(16): p. 6983-7003.
310. Iskander, K., R.J. Barrios, and A.K. Jaiswal, *Disruption of NAD(P)H:quinone oxidoreductase 1 gene in mice leads to radiation-induced myeloproliferative disease.* Cancer Res, 2008. **68**(19): p. 7915-22.
311. Radjendirane, V., et al., *Disruption of the DT diaphorase (NQO1) gene in mice leads to increased menadione toxicity.* J Biol Chem, 1998. **273**(13): p. 7382-9.
312. Iskander, K., et al., *Lower Induction of p53 and Decreased Apoptosis in NQO1-Null Mice Lead to Increased Sensitivity to Chemical-Induced Skin Carcinogenesis.* Cancer Research, 2005. **65**(6): p. 2054-2058.
313. Peng, Q., et al., *The NQO1 Pro187Ser polymorphism and breast cancer susceptibility: evidence from an updated meta-analysis.* Diagn Pathol, 2014. **9**: p. 100.
314. Yuan, W., et al., *Evidence on the association between NQO1 Pro187Ser polymorphism and breast cancer risk in the current studies: a meta-analysis.* Breast Cancer Res Treat, 2011. **125**(2): p. 467-72.
315. Yang, Y., et al., *Clinical implications of high NQO1 expression in breast cancers.* J Exp Clin Cancer Res, 2014. **33**: p. 14.
316. Ma, Y., et al., *NQO1 overexpression is associated with poor prognosis in squamous cell carcinoma of the uterine cervix.* BMC Cancer, 2014. **14**(1): p. 414.
317. Cheng, Y., et al., *The expression of NAD(P)H:quinone oxidoreductase 1 is increased along with NF-kappaB p105/p50 in human cutaneous melanomas.* Oncol Rep, 2010. **23**(4): p. 973-9.
318. Yang, Y., et al., *Clinical implications of high NQO1 expression in breast cancers.* J Exp Clin Cancer Res, 2014. **33**(1): p. 14.
319. Lin, L., et al., *Significance of NQO1 overexpression for prognostic evaluation of gastric adenocarcinoma.* Experimental and Molecular Pathology, 2014. **96**(2): p. 200-205.
320. Cui, X., et al., *High expression of NQO1 is associated with poor prognosis in serous ovarian carcinoma.* BMC Cancer, 2015. **15**(1): p. 244.
321. Ji, M., et al., *Clinicopathological implications of NQO1 overexpression in the prognosis of pancreatic adenocarcinoma.* Oncol Lett, 2017. **13**(5): p. 2996-3002.

322. Lee, H., et al., *NQO1-induced activation of AMPK contributes to cancer cell death by oxygen-glucose deprivation.* Scientific Reports, 2015. **5**(1): p. 7769.
323. Kennedy, K.A., S. Rockwell, and A.C. Sartorelli, *Preferential activation of mitomycin C to cytotoxic metabolites by hypoxic tumor cells.* Cancer Res, 1980. **40**(7): p. 2356-60.
324. Pink, J.J., et al., *NAD(P)H:Quinone oxidoreductase activity is the principal determinant of beta-lapachone cytotoxicity.* J Biol Chem, 2000. **275**(8): p. 5416-24.
325. Gerber, D.E., et al., *Phase 1 study of ARQ 761, a beta-lapachone analogue that promotes NQO1-mediated programmed cancer cell necrosis.* Br J Cancer, 2018. **119**(8): p. 928-936.
326. Beg, M.S., et al., *708P - A phase I/Ib, multi-center trial of ARQ-761 (Beta-Lapachone) with gemcitabine/nab-paclitaxel in patients with advanced pancreatic cancer.* Annals of Oncology, 2019. **30**: p. v271.
327. Shin, E. and J.S. Koo, *Glucose Metabolism and Glucose Transporters in Breast Cancer.* Front Cell Dev Biol, 2021. **9**: p. 728759.
328. Patra, S., et al., *Mechanisms Governing Metabolic Heterogeneity in Breast Cancer and Other Tumors.* Front Oncol, 2021. **11**: p. 700629.
329. Pelicano, H., et al., *Mitochondrial dysfunction in some triple-negative breast cancer cell lines: role of mTOR pathway and therapeutic potential.* Breast Cancer Res, 2014. **16**(5): p. 434.
330. Gong, Y., et al., *Metabolic-Pathway-Based Subtyping of Triple-Negative Breast Cancer Reveals Potential Therapeutic Targets.* Cell Metab, 2021. **33**(1): p. 51-64.e9.
331. Kourtidis, A., et al., *An RNA interference screen identifies metabolic regulators NR1D1 and PBP as novel survival factors for breast cancer cells with the ERBB2 signature.* Cancer Res, 2010. **70**(5): p. 1783-92.
332. Kim, S., Y. Lee, and J.S. Koo, *Differential Expression of Lipid Metabolism-Related Proteins in Different Breast Cancer Subtypes.* PLOS ONE, 2015. **10**(3): p. e0119473.
333. Jin, Q., et al., *Fatty acid synthase phosphorylation: a novel therapeutic target in HER2-overexpressing breast cancer cells.* Breast Cancer Res, 2010. **12**(6): p. R96.
334. Sarmiento-Salinas, F.L., et al., *Breast Cancer Subtypes Present a Differential Production of Reactive Oxygen Species (ROS) and Susceptibility to Antioxidant Treatment.* Frontiers in Oncology, 2019. **9**(480).
335. Daemen, A., et al., *Pan-Cancer Metabolic Signature Predicts Co-Dependency on Glutaminase and De Novo Glutathione Synthesis Linked to a High-Mesenchymal Cell State.* Cell Metabolism, 2018. **28**(3): p. 383-399.e9.
336. Timmerman, Luika A., et al., *Glutamine Sensitivity Analysis Identifies the xCT Antiporter as a Common Triple-Negative Breast Tumor Therapeutic Target.* Cancer Cell, 2013. **24**(4): p. 450-465.
337. Wang, Z., Q. Jiang, and C. Dong, *Metabolic reprogramming in triple-negative breast cancer.* Cancer Biology & Medicine, 2020. **17**: p. 44 - 59.
338. McGuirk, S., et al., *PGC-1α supports glutamine metabolism in breast cancer.* Cancer Metab, 2013. **1**(1): p. 22.
339. Brauer, H.A., et al., *Impact of tumor microenvironment and epithelial phenotypes on metabolism in breast cancer.* Clin Cancer Res, 2013. **19**(3): p. 571-85.
340. Dias, A.S., et al., *Metabolic crosstalk in the breast cancer microenvironment.* European Journal of Cancer, 2019. **121**: p. 154-171.

341. Faubert, B., A. Solmonson, and R.J. DeBerardinis, *Metabolic reprogramming and cancer progression.* Science, 2020. **368**(6487).
342. Wang, L., S. Zhang, and X. Wang, *The Metabolic Mechanisms of Breast Cancer Metastasis.* Front Oncol, 2020. **10**: p. 602416.
343. Schafer, Z.T., et al., *Antioxidant and oncogene rescue of metabolic defects caused by loss of matrix attachment.* Nature, 2009. **461**(7260): p. 109-13.
344. Evans, K.W., et al., *Oxidative Phosphorylation Is a Metabolic Vulnerability in Chemotherapy-Resistant Triple-Negative Breast Cancer.* Cancer Res, 2021. **81**(21): p. 5572-5581.
345. Davis, R.T., et al., *Transcriptional diversity and bioenergetic shift in human breast cancer metastasis revealed by single-cell RNA sequencing.* Nat Cell Biol, 2020. **22**(3): p. 310-320.
346. Dupuy, F., et al., *PDK1-Dependent Metabolic Reprogramming Dictates Metastatic Potential in Breast Cancer.* Cell Metabolism, 2015. **22**(4): p. 577-589.
347. Kuntz, E.M., et al., *Targeting mitochondrial oxidative phosphorylation eradicates therapy-resistant chronic myeloid leukemia stem cells.* Nature Medicine, 2017. **23**(10): p. 1234-1240.
348. Whitaker-Menezes, D., et al., *Hyperactivation of oxidative mitochondrial metabolism in epithelial cancer cells in situ: visualizing the therapeutic effects of metformin in tumor tissue.* Cell Cycle, 2011. **10**(23): p. 4047-64.
349. Chiche, J., et al., *GAPDH Expression Predicts the Response to R-CHOP, the Tumor Metabolic Status, and the Response of DLBCL Patients to Metabolic Inhibitors.* Cell Metabolism, 2019. **29**(6): p. 1243-1257.e10.
350. Viale, A., et al., *Oncogene ablation-resistant pancreatic cancer cells depend on mitochondrial function.* Nature, 2014. **514**(7524): p. 628-32.
351. Haq, R., et al., *Oncogenic BRAF regulates oxidative metabolism via PGC1α and MITF.* Cancer Cell, 2013. **23**(3): p. 302-15.
352. Bekele, R.T., et al., *Oxidative stress contributes to the tamoxifen-induced killing of breast cancer cells: implications for tamoxifen therapy and resistance.* Scientific Reports, 2016. **6**(1): p. 21164.
353. Deblois, G., et al., *ERRα mediates metabolic adaptations driving lapatinib resistance in breast cancer.* Nature Communications, 2016. **7**(1): p. 12156.
354. Lu, H., et al., *Chemotherapy triggers HIF-1–dependent glutathione synthesis and copper chelation that induces the breast cancer stem cell phenotype.* Proceedings of the National Academy of Sciences, 2015. **112**(33): p. E4600-E4609.
355. Bailey, C.J. and C. Day, *Traditional plant medicines as treatments for diabetes.* Diabetes Care, 1989. **12**(8): p. 553-64.
356. Evans, J.M., et al., *Metformin and reduced risk of cancer in diabetic patients.* Bmj, 2005. **330**(7503): p. 1304-5.
357. Johnson, J.A. and M. Pollak, *Insulin, glucose and the increased risk of cancer in patients with type 2 diabetes.* Diabetologia, 2010. **53**(10): p. 2086-8.
358. Zhang, P., et al., *Association of metformin use with cancer incidence and mortality: a meta-analysis.* Cancer Epidemiol, 2013. **37**(3): p. 207-18.

359. Jiralerspong, S., et al., *Metformin and Pathologic Complete Responses to Neoadjuvant Chemotherapy in Diabetic Patients With Breast Cancer.* Journal of Clinical Oncology, 2009. **27**(20): p. 3297-3302.
360. Bayraktar, S., et al., *Effect of metformin on survival outcomes in diabetic patients with triple receptor-negative breast cancer.* Cancer, 2012. **118**(5): p. 1202-1211.
361. Dowling, R.J., et al., *Metformin in cancer: translational challenges.* J Mol Endocrinol, 2012. **48**(3): p. R31-43.
362. Dowling, R.J.O., P.J. Goodwin, and V. Stambolic, *Understanding the benefit of metformin use in cancer treatment.* BMC medicine, 2011. **9**: p. 33-33.
363. Stumvoll, M., et al., *Metabolic effects of metformin in non-insulin-dependent diabetes mellitus.* N Engl J Med, 1995. **333**(9): p. 550-4.
364. Gunton, J.E., et al., *Metformin rapidly increases insulin receptor activation in human liver and signals preferentially through insulin-receptor substrate-2.* J Clin Endocrinol Metab, 2003. **88**(3): p. 1323-32.
365. Shaw, R.J., et al., *The kinase LKB1 mediates glucose homeostasis in liver and therapeutic effects of metformin.* Science, 2005. **310**(5754): p. 1642-6.
366. Miller, R.A., et al., *Biguanides suppress hepatic glucagon signalling by decreasing production of cyclic AMP.* Nature, 2013. **494**(7436): p. 256-60.
367. Pernicova, I. and M. Korbonits, *Metformin—mode of action and clinical implications for diabetes and cancer.* Nature Reviews Endocrinology, 2014. **10**(3): p. 143-156.
368. Pollak, M., *Insulin and insulin-like growth factor signalling in neoplasia.* Nature Reviews Cancer, 2008. **8**(12): p. 915-928.
369. Dowling, R.J., P.J. Goodwin, and V. Stambolic, *Understanding the benefit of metformin use in cancer treatment.* BMC Med, 2011. **9**: p. 33.
370. Birsoy, K., et al., *Metabolic determinants of cancer cell sensitivity to glucose limitation and biguanides.* Nature, 2014. **508**(7494): p. 108-112.
371. Zhou, G., et al., *Role of AMP-activated protein kinase in mechanism of metformin action.* J Clin Invest, 2001. **108**(8): p. 1167-74.
372. Bridges, H.R., et al., *Effects of metformin and other biguanides on oxidative phosphorylation in mitochondria.* The Biochemical journal, 2014. **462**(3): p. 475-487.
373. Gwinn, D.M., et al., *AMPK phosphorylation of raptor mediates a metabolic checkpoint.* Mol Cell, 2008. **30**(2): p. 214-26.
374. Kalender, A., et al., *Metformin, independent of AMPK, inhibits mTORC1 in a rag GTPase-dependent manner.* Cell Metab, 2010. **11**(5): p. 390-401.
375. Zakikhani, M., et al., *Metformin is an AMP kinase-dependent growth inhibitor for breast cancer cells.* Cancer Res, 2006. **66**(21): p. 10269-73.
376. Griss, T., et al., *Metformin Antagonizes Cancer Cell Proliferation by Suppressing Mitochondrial-Dependent Biosynthesis.* PLoS biology, 2015. **13**(12): p. e1002309-e1002309.
377. Anisimov, V.N., et al., *Metformin extends life span of HER-2/neu transgenic mice and in combination with melatonin inhibits growth of transplantable tumors in vivo.* Cell Cycle, 2010. **9**(1): p. 188-97.
378. Bonanni, B., et al., *Dual effect of metformin on breast cancer proliferation in a randomized presurgical trial.* J Clin Oncol, 2012. **30**(21): p. 2593-600.

379. Schuler, K.M., et al., *Antiproliferative and metabolic effects of metformin in a preoperative window clinical trial for endometrial cancer.* Cancer medicine, 2015. **4**(2): p. 161-173.
380. Dowling, R.J.O., et al., *Changes in insulin receptor signaling underlie neoadjuvant metformin administration in breast cancer: a prospective window of opportunity neoadjuvant study.* Breast cancer research : BCR, 2015. **17**(1): p. 32-32.
381. Niraula, S., et al., *Metformin in early breast cancer: a prospective window of opportunity neoadjuvant study.* Breast Cancer Res Treat, 2012. **135**(3): p. 821-30.
382. Hadad, S., et al., *Evidence for biological effects of metformin in operable breast cancer: a pre-operative, window-of-opportunity, randomized trial.* Breast Cancer Res Treat, 2011. **128**(3): p. 783-94.
383. Goodwin, P.J., et al., *Effect of metformin vs placebo on and metabolic factors in NCIC CTG MA.32.* J Natl Cancer Inst, 2015. **107**(3).
384. Kordes, S., et al., *Metformin in patients with advanced pancreatic cancer: a double-blind, randomised, placebo-controlled phase 2 trial.* Lancet Oncol, 2015. **16**(7): p. 839-47.
385. Thomas, T.S., et al., *Impact of metformin use on pathologic response following chemoradiotherapy in rectal cancer.* Journal of Clinical Oncology, 2018. **36**(15_suppl): p. e15642-e15642.
386. Pimentel, I., et al., *A phase II randomized clinical trial of the effect of metformin versus placebo on progression-free survival in women with metastatic breast cancer receiving standard chemotherapy.* Breast, 2019. **48**: p. 17-23.
387. Cuyàs, E., et al., *The C Allele of ATM rs11212617 Associates With Higher Pathological Complete Remission Rate in Breast Cancer Patients Treated With Neoadjuvant Metformin.* Front Oncol, 2019. **9**: p. 193.
388. Goodwin, P.J., et al., *Effect of Metformin vs Placebo on Invasive Disease–Free Survival in Patients With Breast Cancer: The MA.32 Randomized Clinical Trial.* JAMA, 2022. **327**(20): p. 1963-1973.
389. Gormsen, L.C., et al., *In Vivo Imaging of Human ¹¹C-Metformin in Peripheral Organs: Dosimetry, Biodistribution, and Kinetic Analyses.* Journal of Nuclear Medicine, 2016. **57**(12): p. 1920-1926.
390. Davidoff, F., *Effects of guanidine derivatives on mitochondrial function. 3. The mechanism of phenethylbiguanide accumulation and its relationship to in vitro respiratory inhibition.* J Biol Chem, 1971. **246**(12): p. 4017-27.
391. Stambolic, V., et al., *Utility of metformin in breast cancer treatment, is neoangiogenesis a risk factor?* Breast Cancer Res Treat, 2009. **114**(2): p. 387-9.
392. Iversen, A.B., et al., *Results from 11C-metformin-PET scans, tissue analysis and cellular drug-sensitivity assays questions the view that biguanides affects tumor respiration directly.* Scientific Reports, 2017. **7**(1): p. 9436.
393. Assan, R., et al., *Phenformin-induced lactic acidosis in diabetic patients.* Diabetes, 1975. **24**(9): p. 791-800.
394. Sogame, Y., et al., *A comparison of uptake of metformin and phenformin mediated by hOCT1 in human hepatocytes.* Biopharm Drug Dispos, 2009. **30**(8): p. 476-84.
395. Segal, E.D., et al., *Relevance of the OCT1 transporter to the antineoplastic effect of biguanides.* Biochem Biophys Res Commun, 2011. **414**(4): p. 694-9.

396. Appleyard, M.V., et al., *Phenformin as prophylaxis and therapy in breast cancer xenografts.* Br J Cancer, 2012. **106**(6): p. 1117-22.
397. Janzer, A., et al., *Metformin and phenformin deplete tricarboxylic acid cycle and glycolytic intermediates during cell transformation and NTPs in cancer stem cells.* Proc Natl Acad Sci U S A, 2014. **111**(29): p. 10574-9.
398. Guo, Z., et al., *Phenformin inhibits growth and epithelial-mesenchymal transition of ErbB2-overexpressing breast cancer cells through targeting the IGF1R pathway.* Oncotarget, 2017. **8**(36): p. 60342-60357.
399. Jackson, A.L., et al., *Phenformin has anti-tumorigenic effects in human ovarian cancer cells and in an orthotopic mouse model of serous ovarian cancer.* Oncotarget, 2017. **8**(59): p. 100113-100127.
400. Vara-Ciruelos, D., et al., *Phenformin, But Not Metformin, Delays Development of T Cell Acute Lymphoblastic Leukemia/Lymphoma via Cell-Autonomous AMPK Activation.* Cell Reports, 2019. **27**(3): p. 690-698.e4.
401. Bridges, H.R., et al., *Structural Basis of Mammalian Respiratory Complex I Inhibition by Medicinal Biguanides.* bioRxiv, 2022: p. 2022.08.09.503333.
402. Di Magno, L., et al., *Phenformin Inhibits Hedgehog-Dependent Tumor Growth through a Complex I-Independent Redox/Corepressor Module.* Cell Rep, 2020. **30**(6): p. 1735-1752.e7.
403. Miskimins, W.K., et al., *Synergistic anti-cancer effect of phenformin and oxamate.* PLoS One, 2014. **9**(1): p. e85576.
404. Scharping, N.E., et al., *Efficacy of PD-1 Blockade Is Potentiated by Metformin-Induced Reduction of Tumor Hypoxia.* Cancer Immunol Res, 2017. **5**(1): p. 9-16.
405. Kim, S.H., et al., *Phenformin Inhibits Myeloid-Derived Suppressor Cells and Enhances the Anti-Tumor Activity of PD-1 Blockade in Melanoma.* J Invest Dermatol, 2017. **137**(8): p. 1740-1748.
406. Gravel, S.P., et al., *Serine deprivation enhances antineoplastic activity of biguanides.* Cancer Res, 2014. **74**(24): p. 7521-33.
407. Gui, D.Y., et al., *Environment Dictates Dependence on Mitochondrial Complex I for NAD+ and Aspartate Production and Determines Cancer Cell Sensitivity to Metformin.* Cell Metab, 2016. **24**(5): p. 716-727.
408. Hulea, L., et al., *Translational and HIF-1alpha-Dependent Metabolic Reprogramming Underpin Metabolic Plasticity and Responses to Kinase Inhibitors and Biguanides.* Cell Metab, 2018. **28**(6): p. 817-832.e8.
409. Im, Y.K., et al., *Interplay between ShcA Signaling and PGC-1alpha Triggers Targetable Metabolic Vulnerabilities in Breast Cancer.* Cancer Res, 2018. **78**(17): p. 4826-4838.
410. Urra, F.A., et al., *The Mitochondrial Complex(I)ty of Cancer.* Front Oncol, 2017. **7**: p. 118.
411. Bastian, A., et al., *AG311, a small molecule inhibitor of complex I and hypoxia-induced HIF-1α stabilization.* Cancer Lett, 2017. **388**: p. 149-157.
412. Bastian, A., et al., *A small molecule with anticancer and antimetastatic activities induces rapid mitochondrial associated necrosis in breast cancer.* Journal of Pharmacology and Experimental Therapeutics, 2015: p. jpet.114.220335.
413. Molina, J.R., et al., *An inhibitor of oxidative phosphorylation exploits cancer vulnerability.* Nat Med, 2018. **24**(7): p. 1036-1046.

414. Tsuji, A., et al., *IACS-010759, a potent inhibitor of glycolysis-deficient hypoxic tumor cells, inhibits mitochondrial respiratory complex I through a unique mechanism.* Journal of Biological Chemistry, 2020. **295**(21): p. 7481-7491.
415. Konopleva, M., et al., *Targeting Oxidative Phosphorylation with a Mitochondrial Complex I Inhibitor is limited by Mechanism-based Toxicity*. 2022, Research Square.
416. Janku, F., et al., *First-in-human study of IM156, a novel potent biguanide oxidative phosphorylation (OXPHOS) inhibitor, in patients with advanced solid tumors.* Invest New Drugs, 2022. **40**(5): p. 1001-1010.
417. Quintela-Fandino, M., et al., *Randomized Phase 0/I Trial of the Mitochondrial Inhibitor ME-344 or Placebo Added to Bevacizumab in Early HER2-Negative Breast Cancer.* Clin Cancer Res, 2020. **26**(1): p. 35-45.
418. Luna Yolba, R., et al., *EVT-701 is a novel selective and safe mitochondrial complex 1 inhibitor with potent anti-tumor activity in models of solid cancers.* Pharmacol Res Perspect, 2021. **9**(5): p. e00854.
419. Rocha e Silva, M., *A brief survey of the history of inflammation. 1978.* Agents Actions, 1994. **43**(3-4): p. 86-90.
420. Cen, X., S. Liu, and K. Cheng, *The Role of Toll-Like Receptor in Inflammation and Tumor Immunity.* Front Pharmacol, 2018. **9**: p. 878.
421. Kawasaki, T. and T. Kawai, *Toll-Like Receptor Signaling Pathways.* Frontiers in Immunology, 2014. **5**.
422. Rehwinkel, J. and M.U. Gack, *RIG-I-like receptors: their regulation and roles in RNA sensing.* Nature Reviews Immunology, 2020. **20**(9): p. 537-551.
423. Brennan, J.J. and T.D. Gilmore, *Evolutionary Origins of Toll-like Receptor Signaling.* Mol Biol Evol, 2018. **35**(7): p. 1576-1587.
424. Claesson-Welsh, L., E. Dejana, and D.M. McDonald, *Permeability of the Endothelial Barrier: Identifying and Reconciling Controversies.* Trends in Molecular Medicine, 2021. **27**(4): p. 314-331.
425. Margraf, A., C.A. Lowell, and A. Zarbock, *Neutrophils in acute inflammation: current concepts and translational implications.* Blood, 2022. **139**(14): p. 2130-2144.
426. Paul, William E., *Bridging Innate and Adaptive Immunity.* Cell, 2011. **147**(6): p. 1212-1215.
427. Rossi, J.-F., et al., *Dynamic Immune/Inflammation Precision Medicine: The Good and the Bad Inflammation in Infection and Cancer.* Frontiers in Immunology, 2021. **12**.
428. Borden, E.C., et al., *Interferons at age 50: past, current and future impact on biomedicine.* Nature Reviews Drug Discovery, 2007. **6**(12): p. 975-990.
429. Ortega-Gómez, A., M. Perretti, and O. Soehnlein, *Resolution of inflammation: an integrated view.* EMBO Molecular Medicine, 2013. **5**(5): p. 661-674.
430. Walker, J.A. and A.N.J. McKenzie, *TH2 cell development and function.* Nature Reviews Immunology, 2018. **18**(2): p. 121-133.
431. Basil, M.C. and B.D. Levy, *Specialized pro-resolving mediators: endogenous regulators of infection and inflammation.* Nature Reviews Immunology, 2016. **16**(1): p. 51-67.
432. Zhao, H., et al., *Inflammation and tumor progression: signaling pathways and targeted intervention.* Signal Transduction and Targeted Therapy, 2021. **6**(1): p. 263.

433. Śledzińska, A., et al., *Negative immune checkpoints on T lymphocytes and their relevance to cancer immunotherapy.* Mol Oncol, 2015. **9**(10): p. 1936-65.
434. Takeda, K. and S. Akira, *Toll-like receptors.* Curr Protoc Immunol, 2015. **109**: p. 14.12.1-14.12.10.
435. Kawai, T. and S. Akira, *TLR signaling.* Cell Death & Differentiation, 2006. **13**(5): p. 816-825.
436. Salaun, B., et al., *TLR3 can directly trigger apoptosis in human cancer cells.* J Immunol, 2006. **176**(8): p. 4894-901.
437. Oshiumi, H., et al., *TICAM-1, an adaptor molecule that participates in Toll-like receptor 3–mediated interferon-β induction.* Nature Immunology, 2003. **4**(2): p. 161-167.
438. Oganesyan, G., et al., *Critical role of TRAF3 in the Toll-like receptor-dependent and -independent antiviral response.* Nature, 2006. **439**(7073): p. 208-211.
439. Fitzgerald, K.A., et al., *IKKε and TBK1 are essential components of the IRF3 signaling pathway.* Nature Immunology, 2003. **4**(5): p. 491-496.
440. Liu, T., et al., *NF-κB signaling in inflammation.* Signal Transduction and Targeted Therapy, 2017. **2**(1): p. 17023.
441. Muresan, X.M., et al., *Toll-Like Receptor 3 in Solid Cancer and Therapy Resistance.* Cancers (Basel), 2020. **12**(11).
442. Salmon, H., et al., *Expansion and Activation of CD103(+) Dendritic Cell Progenitors at the Tumor Site Enhances Tumor Responses to Therapeutic PD-L1 and BRAF Inhibition.* Immunity, 2016. **44**(4): p. 924-38.
443. Di, S., et al., *Combined Adjuvant of Poly I:C Improves Antitumor Effects of CAR-T Cells.* Frontiers in Oncology, 2019. **9**.
444. Perrot, I., et al., *TLR3 and Rig-like receptor on myeloid dendritic cells and Rig-like receptor on human NK cells are both mandatory for production of IFN-gamma in response to double-stranded RNA.* J Immunol, 2010. **185**(4): p. 2080-8.
445. Coussens, L.M. and Z. Werb, *Inflammation and cancer.* Nature, 2002. **420**(6917): p. 860-7.
446. Koebel, C.M., et al., *Adaptive immunity maintains occult cancer in an equilibrium state.* Nature, 2007. **450**(7171): p. 903-7.
447. Shalapour, S. and M. Karin, *Immunity, inflammation, and cancer: an eternal fight between good and evil.* J Clin Invest, 2015. **125**(9): p. 3347-55.
448. Dunn, G.P., L.J. Old, and R.D. Schreiber, *The Three Es of Cancer Immunoediting.* Annual Review of Immunology, 2004. **22**: p. 329-360.
449. Zitvogel, L., A. Tesniere, and G. Kroemer, *Cancer despite immunosurveillance: immunoselection and immunosubversion.* Nat Rev Immunol, 2006. **6**(10): p. 715-27.
450. Bidwell, B.N., et al., *Silencing of Irf7 pathways in breast cancer cells promotes bone metastasis through immune escape.* Nat Med, 2012. **18**(8): p. 1224-31.
451. Kim, S.K. and S.W. Cho, *The Evasion Mechanisms of Cancer Immunity and Drug Intervention in the Tumor Microenvironment.* Front Pharmacol, 2022. **13**: p. 868695.
452. Shacter, E. and S.A. Weitzman, *Chronic inflammation and cancer.* Oncology (Williston Park), 2002. **16**(2): p. 217-26, 229; discussion 230-2.
453. Trinchieri, G., *Cancer and Inflammation: An Old Intuition with Rapidly Evolving New Concepts.* Annual Review of Immunology, 2012. **30**: p. 677-706.

454. Grivennikov, S.I., F.R. Greten, and M. Karin, *Immunity, inflammation, and cancer.* Cell, 2010. **140**(6): p. 883-99.
455. Masucci, M.T., M. Minopoli, and M.V. Carriero, *Tumor Associated Neutrophils. Their Role in Tumorigenesis, Metastasis, Prognosis and Therapy.* Frontiers in Oncology, 2019. **9**.
456. Yang, L. and Y. Zhang, *Tumor-associated macrophages: from basic research to clinical application.* J Hematol Oncol, 2017. **10**(1): p. 58.
457. Erez, N., et al., *Cancer-Associated Fibroblasts Are Activated in Incipient Neoplasia to Orchestrate Tumor-Promoting Inflammation in an NF-kappaB-Dependent Manner.* Cancer Cell, 2010. **17**(2): p. 135-47.
458. Kroemer, G., et al., *Immunogenic Cell Death in Cancer Therapy.* Annual Review of Immunology, 2013. **31**: p. 51-72.
459. Harrington, K., et al., *Optimizing oncolytic virotherapy in cancer treatment.* Nature Reviews Drug Discovery, 2019. **18**(9): p. 689-706.
460. Del Prete, A., et al., *Molecular pathways in cancer-related inflammation.* Biochem Med (Zagreb), 2011. **21**(3): p. 264-75.
461. Elinav, E., et al., *Inflammation-induced cancer: crosstalk between tumours, immune cells and microorganisms.* Nature Reviews Cancer, 2013. **13**(11): p. 759-771.
462. Sun, L., et al., *Cyclic GMP-AMP synthase is a cytosolic DNA sensor that activates the type I interferon pathway.* Science, 2013. **339**(6121): p. 786-91.
463. Liu, H., et al., *Nuclear cGAS suppresses DNA repair and promotes tumorigenesis.* Nature, 2018. **563**(7729): p. 131-136.
464. Kwon, J. and S.F. Bakhoum, *The Cytosolic DNA-Sensing cGAS-STING Pathway in Cancer.* Cancer Discov, 2020. **10**(1): p. 26-39.
465. Urban-Wojciuk, Z., et al., *The Role of TLRs in Anti-cancer Immunity and Tumor Rejection.* Front Immunol, 2019. **10**: p. 2388.
466. González-Reyes, S., et al., *Study of TLR3, TLR4 and TLR9 in breast carcinomas and their association with metastasis.* BMC Cancer, 2010. **10**: p. 665.
467. Salaun, B., et al., *TLR3 as a biomarker for the therapeutic efficacy of double-stranded RNA in breast cancer.* Cancer Res, 2011. **71**(5): p. 1607-14.
468. Shrihari, T.G., *Dual role of inflammatory mediators in cancer.* Ecancermedicalscience, 2017. **11**: p. 721.
469. Siegel, P.M. and J. Massagué, *Cytostatic and apoptotic actions of TGF-β in homeostasis and cancer.* Nature Reviews Cancer, 2003. **3**(11): p. 807-820.
470. Schoenborn, J.R. and C.B. Wilson, *Regulation of interferon-gamma during innate and adaptive immune responses.* Adv Immunol, 2007. **96**: p. 41-101.
471. Zaidi, M.R. and G. Merlino, *The two faces of interferon-γ in cancer.* Clin Cancer Res, 2011. **17**(19): p. 6118-24.
472. Wheelock, E.F., *Interferon-Like Virus-Inhibitor Induced in Human Leukocytes by Phytohemagglutinin.* Science, 1965. **149**(3681): p. 310-1.
473. Gocher, A.M., C.J. Workman, and D.A.A. Vignali, *Interferon-γ: teammate or opponent in the tumour microenvironment?* Nature Reviews Immunology, 2022. **22**(3): p. 158-172.
474. Okamura, H., et al., *Regulation of interferon-gamma production by IL-12 and IL-18.* Curr Opin Immunol, 1998. **10**(3): p. 259-64.

475. Trinchieri, G., *Interleukin-12: a cytokine produced by antigen-presenting cells with immunoregulatory functions in the generation of T-helper cells type 1 and cytotoxic lymphocytes.* Blood, 1994. **84**(12): p. 4008-27.
476. Castro, F., et al., *Interferon-Gamma at the Crossroads of Tumor Immune Surveillance or Evasion.* Frontiers in immunology, 2018. **9**: p. 847-847.
477. de Weerd, N.A. and T. Nguyen, *The interferons and their receptors--distribution and regulation.* Immunol Cell Biol, 2012. **90**(5): p. 483-91.
478. Valente, G., et al., *Distribution of interferon-gamma receptor in human tissues.* Eur J Immunol, 1992. **22**(9): p. 2403-12.
479. Bhat, M.Y., et al., *Comprehensive network map of interferon gamma signaling.* J Cell Commun Signal, 2018. **12**(4): p. 745-751.
480. Samarajiwa, S.A., et al., *INTERFEROME: the database of interferon regulated genes.* Nucleic Acids Res, 2009. **37**(Database issue): p. D852-7.
481. Majoros, A., et al., *Canonical and Non-Canonical Aspects of JAK–STAT Signaling: Lessons from Interferons for Cytokine Responses.* Frontiers in Immunology, 2017. **8**.
482. Saha, B., et al., *Gene modulation and immunoregulatory roles of interferon gamma.* Cytokine, 2010. **50**(1): p. 1-14.
483. Huang, S., et al., *Immune Response in Mice that Lack the Interferon-γ Receptor.* Science, 1993. **259**(5102): p. 1742-1745.
484. Dalton, D.K., et al., *Multiple Defects of Immune Cell Function in Mice with Disrupted Interferon-γ Genes.* Science, 1993. **259**(5102): p. 1739-1742.
485. Dalton, D., *IFN-γ and IFN-γ Receptor Knockout Mice*, in *Cytokine Knockouts*. 2003, Humana Press : New Jersey. p. 347-360.
486. Kowanko, I.C. and A. Ferrante, *Stimulation of neutrophil respiratory burst and lysosomal enzyme release by human interferon-gamma.* Immunology, 1987. **62**(1): p. 149-151.
487. Schroder, K., et al., *Interferon-γ: an overview of signals, mechanisms and functions.* Journal of Leukocyte Biology, 2004. **75**(2): p. 163-189.
488. Shankaran, V., et al., *IFNγ and lymphocytes prevent primary tumour development and shape tumour immunogenicity.* Nature, 2001. **410**(6832): p. 1107-1111.
489. Dangaj, D., et al., *Cooperation between Constitutive and Inducible Chemokines Enables T Cell Engraftment and Immune Attack in Solid Tumors.* Cancer Cell, 2019. **35**(6): p. 885-900.e10.
490. Zaidi, M.R. and G. Merlino, *The two faces of interferon-gamma in cancer.* Clin Cancer Res, 2011. **17**(19): p. 6118-24.
491. Hubackova, S., et al., *IFNγ induces oxidative stress, DNA damage and tumor cell senescence via TGFß/SMAD signaling-dependent induction of Nox4 and suppression of ANT2.* Oncogene, 2016. **35**(10): p. 1236-1249.
492. Ossina, N.K., et al., *Interferon-gamma modulates a p53-independent apoptotic pathway and apoptosis-related gene expression.* J Biol Chem, 1997. **272**(26): p. 16351-7.
493. Gooch, J.L., R.E. Herrera, and D. Yee, *The role of p21 in interferon gamma-mediated growth inhibition of human breast cancer cells.* Cell Growth Differ, 2000. **11**(6): p. 335-42.
494. Braumüller, H., et al., *T-helper-1-cell cytokines drive cancer into senescence.* Nature, 2013. **494**(7437): p. 361-5.

495. Homann, L., et al., *IFN-γ and TNF Induce Senescence and a Distinct Senescence-Associated Secretory Phenotype in Melanoma.* Cells, 2022. **11**(9).
496. Zaidi, M.R., *The Interferon-Gamma Paradox in Cancer.* Journal of Interferon & Cytokine Research, 2018. **39**(1): p. 30-38.
497. Katz, J.B., A.J. Muller, and G.C. Prendergast, *Indoleamine 2,3-dioxygenase in T-cell tolerance and tumoral immune escape.* Immunol Rev, 2008. **222**: p. 206-21.
498. Brody, J.R., et al., *Expression of indoleamine 2,3-dioxygenase in metastatic malignant melanoma recruits regulatory T cells to avoid immune detection and affects survival.* Cell Cycle, 2009. **8**(12): p. 1930-4.
499. Ivashkiv, L.B., *IFNγ: signalling, epigenetics and roles in immunity, metabolism, disease and cancer immunotherapy.* Nat Rev Immunol, 2018. **18**(9): p. 545-558.
500. Ihle, J.N., *STATs: signal transducers and activators of transcription.* Cell, 1996. **84**(3): p. 331-4.
501. Shuai, K., et al., *A single phosphotyrosine residue of Stat91 required for gene activation by interferon-gamma.* Science, 1993. **261**(5129): p. 1744-6.
502. Kim, H.S. and M.-S. Lee, *STAT1 as a key modulator of cell death.* Cellular Signalling, 2007. **19**(3): p. 454-465.
503. Kaplan, D.H., et al., *Identification of an interferon-gamma receptor alpha chain sequence required for JAK-1 binding.* J Biol Chem, 1996. **271**(1): p. 9-12.
504. Kotenko, S.V., et al., *Interaction between the components of the interferon gamma receptor complex.* J Biol Chem, 1995. **270**(36): p. 20915-21.
505. Greenlund, A.C., et al., *Ligand-induced IFN gamma receptor tyrosine phosphorylation couples the receptor to its signal transduction system (p91).* Embo j, 1994. **13**(7): p. 1591-600.
506. Schindler, C., et al., *Interferon-dependent tyrosine phosphorylation of a latent cytoplasmic transcription factor.* Science, 1992. **257**(5071): p. 809-13.
507. Darnell, J.E., Jr., I.M. Kerr, and G.R. Stark, *Jak-STAT pathways and transcriptional activation in response to IFNs and other extracellular signaling proteins.* Science, 1994. **264**(5164): p. 1415-21.
508. Taniguchi, T., et al., *IRF family of transcription factors as regulators of host defense.* Annu Rev Immunol, 2001. **19**: p. 623-55.
509. Zhu, X., et al., *Stat1 serine phosphorylation occurs independently of tyrosine phosphorylation and requires an activated Jak2 kinase.* Mol Cell Biol, 1997. **17**(11): p. 6618-23.
510. Gauzzi, M.C., et al., *Interferon-alpha-dependent activation of Tyk2 requires phosphorylation of positive regulatory tyrosines by another kinase.* J Biol Chem, 1996. **271**(34): p. 20494-500.
511. Colamonici, O.R., et al., *p135tyk2, an interferon-alpha-activated tyrosine kinase, is physically associated with an interferon-alpha receptor.* J Biol Chem, 1994. **269**(5): p. 3518-22.
512. Yan, H., et al., *Phosphorylated interferon-alpha receptor 1 subunit (IFNaR1) acts as a docking site for the latent form of the 113 kDa STAT2 protein.* Embo j, 1996. **15**(5): p. 1064-74.

513. Qureshi, S.A., M. Salditt-Georgieff, and J.E. Darnell, Jr., *Tyrosine-phosphorylated Stat1 and Stat2 plus a 48-kDa protein all contact DNA in forming interferon-stimulated-gene factor 3.* Proc Natl Acad Sci U S A, 1995. **92**(9): p. 3829-33.
514. Li, X., et al., *Formation of STAT1-STAT2 heterodimers and their role in the activation of IRF-1 gene transcription by interferon-alpha.* J Biol Chem, 1996. **271**(10): p. 5790-4.
515. Alexander, W.S., et al., *SOCS1 is a critical inhibitor of interferon gamma signaling and prevents the potentially fatal neonatal actions of this cytokine.* Cell, 1999. **98**(5): p. 597-608.
516. Evans, M.K., et al., *Expression of SOCS1 and SOCS3 genes is differentially regulated in breast cancer cells in response to proinflammatory cytokine and growth factor signals.* Oncogene, 2007. **26**(13): p. 1941-1948.
517. Platanias, L.C., *Mechanisms of type-I- and type-II-interferon-mediated signalling.* Nature Reviews Immunology, 2005. **5**(5): p. 375-386.
518. Sun, Y., et al., *Differential expression of STAT1 and p21 proteins predicts pancreatic cancer progression and prognosis.* Pancreas, 2014. **43**(4): p. 619-23.
519. Slattery, M.L., et al., *JAK/STAT/SOCS-signaling pathway and colon and rectal cancer.* Molecular Carcinogenesis, 2013. **52**(2): p. 155-166.
520. Zhang, Y., et al., *The clinical and biological significance of STAT1 in esophageal squamous cell carcinoma.* BMC Cancer, 2014. **14**(1): p. 791.
521. Au, K.K., et al., *STAT1-associated intratumoural T(H)1 immunity predicts chemotherapy resistance in high-grade serous ovarian cancer.* J Pathol Clin Res, 2016. **2**(4): p. 259-270.
522. Widschwendter, A., et al., *Prognostic significance of signal transducer and activator of transcription 1 activation in breast cancer.* Clin Cancer Res, 2002. **8**(10): p. 3065-74.
523. Legrier, M.-E., et al., *Activation of IFN/STAT1 signalling predicts response to chemotherapy in oestrogen receptor-negative breast cancer.* British Journal of Cancer, 2016. **114**(2): p. 177-187.
524. Watson, C.J. and W.R. Miller, *Elevated levels of members of the STAT family of transcription factors in breast carcinoma nuclear extracts.* Br J Cancer, 1995. **71**(4): p. 840-4.
525. Magkou, C., et al., *Prognostic significance of phosphorylated STAT-1 expression in premenopausal and postmenopausal patients with invasive breast cancer.* Histopathology, 2012. **60**(7): p. 1125-32.
526. Chan, S.R., et al., *STAT1-deficient mice spontaneously develop estrogen receptor α-positive luminal mammary carcinomas.* Breast Cancer Res, 2012. **14**(1): p. R16.
527. Meraz, M.A., et al., *Targeted disruption of the Stat1 gene in mice reveals unexpected physiologic specificity in the JAK-STAT signaling pathway.* Cell, 1996. **84**(3): p. 431-42.
528. Koromilas, A.E. and V. Sexl, *The tumor suppressor function of STAT1 in breast cancer.* Jakstat, 2013. **2**(2): p. e23353.
529. Lee, C.K., et al., *Distinct requirements for IFNs and STAT1 in NK cell function.* J Immunol, 2000. **165**(7): p. 3571-7.
530. Schneckenleithner, C., et al., *Putting the brakes on mammary tumorigenesis: loss of STAT1 predisposes to intraepithelial neoplasias.* Oncotarget, 2011. **2**(12): p. 1043-54.
531. Raven, J.F., et al., *Stat1 is a suppressor of ErbB2/Neu-mediated cellular transformation and mouse mammary gland tumor formation.* Cell Cycle, 2011. **10**(5): p. 794-804.

532. Zemek, R.M., et al., *Sensitization to immune checkpoint blockade through activation of a STAT1/NK axis in the tumor microenvironment.* Science Translational Medicine, 2019. **11**(501): p. eaav7816.
533. Lesinski, G.B., et al., *The antitumor effects of IFN-alpha are abrogated in a STAT1-deficient mouse.* J Clin Invest, 2003. **112**(2): p. 170-80.
534. Battle, T.E., R.A. Lynch, and D.A. Frank, *Signal transducer and activator of transcription 1 activation in endothelial cells is a negative regulator of angiogenesis.* Cancer Res, 2006. **66**(7): p. 3649-57.
535. Alvaro, T., et al., *The presence of STAT1-positive tumor-associated macrophages and their relation to outcome in patients with follicular lymphoma.* Haematologica, 2006. **91**(12): p. 1605-12.
536. Kusmartsev, S. and D.I. Gabrilovich, *STAT1 signaling regulates tumor-associated macrophage-mediated T cell deletion.* J Immunol, 2005. **174**(8): p. 4880-91.
537. Zellmer, V.R., et al., *Tumor-induced Stromal STAT1 Accelerates Breast Cancer via Deregulating Tissue Homeostasis.* Molecular Cancer Research, 2017. **15**(5): p. 585-597.
538. Kumar, A., et al., *Defective TNF-alpha-induced apoptosis in STAT1-null cells due to low constitutive levels of caspases.* Science, 1997. **278**(5343): p. 1630-2.
539. Cao, Z.H., et al., *STAT1-mediated down-regulation of Bcl-2 expression is involved in IFN-γ/TNF-α-induced apoptosis in NIT-1 cells.* PLoS One, 2015. **10**(3): p. e0120921.
540. Chin, Y.E., et al., *Activation of the STAT signaling pathway can cause expression of caspase 1 and apoptosis.* Mol Cell Biol, 1997. **17**(9): p. 5328-37.
541. Xu, X., et al., *IFN-γ Induces Cell Growth Inhibition by Fas-mediated Apoptosis: Requirement of STAT1 Protein for Up-Regulation of Fas and FasL Expression1.* Cancer Research, 1998. **58**(13): p. 2832-2837.
542. Choi, E.A., et al., *Stat1-dependent induction of tumor necrosis factor-related apoptosis-inducing ligand and the cell-surface death signaling pathway by interferon beta in human cancer cells.* Cancer Res, 2003. **63**(17): p. 5299-307.
543. Miura, Y., et al., *TRAIL expression up-regulated by interferon-gamma via phosphorylation of STAT1 induces myeloma cell death.* Anticancer Res, 2006. **26**(6b): p. 4115-24.
544. Kaplan, D.H., et al., *Demonstration of an interferon gamma-dependent tumor surveillance system in immunocompetent mice.* Proc Natl Acad Sci U S A, 1998. **95**(13): p. 7556-61.
545. Kovacic, B., et al., *STAT1 acts as a tumor promoter for leukemia development.* Cancer Cell, 2006. **10**(1): p. 77-87.
546. Klover, P.J., et al., *Loss of STAT1 from mouse mammary epithelium results in an increased Neu-induced tumor burden.* Neoplasia, 2010. **12**(11): p. 899-905.
547. Khodarev, N.N., et al., *STAT1 is overexpressed in tumors selected for radioresistance and confers protection from radiation in transduced sensitive cells.* Proc Natl Acad Sci U S A, 2004. **101**(6): p. 1714-9.
548. Zimmerman, M.A., et al., *Unphosphorylated STAT1 promotes sarcoma development through repressing expression of Fas and bad and conferring apoptotic resistance.* Cancer Res, 2012. **72**(18): p. 4724-32.

549. Hix, L.M., et al., *Tumor STAT1 transcription factor activity enhances breast tumor growth and immune suppression mediated by myeloid-derived suppressor cells.* J Biol Chem, 2013. **288**(17): p. 11676-88.
550. Garcia-Diaz, A., et al., *Interferon Receptor Signaling Pathways Regulating PD-L1 and PD-L2 Expression.* Cell Reports, 2017. **19**(6): p. 1189-1201.
551. Kharma, B., et al., *STAT1 Drives Tumor Progression in Serous Papillary Endometrial Cancer.* Cancer Research, 2014. **74**(22): p. 6519-6530.
552. Ahn, R., et al., *The Shc1 adaptor simultaneously balances Stat1 and Stat3 activity to promote breast cancer immune suppression.* Nature Communications, 2017. **8**(1): p. 14638.
553. Peng, M., et al., *Aerobic glycolysis promotes T helper 1 cell differentiation through an epigenetic mechanism.* Science, 2016. **354**(6311): p. 481-484.
554. Chang, C.H., et al., *Posttranscriptional control of T cell effector function by aerobic glycolysis.* Cell, 2013. **153**(6): p. 1239-51.
555. Wang, F., et al., *Interferon Gamma Induces Reversible Metabolic Reprogramming of M1 Macrophages to Sustain Cell Viability and Pro-Inflammatory Activity.* EBioMedicine, 2018. **30**: p. 303-316.
556. Shima, K., et al., *Interferon-gamma interferes with host cell metabolism during intracellular Chlamydia trachomatis infection.* Cytokine, 2018.
557. Su, X., et al., *Interferon-γ regulates cellular metabolism and mRNA translation to potentiate macrophage activation.* Nature Immunology, 2015. **16**(8): p. 838-849.
558. Wang, W., et al., *CD8+ T cells regulate tumour ferroptosis during cancer immunotherapy.* Nature, 2019. **569**(7755): p. 270-274.
559. Parker, J.L., et al., *Molecular basis for redox control by the human cystine/glutamate antiporter system xc−.* Nature Communications, 2021. **12**(1): p. 7147.
560. McCann, K.J., et al., *IFNγ regulates NAD+ metabolism to promote the respiratory burst in human monocytes.* Blood Advances, 2022. **6**(12): p. 3821-3834.
561. Tai, Y., et al., *Enhanced mitochondrial pyruvate transport elicits a robust ROS production to sensitize the antitumor efficacy of interferon-γ in colon cancer.* Redox Biol, 2019. **20**: p. 451-457.
562. Wang, W., et al., *Effector T Cells Abrogate Stroma-Mediated Chemoresistance in Ovarian Cancer.* Cell, 2016. **165**(5): p. 1092-1105.
563. Pitroda, S.P., et al., *STAT1-dependent expression of energy metabolic pathways links tumour growth and radioresistance to the Warburg effect.* BMC Med, 2009. **7**: p. 68.
564. Jitschin, R., et al., *Inflammation-induced glycolytic switch controls suppressivity of mesenchymal stem cells via STAT1 glycosylation.* Leukemia, 2019. **33**(7): p. 1783-1796.
565. Huffaker, T.B., et al., *A Stat1 bound enhancer promotes Nampt expression and function within tumor associated macrophages.* Nature Communications, 2021. **12**(1): p. 2620.
566. Bhattacharya, A., et al., *Superoxide Dismutase 1 Protects Hepatocytes from Type I Interferon-Driven Oxidative Damage.* Immunity, 2015. **43**(5): p. 974-86.
567. Wang, H., et al., *Protective effect of silencing Stat1 on high glucose-induced podocytes injury via Forkhead transcription factor O1-regulated the oxidative stress response.* BMC Molecular and Cell Biology, 2019. **20**(1): p. 27.

568. Kim, J. and R.J. DeBerardinis, *Mechanisms and Implications of Metabolic Heterogeneity in Cancer.* Cell Metab, 2019. **30**(3): p. 434-446.
569. Hulea, L., et al., *Translational and HIF-1alpha-Dependent Metabolic Reprogramming Underpin Metabolic Plasticity and Responses to Kinase Inhibitors and Biguanides.* Cell Metab, 2018. **28**(6): p. 817-832 e8.
570. Ahn, R., et al., *The Shc1 adaptor simultaneously balances Stat1 and Stat3 activity to promote breast cancer immune suppression.* Nat Commun, 2017. **8**: p. 14638.
571. Ursini-Siegel, J., et al., *ShcA signalling is essential for tumour progression in mouse models of human breast cancer.* EMBO J, 2008. **27**(6): p. 910-20.
572. Wall, E.M., et al., *Spontaneous mammary tumors differ widely in their inherent sensitivity to adoptively transferred T cells.* Cancer Res, 2007. **67**(13): p. 6442-50.
573. Rose, A.A., et al., *Osteoactivin promotes breast cancer metastasis to bone.* Mol Cancer Res, 2007. **5**(10): p. 1001-14.
574. Savage, P., et al., *A Targetable EGFR-Dependent Tumor-Initiating Program in Breast Cancer.* Cell Rep, 2017. **21**(5): p. 1140-1149.
575. Darini, C., et al., *An integrated stress response via PKR suppresses HER2+ cancers and improves trastuzumab therapy.* Nat Commun, 2019. **10**(1): p. 2139.
576. Cao, L., et al., *Tumor-selective, futile redox cycle-induced bystander effects elicited by NQO1 bioactivatable radiosensitizing drugs in triple-negative breast cancers.* Antioxid Redox Signal, 2014. **21**(2): p. 237-50.
577. Longhi, M.P., et al., *Dendritic cells require a systemic type I interferon response to mature and induce CD4+ Th1 immunity with poly IC as adjuvant.* The Journal of experimental medicine, 2009. **206**(7): p. 1589-1602.
578. Dankner, M., et al., *Classifying BRAF alterations in cancer: new rational therapeutic strategies for actionable mutations.* Oncogene, 2018. **37**(24): p. 3183-3199.
579. Listgarten, J., et al., *Predictive models for breast cancer susceptibility from multiple single nucleotide polymorphisms.* Clin Cancer Res, 2004. **10**(8): p. 2725-37.
580. Mookerjee, S.A., et al., *Quantifying intracellular rates of glycolytic and oxidative ATP production and consumption using extracellular flux measurements.* J Biol Chem, 2017. **292**(17): p. 7189-7207.
581. Mamer, O., et al., *The complete targeted profile of the organic acid intermediates of the citric acid cycle using a single stable isotope dilution analysis, sodium borodeuteride reduction and selected ion monitoring GC/MS.* Metabolomics, 2013. **9**(5): p. 1019-1030.
582. Bolger, A.M., M. Lohse, and B. Usadel, *Trimmomatic: a flexible trimmer for Illumina sequence data.* Bioinformatics, 2014. **30**(15): p. 2114-20.
583. Dobin, A., et al., *STAR: ultrafast universal RNA-seq aligner.* Bioinformatics, 2013. **29**(1): p. 15-21.
584. Liao, Y., G.K. Smyth, and W. Shi, *featureCounts: an efficient general purpose program for assigning sequence reads to genomic features.* Bioinformatics, 2014. **30**(7): p. 923-30.
585. Love, M.I., W. Huber, and S. Anders, *Moderated estimation of fold change and dispersion for RNA-seq data with DESeq2.* Genome Biol, 2014. **15**(12): p. 550.
586. Li, H., et al., *The Sequence Alignment/Map format and SAMtools.* Bioinformatics, 2009. **25**(16): p. 2078-9.

587. Quinlan, A.R. and I.M. Hall, *BEDTools: a flexible suite of utilities for comparing genomic features.* Bioinformatics, 2010. **26**(6): p. 841-2.
588. Wheaton, W.W., et al., *Metformin inhibits mitochondrial complex I of cancer cells to reduce tumorigenesis.* Elife, 2014. **3**: p. e02242.
589. Alimova, I.N., et al., *Metformin inhibits breast cancer cell growth, colony formation and induces cell cycle arrest in vitro.* Cell Cycle, 2009. **8**(6): p. 909-15.
590. Liu, B., et al., *Metformin induces unique biological and molecular responses in triple negative breast cancer cells.* Cell Cycle, 2009. **8**(13): p. 2031-40.
591. Larsson, O., et al., *Distinct perturbation of the translatome by the antidiabetic drug metformin.* Proceedings of the National Academy of Sciences, 2012. **109**(23): p. 8977-8982.
592. Goodwin, P.J., et al., *Effect of Metformin vs Placebo on Invasive Disease-Free Survival in Patients With Breast Cancer: The MA.32 Randomized Clinical Trial.* Jama, 2022. **327**(20): p. 1963-1973.
593. Pollak, M., *Overcoming Drug Development Bottlenecks With Repurposing: Repurposing biguanides to target energy metabolism for cancer treatment.* Nature Medicine, 2014. **20**(6): p. 591-593.
594. Eikawa, S., et al., *Immune-mediated antitumor effect by type 2 diabetes drug, metformin.* Proceedings of the National Academy of Sciences, 2015. **112**(6): p. 1809-1814.
595. Andrzejewski, S., et al., *Metformin directly acts on mitochondria to alter cellular bioenergetics.* Cancer Metab, 2014. **2**: p. 12.
596. Bridges, H.R., et al., *Effects of metformin and other biguanides on oxidative phosphorylation in mitochondria.* Biochem J, 2014. **462**(3): p. 475-87.
597. Ramana, C.V., et al., *Stat1-dependent and -independent pathways in IFN-gamma-dependent signaling.* Trends Immunol, 2002. **23**(2): p. 96-101.
598. Braumuller, H., et al., *T-helper-1-cell cytokines drive cancer into senescence.* Nature, 2013. **494**(7437): p. 361-5.
599. Stojdl, D.F., et al., *VSV strains with defects in their ability to shutdown innate immunity are potent systemic anti-cancer agents.* Cancer Cell, 2003. **4**(4): p. 263-75.
600. Cheng, Y.S. and F. Xu, *Anticancer function of polyinosinic-polycytidylic acid.* Cancer Biol Ther, 2010. **10**(12): p. 1219-23.
601. Dempoya, J., et al., *Double-stranded RNA induces biphasic STAT1 phosphorylation by both type I interferon (IFN)-dependent and type I IFN-independent pathways.* J Virol, 2012. **86**(23): p. 12760-9.
602. Longhi, M.P., et al., *Dendritic cells require a systemic type I interferon response to mature and induce CD4+ Th1 immunity with poly IC as adjuvant.* J Exp Med, 2009. **206**(7): p. 1589-602.
603. Trumpfheller, C., et al., *The microbial mimic poly IC induces durable and protective CD4+ T cell immunity together with a dendritic cell targeted vaccine.* Proc Natl Acad Sci U S A, 2008. **105**(7): p. 2574-9.
604. Rose, A.A., et al., *ADAM10 releases a soluble form of the GPNMB/Osteoactivin extracellular domain with angiogenic properties.* PLoS One, 2010. **5**(8): p. e12093.

605. Dowling, R.J., et al., *Metformin Pharmacokinetics in Mouse Tumors: Implications for Human Therapy.* Cell Metab, 2016. **23**(4): p. 567-8.
606. Pollak, M., *Potential applications for biguanides in oncology.* J Clin Invest, 2013. **123**(9): p. 3693-700.
607. Chandel, N.S., et al., *Are Metformin Doses Used in Murine Cancer Models Clinically Relevant?* Cell Metab, 2016. **23**(4): p. 569-70.
608. Fendt, S.M., et al., *Reductive glutamine metabolism is a function of the alpha-ketoglutarate to citrate ratio in cells.* Nat Commun, 2013. **4**: p. 2236.
609. Kirtonia, A., G. Sethi, and M. Garg, *The multifaceted role of reactive oxygen species in tumorigenesis.* Cell Mol Life Sci, 2020.
610. Perillo, B., et al., *ROS in cancer therapy: the bright side of the moon.* Exp Mol Med, 2020. **52**(2): p. 192-203.
611. Nehme, A., et al., *Mechanism of interaction between cisplatin and human recombinant interferon gamma in human ovarian-cancer cell lines.* Int J Cancer, 1995. **61**(5): p. 643-8.
612. Jeon, S.M., N.S. Chandel, and N. Hay, *AMPK regulates NADPH homeostasis to promote tumour cell survival during energy stress.* Nature, 2012. **485**(7400): p. 661-5.
613. Ford, J.M., J.M. Yang, and W.N. Hait, *Effect of buthionine sulfoximine on toxicity of verapamil and doxorubicin to multidrug resistant cells and to mice.* Cancer Res, 1991. **51**(1): p. 67-72.
614. Traver, R.D., et al., *NAD(P)H:Quinone Oxidoreductase Gene Expression in Human Colon Carcinoma Cells: Characterization of a Mutation Which Modulates DT-Diaphorase Activity and Mitomycin Sensitivity.* Cancer Research, 1992. **52**(4): p. 797-802.
615. Nathan, D.M., et al., *Medical management of hyperglycemia in type 2 diabetes: a consensus algorithm for the initiation and adjustment of therapy: a consensus statement of the American Diabetes Association and the European Association for the Study of Diabetes.* Diabetes Care, 2009. **32**(1): p. 193-203.
616. Li, Z., et al., *NQO1 protein expression predicts poor prognosis of non-small cell lung cancers.* BMC Cancer, 2015. **15**: p. 207.
617. Cresteil, T. and A.K. Jaiswal, *High levels of expression of the NAD(P)H:quinone oxidoreductase (NQO1) gene in tumor cells compared to normal cells of the same origin.* Biochem Pharmacol, 1991. **42**(5): p. 1021-7.
618. Huang, X., et al., *Leveraging an NQO1 Bioactivatable Drug for Tumor-Selective Use of Poly(ADP-ribose) Polymerase Inhibitors.* Cancer Cell, 2016. **30**(6): p. 940-952.
619. Silvers, M.A., et al., *The NQO1 bioactivatable drug, beta-lapachone, alters the redox state of NQO1+ pancreatic cancer cells, causing perturbation in central carbon metabolism.* J Biol Chem, 2017. **292**(44): p. 18203-18216.
620. Postovit, L., et al., *Harnessing Oxidative Stress as an Innovative Target for Cancer Therapy.* Oxid Med Cell Longev, 2018. **2018**: p. 6135739.
621. Vangapandu, H.V., et al., *Biological and metabolic effects of IACS-010759, an OxPhos inhibitor, on chronic lymphocytic leukemia cells.* Oncotarget, 2018. **9**(38): p. 24980-24991.
622. Sullivan, L.B., et al., *Supporting Aspartate Biosynthesis Is an Essential Function of Respiration in Proliferating Cells.* Cell, 2015. **162**(3): p. 552-63.

623. Cardaci, S., et al., *Pyruvate carboxylation enables growth of SDH-deficient cells by supporting aspartate biosynthesis.* Nat Cell Biol, 2015. **17**(10): p. 1317-26.
624. Liu, X., et al., *Metformin Targets Central Carbon Metabolism and Reveals Mitochondrial Requirements in Human Cancers.* Cell Metab, 2016. **24**(5): p. 728-739.
625. Appleyard, M.V.C.L., et al., *Phenformin as prophylaxis and therapy in breast cancer xenografts.* British journal of cancer, 2012. **106**(6): p. 1117-1122.
626. Tully, E., et al., *Biguanide drugs enhance cytotoxic effects of cisplatin by depleting aspartate and NAD+ in sensitive cancer cells.* Cancer Biology & Therapy, 2021. **22**(10-12): p. 579-586.
627. Cipak Gasparovic, A., et al., *Chronic Oxidative Stress Promotes Molecular Changes Associated with Epithelial Mesenchymal Transition, NRF2, and Breast Cancer Stem Cell Phenotype.* Antioxidants (Basel), 2019. **8**(12).
628. Wolf, D.A., *Is reliance on mitochondrial respiration a "chink in the armor" of therapy-resistant cancer?* Cancer Cell, 2014. **26**(6): p. 788-795.
629. Britten, R.A., J.A. Green, and H.M. Warenius, *Cellular glutathione (GSH) and glutathione S-transferase (GST) activity in human ovarian tumor biopsies following exposure to alkylating agents.* Int J Radiat Oncol Biol Phys, 1992. **24**(3): p. 527-31.
630. Greenwood, H.E., et al., *Measurement of tumor antioxidant capacity and prediction of chemotherapy resistance in preclinical models of ovarian cancer by positron emission tomography.* Clinical Cancer Research, 2019: p. clincanres.3423.2018.
631. Parekh, A., et al., *Multi-nucleated cells use ROS to induce breast cancer chemo-resistance in vitro and in vivo.* Oncogene, 2018. **37**(33): p. 4546-4561.
632. Lee, J., et al., *Effective breast cancer combination therapy targeting BACH1 and mitochondrial metabolism.* Nature, 2019. **568**(7751): p. 254-258.
633. Lien, E.C., et al., *Glutathione biosynthesis is a metabolic vulnerability in PI(3)K/Akt-driven breast cancer.* Nat Cell Biol, 2016. **18**(5): p. 572-8.
634. Lin, N.U., et al., *Clinicopathologic features, patterns of recurrence, and survival among women with triple-negative breast cancer in the National Comprehensive Cancer Network.* Cancer, 2012. **118**(22): p. 5463-72.
635. Liedtke, C., et al., *Response to neoadjuvant therapy and long-term survival in patients with triple-negative breast cancer.* J Clin Oncol, 2008. **26**(8): p. 1275-81.
636. Weldon, C.B., et al., *Barriers to the Use of Personalized Medicine in Breast Cancer.* Journal of Oncology Practice, 2012. **8**(4): p. e24-e31.
637. Di Magno, L., et al., *The Mechanism of Action of Biguanides: New Answers to a Complex Question.* Cancers, 2022. **14**(13): p. 3220.
638. Krishnamurthy, S., et al., *Phenformin-loaded polymeric micelles for targeting both cancer cells and cancer stem cells in vitro and in vivo.* Biomaterials, 2014. **35**(33): p. 9177-86.
639. Di Magno, L., et al., *Phenformin Inhibits Hedgehog-Dependent Tumor Growth through a Complex I-Independent Redox/Corepressor Module.* Cell Rep, 2020. **30**(6): p. 1735-1752 e7.
640. Vara-Ciruelos, D., et al., *Phenformin, But Not Metformin, Delays Development of T Cell Acute Lymphoblastic Leukemia/Lymphoma via Cell-Autonomous AMPK Activation.* Cell Rep, 2019. **27**(3): p. 690-698.e4.

641. Hawley, S.A., et al., *Use of cells expressing gamma subunit variants to identify diverse mechanisms of AMPK activation.* Cell Metab, 2010. **11**(6): p. 554-65.
642. Wang, Y., et al., *Phenformin and metformin inhibit growth and migration of LN229 glioma cells in vitro and in vivo.* Onco Targets Ther, 2018. **11**: p. 6039-6048.
643. Veiga, S.R., et al., *Phenformin-Induced Mitochondrial Dysfunction Sensitizes Hepatocellular Carcinoma for Dual Inhibition of mTOR.* Clin Cancer Res, 2018. **24**(15): p. 3767-3780.
644. Sancho, P., et al., *MYC/PGC-1α Balance Determines the Metabolic Phenotype and Plasticity of Pancreatic Cancer Stem Cells.* Cell Metab, 2015. **22**(4): p. 590-605.
645. Izreig, S., et al., *Repression of LKB1 by miR-17 approximately 92 Sensitizes MYC-Dependent Lymphoma to Biguanide Treatment.* Cell Rep Med, 2020. **1**(2): p. 100014.
646. Prawan, A., et al., *Inflammatory cytokines suppress NAD(P)H:quinone oxidoreductase-1 and induce oxidative stress in cholangiocarcinoma cells.* J Cancer Res Clin Oncol, 2009. **135**(4): p. 515-22.
647. Rusinova, I., et al., *Interferome v2.0: an updated database of annotated interferon-regulated genes.* Nucleic Acids Res, 2013. **41**(Database issue): p. D1040-6.
648. Ross, D. and D. Siegel, *Functions of NQO1 in Cellular Protection and CoQ10 Metabolism and its Potential Role as a Redox Sensitive Molecular Switch.* Front Physiol, 2017. **8**: p. 595.
649. Montano, M.M., A.K. Jaiswal, and B.S. Katzenellenbogen, *Transcriptional Regulation of the Human Quinone Reductase Gene by Antiestrogen-liganded Estrogen Receptor-α and Estrogen Receptor-β*.* Journal of Biological Chemistry, 1998. **273**(39): p. 25443-25449.
650. Kitaya, K., et al., *Genes regulated by interferon-gamma in human uterine microvascular endothelial cells.* Int J Mol Med, 2007. **20**(5): p. 689-97.
651. Lajin, B. and A. Alachkar, *The NQO1 polymorphism C609T (Pro187Ser) and cancer susceptibility: a comprehensive meta-analysis.* Br J Cancer, 2013. **109**(5): p. 1325-37.
652. Freriksen, J.J.M., et al., *Genetic polymorphism 609C>T in NAD(P)H:quinone oxidoreductase 1 enhances the risk of proximal colon cancer.* Journal of Human Genetics, 2014. **59**(7): p. 381-386.
653. Yin, Z., et al., *Targeting T cell metabolism in the tumor microenvironment: an anti-cancer therapeutic strategy.* Journal of Experimental & Clinical Cancer Research, 2019. **38**(1): p. 403.
654. Pereira, F.V., et al., *Metformin exerts antitumor activity via induction of multiple death pathways in tumor cells and activation of a protective immune response.* Oncotarget, 2018. **9**(40): p. 25808-25825.
655. Li, X., et al., *NQO1 targeting prodrug triggers innate sensing to overcome checkpoint blockade resistance.* Nature communications, 2019. **10**(1): p. 3251-3251.
656. Pollak, M.N., *Investigating metformin for cancer prevention and treatment: the end of the beginning.* Cancer Discov, 2012. **2**(9): p. 778-90.
657. Trachootham, D., J. Alexandre, and P. Huang, *Targeting cancer cells by ROS-mediated mechanisms: a radical therapeutic approach?* Nat Rev Drug Discov, 2009. **8**(7): p. 579-91.